

中華民國核醫學學會 2019年會暨國際學術研討會

2019 Annual Meeting and International Symposium
of The Society of Nuclear Medicine, Taiwan (R.O.C)


奇美醫院

2019

November 16

(六)

■ 地點 ■ 奇美醫學中心永康總院第五醫療大樓5樓

■ 主辦單位 ■  中華民國核醫學學會



奇美醫學中心永康總院



行政院原子能委員會核能研究所

目次

■ 大會致詞	2
■ 會場平面圖	3
■ 大會議程表	4
■ 講師及演講摘要	5
■ 口頭論文發表摘要 - 基礎組	29
■ 口頭論文發表摘要 - 臨床組	39
■ 壁報論文發表摘要 - 基礎組	51
■ 壁報論文發表摘要 - 臨床組	94
■ 大會組織	228
■ 贊助廠商	229



李將瑄 會長

Dear Distinguished Guests, Ladies and Gentlemen, and Friends !

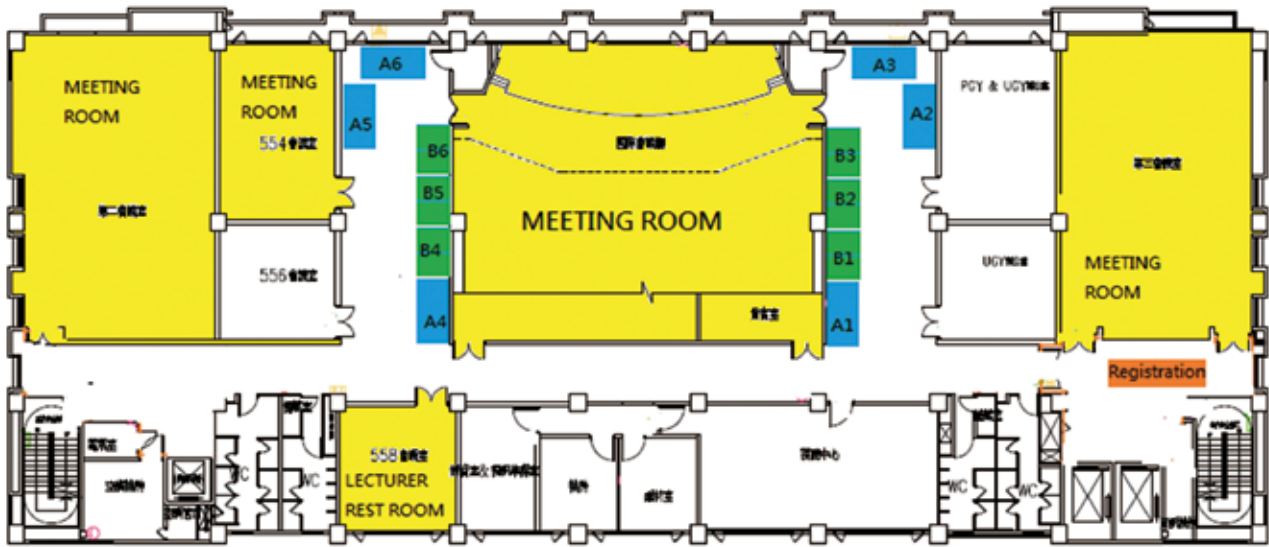
On behalf of Society of Nuclear Medicine, Taiwan, and Chi Mei Hospital, I am honored and glad to cordially invite you to the 2019 Annual Meeting of our society. The meeting will be held on November 16th at Chi Mei Medical Center in Tainan City, the oldest city in Taiwan known for its history, temples, and traditional snack food.

Chi Mei Hospital is an integrated health care system providing safe and quality health care in Southern Taiwan with totally more than 2500 beds capacity in Chi Mei Medical Center and Shulin campus, Chi Mei Hospital Liouying branch and Chiali branch. Our Nuclear Medicine department was organized in 1996, offering service including radioimmunoassay, single-photon emission computerized tomography (SPECT) scan, positron emission tomography (PET) scan, and radiopharmaceutical therapies.

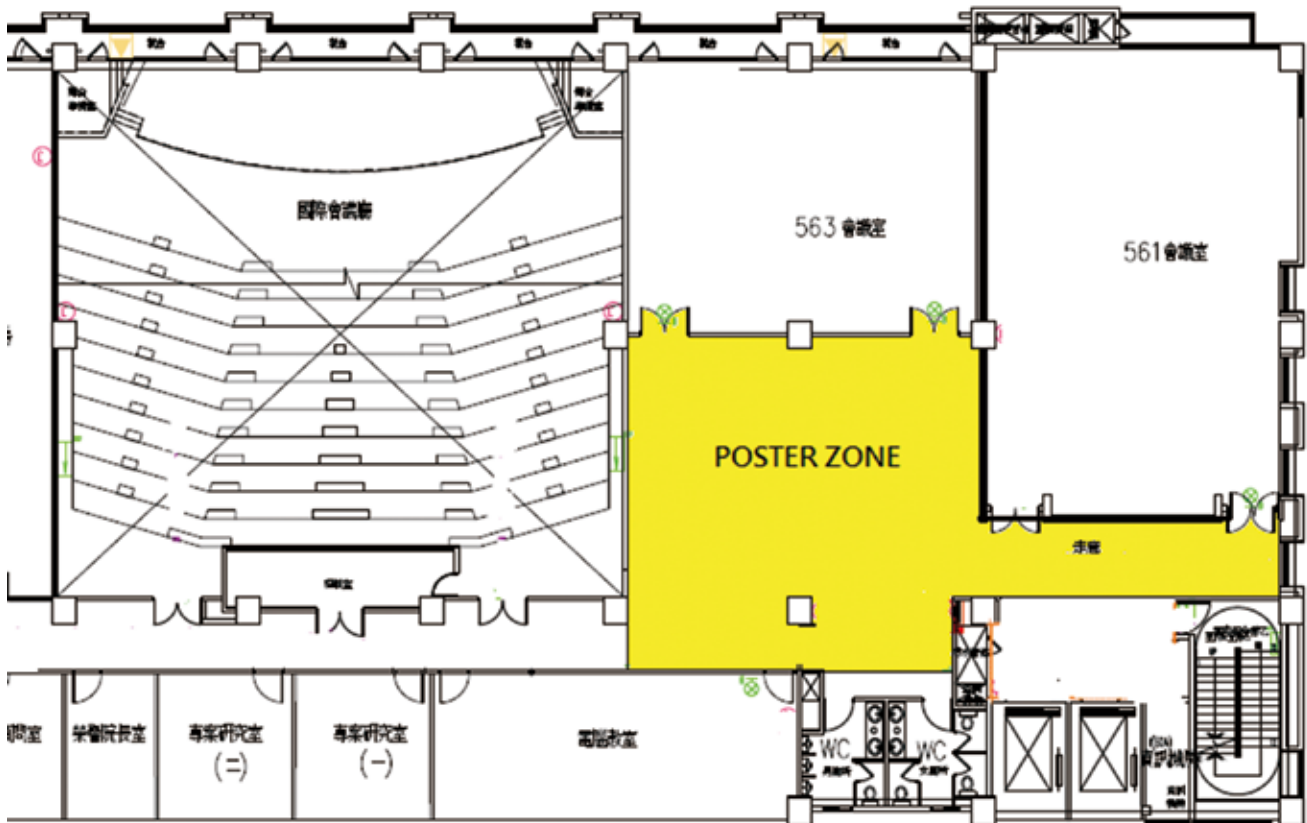
Precision medicine is emerging in recent years, and Theranostics of nuclear medicine plays an important part in it worldwide. This year, we invited well-known experts to give us an update on Theranostics and to share experiences of Theranostics Practice. I hope Theranostics will be well-established and popularized in Taiwan as soon as possible for better health, well-being and outcome of our patients.

李將瑄

5 樓平面圖



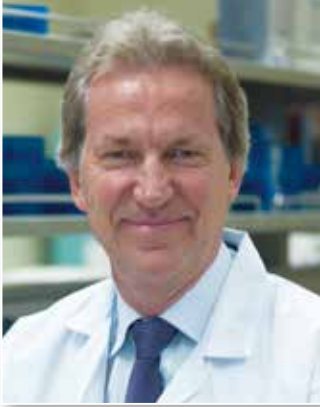
6 樓平面圖



中華民國核醫學學會 2019 年會暨國際學術研討會議程

大會議程表

時間 / 地點	奇美醫學中心永康總院第五醫療大樓 5 樓		
08:00~09:00	大會報到		
09:20~09:30	大會開幕 (奇美院長邱仲慶、理事長顏若芳)		
	國際會議廳 (5F)(247 人)	第二會議室 (5F)(129 人)	554 會議室 (5F)(37 人)
09:30~10:00	Translational PET Neuroimaging and Drug Development 主講: Prof. Christer Halldin 座長: 馬國興教授	09:30~10:30 臨床大數據分析及醫療影像量化 / 視覺化趨勢 主講: 瑞特資訊系統股份有限公司總經理劉光筠 座長: 杜高望組長	
10:00~10:30	Imaging Prostate Cancer with Fluciclovine PET 主講: Prof. David M. Schuster 座長: 鄭澄意副院長、高潘福主任		
10:30~10:50	Coffee break、廠商展示		
10:50~11:20	Lutetium-177 PSMA Radioligand Therapy in Metastatic Castration-Resistant Prostate Cancer. 主講: Haim Golan (Medical Director at Theragnostica-Israel) 座長: 彭南靖主任、劉仁賢主任		10:50~11:30 口頭論文基礎 座長: 張志賢組長、黃詠暉副教授
11:20~11:50	Nuclear Medicine Practice in treatment of mCRPC bony metastases with Ra-223 主講: Prof. Joe O'Sullivan (英國愛丁堡 Queen's University Belfast 核醫學教授) 座長: 譚鴻遠主任、黃玉儀主任	10:50~12:30 台韓醫技經驗交流 主講: Jun-Mo Park Min-Ho Park Jun-young Park 座長: Won -Guk Lee、黃奕瑾組長	
11:50~12:20	Radioactive iodine refractory thyroid cancer: molecular mechanisms and therapeutic approaches 主講: Prof. Byeong-Cheol Ahn (韓國大邱 Kyungpook National University 核醫學教授) 座長: 吳鴻昇院長、譚鴻遠主任		11:30~12:20 口頭論文基礎 座長: 陳傳霖副教授、黃雅瑤博士
12:20~12:30	會員大會		
	Lunch Symposium		
12:30~13:30	第二會議室	554 會議室	
	Digital PET/CT and Motion Management 主講: Tinsu Pan, Ph.D. 座長: 劉仁賢主任	Veriton, A New Design With Ring Type CZT – Whole Body Scanner 主講: Mr. Roland Schöll 座長: 蔡秋德 (常捷生醫科技股份有限公司 - 總經理)	
13:40~14:10	Precision imaging and theranostics: Liverpool Hospital experience 主講: Prof. Peter Lin, M.D. (University of Sydney) 座長: 黃文盛主任、張智勇醫師	13:40~14:00 1. Application of I-123 MIBG in oncology 主講: 台大 - 盧孟佑醫師 座長: 曾凱元醫師	13:40~14:40 第一年住院醫師考試
		14:00~14:20 2. Application of I-123 MIBG in cardiology 主講: 亞東 - 汪姍瑩主任 座長: 吳彥雯主任	
		14:20~14:40 3. Application of I-123 MIBG in neurology 主講: 秀傳 - 邱百韻主任 座長: 邱南津主任	
14:10~14:40	PET imaging in Interstitial lung Disease. 主講: Prof. Ashley Groves 座長: 謝孟哲主任、陳世欣主任	14:40~15:00 4. Imaging protocol & analysis of I-123 MIBG (秀傳 - 洪光威副院長) 座長: 蔡世傳主任	
14:40~15:10	Imaging and staging of Lung cancer: What the Chest physician want to know 主講: Prof. Thida Win 座長: 賴建豪主任、何恭之主任	15:00~15:20 討論: 座長: 林昆儒醫師	14:40~15:40 口頭論文 臨床 座長: 邱創新主任、許幼青放射師
15:10~15:30	Coffee break		
15:30~15:50	FCH PET 臨床應用: FCH 的備製與品管 主講: 花蓮慈濟高志浩博士 座長: 薛晴彥教授	15:30~16:10 Randox 外部能力試驗結果解說 主講: 陳翰逸業務專員 Randox 相關品管試劑業務 座長: 王安美主任	15:40~16:30 口頭論文 臨床 座長: 詹勝傑醫師、邱宇莉醫師
15:50~16:10	FCH PET 臨床應用: FCH 在肝癌的應用 主講: 中山醫大附醫高潘福主任 座長: 曾凱元醫師、陳輝堉主任		
16:10~16:30	FCH PET 臨床應用: FCH 在攝護腺癌的應用 主講: 臺大醫院路景竹醫師 座長: 曾凱元醫師、陳輝堉主任		
16:30~16:50	FCH PET 臨床應用: FCH 在副甲狀腺腫瘤的應用 主講: 花蓮慈濟陳昱宏醫師 座長: 曾凱元醫師、陳輝堉主任	16:10~16:50 放射免疫分析實驗室風險管理之經驗分享 主講: 王安美 (馬偕紀念醫院核醫科技術主任) 座長: 陳宜伶放射師	
16:50 ~	閉幕		



Name: **Christer Halldin**

Title: Professor

Institute: BSc in Chemistry, Uppsala Organic Chemistry and Radiochemistry

Translational PET Neuroimaging and Drug Development

Professor Halldin's scientific research activities have been focusing on the development of PET radioligands for the central nervous system and their applied use in translational imaging from animal to clinical use in patients. In recent years the primary focus has been in the development of imaging biomarkers for diseases such as Parkinson and Alzheimer and tracers for measuring neurotransmitter release.



Name: **David M. Schuster**

Title: Professor

Institute: B.Sc. in Chemistry, University of Uppsala

Imaging Prostate Cancer with Fluciclovine PET

Prostate cancer is a leading cause of cancer death worldwide. Up to 50% of patients after initial therapy will develop biochemical failure. The differentiation of local from extraprostatic recurrence plays a critical role in patient management. The use of functional imaging targeting features of cancer metabolism has proven highly useful. Amino acid transport is upregulated in prostate cancer. Fluciclovine (*anti*-1-amino-3-F-18-fluorocyclobutane-1-carboxylic acid, FACBC, Axumin™) is an artificial amino acid PET tracer that was approved in 2016 by the U.S. Food and Drug Administration for detection of suspected recurrent prostate cancer.

This talk will provide an overview of fluciclovine PET for recurrent prostate cancer, including published comparisons to conventional imaging and other molecular imaging agents. The talk will also review the fluciclovine PET imaging procedure and image interpretation, including physiologic and pathologic uptake patterns and pitfalls.



Name: **Haim Golan**

Title: Director

Institute: Ben-Gurion University, Nuclear Medicine at Soroka Medical Center

Lutetium-177 PSMA Radioligand Therapy in Metastatic Castration-Resistant Prostate Cancer

Among PET radiotracers, prostate-specific membrane antigen (PSMA)-based compounds in advanced prostate cancer are gaining growing interest, mostly due to their relevance as theranostic agents.

The impact of PSMA-based PET/CT imaging on treatment strategies and prognosis will be discussed with regard to application in PSMA-directed RLT, as well as monitoring treatment response and assessment of the spread of prostate cancer.

Lutetium-177 (^{177}Lu) is a short path beta emitter with a mean length of 1 mm, average penetration of 0.3 mm, and a 6.7-day half-life.

Radioligand therapy with ^{177}Lu -PSMA in metastatic castration resistant prostate cancer (mCRPC) published data suggest a high activity of ^{177}Lu showing in some cases complete treatment response after two cycles of ^{177}Lu -PSMA-617.

Data from prospective trials from Australia and Germany will be presented with regard to overall survival, progression free survival, quality of life and treatment toxicity.



Name: **Joe O'Sullivan**

Title: Professor (Clinical) of Radiation Oncology

Institute: School of Medicine, Dentistry and Biomedical Sciences, Queen's University Belfast, United Kingdom

Nuclear Medicine Practice in Treatment of mCRPC Bony Metastases with Ra-223

The aim of targeted radionuclide therapy is to deliver systemic radiation selectively to cancer cells, minimizing toxicity to healthy tissues. The ideal radionuclide for targeted therapy is persistent, short-range, and powerful. The high decay energy and short range of alpha particles confers a high radiobiological effectiveness and is likely to lead to irreparable double strand DNA breaks and cell death. There is no known mechanism of resistance to alpha particle irradiation. Radium 223 dichloride, the only approved alpha particle bone targeted therapy, delivered survival gain in men with bone metastases due to castrate resistant prostate cancer. As more life-prolonging agents available, more decisions were considered in current mCRPC treatment landscape. How to select eligible patients, have initial discuss, monitor/manage patients from first infusion to completion of 6 months of therapy will be discussed under this topic.



Name: **Byeong-Cheol Ahn**

Title: Professor

Institute: Department of Nuclear Medicine, School of Medicine, Kyungpook National University

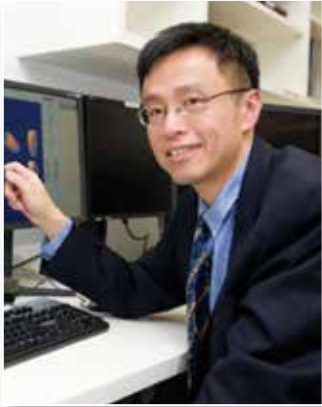
Radioactive Iodine Refractory Thyroid Cancer: Molecular Mechanisms and Therapeutic Approaches

Although most differentiated thyroid cancers show excellent prognosis, treating radioactive iodine (RAI) refractory differentiated thyroid cancers (DTCs) is challenging. Various therapies, including chemo-, radio-, and targeted therapies, have been applied for treating RAI refractory DTCs but show limited effectiveness. The pathogenesis of thyroid cancer is closely associated with genetic mutations, rearrangements and epigenetic alterations, which activate certain signaling cascades, which might produce silencing of iodide metabolizing genes. The activated signaling pathways by the genetic mutations are crucial underlying mechanisms of the RAI refractoriness in DTCs.

Blockade of the signaling cascades may lead to redifferentiation of RAI refractory DTCs that are respond to RAI therapy. Redifferentiation followed by RAI therapy might be a promising new alternative therapy for the RAI refractory DTCs.

Extracellular vesicles (EVs), heterogeneous lipid-bound nanovesicles which released by cells, play a vital role in cell-to-cell communications. The EVs can be used as delivery vehicles for RNAs, proteins, and drugs, and the EV technology can revert RAI refractory DTCs to RAI sensitive cancers.

This presentation will discuss molecular mechanisms of RAI refractory DTCs and therapeutic strategies based on tacking the mechanisms. In addition, EV technologies for the strategies will be touched as well.



Name: **Peter Lin**
Title: Professor
Institute: University of Sydney, MDr

Precision Imaging and Theranostics: Liverpool Hospital Experience

The presentation will provide an overview of our Medical Imaging service, and molecular imaging and targeted therapy program in my Department.

Discuss PSMA imaging and theranostics using Ga68-PSMA-11 HBED-CC, and more recently newer generation F18 and Lu177 labelled PSMA ligands with PSMA-1007, PSMA-617 and PSMA I&T, and share our clinical experiences, and also lessons learnt in planning and establishing a “precision” theranostics and targeted molecular therapy service.



Name: **Peter Ashley Groves**

Title: Professor

Institute: SpR Nuclear Medicine (London) and Radiology (Cambridge),
University of Newcastle Upon Tyne

PET Imaging in Interstitial Lung Disease

Added Clinical Value for PET/MR in Oncology Initial clinical research comparing the diagnostic performance of PET/MRI and PET/CT has largely shown equivalent diagnostic capabilities for these modalities in oncology. These uncertainties about the magnitude of diagnostic benefit are compounded by the considerable health economic challenges associated with clinical implementation. Therefore, there is a need to identify ways to extend the use of this technology beyond simple diagnosis so that PET/MRI can add sufficient clinical value beyond PET/CT or MRI alone and become a cost-effective imaging modality in clinical practice. A major advantage of PET/MRI over other imaging modalities is the ability to generate multiple quantitative images from a single examination. A multiparametric PET/MRI approach not only can add clinical value through contributing to precision medicine but also can establish PET/MRI as a potentially cost-effective imaging modality in oncology.



Name: **Thida Win**

Title: Professor

Institute: INSTITUTE OF MEDICINE II MBBS (Yangon, Myanmar)

Imaging and Staging of Lung Cancer: What the Chest Physician Want to Know

We prospectively performed spirometry and quantitative ventilation-perfusion scintigraphy on consecutive patients undergoing lobectomy for lung cancer. we found that ventilation scintigraphy alone provided the best correlation between the predicted and actual postoperative values and recommend its use to predict postoperative lung function. Combining FDG-PET and dynamic contrast CT could assess vascular and metabolic tumour types of NSCLC. The low metabolism with high vascularity phenotype was significantly more common among adenocarcinomas, whereas the high metabolism with high vascularity phenotype was more common among squamous cell carcinomas. Other non-small cell lung carcinoma tumor types demonstrated a high prevalence of the high metabolism with low vascularity phenotype. Texture analysis could obtain survival-predictors such as CT-derived heterogeneity, PET-derived heterogeneity in addition to CT-derived permeability and stage. These predictors were independent of patient treatment and could assist the management of many patients with NSCLC.



Name: 高志浩

Title: 製藥科主任

Institute: 環境健康科學系〔放射藥物化學學程〕美國約翰霍普金斯大學公共衛生學院博士

FCH PET 臨床應用： FCH 的備製與品管

以目前台灣衛生主管機關針對正子藥品的規定，醫院可以有條件的提供 FCH 正子斷層掃描。花蓮慈濟醫院自 2013 年起逐漸提高生產 FCH 的頻率，產能足以供應院內兩案臨床試驗需求，但並無供應常規性臨床服務。臺大醫院則選擇向食品藥物管理署申請 FCH 的生產品質查核，以 EP 標準進行 FCH 藥品產品品質檢驗，並於 2018 年通過查核，因此臺大醫院所生產的 FCH 可以供應常規性臨床正子斷層掃描檢查。

由於整體國際醫療市場對 FCH 的需求逐漸增加，FCH 的自動化生產製造也因此不斷得到精進改良，目前已經可以有量產規模，其品質又已經得到歐洲藥典的明確規範，國內的正子藥品製造機構將可逐步推動 FCH 的商業化生產，使此項先進的正子斷層掃描技術得以在台灣普及。



Name: 高潘福

Title: 教授兼副系主任

Institute: 1. Johns Hopkins University, Master of Science

2. 中山醫學大學臨床醫學研究所博士

FCH PET 臨床應用： FCH 在肝癌的應用

近十年臨床研究結果顯示在診斷肝癌方面，雖然 ^{18}F -FDG 造影對於診斷高分化的肝癌靈敏度偏低，但整體而言 ^{18}F -FDG 造影能提供預後與治療方式選擇的有用資訊。相反的，脂肪代謝的 ^{11}C -醋酸鹽或 ^{18}F -膽鹼造影對於診斷高分化的肝癌有較好的靈敏度，卻對低分化的肝癌靈敏度偏低。這不僅在同一病患的不同肝癌病灶，即使在同一肝癌病灶內的不同部分，都可能呈現兩種放射製劑互補攝取的現象。目前研究學者一致主張合併 ^{18}F -FDG 和 ^{18}F -膽鹼兩種放射製劑造影，對於偵測肝癌肝內腫瘤和全身癌轉移病灶將有最佳的診斷率，以及在預測手術後復發等都能達到最好的效果。



Name: 路景竹

Title: 主治醫師

Institute: Ph.D., Graduate Institute of Epidemiology and Preventive Medicine

FCH PET 臨床應用： FCH 在攝護腺癌的應用

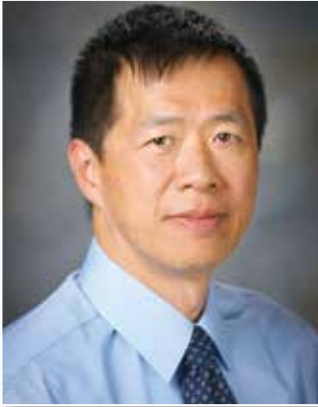
近十年臨床研究結果顯示在診斷肝癌方面，雖然 ^{18}F -FDG 造影對於診斷高分化的肝癌靈敏度偏低，但整體而言 ^{18}F -FDG 造影能提供預後與治療方式選擇的有用資訊。相反的，脂肪代謝的 ^{11}C -醋酸鹽或 ^{18}F -膽鹼造影對於診斷高分化的肝癌有較好的靈敏度，卻對低分化的肝癌靈敏度偏低。這不僅在同一病患的不同肝癌病灶，即使在同一肝癌病灶內的不同部分，都可能呈現兩種放射製劑互補攝取的現象。目前研究學者一致主張合併 ^{18}F -FDG 和 ^{18}F -膽鹼兩種放射製劑造影，對於偵測肝癌肝內腫瘤和全身癌轉移病灶將有最佳的診斷率，以及在預測手術後復發等都能達到最好的效果。



Name: 陳昱宏
Title: 主治醫師
Institute: 慈濟大學醫學系學士

FCH PET 臨床應用： FCH 在副甲狀腺腫瘤的應用

近十年臨床研究結果顯示在診斷肝癌方面，雖然 ^{18}F -FDG 造影對於診斷高分化的肝癌靈敏度偏低，但整體而言 ^{18}F -FDG 造影能提供預後與治療方式選擇的有用資訊。相反的，脂肪代謝的 ^{11}C -醋酸鹽或 ^{18}F -膽鹼造影對於診斷高分化的肝癌有較好的靈敏度，卻對低分化的肝癌靈敏度偏低。這不僅在同一病患的不同肝癌病灶，即使在同一肝癌病灶內的不同部分，都可能呈現兩種放射製劑互補攝取的現象。目前研究學者一致主張合併 ^{18}F -FDG 和 ^{18}F -膽鹼兩種放射製劑造影，對於偵測肝癌肝內腫瘤和全身癌轉移病灶將有最佳的診斷率，以及在預測手術後復發等都能達到最好的效果。



Name: **Tinsu Pan, Ph.D.**

Title: Professor

Institute: Department of Imaging Physics, Division of Diagnostic Imaging,
The University of Texas MD Anderson Cancer Center, Houston, TX

Digital PET/CT and Motion Management

New digital PET/CT has a larger axial field of view resulting in higher sensitivity, and has a finer cut of scintillation crystal leading to higher spatial resolution than the conventional photomultiplier tube (PMT) based PET/CT. Not only can a digital PET/CT shorten the scan time, it can also reduce the injection activity and/or improve the image quality. We will share our experiences of digital PET/CT imaging at M.D. Anderson Cancer Center.

New technology of data driven gating (ddg), which does not require a respiratory monitoring device for PET gating, is almost ready for clinical use. As PET gating improves, it becomes evident that ddg CT is needed for ddg PET. We will demonstrate the first application of ddg CT for ddg PET, and compare the ddg PET/CT with average PET/CT in the application of Ga-68 Dotatate imaging.

The information contained in this e-mail message may be privileged, confidential, and/or protected from disclosure. This e-mail message may contain protected health information (PHI); dissemination of PHI should comply with applicable federal and state laws. If you are not the intended recipient, or an authorized representative of the intended recipient, any further review, disclosure, use, dissemination, distribution, or copying of this message or any attachment (or the information contained therein) is strictly prohibited. If you think that you have received this e-mail message in error, please notify the sender by return e-mail and delete all references to it and its contents from your systems.



Name: **Mr. Roland Schöll**
 Title: Business Development Director APAC
 Institute: ■ BSc, Medical Radiation Technology (Nuclear Medicine),
 University of Sydney (1994)
 ■ CPD accreditation Nuclear Medicine
 ■ Sales one-on-One, Leadership Framework Certification,
 Corporate Compliance Training
 ■ Strategic Blue Ocean Training Course –Siemens AG

Veriton, A New Design With Ring Type CZT – Whole Body Scanner

The VERITON-CT[®] (SPECT/CT) with diagnostic 16 or 64 slice CT capabilities has a unique 360° CZT[™] design, more closely resembling a PET ring gantry than traditional dual head nuclear camera.

It follows the adaptation of the ground-breaking D-SPECT[®] cardiac design which focuses on close detector proximity to the patient for optimized SPECT imaging.

VERITON-CT[®] uses a similar strategy using multiple telescopic detectors to establish the optimal minimum source to detector distance. Swiveling detector assemblies, acquisition modes and reconstructions, as well as new, unique capabilities added to VERITON maximize the impact of 360° CZT. Acquisitions are always 3D offering full tomographic detail.

The time has come to re-consider the way that SPECT imaging is used in routine clinical practice.





Name: 劉光筠
Title: 總經理
Institute: 瑞特資訊系統股份有限公司

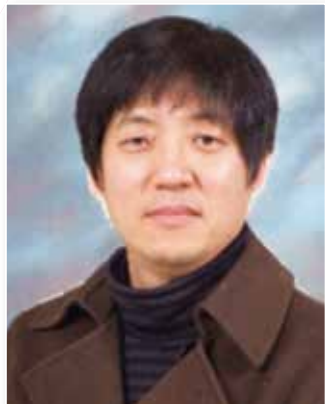
臨床大數據分析及醫療影像量化 / 視覺化趨勢

因應時代的變遷，當移動式裝置逐漸取代了 Win-tel 系統為主的電腦系統，智慧型手機取代了一般的電話手機，醫療環境漸漸起了變化，以往的總總限制似乎有了新的解決方案，面對新的裝置崛起，猶豫思量等待守候亦或是義無反顧迎合發展，在在考驗醫療界專家的智慧。

醫療資訊發展至今，很多人都覺得已經到了盡頭，其實並不竟然，單看 DICOM/HL7 的發展就可窺知一二。舉例而言，DICOM3.0 自 Part 18 提到 Web Services 之後，提供了一個跨平台與醫院系統介接的方式；這兩年新增的 Part 19 及 Part 20 所談到的 Application Hosting 及 DICOM/HL7 的串接轉換，在在提醒我們數位影像的移動型趨勢及背後的資料資訊整合，再加上新增的 Part 21 對於量化影像資料的儲存傳輸的流程制定，HL7 推出 FHIR 的新規範，在在顯示醫療影像量化及醫療資訊交流對於未來的影響就是各個醫療單位科室的系統會更趨於獨特性及客製化，且臨床資訊視覺化顯示提點會更受臨床醫護人員的依賴；如此醫療資訊應用勢必多樣性的發展，以符合未來資訊整合的需求。

因應醫療影像環境的趨勢，人工智慧的相關技術與臨床工作結合已非夢想，思索是否可以解決過去需要醫療環境下所造成的盲點，若能將系統內容提供即時及主動提示，這已不只是增加工作效率而已，對於臨床品質的提升更是有莫大的助益，面對人工智慧浪潮排山倒海而來，臨床相關專家是否有正確的觀念及投資方向，將有助於未來人工智慧醫療環境的到來。

鑑往知來，當趨勢莫之能禦時，若能順勢而為、掌握機先方是上策，尤其是醫療大數據收集、資料視覺化及人工智慧的應用接踵而來，這會是醫療資訊的重大革命，若等到所有趨勢已成定局方才修正，恐怕是為時已晚，屆時就算投入更大的資源也無法彌補彼此的醫療品質差異，這就是這些新興科技在這個時代的關鍵意義。



Name: **Jun Mo Park**
 Title: Medical Laboratory Technologist
 Institute: Department of nuclear medicine, Yeouido ST.Mary's hospital
 Catholic University, Seoul, Korea

ARC Availability Experiment by Comparing Plasma Renin Activity (PRA) and Active Renin Concentration (ARC)

Purpose: Renin is a proteolytic enzyme synthesized and secreted from epidermal (juxtaglomerular) cells in kidney. Renin acts on the renin substrate angiotensinogen to produce angiotensin I, and then angiotensin II is produced by the action of angiotensin converting enzyme. This causes the adrenal glands to boost blood pressure (vasoconstriction) and promote aldosterone secretion. While Plasma renin activity (PRA) is to test angiotensin I, the active renin concentration (ARC) is a renin test directly. They have different test methods and their own substrates. However, these two methods are sometimes interpreted as the same as a result. The purpose of this study was to evaluate the usefulness of the ARC test by comparing the results between PRA and ARC.

Materials and Methods: For the diversity of the experiment, 26 samples were requested to test with PRA (company A) and ARC (company C) to other institution. We compared and analyzed PRA (company B) and ARC (company C) tests using 28 samples from September 15th to October 13th in 2017. The statistical analysis method for PRA/ARC evaluated the usefulness using Microsoft Excel program by verifying a correlation analysis of Aldosterone/PRA ratio and a correlation analysis of Aldosterone/ARC ratio and conducting T-test.

Results: The regression equation of the PRA (company B)/ARC (company C), which was tested in the department, was $y = 0.0637x + 0.3285$ and the correlation coefficient was 0.73. The regression equation of the PRA (company A)/ARC (company C), which was tested in the other institution, was $y = 0.0888x + 0.3316$ and the correlation coefficient was 0.90. In addition, The regression equation of Aldosterone / PRA ratio and Aldosterone / ARC ratio was $y = 0.875x - 11.688$ and the correlation coefficient was 0.87. Plus T – test showed no significant difference ($P > 0.05$).

Conclusion: Both tests showed a strong positive correlation, but this only represents the strength and direction of the relationship between the two tests. Furthermore, the actual results showed somewhat differences. It is presumed that the measured value was influenced by the endogenous renin group mass in the plasma, the condition of the enzyme reaction and the kind of the inhibitor. When the active renin concentration (ARC) test is performed, it is useful to distinguish between the two tests as they are complementary.

Keywords: Plasma renin activity (PRA), Active renin concentration (ARC), Aldosterone



Name: **Min-Ho Park**
Title: Employee
Institute: Department of Nuclear Medicine, Seoul National University Hospital, Seoul, Korea

Glomerular Filtration Rate Test Methods and Guidelines

Purpose: The glomerular filtration rate (GFR) test is an important indicator of glomerular filtration and has been used to test renal function and the extent of its function. The GFR test is performed by intravenous injection of radioactive medicines made of $^{51}\text{Cr-EDTA}$, and blood concentration is measured by taking blood according to the elapsed time. also, PET-CT, bone scan, transfusion and so on will affect the outcome. Therefore, we will improve the quality of the test by providing guidelines for the GFR test for more accurate testing.

Materials and Methods: 5 mL of physiological saline solution and 2 mL of $^{51}\text{Cr-EDTA}$ solution are used to make 5 mL of the radiopharmaceutical solution to be injected into the patient. First, the syringe weight is measured before the injection, and then the radioactive medicine is injected into the patient's vein and the syringe weight is measured after the injection. Blood sampling is performed twice in total. In adults, blood is collected 3 hours / 5 hours after injection and in children 2 hours / 5 hours after injection. The blood sample is centrifuged at 3300 rpm for 5 minutes. Standard solution is prepared by filling diluent water up to the scale indicated in the 200-mL volumetric flask, discarding 500 μL , injecting 500 μL of GFR reagent and mixing well. 500 μL each of the standard solution is dispensed into two test tubes, and 500 μL of each of the plasma samples collected in time is dispensed into two test tubes and measured with a Cobra Counter.

Results: At present, the reference range applied in this study is 119.5 ± 30.3 ml / min / 1.73 m² for males and 125.2 ± 28.2 ml / min / 1.73 m² for females.

Conclusion: The GFR test is conducted using radioactive medical products. GFR testing is performed as a scheduled test, but PET-CT, dialysis and transfusion, which may affect GFR testing, may be scheduled during GFR testing. Therefore, we could get accurate GFR test results by notifying the ward and department beforehand when booking.

Keyword: Glomerular filtration rate, $^{51}\text{Cr-EDTA}$, Cobra Counter



Name: **Jun-Young Park**

Title: Radiochemist

Institute: Department of Nuclear Medicine, Severance Hospital, Yonsei University College of Medicine

Tungsten Shielding Device for Protection of Bremsstrahlung Radiation from Y-90 Microspheres

Purpose: Yttrium-90 (Y-90) is high-energy beta emitters ($E\beta$, max = 2.28 MeV) with the mean penetration depth of 2.5 mm in tissue. Radioactive microspheres containing Y-90 is widely used for the transarterialradioembolization ofhepatocellular carcinoma. However, bremsstrahlung radiation from Y-90 can cause the external radiation exposure to medical staff who handle the Y-90 microspheres. In this study, shielding device for Y-90 microspheres was developed to minimize the external radiation exposure.

Materials and Methods: Y-90 microsphere shieldingdevice was made from 6 mm thicknesses of tungsten including the lead glass window. Radiation shielding ability of Y-90 microsphere shielding device was evaluated using 4 GBq of SIR-Spheres[®] Y-90 microspheres. The bremsstrahlung radiation wasmeasured usingradiation survey meter (Alert[™], Inspector, USA).

Results: The mean radiation dose of SIR-Spheres[®] Y-90 in acrylic shield was $261.7 \pm 2.3 \mu\text{Sv/h}$ (n = 5) at 10 cm away from the shield. With the additional tungsten shielding device, it was $23.7 \pm 1.3 \mu\text{Sv/h}$ (n = 5). Thus, the bremsstrahlung radiation dose was decreased by 90.9%. At 50 cm away from the shield, bremsstrahlung radiation was reduced by 89.2% after using tungsten shielding device.

Conclusion: During the preparation and radioembolization of Y-90 microsphere, medical staff areexposed toexternal radiation. In this study, we demonstrated thatthe use of tungsten shielding device devices significantly reduced the amount of bremsstrahlung radiation. Y-90 microsphere tungstenshieldingdevice can be highly effective in reducing the bremsstrahlung radiation.

Keywords: Y-90, Radiotherapy, Bremsstrahlung, Radiation shield, Radiation Exposure



Name: 盧孟佑

Title: Assistant Professor

Institute: National Taiwan University, College of Medicine

Application of I-123 MIBG in Oncology

MIBG 之化學結構與交感神經傳導物質相似，能與腎上腺素受體結合，且具有高度特異性，因此加上放射線碘 (I-123/131) 可作為顯像劑，使富含腎上腺素受體的組織和器官，如腦神經、心肌造影和腎上腺髓質。在癌症方面的應用主要是某些神經內分泌腫瘤 (Neuroendocrine tumor, NET)：如神經母細胞瘤 (neuroblastoma)、嗜鉻細胞瘤 (pheochromocytoma, paraganglionma) 的偵測與治療。在兒童的神經母細胞瘤的應用上，因為分期、骨髓和遠端轉移的偵測判定，I-123/131 MIBG 檢查更是列為必要的檢查項目。

神經母細胞瘤為孩童第四種常見癌症，全台灣每年約新增 20-30 名病患 (百萬分之 4-8 的發病率)，其中 50% 在二歲以前發病，75% 在五歲以前發病。不幸的是，神經母細胞瘤是兒童癌症中最難纏的一種，治療效果一向很差，而且這些病患中 70% 在診斷時即為疾病高危險群 (第三、四期)，預後十分不好。常用的治療方式有三種：手術、放射線治療及化學治療，甚至加上自體造血幹細胞移植。I-123/131 MIBG 檢查在診斷時用來確定分期，遠端轉移 (尤其是骨髓轉移) 判定，更進一步有半定量評分可以用作預後指標和評估治療反應的指標。

I-123 MIBG 與 I-131 MIBG 比較，I-123 MIBG 能夠比 I-131 MIBG 提供較佳的影像，更高的敏感度，並減低輻射曝露，能與 CT 同時進行 SPECT 檢查改善其定位，但在國內因生產與 I-123 短半期的緣故，一直無法使用。只能進口較差的 I-131 MIBG 來使用，而且因進口等待期長，往往無法及時在初診斷時進行。2008-2012 年台大醫院與核能所合作，進行 I123-MIBG 於神經母細胞瘤之診斷與追蹤。現在 I-123 MIBG 已經通過 TFDA 查驗登記，國內可常規進行 I-123 MIBG 檢查，對於神經母細胞瘤孩童將是一大進步。



Name: 汪 姍 瑩
Title: 核醫科主任
Institute: 台灣大學醫學院醫學系

Application of I-123 MIBG in Cardiology

Heart failure is a progressive condition with high morbidity and mortality. With each acute event, myocardial injury may contribute to progressive LV dysfunction. Increasing frequency of acute events with disease progression leads to high rates of hospitalization and increased risk of mortality. Imaging biomarker - guided therapy provides accurate diagnosis, better monitoring prognosis, and precise treatment-guidance. Quantitative parameters derived from I-123-MIBG imaging includes primary heart/mediastinum ratio on 4-hour delayed planar imaging, and secondary quantitative results from both planar and SPECT. Intermediate MIBG defects associated with higher arrhythmic risks.



Name: 邱百諠
Title: 神經內科主任
Institute: 中山醫學大學醫學研究所博士

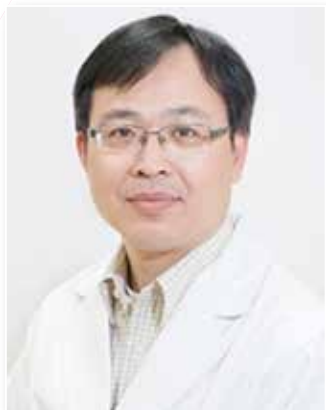
Application of I-123 MIBG in Neurology

The fourth consensus criteria for the diagnosis of dementia with Lewy bodies (DLB) has been published two years ago. The newest criteria provide some important changes of the clinical features and indicative biomarkers for the clinical diagnosis of DLB. Compared with the previous consensus criteria, fluctuation of cognition, recurrent visual hallucinations, spontaneous parkinsonism, and decreased dopamine receptor uptake are not changed of their status. Nuclear medicine biomarkers such as [123I]meta-iodobenzylguanidine (MIBG) myocardial scintigraphy, dopamine transporter imaging, and imaging to detect the metabolism or perfusion of occipital lobes are important for the clinical diagnosis of DLB.

In recent years, [123I]meta-iodobenzylguanidine (MIBG) myocardial scintigraphy has been used for visual assessment of the sympathetic nerve terminals, based on the fact that MIBG, a noradrenaline storage analogue, shares the same metabolic pathways as noradrenaline. The uptake and storage in presynaptic vesicles of MIBG is probably identical to norepinephrine. MIBG is released into the synaptic cleft but is not metabolized. The decreased cardiac uptake of MIBG in LBD reflects the postganglionic cardiac sympathetic denervation.

MIBG cardiac scintigraphy has been also proposed as a method to differentiate between DLB and dementia due to Alzheimer's disease. There are several studies that support the evidence of MIBG imaging for the clinical differential diagnosis of DLB from other neurodegenerative disorders. Therefore, followed the dopamine transporter imaging, it becomes one of the indicative biomarkers for the diagnosis of DLB in the fourth consensus criteria.

However, there is still no molecular imaging that targeting alpha synuclein which is regarded as the primary pathological abnormality of DLB. Effectiveness of the current medication for AD, such as acetylcholinesterase inhibitors or memantine, on DLB is still controversial. Fortunately, there are few countries agreed with the clinical use of donepezil in patients with DLB and we hope there will be more clinical researches to develop new technics for the diagnosis and new drugs for the treatment of DLB.



Name: 洪光威
Title: 醫療副院長
Institute: 高雄醫學大學

Imaging Protocol & Analysis of I-123 MIBG

Myocardial sympathetic imaging with I-123 metaiodobenzylguanidine (I-123 MIBG) has been found very useful for diagnosis of Lewy body disease (LBD, including dementia with Lewy bodies and Parkinson's disease) and for risk stratification of heart failure (HF). However, I-123 MIBG is still not widely used in the daily routine in Taiwan due to non-availability of locally produced radiotracer and the difficulty of importing the radiotracer from other countries. Recently, I-123 MIBG produced by the institute of nuclear energy research (INER) was just approved by Taiwan Food and Drug Administration for clinical usage and marketing. Before introducing this new useful imaging to neurologists and cardiologists, it is very important to prepare standard imaging protocol & analysis method for producing high-quality images and reliable interpretations.

For diagnosis of LBD and HF, quantitative analysis with measuring heart-to-mediastinum (H/M ratio) of I-123 MIBG myocardial imaging has been a most commonly used marker. The Japanese society of nuclear medicine working group had constructed normal database and suggested a lower limit of referenced normal value by MEGP collimator is 2.2. In addition, there was no age or sex difference of H/M ratio on early or delayed imaging. In addition, the suggested protocol was as follows, injection dose: 111 MBq, early imaging at 20 mins & delayed imaging at 3-4 hrs after injections, energy window: 159 keV \pm 10% (planar) & 159 keV \pm 7.5% (SPECT), acquisition time: 2-10 min (planar) & 30 s/view/step&shoot/6 degree (SPECT). In addition, MEGP collimator is preferred. If MEGP is not available, LMEGP, LEHR or LEGP may also be used but standardization to MEGP is necessary. The conversion coefficients were 0.55, 0.59 and 0.82 for LEHR, LEGP and LMEGP, respectively.

In conclusion, standardization of imaging protocol & analysis is critical for I-123 MIBG myocardial imaging. H/M ratio standardized to MEGP should be used as a quantitative marker of diagnosing LBD or HF.



Name: 陳翰逸

Title: 業務專員

Institute: 台北科技大學科系 / 化學工程與生物科技系

Radox 外部能力試驗結果解說

能力試驗 (Proficiency testing, 簡稱 PT) 是實驗室品質改善過程的一個工具，亦是對於實驗室與同儕間準確度比較。對於實驗室顧客、認證機構和主管機關而言，PT 提供了實驗室展現能力的客觀證據。

本公司所代理之能力試驗是有獨特資訊來源，其數據運算也有別於其他能力試驗，因此本公司特別藉此機會，對放射免疫分析實驗室使用本產品之客戶詳細介紹本產品之優勢及如何判讀，以利各實驗室若有問題能知道如何改善，以提升實驗室之品質。



Name: 王安美
Title: 馬偕紀念醫院核醫科技術主任
Institute: 大同大學生物工程碩士

放射免疫分析實驗室之風險管理分享

所謂風險 (Risk) 乃是「某種傷害 (Harm) 發生的不確定性」。ISO 15189:2012 新版規範中其第 4.14.6 節「風險管理」載明「實驗室應針對影響病人安全的工作流程與檢驗結果之潛在失效的衝擊進行評估，並應調整流程以減少或消除已鑑別的風險，並將決定及採行措施予以文件化」，故將風險管理 (Risk Management) 納入評估與稽核、管理審查活動等。美國聯邦醫療保險及低收入戶居民健保服務中心 (Centers for Medicare and Medicaid Services, CMS) 所發佈著重風險管理的品管計畫 IQCP (Individual quality control plan) 將於 2016 年 1 月 1 日起生效。

醫學實驗室目前實施的日常品管 (Daily Control) 或能力試驗 (Proficiency test) 作業並不同「病人安全」。因為分析前階段 (Preanalytical phase) 與分析後階段 (Postanalytical phase) 的錯誤率 (errors rate) 遠超過分析階段 (Analytical phase)。從病人準備到報告解讀的過程中存在著已知或未知的危險 (Hazard) 與潛在失效 (Fail)，直接或間接的對病人造成不同程度的傷害 (Harm)。醫學實驗室聯合相關人員與專家建立風險評鑑 (Risk assessment)、風險處理 (Risk treatment)、風險監控 (Risk monitor) 的風險管理程序 (Risk management process)，避免 (avoid) 或緩解 (mitigate) 不可接受的風險 (unacceptable Risk) 已是必然趨勢。

風險管理是預防措施 (Preventive action) 與矯正措施 (Corrective action) 執行的一部分，風險管理流程的建立可降低錯誤的發生率使「病人安全」更有保障。

OB001

Study on the Effectiveness of Radiation Health Education for Bone Scan Patients' Learning

骨骼掃描受檢者學習輻射知識之成效評估

Chun-Mei Chang^{1,2}, Han-Zong Chen¹, Chang-Ching Yu¹, Hung-Pin Chan¹

¹Department of Nuclear Medicine, Kaohsiung Veterans General Hospital, Kaohsiung, Taiwan

²Graduate Institute of Adult Education, National Kaohsiung Normal University, Kaohsiung, Taiwan

Background: People believes that radiation could cause cancer and is anxious about receiving radiation-related tests. This study aimed to evaluate the teaching effect of using multimedia educational videos in patients undergoing whole body bone scan.

Methods: From November to December 2018, we conducted a prospective randomized control trial at Kaohsiung Veterans General Hospital, a medical center of 1300 beds in Taiwan. During this period, 560 individuals was scheduled whole body bone scan examination. After excluding 500 individuals who were either unconscious or did not consent to participate, 60 patients who fulfilled the recruitment criteria and provided consent were enrolled. They were randomly assigned to the experimental and control groups. Each group comprised 30 individuals. The control group received regular educational brochure instructions. The experimental group received a 12-minute educational compact disc about radiation. Patients' knowledge on radiation and a health behavioral scale were compared by pre- and post evaluation test tools.

Results: The experimental group comprised 13 male and 17 female patients, with average age of 50.83 ± 13.06 years. The control group included 14 male and 16 female participants, with average age of 51.17 ± 12.51 years. There was no statistic difference in educational level between these two groups. The pre-test scores regarding the awareness of radiation of the two groups did not reveal significant difference. However, the experimental group (pre-test score: 6.30 ± 1.26 , post-test score: 7.90 ± 1.32 , improvement: 1.60 ± 1.54) displayed significant greater increase in post-test knowledge scores compared with the control group (pre-test score: 6.77 ± 1.61 , post-test score: 7.50 ± 1.48 , improvement: 0.73 ± 1.64 , $P < 0.05$). Although there appeared higher post-test behavior scale in the experimental group (pre-test scale: 3.93 ± 0.80 , post-test scale: 4.59 ± 0.54 , increase: 0.66 ± 0.81) than the control group (pre-test scale: 3.78 ± 0.58 , post-test scale: 4.28 ± 0.62 , increase: 0.50 ± 0.65 marks), there was no significant difference ($P > 0.05$).

Discussion and Conclusion: The results of this study display that multimedia educational videos is effective in enhancing the understanding of radiation for patients undergoing whole body bone scan examination. However, further research is necessary to explore why there was no significant behavioral change. Take-home Message: Educational videos is more efficient than brochure in teaching the knowledge of radiation.

OB002

The Survey and Establishment of Diagnostic Reference Levels for CT-based Attenuation Correction in Whole Body PET/CT Examination

Bang-Hung Yang, Wen-Sheng Huang

Department of Nuclear Medicine, Taipei Veterans General Hospital, Taiwan, R.O.C

Abstract

Introduction: Diagnostic reference level (DRL) is one of methods to monitor and reduce medical exposure to patients. However, the radiation dose of CT-base attenuation correction in PET/CT scan is usually neglected. According to references, the maximum effective dose of whole body PET/CT scan is approximately 15-26 mSv. The purpose of this study is survey and establishment of diagnostic reference levels for CT-based attenuation correction in whole body PET/CT examination.

Methods: The rando phantom inserted 131 TLDs was used to acquire images with routine whole body PET/CT protocols. Effective dose was calculated by TLD and CT-EXPO software. Questionnaires were sent to 69 departments of PET/CT centers in Taiwan. Information of 68 patients (61.8%) was recruited in our study and calculated $CTDI_{vol}$, DLP and ED by CT-EXPO software.

Results: The results showed that mean, median and 75th percentile of $CTDI_{vol}$ was 5.15 mGy, 4.5 mGy and 7 mGy, respectively, and mean, median and 75th percentile of DLP was 533.9 mGy•cm, 439 mGy•cm, 693.75 mGy•cm, respectively. 75th percentile of $CTDI_{vol}$ in U.S. and France was 9.8 mGy and 7.7 mGy, respectively. In our previous study, we determined that k factor for whole body CT scan was 0.016. Mean, median and 75th percentile of effective dose of 68 patients was 8.54 mSv, 7.02 mSv, 11.1 mSv, respectively.

Conclusions: The effective dose from PET radiopharmaceuticals injection was 6.6-7.2 mSv, meaning effective dose of a whole body PET/CT scan is 15-20 mSv in Taiwan.

OB003

整合式 PET/MR 衰減校正影像資訊準確度

楊邦宏¹ 謹立成² 陳志成²

¹ 臺北榮民總醫院核醫部

² 國立陽明大學生物醫學影像暨放射科學系

背景介紹：整合式 PET/MR 因缺乏如 CT 之能量線性衰減資訊，必須以磁共振造影影像資訊做光子衰減修正 (magnetic resonance attenuation correction, MRAC)，目前藉由 MRI 本身之狄克森法脈衝程序 (Dixon pulse sequence) 產生之影像進行衰減修正。然而 MRI 資訊反映的是物體的磁性特徵而並非如 CT 反映的是電子密度與組織之衰減係數，故 MR 數值與衰減係數沒有直接關係，使用 MRAC 產生之衰減修正圖譜為估計之結果，故本研究目的在找尋 PET/CT 及 PET/MR 在定量數值之關係性，以及如何將兩者進行正規化與轉換。

方法：本研究使用物理假體，並以臺北榮民總醫院核醫部之 PET/CT 以及 PET/MR 個別掃描後，分別依機器本身之 CTAC 與 MRAC 進行衰減修正後進行比較，圈選 ROI (region of interest) 計算其標準攝取值 (standard uptake value) SUV 及放射濃度 (Bq/ml) 計算其不同衰減修正之方法對 SUV 及放射濃度 (Bq/ml) 定量之差異，並設法找尋其關係性。

結果：結果發現 PET/CT 及 PET/MR 之 SUV 及放射濃度具有高度相關且可透過線性公式進行轉換，其中在腹部使用 $SUVPETCT = 1.3103 \times SUVPETMR + 0.0541$ ，在肺部使用 $SUVPETCT = 1.762 \times SUVPETMR + 0.0929$ ，以及在頭部使用 $SUVPETCT = 1.5688 \times SUVPETMR + 0.2821$ 。

結論：本方法可應用於臨床提高臨床診斷和治療規劃的準確性，提供跨 PET/MR 與 PET/CT 平台之比較依據。

OB004

Imaging Dynamic Activity of Inducible Nitric Oxide Synthase (iNOS) in Neuroinflammation with [¹⁸F]FBAT PET

Chin-Wei Chang¹, Wen-Sheng Huang^{1,2a}, Chuang-Shin Chiu², Haibin Tian³,
Tsung-Hsun Yu⁴, Pao-Yeh Wang⁴, Yu-Yeh Kuo¹, Skye Hsin-Hsien Yeh⁴

¹Department of Nuclear Medicine, Taipei Veterans General Hospital, Taipei, Taiwan

²Department of Nuclear Medicine, Tri-Service General Hospital, Taipei, Taiwan

³Departments of Biomedical Engineering and Radiology, Case Western Reserve University, Cleveland, Ohio, USA

⁴Brain Research Center, National Yang-Ming University, Taipei, Taiwan.

^aEqual Contribution

Introduction: Microglia, as cellular mediators of neuroinflammation, are implicated in the pathogenesis of a wide range of neurodegenerative diseases. Positron emission tomography (PET) imaging of microglia has matured over the last 20 years, through the development of radiopharmaceuticals targeting several molecular biomarkers of microglial activation and, among these, mainly the inducible nitric oxide synthase (iNOS). The roles of inducible nitric oxide synthase (iNOS) as a family of nitric oxide synthases in the pathogenesis of neuroinflammation has been largely investigated for microglia function in inflammatory process, suggesting iNOS as an important biomarker to assess risk factors for neuroinflammation.

In this research proposal, we carefully lay out the strategic plan to develop iNOS targeted molecular PET imaging with [¹⁸F]FBAT tracer for detecting iNOS expression in lipopolysaccharide (LPS) induced inflammatory brain using the mouse models and evaluate the potential of [¹⁸F] FBAT as a prognostic utility in the progression of neuroinflammation mediated brain disease.

Methods: 3 groups of male C57BL/6 mice (age 8 weeks) were used for the dynamic micro PET/CT (SEDECAL, Madrid, Spain) or PET/MRI (Bruker, Germany) study: group 1 or 2 was intraperitoneally injection injected with 5 mg/kg LPS in 0.1 mL saline (Sigma-Aldrich, Saint Louis, MO, USA) 3 h or 24 h prior to [¹⁸F]FBAT (11.1 MBq; 0.3 mCi) injection (n = 6 per group); group 3 received 0.9% NaCl by ip as control (n = 6). Data were analyzed with PMOD 3.7 software (PMOD Technologies Ltd., Zurich, Switzerland). Immunohistochemistry study was performed after PET imaging.

Results: We found that LPS challenge elicited a stronger iNOS induction. At 30 minutes after injection of radiotracer, in the LPS-3 hours group, the whole brain, cortex, midbrain, hypothalamus, brain stem had a longer retention time of [¹⁸F]FBAT-derived radioactivity when compared to other regions. Averagely, the accumulation of [¹⁸F]FBAT in LPS-3 hrs. group had 1.64 and 1.28 folds higher than that of controls and LPS-24 hrs, respectively. There was similar accumulations of [¹⁸F]FBAT-derived radioactivity in the control and LPS-24 hours groups.

Integrated activity (AUC; SUV·min 0-30 mins.) showed more retention of [¹⁸F]FBAT in the LPS 3 hrs. group in comparison to control or LPS 24 hrs. Mice. The *K_i* value of [¹⁸F]FBAT of the LPS 3 hrs. group was dramatic increase when compared to the LPS 24 hrs. or controls group whereas there was also significantly difference between the LPS 24 hrs. and controls group.

iNOS immunoreactivity in the cortex, CA2, CA3 and dentate gyrus showed a significantly higher immunoreactivity at 3 hrs. after administration of LPS whereas iNOS expression in CA1 was similar in all 3 study conditions. After 24 hrs, there was similar immunoreactivity in the control or LPS 24 hrs. groups; however, an increase in NOS activity was observed in the cerebellum but no statistically significant difference. Apoptosis-inducing factor (AIF) immunoreactivity showed similar pattern with iNOS.

Conclusions: The evaluation of [^{18}F]FBAT which carried out by *in vivo* PET imaging as well as immunochemistry staining showed a novel [^{18}F]FBAT could be Our approach is feasible to visualize and quantify the iNOS expression by [^{18}F]FBAT.

OB005

Nuclear Image Targeting to GZMB for Monitoring Exhaustion of CD8⁺ T Cells with Loss of Anti-tumor Activity in Cigarette Smokers and Tumor Patients

Chun-Chia Cheng¹, Ya-Wen Chiang^{2,3}, Cheng-Liang Peng⁴, Jungshan Chang⁶,
Bi-Ling Yang⁷, Ken-Hong Lim^{2,3,5}, Ai-Sheng Ho^{7*}, Yi-Fang Chang^{2,3,5}

¹Radiation Biology Research Center, Institute for Radiological Research,
Chang Gung University / Chang Gung Memorial Hospital at Linkou, Taiwan;

²Division of Hematology and Oncology, Department of Internal Medicine, Mackay Memorial Hospital, Taipei, Taiwan

³Laboratory of Good Clinical Research Center, Department of Medical Research, Mackay Memorial Hospital,
Tamsui District, New Taipei City, Taiwan

⁴Institute of Nuclear Energy Research, Atomic Energy Council, Taoyuan

⁵Department of Medicine, Mackay Medical College, New Taipei City, Taiwan

⁶Graduate Institute of Medical Sciences, School of Medicine, College of Medicine,
Taipei Medical University, Taipei, Taiwan

⁷Division of Gastroenterology, Cheng Hsin General Hospital, Taipei, Taiwan

Introduction: Since the status of CD8⁺ T cells in patients with cancers play an important role for obtaining the immunotherapeutic success, and smoking has been demonstrated to affect the immunological activity. This study aimed to investigate the molecular effect of smoking (nicotine) on exhaustion of CD8⁺ T cells in healthy volunteer and patient with cancers by targeted imaging to granzyme B (GZMB).

Methods: The anti-tumor capacity of CD8⁺ T cells were investigated against the lung cancer EGFR-positive tumors. RNAseq and qPCR were utilized to search for the driver genes maintaining the activity of CD8⁺ T cells. Then the humanized tumor xenografts were used for validating the peripheral blood mononuclear cells (PBMCs)-mediated anti-tumor effect through targeting GZMB by nuclear imaging platform.

Results: We found that CD8⁺ T cells lost anti-HCC827 cells *in vitro* in the healthy cigarette smokers. The RNAseq and qPCR data revealed that *IL2RB* and *GZMB* decreased in CD8⁺ T cells from a smoker, whereas *IL2RB* involved in IL2-mediated signaling pathway to mediate *GZMB* expression. We validated that *IL2RB* and *GZMB* were diminished by nicotine treatment and in patients with cancers, resulting in decrease of PBMCs-mediated anti-HCC827 ability. GZMB-targeted nuclear imaging revealed a lower radioactive signal in nicotine-treated PBMCs from a healthy volunteer and in patients with cancers.

Conclusions: This study demonstrated that lung cancer HCC827 cells sensitized the cytotoxicity of CD8⁺ T cells, and the low expression of *IL2RB* and *GZMB* caused by nicotine led to loss of anti-HCC827 effect in CD8⁺ T cells. Moreover, we validated that granzyme B-targeted radioactive agent was able to measure the cytotoxic activity of CD8⁺ T cells in a humanized HCC827-derived tumor xenograft model, that may be applied for monitoring immunotherapeutic efficacy.

OB006

Survey of Impurities, Stability, Degradation Derivatives and Causes of M-iodobenzylguanidine Hemisulfate (MIBGHS), a Precursor for Neuroendocrine Tumors Radiopharmaceutical by HPLC-tandem Mass Spectrometry

Wei-Hsi Chen¹, Tsai-Yueh Luo², Yu Chang¹, Ching-Yun Lee¹,
Shiu-Wen Liu¹, Wen-Ching Wu²

¹Chemistry Division, Institute of Nuclear Energy Research, 1000, Wunhua Rd., Chiaan Village,
Longtan District, Taoyuan City, Taiwan

²Isotope Application Division, Institute of Nuclear Energy Research, 1000, Wunhua Rd., Chiaan Village,
Longtan District, Taoyuan City, Taiwan

Introduction: Meta-iodobenzylguanidine hemisulfate (MIGBHS) is the precursor to prepare of radio-iodine labeled MIBG radiopharmaceutical which is served as radio-imaging or therapy for patients with neuroendocrine tumors and myocardial. New Drug Application (NDA) for I-123-MIBG in Taiwan has being submitted to FDA, Taiwan by INER. It is necessary to define chemical characters of MIBG clearly to assure its quality, efficiency and safety. The aim of the report is to figure out stability, contaminants, degenerates and causes for MIBGHS.

Methods: Purity assay based on reversed phase (butyl-phenyl column) HPLC and identify impurities in MIBGHS by electrospray ionization tandem mass spectrometric analytical method.

Results: Process related impurities were determined in MIBGHS included m-bromo benzylguanidine (MBrBG), bis(3-iodobenzyl)-4H-triazole-3,5-iamine and 1,3-bis(3-iodobenzyl)guanidine. MBrBG came from starting material, m-iodobenzylamine (MIBA) which was polluted by m-bromobenzylamine. The later both arose from over reacted byproducts in MIBGHS synthesis procedure. The purity data (> 99%) of long-term stability and accelerated stability examination showed that MIBG is stable for at least 12 and 6 months respectively under normal store environment. Forced degradation demonstrated that MIBG would be decomposed by UV, alkaline and oxidation factors but inert against acidic and thermal effects.

Conclusions: The synthesized product quality of MIBGHS (purity > 99%) by INER is satisfied even stored over 12 months under normal condition. Trace impurities were excessive reaction byproducts. MIBGHS is stable under thermal and acidic conditions which employed in labeling radio-iodine process (1 h), although guanidine and iodide were the active chemical bond to form degenerates under UV exposed, alkaline and oxidative atmosphere.

OB007

口頭論文發表摘要·基礎組

Improved Purification of 2-(1-{6-[(2-2'-[¹⁸F] Fluoroethoxyethyl)(methyl)amino]-2-naphthyl}ethylidene) malononitrile ([¹⁸F]FEONM) as an Alzheimer's Disease Imaging Agent

Jenn-Tzong Chen^{1,+}, Shiou-Shiow Farn^{1,+}, Tsai-Yueh Luo²,
Wuu-Jyh Lin^{2*}, Chyng-Yann Shiue^{3,4}

¹Isotope Application Department, Institute of Nuclear Energy Research, Taoyuan, Taiwan

²Institute of Nuclear Energy Research, Taoyuan, Taiwan

³National Taiwan University Hospital, Taipei, Taiwan

⁴Tri-Service General Hospital, Taipei, Taiwan

⁺Equal Contribution

^{*}Corresponding Author

Introduction: [¹⁸F]FDDNP was the first PET tracer developed to target tau protein. However, its specificity and selectivity were found to be relative low in vivo. In order to increase its brain uptake as well as its specificity and selectivity, we have synthesized and evaluated its analog, [¹⁸F]FEONM as an Alzheimer's disease imaging agent. In the original synthesis, [¹⁸F]FEONM was purified by SPE method and had low chemical purity. We report herein an improved purification of [¹⁸F]FEONM and evaluate it as an Alzheimer's disease imaging agent

Methods: [¹⁸F]FEONM was synthesized as reported previously with some modifications on its purification. After radiofluorination, the crude product of [¹⁸F]FEONM was purified with a semi-preparative HPLC system (Column: Fortis[®] Part No. FPH 100905, 5 μm diphenyl, size: 250 X 10 mm; Mobile phase: 95% ethanol; Flow rate: 1.6 ml/min, pump: Eldex 2SMP). The final product was collected into a sterilized vial, adjusted with saline to keep its ethanol concentration < 10% and passed through a millipore filter for injection. The purity of [¹⁸F]FEONM was determined by analytical HPLC system (Column: Fortis PN: FPH-050905 5um, Size: 250 X 4.6 mm; Mobile phase: 95% Acetonitrile; Flow rate: 0.3 ml/min; Water 600 controller and pump. Waters 2489 UV detector).

Results: The purity of [¹⁸F]FEONM purified by HPLC method was much better than that of purified by the SPE method. In addition, it is better to use ethanol as mobile phase than using toxic organic solvent as mobile phase for HPLC purifications.

Conclusions: The purity of [¹⁸F]FEONM purified by HPLC method was much better than that of purified by the SPE method. The [¹⁸F]FEONM purified by HPLC method is under evaluation as an Alzheimer's disease imaging agent.

OB008

The Preparation and Biological Characterization of Novel CXCR4 Antagonist for Tumor Mice Imaging

Chien-Chung Hsia, Chung-Hsin Yeh, Cheng-Liang Peng, Chun-Tang Chen

Institute of Nuclear Energy Research, Tau-Yen, Taiwan

Introduction: CXCR4 and CXCL12 play a pivotal role in tumor development and metastasis. This has been demonstrated for a variety of cancer entities, including breast, prostate and colorectal cancer...etc. The level of CXCR4 expression is predictive for the metastatic potential of a given tumor type and mediates organ-specific metastasis. CXCR4-antagonist AMD3100, the first FDA approved for the therapy of lymphoma and myeloma and had been labeled with Cu-64, Ga-67...etc. for tumor imaging. However, poor in vivo stability and poor T/NT ratio limited its further imaging application. This research designed novel AMD3100-derivative small molecular and proved it's effective.

Methods: Novel CXCR4 receptor antagonist ABE-01 was used by artificial intelligence (A.I.). The structure-based design and molecular docking to CXCR4 was analyzed by BIOVIA Discovery Studio. In-111 isotope was labeled with buffer under room temperature reaction. Radiochemical purity of ^{111}In -ABE-01 was analyzed by radio-TLC. Balb/c nude mice were inoculated with CXCR4 over-expression MDA-MB-231 breast cancer for evaluating tracer's biological characterization. ^{111}In -AMD3100 and cold AMD3465 were also been done as the control group and CXCR4-binding competitor, respectively.

Results: The radio-chemical purity of ^{111}In -ABE-01 was over 95%. The T/NT ratio of ^{111}In -ABE-01 and ^{111}In -AMD3100 were 6.98 ± 0.12 ($n = 3$) and 1.78 ± 0.26 ($n = 2$) after the tail vein injection for 4 hours in NanoSPECT images, respectively. Overdose of AMD3465 (AMD3100-derivative) suppressed tumor's uptake of ^{111}In -ABE-01, obviously.

Conclusions: By the assistant of A.I. technology, novel CXCR4 antagonist structures were been designed by considering the molecular docking and pharmacophore binding. The tumor model of SPECT image proved its effective and improving the CXCR4 targeting effect than AMD3100. CXCR4-directed theranostics in oncology and inflammation were been evaluated and executed, actively.

OB009

Initial Testing of Conjugation and Radiolabeling of Anti-PD-L1 mAb with Zirconium-89 for PET Imaging Study

Shiou-Shiow Farn^{1,+}, Jenn-Tzong Chen^{1,+}, Ting-Shien Duh^{1,+},
Fang-Yu Ou Yang¹, Chih-Hsien Chang^{1*}

¹Isotope Application Department, Institute of Nuclear Energy Research, Taoyuan, 32546, Taiwan

⁺Equal contribution

^{*}Corresponding Author

Introduction: In recent years, Zirconium-89 (⁸⁹Zr) has become the most commonly studied positron emitting radionuclide for immuno-PET imaging because the physical half-life (78.41 h) is a good characteristic with the biological half-life of mAbs, so increasing the utility of PET in the development of compounds. The aim of the study, we report the initial testing of cyclotron irradiation, chemical separation of [⁸⁹Zr]Zr-oxalate solution, conjugation and radiolabeling of anti-PD-L1 mAb with [⁸⁹Zr]Zr-oxalate solution in INER.

Methods: ⁸⁹Zr was produced via the ⁸⁹Y(p,n)⁸⁹Zr transmutation reaction on a TR15/30 cyclotron at 14~15 MeV beam energy and 15-30 uA beam current with irradiation time of 1-16 hours. The [⁸⁹Zr]Zr-oxalate solution was isolated by hydroxamate resin and theoretical calculated specific activity of that was 22~106 MBq/mg (0.38~2.887 mCi/mg). The anti-PD-L1 mAb was conjugated to the p-Isothiocyanatobenzyl-desferrioxamine (Df-Bz-NCS) and radiolabelled with [⁸⁹Zr]Zr-oxalate solution based on a published procedure described by Maria J W D Vosjan1 et al. Calculation of radiolabelling efficiency of anti-PD-L1 mAb was achieved by using ITLC analysis.

Results: Production of ⁸⁹Zr with 1 mm thick yttrium-89 plate (purity: ≥ 99%) at incident proton beam energy of 14.5 MeV, 30 beam current and irradiation time of 5.88 hours results in a yield of 46 MBq/uAh after EOB. ⁸⁹Zr was achieved in high radionuclidic purity (≥ 98%) with 30-70% recovery of the radioactivity.

The conjugation and purification chemistry was found to proceed in a moderate yield (50~57%). Radiolabeling of anti-PD-L1 mAb with [⁸⁹Zr]Zr-oxalate was achieved at room temperature, in slightly alkaline solutions (pH 6.8~7.2), with crude radiochemical purity (91.45%). Till now, facile purification of anti-PD-L1 mAb with ⁸⁹Zr-oxalate from small-molecule radiolabeled impurities has been achieving by using either size-exclusion chromatography or spin-column centrifugation.

Conclusion: The initial testing described will startup the use of ⁸⁹Zr in basic science research of immuno-PET in Taiwan. Further studies to optimize cyclotron irradiation, chemical separation of [⁸⁹Zr]Zr-oxalate solution, conjugation and the radiolabelling conditions based on ⁸⁹Zr-oxalate are currently underway.

OC001

Predicting Pathological Complete Response in Rectal Cancer After Chemoradiotherapy Through a Random Forest Using Radiomics from FDG-PET/CT

Yung-Chi Lai¹, Wei-Chih Shen², Shang-Wen Chen^{3,4,5}, Kuo-Chen Wu⁶, Peng-Yi Lee³, Chun-Lung Feng⁷, Te-Chun Hsieh^{1,8}, Kuo-Yang Yen^{1,8}, Chia-Hung Kao^{1,9,10}

¹Department of Nuclear Medicine and PET Center, China Medical University Hospital, Taichung, Taiwan

²Department of Computer Science and Information Engineering, Asia University, Taichung, Taiwan

³Department of Radiation Oncology, China Medical University Hospital, Taichung, Taiwan

⁴School of Medicine, College of Medicine, China Medical University, Taichung, Taiwan

⁵School of Medicine, College of Medicine, Taipei Medical University, Taipei, Taiwan

⁶Department of Computer Science and Engineering, National Chung Hsing University, Taichung, Taiwan

⁷Division of Hepato-Gastroenterology, Department of Internal Medicine, China Medical University Hospital, Taichung, Taiwan

⁸Department of Biomedical Imaging and Radiological Science, China Medical University, Taichung, Taiwan

⁹Graduate Institute of Biomedical Sciences, School of Medicine, College of Medicine, China Medical University, Taichung, Taiwan

¹⁰Department of Bioinformatics and Medical Engineering, Asia University, Taichung, Taiwan

Background: Neoadjuvant chemoradiotherapy (NCRT) followed by surgery is the standard treatment for patients with locally advanced rectal cancer. This study constructed a random forest to predict a pathological complete response (pCR) based on radiomics derived from baseline ¹⁸F-fluorodeoxyglucose (¹⁸F[FDG]) positron emission tomography (PET)–computed tomography (CT).

Methods: This study analyzed 169 patients with newly diagnosed rectal cancer. All completed the allocated ¹⁸F[FDG]-PET/CT, NCRT, and surgery. A total of 68 radiomic features were extracted from the metabolic tumor volume. The numbers of splits in a decision tree and trees in a random forest were determined based on their effects on predictive performance. Receiver operating characteristic curve analysis was performed to evaluate predictive performance and ascertain the optimal threshold for maximizing the prediction accuracy.

Results: After NCRT, 22 patients (13%) achieved pCRs. Forty-two features were capable of differentiating the tumors with pCR and were used to construct the random forest. The suitable numbers of the decision trees and splits were six and seven, respectively. Accordingly, the classification results disclosed the sensitivity, specificity, positive predictive value, negative predictive value, and accuracy for prediction were 81.8%, 97.2%, 81.8%, 97.2%, and 95.3%, respectively.

Conclusion: Through a random forest, radiomics derived from baseline ¹⁸F[FDG]-PET/CT can provide accurate predictions of pCRs in patients with rectal cancer. High accuracy and predictive values can be achieved but should be externally validated.

OC002

口頭論文發表摘要·臨床組

PET Scan in RAI Treatment Patient with TENIS Syndrome

Shanfan YAO, Wen-Sheng Huang

Nuclear Medicine department, Taipei Veterans General Hospital

Introduction: Differentiated thyroid cancer with elevated thyroglobulin but negative Iodine scintigraphy. Under the flip-flap phenomenon, lesion tend to be showed from FDG-PET.

Methods: 19 FDG-PET/CT was performed in 241 patients between Oct. 2018 to Sep. 2019. 54 patients was referred with no post therapy scintigraphy and was excluded.

Scintigraphy from post radioiodine therapy was review by nuclear physician and patient with negative result was underwent FDG-PET/.CT scan within 14 days.

Results: 19 patients, 6 males and 13 females. Mean days from Iodine scintigraphy to FDG-PETG scan is 5.05 ± 3.73 days (range 1 – 15 days). Mean-Thyroglobulin level $60.8 \text{ ng/ml} \pm 79.5$ (range 0-269). PET avid disease was identified in 13/17 scans (sensitivity 76%).

Conclusions: Dynamic SPECT/CT demonstrates the feasibility in absolute FDG-PET/CT scan is helpful in TENIS syndrome, especially in patients just received radioactive Iodine therapy.

OC003

碘 -131 在甲狀腺癌患者 消融治療時的體內動力學研究

黃兆駿^{1,2} 賴佳玟¹ 陳雅鳳¹ 李柏葦¹ 汪姍瑩¹ 吳彥雯¹ 潘榕光²

¹ 亞東紀念醫院核子醫學科

² 中臺科技大學醫學影像暨放射科學系

背景介紹：體內動力學模型是一用來描述人體攝入特定放射性物質後，放射性物質在人體內的分佈路徑、強度、循環以及排泄的情形。國際放射防護委員會 (International Commission on Radiological Protection, ICRP) 在 30 號報告中提出了碘的體內動力學模型。然而，模型的數據來源是標準健康受試者，對於臨床上甲狀腺全切除術的甲狀腺癌患者是否適用仍有待評估。本研究針對九位甲狀腺已切除並即將接受碘 -131 消融治療之患者進行體內動力學研究。

方法：受試者口服碘 -131 劑量皆為 1110 MBq (30 mCi)，分別於服藥後 1、4、24、48、72 及 168 小時接受全身掃描。造影儀器使用 GE Healthcare Infinia Hawkeye 4 SPECT/CT，搭配 High energy general purpose collimator (HEGP) 準直儀。參數設定掃描速度 (Scan speed) 10 cm/min，峰值能窗 (width of the energy window) 10%。數據分析以 ICRP 所提出的碘的體內動力學模型數據為基礎建立一聯立方程式，以逆運算法在 MATLAB 中以自行開發的程式求出與受試者全身掃描數據最佳擬合結果。

結果：九位受試者的胃、體液、甲狀腺和全身的平均碘生物半衰期分別為 0.54 ± 0.32 、 12.6 ± 1.8 、 42.8 ± 5.1 及 12.6 ± 1.8 小時；平均路徑強度體液至甲狀腺 (I_{23})、體液至排泄 (I_{25}) 分別為 0.21 ± 0.14 及 0.79 ± 0.14 。

結論：研究結果與 ICRP 模型所描述的胃、體液、甲狀腺和全身的平均碘生物半衰期 0.696、6、1920 及 12 小時，路徑強度 I_{23} 、 I_{25} 為 0.3、0.7 相較之下，碘 -131 在甲狀腺癌患者消融治療時其胃、體液、甲狀腺及全身的平均碘生物半衰期、平均路徑強度皆有顯著變化。

OC004

口頭論文發表摘要·臨床組

The Prognostic Benefit of Recombinant Human Thyroid-Stimulating Hormone in the Treatment of Distant Metastasis in Patients with Papillary Thyroid Cancer

His-Chen Tsai¹, Kung-Chu Ho¹, Kun-ju Lin¹, Ju-Chin Cheng², Miaw-Jene Liou³

¹Department of Nuclear Medicine, Linkou Chang Gung Memorial Hospital, Taoyuan, Taiwan

²Department of Nuclear Medicine, Keelung Chang Gung Memorial Hospital, Keelung, Taiwan

³Department of Metabolism and Endocrinology, Linkou Chang Gung Memorial Hospital, Taoyuan, Taiwan

Background: The thyroid cancer mortality rate has been reported to increase annually. The annual increase in mortality rate was restricted to patients with papillary thyroid cancer (PTC), but was statistically significant only for PTC patients with distant metastasis. In this study, we sought to evaluate the survival outcomes of PTC patients with distant metastasis between two groups of preparation modes (recombinant human TSH (rhTSH) vs. thyroid hormone withdrawal (THW)) prior to high-dose radioiodine (RAI) therapy.

Material and Methods: We retrospectively reviewed the clinical records of patients receiving high dose RAI between 2007 to 2019. Patients with histologically proven PTC with distant metastases and prepared by either rhTSH or THW mode were included. Since only four eligible patients were dead in follow-up period, progression free survival (PFS) was used for outcome evaluation.

Results: Of these 88 eligible patients, 52 (59%) were prepared with THW and 36 (41%) with rhTSH. In THW group, 29 patients showed disease progression; in rhTSH group, 13 patients did. With multivariate analysis, we identified preparation (THW vs. rhTSH, p value = 0.048, 95% CI = 0.251–0.994, HR = 0.500) and age (< 45 vs. ≥ 45, p value = 0.085, 95% CI = 0.300–1.080, HR = 0.057) as independent prognostic factors for PFS. Then, a prognostic scoring system was devised by summing up the factors of preparation and age, the two most significant independent predictors identified in multivariate analysis, from 0 to 2. The PFS outcomes of patients with score of 0 (rhTSH & age < 45), 1 (rhTSH & age ≥ 45 or THW & age < 45), and 2 (THW & age ≥ 45) were 54.7% (p value = 0.048), 42.0% (p value = 0.098, 95% CI = (0.846–7.100), HR = 2.456), 21.9% (p value = 0.016, 95% CI = (1.292–12.127), HR = 3.958), respectively.

Conclusion: PTC patients with distant metastasis who prepared by rhTSH prior to high-dose RAI have better progression free survival outcomes, especially for younger age.

OC005

Gamma Camera 對於甲狀腺腫大 受檢者攝取率測量之應用

吳忠順¹ 胡瑋¹ 彭南靖^{1,2}

¹ 高雄榮民總醫院核醫科

² 陽明大學醫學院

背景介紹：使用甲狀腺攝取儀測量放射性碘攝取率因其無法顯示影像，可能因為偵測中心點不正確而產生測量誤差，而甲狀腺腫大之受檢者因為甲狀腺攝取儀的偵測範圍受限更可能造成不同程度之低估。使用 Gamma Camera 測量甲狀腺攝取率可避免以上兩者產生的誤差，還可以觀察甲狀腺大小、形狀及其外形。常規使用 Gamma Camera 替代攝取儀測量甲狀腺攝取率需針對各種測量條件、造影參數與影像處理方法進行探討與分析比對。

方法：Gamma Camera 使用 Siemens Symbia T 配置中能量準直儀；甲狀腺攝取儀為 BIODEX Atomlab 950。以假體實驗測量影響 Gamma Camera 計數 (counts) 之因素後，44 位臨床受測者同時使用以上兩種儀器測量甲狀腺攝取率，研究比對後發現當 Gamma Camera 使用相同偵測距離 10 公分、矩陣設定為 256 x 256、放大倍率 1 及 ROI 選取為 10 x 10 公分時 (10,000 mm²) 的方式最佳，兩者相關性為 0.992 ($p < 0.001$)、 β 值為 0.989 ($p < 0.001$)、差異性為 0.6 ($p = 0.078$)。但甲狀腺腫大之受檢者甲狀腺 ROI 選取若為 10,000 mm² 會發現甲狀腺因為未完全被圈入 ROI 內而導致測量值被低估。

結果：以本研究中之受檢者為例，受檢者之甲狀腺具活性部分經測量約為 12.3 x 13.4 公分，10,000 mm² 的 ROI 明顯未能完全涵蓋。為使其給予劑量測量值與其他人為相同基準，故碘 -131 膠囊 ROI 選取統一為 10,000 mm²，而甲狀腺 ROI 選取為 10,000 mm² 時，測量之攝取率為 32.9% (以此假設若使用甲狀腺攝取儀時將得到此近似值)，若將甲狀腺完全圈入時 ROI 選取約為 22,764 mm²，此時測量之攝取率為 49.8%。

結論：甲狀腺腫大受檢者之攝取率若使用甲狀腺攝取儀會造成不同程度之低估，此時使用 Gamma Camera 定位與測量，並視甲狀腺實際大小調整 ROI，可以獲得正確的數值，但常規使用 Gamma Camera 測量甲狀腺攝取率之前，需針對各種測量條件、造影參數與影像處理方法與甲狀腺攝取儀進行統計分析。

OC006

Deep Learning for Predicting Lesion Via the Images of SPECT Myocardial Perfusion

Tien-Hsin Chang^{1,2}, Da-Chuan Cheng², Cing-Yuan Chen¹

¹*Department of Nuclear Medicine, Taichung Tzu Chi Hospital, Buddhist Tzu Chi Medical Foundation*

²*Department of Biomedical Imaging and Radiological Science, China Medical University, Taichung, Taiwan*

Introduction: Recent years, research about artificial intelligence (AI) is a universality to improving human health. SPECT myocardial perfusion image (MPI) is widely used for the diagnosis of coronary artery disease (CAD) and there are more than 150000 scans performed annually in Taiwan.

The purpose of this study is improving the correctness of diagnosis via MPI.

Methods: A total of patients 243 (79% men) were studied, patients underwent stress and rest Tl-201 MPI scan, all patients underwent cardiac catheterization within half year after MPI. The post-processing image of cardiac in nuclear medicine are analyzed via Xeleris 3.0 and it generated polar maps from 200 training datasets and 43 testing datasets. Deep learning and analysis using MATLAB suite software.

Results: The accuracy rate of prediction via AI is 77% for pre-patient and 78% for pre-vessel and the sensitivity is 81.25%, the specificity is 74%.

Conclusions: Deep learning has potential for development in the future, and the applications can provide some help in medical.

OC007

First-year Bone Scan of the Newly Diagnosed Patients with Breast Cancer and the Subtypes of those with Distant Metastasis

Che Lin^{1,3}, Kuang-Tao Yang^{2*}, Ding-Ru Chen¹

¹Breast Cancer Center, Department of Surgery, Changhua Christian Hospital, Changhua, Taiwan

²Department of Optometry, Chung Hwa University of Medical Technology, Tainan, Taiwan

³Department of Nuclear Medicine, Changhua Christian Hospital, Changhua, Taiwan

Introduction: According to the National Comprehensive Cancer Network (NCCN)-breast cancer 2019 guideline with references, it is not recommended to use Tc-99 MDP bone scan to follow up stage 0 to stage II breast cancer patients, except clinical suspicion (such as patients feel localized bone pain or elevated alkaline phosphatase). However, physicians in Taiwan keep using baseline Tc-99 MDP bone scan to long term follow up the newly diagnosed breast cancer patients. There are no studies yet that explore whether the NCCN Breast Cancer Guidelines and other Western studies are suitable for Asians (including Taiwan).

Methods: According to the data from Changhua Christian Hospital cancer registration service, bone scan results from 3875 breast cancer patients between January 1, 2011, and December 31 2015 were collected. Excluding patients whose primary tumor cannot be assessed or with incomplete information (pathological or surgical report), 1862 patients have their first bone scan within a year after diagnosed breast cancer: Stage 0: 119, stage I: 605, stage II: 816, stage III: 322 patients were analyzed. (Stage II upstage to IV: 4 patients, Stage III upstage to IV: 37 patients).

Results: There is no bone metastasis found in stage 0 and stage I (total 724 patients). Four bone metastases were found in stage II (0.49%, 4/816), 16 in stage III (5%, 16/322). Bone scan true positivity in stage 0 and stage I 0% (0/724), stage II 0.49% (4/812) and stage III 4% (13/322). Using bone scan typical metastasis changes as our standard, in 41 stage IV patients 20 were found to have bone metastasis, 20 with neo-adjuvant chemotherapy, 36 under hormonal receptor and her2/neu immunohistochemistry stains (2017 St. Gallen criteria, ER+ her2/neu negative A-like 6 [17%], ER+ her2/neu negative B-like 5 [14%], ER+her2/neu positive 10 [28%], ER negative her2/neu positive 8 [22%], ER negative her2/neu negative 7 [19%]; bone metastasis 50% [18/36], ER+her2/neu positive 70% [7/10], ER+ her2/neu negative A-like 67% [4/6], ER negative her2/neu negative 29% [2/17], ER+her2/neu negative B-like 20% [1/5]; no bone metastasis in stage 0 and stage I; bone metastasis, 14 in stage III[ER+her2/neu negative A-like 6, ER negative her2/neu 8]; bone scan positivity, true positive 89% [16/18], false positive 6% [1/18], false negative 11% [2/18, ER+her2/neu positive subtype]).

Conclusion: Health, cost effectiveness and radiation health risk for First-year routine bone scan needs further investigation for the Asian breast cancer patients (including Taiwanese).

OC008

Developing an Objective Structured Clinical Examination (OSCE) Case for Medical Radiation Technologists

Bi-Fang Lee

Department of Imaging Medicine, National Cheng-Kung University Medical College and Hospital, Tainan, Taiwan

Introduction: An objective structured clinical examination (OSCE) has been developing as an addition to the entry-to practice examination for all the medical personnel (non-physician) at a southern medical center in Taiwan. The medical personnel (non-physician) includes dentists, nursing personnel, social work specialists, psychologists, respiratory therapists, medical technologists, medical radiation technologists, dieticians, hearing specialists, speech therapists, physical therapists, and occupational therapists. This study is to investigate the developing OSCE case for medical radiation technologists.

Methods: A “blueprint” is a template used to guide the development of OSCE stations to ensure tasks and problems depicted in simulations are relevant to competencies being measured. An OSCE blueprint format and an OSCE test format for entry-to-practice medical personnel (non-physician) were designed. A retrospective analysis with descriptive statistics were applied to scaled survey items. Qualitative analysis through independently coded responses to open-ended survey responses using word processing were conducted. Line-by-line content analysis supported collaborative development of overall themes.

Results: From 2018 to 2019, two courses of developing an OSCE case for all the medical personnel (non-physician) at a southern medical center in Taiwan were conducted. Forty-five persons participated in this activity, and 45 questionnaires were returned. Satisfaction with the activity was 4.55 points (4 = satisfied; 5 = very satisfied).

Conclusions: OSCE could be used across medical personnel as a strategy to assess clinical competence, prepare for clinical education, and conduct program evaluation, indicating compliance with educational standards. Of course, OSCE is not intended to replace other clinical assessment, such as Direct Observation of Procedural Skills, but to assess clinical competence not currently addressed by other means.

OC009

Lymphoscintigraphy in Breast Cancer Related Unilateral Limb Lymphedema

Bi-Fang Lee¹, Chien-Liang Ho², Nan-Tsing Chiu¹

¹*Department of Imaging Medicine*

²*Department of Surgery, National Cheng-Kung University Medical College and Hospital, Tainan, Taiwan*

Introduction: No global consensus has been reached for diagnosis and staging for patients with breast cancer related unilateral arm lymphedema among medical specialties to receive the appropriate management.

Methods: This study was approved by the National Cheng-Kung University Hospital, Tainan, Taiwan, Institutional Review Board. All patients were classified by the International Society of Lymphology clinical stages from 0 to 3. All patients with unilateral extremity lymphedema and breast cancer were included to receive lymphoscintigraphy to confirm the lymphedema diagnosis. Duplex ultrasound will be used for the assessment of any concomitant vascular anomaly.

Results: We included 36 patients with unilateral extremity lymphedema using lymphoscintigraphy. Lymphoscintigraphy was correlated to clinical symptoms and signs, and classified into normal lymphatic drainage, partial obstruction, and total obstruction.

Conclusions: Our results demonstrate the role of radionuclide lymphoscintigraphy for early detection and management of breast cancer related unilateral arm lymphedema.

OC010

Nuclear Pharmacy for Medical Clerks: Interprofessional Education

Chen-Ching Ho¹, Bi-Fang Lee^{2,3}, Yu-Chin Wu¹, Ching-Lan Cheng¹, Nan-Tsing Chiu³

¹*Department of Pharmacy, National Cheng Kung University Hospital, College of Medicine,
National Cheng Kung University, Tainan, Taiwan*

²*Education Center, National Cheng Kung University Hospital, College of Medicine,
National Cheng Kung University, Tainan, Taiwan*

³*Department of Imaging Medicine, National Cheng Kung University Hospital, College of Medicine,
National Cheng Kung University, Tainan, Taiwan*

Introduction: Interprofessional education (IPE) is an important step in advancing health professional education when students from two or more professions in health and social care learn together. For medical clerks, nuclear pharmacists could prepare them for physician and pharmacist collaboration in the future.

Methods: We arranged 1 hour of IPE from nuclear pharmacists for medical clerks during the medical clerks' orientation training. First, routine nuclear pharmacy works were introduced, focusing on the services that physicians utilize or participate in. Subsequently, the clerks visited the nuclear pharmacy department to experience the daily work of nuclear pharmacists. Pre- and post-activity questionnaires scored using 5-point Likert scales were employed to evaluate the outcomes.

Results: From 2018 to 2019, 51 clerks participated in this activity, and 51 questionnaires were returned. Satisfaction with the activity was 4.89 points (4 = satisfied; 5 = very satisfied).

Conclusions: IPE increased the recognition of nuclear pharmacists' services among medical clerks. By performing this pedagogical activity, the medical clerks learned about the role and responsibility of nuclear pharmacists in the medical team.

OC011

¹²³I-mIBG SPECT/CT and ¹⁸F-FDG PET/CT in Detection of Pediatric Neuroblastoma: Case Series and Review of Literature

Jiun-Chang Wu, Chin-Ho Tsao

Department of Nuclear Medicine, Mackey Memorial Hospital, Taipei, Taiwan

Introduction: Neuroblastoma is a malignant neuroectodermal tumor. It is highly malignant since nearly 60% of neuroblastomas are stage IV at the time of presentation; therefore, accurate imaging methods are crucial for staging and defining appropriate treatment. Meta-iodobenzylguanidine (mIBG) is a noradrenaline analogue, utilized for imaging since tumor cells express the norepinephrine transporter. In contrast, ¹⁸F-fluorodeoxyglucose (FDG) is a glucose analogue, entrapped in neoplastic tissue. We present case series and discuss which study is more beneficial for patients with neuroblastoma, ¹²³I-mIBG SPECT/CT or ¹⁸F-FDG PET/CT.

Methods: Ten patients with neuroblastoma comprising of six males and four females ranging from 0 to 5 years (average 2.5 years) participated in this study. All patients underwent whole-body planar imaging 6 hours and 24 hours, and SPECT/CT 24 hours following administration of ¹²³I-mIBG, as well as PET/CT 60 minutes following administration of ¹⁸F-FDG. Two diagnostic tools were done within 6 days.

Result: Two patients revealed consistent findings in both diagnostic tools. Inconsistent findings were found in the other three patients, all as stage IV at the time of presentation. Five patients were interpreted as negative finding. Overall, ¹²³I-mIBG SPECT/CT unveil more lesions than ¹⁸F-FDG PET/CT among these patients.

Discussion: In literature reviews, mIBG is an ideal agent for diagnosing neuroblastoma with straightforward identification of osseous metastasis, while there are several disadvantages including difficulty in detecting small lesions, approximately 10% neuroblastoma not take up mIBG, and some tumor cells losing expression of transporter after therapy. ¹⁸F-FDG is less specific than mIBG; however, could be a useful tool when neuroblastoma fail to uptake mIBG at initial presentation, during, or after therapy.

Conclusion: Among ten patients, ¹²³I-mIBG SPECT/CT is more sensitive than ¹⁸F-FDG PET/CT; however, neither diagnostic tool is completely superior to the other. We suggest both examinations are necessary, especially for stage IV neuroblastoma.

OC012

口頭論文發表摘要·臨床組

Prognostic Value of Attenuation Corrected Myocardial Perfusion Imaging among Patients with Suspected Coronary Artery Disease

Jeii-Yie Huang^{1,2}, Chi-Lun Ko¹, Yen-Wen Wu^{1,3,4-6}, Chia-Ju Liu^{1,7},
Kuo-Liong Chien^{2,3}, Ruoh-Fang Yen¹

¹*Department of Nuclear Medicine, National Taiwan University Hospital and National Taiwan University College of Medicine, Taipei, Taiwan*

²*Institute of Epidemiology and Preventive Medicine, College of Public Health, National Taiwan University, Taipei, Taiwan*

³*Department of Internal Medicine, National Taiwan University Hospital and National Taiwan University College of Medicine, Taipei, Taiwan*

⁴*Department of Nuclear Medicine, and*

⁵*Cardiology Division of Cardiovascular Medical Center, Far Eastern Memorial Hospital, New Taipei City, Taiwan*

⁶*National Yang-Ming University School of Medicine, Taipei, Taiwan*

⁷*Department of Nuclear Medicine, National Taiwan University Hospital, Yun-Lin Branch, Yun-Lin County, Taiwan*

Introduction: Multiple studies demonstrated the evidence of improving diagnostic accuracy after attenuation correction (AC). However, as regards the prognostic value of AC, there have been few published reports with controversial results. Therefore, the aim of this study was to investigate the prognostic value of AC MPI.

Methods: One-hundred and eight patients underwent TI-201 MPI by a hybrid SPECT/CT system. AC and non-corrected (NAC) images were interpreted blindly using a 17-segment model and the summed stress scores (SSS) was calculated. Severity of disease was divided by SSS of 4, 8 and 12. The primary endpoint was all cause mortality and secondary endpoints were cardiovascular (CV) related re-admission and heart failure (HF) related admission.

Results: During a follow-up of 8 to 10 years, 25% (27/108) of deaths, 38% (41/108) of CV related re-admission, 59% (64/108) of deaths plus CV related re-admission and 5% (5/108) of HF admission occurred. Kaplan-Meier analysis of all cause mortality plus CV related re-admission showed significant differences between both AC and NAC SSS groups. In the univariable Cox regression, NAC SSS, AC SSS, NAC SSS by groups and AC SSS by groups all yielded significant higher hazards ratios for all cause mortality. In the multivariable model, NAC SSS, AC SSS, NAC SSS by groups and AC SSS by groups were significant predictors for prediction of composite endpoints of all cause mortality plus CV readmission.

Conclusions: Our results showed that AC and NAC MPI showed equivalent value for predicting the composite endpoints of all cause mortality plus CV re-admission. However, the effectiveness of additional AC for predicting all cause mortality was challenged.

PB001

I-131 廢水槽溢水位警示異常之處理及改善

陸建華¹ 吳志順¹ 李將瑄^{2*}

¹ 奇美醫療財團法人柳營奇美醫院核子醫學科

² 奇美醫療財團法人奇美醫院核子醫學科

背景介紹：I-131 廢水槽為儲放 I-131 治療病人排放之放射性廢液使用，當廢水槽儲滿後電動閥開關自動關閉，讓廢液靜置衰減，等放射性活度低於外釋排放標準後始可排放，如槽體溢水位警示產生，則可能是開關處異物堵塞無法關閉，或是浮球異常，浮球異常部分則須等槽內廢液排空後始可檢修，影響檢修時效及槽體使用率，故改善浮球檢修方式以提高槽體之正常使用率，不影響病人之住院排程。

方法：在每一廢水槽浮球擺放位置之槽體上方開一檢測口，平時予以封閉，如遇溢水位警示時，打開檢測口，直接檢測浮球擺放高度是否移位或損壞，則可判斷是否只是訊號異常，並無廢水再次流入槽內，如浮球檢測皆正常，則可判定為開關處異物阻塞，槽體無法關閉，廢液一直滲入槽內，造成溢水位警示，此時僅需維修電動閥開關，就可解決溢水位問題，如此一來可以縮短檢查及維修時效。

結果：以往溢水位警示產生後，工務室人員均先維修電動閥開關，如溢水位警示燈號仍持續閃爍，則需等槽內廢液排空後始可維修浮球部分，現今則可立刻判斷處理，可維持槽體正常運作使用。

結論：I-131 廢水槽之使用及運作，可以直接影響到 I-131 病人之治療，如廢水活度未達排放標準，則槽內廢液不得排放，廢水槽則無法使用，就不能收受治療病人，故廢水槽之管理及問題之排除改善，亦是 I-131 病室對病人治療上很重要之環節。

PB002

人員生物劑量國際能力試驗比對

林婉琪¹ 歐陽芳鈺¹ 莊程惠¹ 張剛璋²

¹ 行政院原子能委員會核能研究所

² 台北醫學大學

背景介紹:國內目前有輻射工作人員 50,000 餘人，涵蓋核能電廠、工業、醫院、研究機構等各類領域，當發生輻射意外曝露事件，人員生物劑量評估為事故發生後可採取的措施，並用以評估人員接受之劑量，做為醫療照護的參考。本研究建立人員生物劑量 (Biodosimetry) 評估相關技術，並發展出具有國際水準的生物劑量實驗室。為保持實驗室之分析能力能與國際接軌，參與了由加拿大衛生部 Wilkins 教授舉辦的國際能力試驗，與其它六個國家十一間實驗室進行比對。

方法:接收到加拿大衛生部統一製作之盲樣血液後，進行培養、純化後噴片取得染色體樣品，再以顯微鏡進行影像掃描。根據規範，每個盲樣樣品進行五十個細胞染色體分析，若已發現三十個染色體變異則停止分析。於每十個、二十個及五十個分析後進行數據統計，計算其劑量與 95% 信賴區間內的上下限及統計時間。最後將所有數據回傳加拿大進行最後計算統計。

結果:經加拿大衛服部統計之後，本實驗室 (Lab 9) 之分析結果，十個盲樣中有七個分析數值皆落在 95% 信任區間範圍內，其於三個雖未落於範圍內但與正確數值差異不大，由 Z-Score 分析可得知所有數據皆落在 ± 2 之內，表示分析之數據結果皆在誤差範圍之內。

結論:藉由參加國際比對与其它實驗室一同進行分析，除了可以了解本實驗室分析能力確實有與國際接軌，也證明本實驗室分析之數據確實具有可信度，於發生緊急曝露事件時可以有效分析評估劑量進行後續之醫療行動。

PB003

評估放射性銥 -111 標誌長半衰期 RGD 胜肽 在人類腦癌模式的特性

羅瑋霖 羅世偉 陳明偉 黃永睿 陳亮丞 李銘忻

行政院原子能委員會核能研究所

背景介紹：最近的研究表明，將 RGD 胜肽結合伊凡氏藍分子 (Evans blue) 片段，可以改善血液半衰期和腫瘤攝取量。本研究的目的是通過生物分佈和 nanoSPECT / CT 研究放射性銥 -111 標誌長半衰期型 RGD 胜肽在 U-87 MG 人類腦癌皮下腫瘤動物模式中的藥物分布特性。

方法：長半衰期 RGD 胜肽 (DOTA-EB-cRGDfK) 在核能研究所 (INER) 中用銥 -111 標誌。以皮下注射 3×10^6 U-87MG 細胞在 6 週齡雌性 BALB/c 裸鼠，建立產生人類腦癌皮下腫瘤動物模式。給藥方式為尾靜脈注射，並使用 nanoSPECT / CT 成像和生物分布試驗來研究放射性標記胜肽在動物體內分布。

結果：生物分布數據顯示 ^{111}In -DOTA-EB-cRGDfK 在腎，肝，脾和腫瘤等部位累積。腫瘤累積量最高達 $27.12 \pm 2.7\%$ ID/g，給藥 24 小時後腫瘤累積量比肌肉部位高約 22 倍。 ^{111}In -DOTA-EB-cRGDfK 的 NanoSPECT / CT 圖像顯示腫瘤部位的信號隨時間增加，且 72 小時後信號仍然明顯。

結論：本研究顯示放射性標記的長半衰期 RGD 胜肽 (^{111}In -DOTA-EB-cRGDfK) 可在腫瘤部位明顯積累，本藥物具有腫瘤診療的潛力。

PB004

Using Filtered Backprojection (FBP) to Improve Truncation Artifacts Generated by the Patient's Bladder or Injection Site in PET Image

Ya-Lien Chang^{1,2}, Chiang-Hsuan Lee³

¹Division of Nuclear Medicine, Department of Medical Image, Chi Mei Medical Center, Liouying, Tainan, Taiwan

²Department of Medical Imaging and Radiological Sciences, Kaohsiung Medical University

³Division of Nuclear Medicine, Department of Medical Image, Chi Mei Medical Center, Yongkang, Tainan, Taiwan

Purpose: In PET/CT, since FDG is mostly excreted in urine, occasionally the image may produce truncation artifacts due to the patient's bladder urine or the injection site. The artifact will cause some of the image information to be lost, thereby affecting the image quality. Before the patient can't re-scan, we hope to compensate part of the image information by different image reconstruction methods.

Method: Iterative reconstruction has a better signal-to-noise ratio and no streaky artifacts, and has now replaced FBP in PET image. This method uses a computer to estimate the data, and use this data to generate a set of images, the set of images are compared to the original projection view captured by the patient, we can get the difference or ratio of the two projection views and use it to correct the original transaxial slice estimated by the computer, repeat again and again. In the iterative reconstruction method, the OSEM algorithm can be used to save computer computing time.

Filtered backprojection (FBP) has been widely used in the past for nuclear medical tomographic reconstruction. Since this reconstruction method preserves all the information on each back projection path, it produces star artifacts. Although increasing the number of projected views can improve the star artifacts, the surrounding objects are still blurred and have a halo appearance, called backprojection artifacts. This artifact can be improved by filtering and Fourier transform.

The reconstruction method of the original PET image preset is OSEM. In an attempt to improve the truncation artifacts, the original data were reconstructed using the FBP reconstruction method for comparison.

Results and Discussion: The reconstruction method of the original PET image preset is OSEM. After using the FBP reconstruction method, although the image has noise, it can eliminate the truncation and compensate for the lost information. The GE company application engineer said in the newer models, there are also options to chose, which may improve the truncation artifacts. However, since this option is not available in our model, we chose to change the reconstruction method.

Conclusion: The OSEM reconstruction method uses a computer to estimate the data, and uses this data to generate a set of transaxial slices, and then use this transaxial slice to compare with the original projected view; the FBP reconstruction method directly produces transaxial slices from the data obtained by the camera. The process of the two reconstruction methods is different, which makes the image results different.

PB005

利用田口方法在 R-CAMERA 下 探討最佳空間解析度

葉馨潔¹ 潘榕光²

¹ 台中慈濟醫院核子醫學科

² 中台科技大學醫學影像暨放射科學系

背景介紹：核子醫學科心肌血流灌注造影 (MPI) 所使用的藥物，可以使用在評估懷疑或證實為冠狀動脈心臟疾病，也可以使用在腫瘤的追蹤，Tl-201 化學性質和鉀離子相似，靜脈注射後，會隨血液循環流經冠狀動脈，再由鈉 - 鉀幫浦主動運輸之機轉進入心肌細胞內。

目的是找出 Tl-201 於 SPECT 造影時，準直儀、距離、掃描時間、能窗、矩陣大小、放大倍率等 6 個因子，探討最佳影像品質條件。

方法：以田口 L18 直交表進行實驗設計，將 0.8 mCi 的 Tl-201 稀釋到 5 cc 的空針內 (使用藍色墨水染色)，再注入壓克力假體，使用 GE Infinia Hawkeye 4 SPECT/CT 收取 18 組不同條件的影像，找出之最佳化組合並進行驗證。

結果：從因子反應圖中，得到最佳化的結果是 LEHR、距離 3 cm、掃描時間 350 sec、能窗 25%、矩陣大小 256×256、放大倍率 1.00。但這結果並不在田口 L18 直交表內，所以使用了上述條件去收取影像做驗證。

結論：使用藥物 Tl-201 的特性，不只能應用於冠狀動脈疾病的診斷，也可應用於腫瘤追蹤。透過田口方法，能有效率又快速地，找出影響 Tl-201 影像的關鍵是 Detector 與病人之間的距離，這對未來於臨床的應用和醫師的影像判讀上有很大的幫助。

PB006

壁報論文發表摘要·基礎組

Three-year Production Experience of GMP-Compliant [¹⁸F]FSPG Injection with a Modified TracerLab FxFDG Module

Ya-Yao Huang^{1*}, Yu-Ning Cheng¹, Wei-Hua Kuo¹, Kuang-Hua Tang¹,
Mei-Fang Cheng^{1,2}, Yu-Wen Tien^{3,4}, Kai-Yuan Tzen^{1,5},
Ruoh-Fang Yen^{1,5}, Chyng-Yann Shiue^{1,5,6}

¹*PET Center, Department of Nuclear Medicine, National Taiwan University Hospital, 7,
Chung-Shan S. Road, Taipei, 100, Taiwan*

²*Institute of Occupational Medicine and Industrial Hygiene, National Taiwan University, Taipei, Taiwan*

³*Department of Surgery, National Taiwan University College of Medicine and Hospital, Taipei, Taiwan*

⁴*Department of Surgery, College of Medicine, National Taiwan University, Taipei, Taiwan*

⁵*Molecular Imaging Center, National Taiwan University, Taipei, Taiwan*

⁶*PET Center, Department of Nuclear Medicine, Tri-Service General Hospital, Taipei, Taiwan*

Introduction: [¹⁸F]FSPG has been proved to be a promising tracer for imaging xC- transporter (xCT-) and clinically applied in various oncological studies. In order to fulfil the clinical need of several studies in Taiwan, we have modified TracerLab FxFDG module to automatically synthesize [¹⁸F]FSPG with GMP compliance since Sep. 2016. We reported herein our three-year experience on the production of this imaging agent.

Methods: Based on reported radiosynthesis method, the [¹⁸F]FSPG was automatically produced with our modified TracerLab FxFDG module. The QC tests of [¹⁸F]FSPG were performed based on USP monographs of [¹⁸F]FDG and the residual [¹⁸F]Fluoride level was measured by radio-TLC method.

Results: In our three years production experience, [¹⁸F]FSPG was reliably produced with a radiochemical yield of $4.4 \pm 2.4\%$ (EOS) in a synthesis time of 83 ± 9 min from EOB (n = 53). Both the chemical and radiochemical purity of [¹⁸F]FSPG were > 95% with a specific activity of 377 ± 162 mCi/ μ mol. The quality of [¹⁸F]FSPG was found to be suitable for clinical applications.

Conclusions: With the modified FxFDG module, [¹⁸F]FSPG could be reliably produced for preclinical and clinical studies. After preclinical imaging validation studies, clinical study of [¹⁸F]FSPH for cancer patients is still ongoing at NTUH.

PB007

Long-Term Validation of Pharmaceutical-Grade GalliaPharm® ⁶⁸Ge/⁶⁸Ga Generator

Ya-Yao Huang¹, Chih-Chen Yu¹, Yu-Ning Chang¹, Ruoh-Fang Yen^{1,2}

¹PET Center, Department of Nuclear Medicine, National Taiwan University Hospital, Taipei, Taiwan

²Molecular Imaging Center, National Taiwan University, Taipei, Taiwan

Introduction: GalliaPharm® ⁶⁸Ge/⁶⁸Ga generator (Eckert & Ziegler Eurotope GmbH, Germany) has been a well-known pharmaceutical-grade generator receiving marketing authorization in Europe. Since 2017, PET center of National Taiwan University Hospital (NTUH) has sequentially used two GalliaPharm® ⁶⁸Ge/⁶⁸Ga generator for GMP-compliant production of [⁶⁸Ga]Ga-DOTA-TOC and [⁶⁸Ga]Ga-PSMA. As one of starting materials for above ⁶⁸Ga-labeled radiopharmaceuticals, we routinely validated and monitored ⁶⁸Ge/⁶⁸Ga generator eluate for quality confirmation. This study aimed to organize and present our results here.

Methods: One GalliaPharm® ⁶⁸Ge/⁶⁸Ga generator loaded with 1110 MBq (30 mCi) of ⁶⁸Ge and the other one generator loaded with 1850 MBq (50 mCi) of ⁶⁸Ge were evaluated in these study, respectively. Both generators were automatically eluted using 0.1 M HCl (Ultrapure trace-metal-free). The QC processes for the elute ([⁶⁸Ga]GaCl₃) at NTUH was routinely performed based on EP monograph of [⁶⁸Ga]GaCl₃. Briefly, there are two types of QC tests: physicochemical tests and biological tests. The radiochemical purity of the final dose was validated using radio-TLC. The quality control of clinical doses included tests of their endotoxin level, radionuclide identity, filter integrity, pH, sterility and ⁶⁸Ge breakthrough.

Results: Over a period of one year, ⁶⁸Ga elution yields from these two generators were 57~73% and 61~65%, respectively. ⁶⁸Ge breakthrough was less than 0.001% all the time (expressed as percentage of ⁶⁸Ge activity present in the generator at the time of elution), and all qualities fit the criteria listed in EP.

Conclusions: The GMP-certified GalliaPharm® ⁶⁸Ge/⁶⁸Ga generator system was studied for two years. The generator system is contained within the fluidic labeling module, and it is compact, self-shielded, and easy to automatically operate. The results indicated the unique characteristics of these two GalliaPharm® ⁶⁸Ge/⁶⁸Ga generators including the ⁶⁸Ge levels in the elute were under the detection limits at all times.

PB008

In Vivo Whole-Body Biodistribution and Radiation Dosimetry of [¹⁸F]FPA

Ya-Yao Huang¹, Chia-Ling Tsai¹, Yu-Ning Chang¹, Chi-Han Wu³, Ruoh-Fang Yen^{1,3}

¹*PET Center, Department of Nuclear Medicine, National Taiwan University Hospital, Taipei, Taiwan*

²*Department of Anesthesiology, Wan Fang Hospital, Taipei Medical University, Taipei, Taiwan*

³*Molecular Imaging Center, National Taiwan University, Taipei, Taiwan*

Introduction: Fatty acid synthase (FASN) is a key enzyme in fatty acid synthesis pathways and its expression has been known to be an indicator of poor prognosis in breast cancer (BC). Recently, a hypothetical model for FASN-regulated ER signaling in BC cells has been suggested. As one of the short fatty acids, [¹⁸F]2-fluoropropionic acid ([¹⁸F]FPA) has been proved as a promising oncological imaging agent. Accordingly, the aim of this study was to further assess the safety and usefulness of [¹⁸F]FPA via microPET imaging. Finally, the radiation dosimetry of [¹⁸F]FPA will be further assessed for the issue of the radiation safety.

Methods: [¹⁸F]FPA was automatically synthesized based on reported methods with FLEXLAB module (iPHASE Technologies, Australia) and its complete QC tests were carried out for quality confirmation. For animal study, male ICR mice (30-40 g) were injected with a bolus of about 300 μCi of [¹⁸F]FSPG. By using small-animal Argus PET/CT scanner, dynamic sinograms were produced and VOIs were defined on co-registered PET/CT images.

Results: The RCY of [¹⁸F]FPA was $39.1 \pm 12.6\%$ (n = 6, EOB after HPLC isolation) and the synthesis time without formulation was about 85 min at end of synthesis. The radiochemical purity was > 90% as determined by analytical HPLC and TLC methods. During scanning, [¹⁸F]FPA injection did not produce overt adverse effects in mice and its significant uptake in bladder of mice only. The results from microPET imaging showed that the target organs of [¹⁸F]FPA Injection were lungs, kidneys and bladder, and the estimated effective doses extrapolated from non-fasted mice were $18.5 \pm 0.06 \mu\text{Sv}/\text{MBq}$ (n = 3).

Conclusions: MicroPET images in normal mice showed that [¹⁸F]FPA had significantly accumulated in bladder and urinary elimination was suggested to be a significant clearance pathway of [¹⁸F]FPA. Additionally, its radiation dosimetry has been evaluated for incoming human studies.

PB009

Production Experience of GMP-Compliant [^{18}F]FCH Injection with Cassette-Type TracerLab MxFDG Module

Ya-Yao Huang¹, Chin-Hung Chiu¹, Wei-Hua Kuo¹, Yu-Ning Chang¹,
Kuang-Hua Tang¹, Ruoh-Fang Yen^{1,2}

¹*PET Center, Department of Nuclear Medicine, National Taiwan University Hospital*

²*Molecular Imaging Center, National Taiwan University*

Introduction: [^{18}F]Fluoromethylcholine ([^{18}F]FCH) has been a well-known imaging agent in clinic. Since 2018, GMP-compliant automated production of [^{18}F]FCH with cassette-type MxFDG module has been well validated and produced [^{18}F]FCH injection has been approved for clinical use at by TFDA at NTUH. Here we report on our 1.5 year experience with an automated system for [^{18}F]FCH at NTUH.

Methods: In this study, [^{18}F]FCH will be radiosynthesized based on reported methods but with a cassette-type TracerLab MXFDG module. Analytic HPLC and TLC procedures of radiochemical purity and chemical impurity (Tetrabutylammonium ion) were verified in advance and all QC tests were performed based on EP monograph.

Results: Automated production of [^{18}F]FCH were successfully validated under GMP conditions, resulting in radiochemical yield of $25 \pm 4\%$ (EOS) within 51 ± 0 min ($n > 30$) of synthesis time. For on-site produced [^{18}F]FCH injection at NTUH, all QC criteria listed in EP were fully satisfied. Particularly, radiochemical purity of [^{18}F]FCH was $98 \pm 1\%$ and residual [^{18}F]Fluoride and DMAE levels were $0.2 \pm 0.1\%$ and 0.6 ± 0.4 ppm.

Conclusions: A 1.5-year production experiment for clinical study supply showed that our production method of [^{18}F]FCH has the advantages of a high stable production and radiochemical yields for many patients in Taiwan.

PB010

壁報論文發表摘要·基礎組

Evaluation C-11 Sodium Acetate Synthesis and Quality Control in cGMP Condition

Wen-Yi Chang¹, Shih-Pei Chen¹, Jyh-Hwa Chen¹,
Ren-Shyan Liu², Wen-Sheng Huang¹

¹*Department of Nuclear Medicine, Veterans General Hospital, Taipei, Taiwan*

²*Department of Biomedical Imaging and Radiological Sciences, National Yang-Ming University, Taipei, Taiwan*

Introduction: C-11 Sodium Acetate has been widely used for diagnosis prostate cancer, hepatocellular, lung cancer, bladder carcinoma, brain tumor and assessment of regional myocardial oxygen consumption in clinical. C-11 Sodium Acetate may act as a probe of tissue intermediary metabolism through acetyl-CoA-mediated entry into anabolic pathways. There are only three hospitals which provide C-11 Sodium Acetate PET scan in Taiwan. The National PET/Cyclotron Center of Taipei Veterans General Hospital was established by the end of 1992 and supplied C-11 Sodium Acetate in 2012 by Taiwan FOOD and Drug Administration (TFDA) approved.

Methods: In this study, we summarized the results of quality control data from 2016 to present. The standard criteria for production radiopharmaceutical are according Current Good Manufacturing Practice (cGMP) and the specification are according European Pharmacopeia (EP).

Results: The cGMP clean room is under the appropriate pressure differences, air flow direction and air quality. The radio-chemical synthesis is using close and automated system (Hot cell) in a Class 1,0000 environment. Aseptic dispensing activities is carried out in a Class 100 isolator. The radio-activity, radio-chemical yield, pH value and radio-chemical purity of C-11 Sodium Acetate were 909 ± 280 mCi, $48 \pm 14\%$, 8.0 and $> 99.9\%$, respectively.

Conclusions: The National PET/Cyclotron Center of Taipei Veterans General Hospital is stably providing high quality C-11 Sodium Acetate for clinical need by keeping analysis the trend of C-11 Sodium Acetate production in cGMP condition.

PB011

Automated cGMP-Grade Production of F-18 Fallypride as a D2 Dopamine Receptor Ligand for Brain Disorders

Wen-Yi Chang¹, Shih-Pei Chen¹, Chun-Tse Hung¹, Geng-Ying Li¹,
Chi-Wei Chang¹, Ren-Shyan Liu², Wen-Sheng Huang¹

¹*Department of Nuclear Medicine, Veterans General Hospital, Taipei, Taiwan*

²*Department of Biomedical Imaging and Radiological Sciences, National Yang-Ming University, Taipei, Taiwan*

Introduction: The imaging of dopamine D2 receptor is essential for diagnosis brain diseases with high correlation with dopaminergic system. C-11 raclopride is the first generation D2 receptor imaging probe and record in European Pharmacopeia (EP) and United State Pharmacopeia (USP). But, the affinity of C-11 raclopride is not enough to imaging those receptors in extra-striatal brain areas. F-18 fallypride is a high-affinity dopamine D2 receptor imaging probe and designed to make possible to imaging extra-striatal dopamine D2 receptor with clinical PET.

Methods: Synthesis F-18 fallypride was followed by the reported method by Byung Seok Moon et al. In National PET/Cyclotron Center of Taipei Veterans General Hospital, F-18 fallypride was performed by Eckert & Ziegler (EZ) synthesizer. Radio-labeling precursor and reagents were commercially available. The standard criteria for production radiopharmaceutical are according Current Good Manufacturing Practice (cGMP). Quality control included radio-chemical purity, pH value, MCA analysis and specific activity analysis, et al. Stability test was performed up to 6 hours after end of synthesis.

Results: cGMP production of F-18 fallypride was successful performed in our center with $5.3 \pm 2.1\%$ radiochemical yield. QC results of radio-chemical purity, pH value, and specific activity analysis were 99.9%, 7.0, 458.5 ± 218.5 GBq/ μmol , respectively. F-18 fallypride was had high stability in normal saline solution ($> 99\%$, purity after 6h incubation).

Conclusions: Now, cGMP production of F-18 fallypride is successful setup in National PET/Cyclotron Center of Taipei Veterans General Hospital. F-18 fallypride may be used as PET probes for noninvasive evaluation of D2 receptor-related brain disease.

PB012

壁報論文發表摘要·基礎組

核醫藥品銻 ^{99m}MAA 、 DTPA 、 Phytate 凍晶組套 (Lyophilized kits) 分裝後效益分析

吳元鍾 林欣純 張文議 黃文盛

臺北榮民總醫院核醫部

背景介紹：核醫藥品 (Radiopharmaceutical) 在醫院採購成本上已呈現逐年成長趨勢，但全民健康保險醫療服務給付項目及支付標準針對核醫檢查卻已數十年都未調整，因此該研究目的是將原廠銻 ^{99m}MAA 、 DTPA 、 Phytate 凍晶組套分裝成若干份，並配合臨床所需用量來標幟 (Labeling) 已分裝完成之組套，以降低用藥成本及提供臨床供藥的穩定性。

方法：將核醫藥品銻 ^{99m}MAA 加入 3 ml 生理食鹽注射液溶解凍晶組套 (Lyophilized kits) 中之結晶物，使該溶液分成二等份 (稀釋比例 2:1)，並冷凍於 -20 冰箱中 0、7、14 天。另外銻 $^{99m}\text{DTPA}$ 、 Phytate 分別加入 2 ml 生理食鹽注射液溶解凍晶組套 (Lyophilized kits) 中之結晶物，使該溶液分成二等份 (稀釋比例 2:1)，並冷凍於 -20 冰箱中 0、7、14 天。

結果：分裝後的三種凍晶組套 (Lyophilized kits) 藥品後續所標幟的活性為銻 99m 30 mCi \pm 10%，經 0、7、14 天後取出標幟後第 10 分鐘及第 6 小時放射化學純度 (Radiochemical purity) 皆大於 90% ($n = 106$)。

結論：核醫藥品銻 ^{99m}MAA 、 DTPA 、 Phytate 凍晶組套 (Lyophilized kits) 分裝後的放射化學純度 (Radiochemical purity) 可達到美國藥典要求，經扣除分裝過程及放射化學純度分析耗材等成本後，成本可降低至約採購價的一半，並可增加臨床供藥的穩定性。

PB013

以 ACR 假體比較三台不同正子造影儀器 於標準攝取值之差異

陳奕倫 楊邦宏 黃文盛

臺北榮民總醫院核子醫學部

背景介紹：正子檢查是提供現代診斷癌症常用之工具，正子造影儀器隨科技進步，無論軟、硬體上皆有大幅度的提升，而能得到更佳的影像與更準確的半定量分析。然而，過去以 BGO 晶體當成標準的標準攝取值 (Standard uptake value, SUV) 卻無法直接於新的儀器上使用。因此，本研究目的在比較三台儀器於半定量分析的差異，並尋找其相慣性與轉換之方法。

方法：使用兩台新的正子造影儀器 PET/CT-Discovery MIDR、PET/MR-SIGNA 與 BGO 晶體之正子造影儀器 PET/CT-Discovery VCT 進行 ACR 假體實驗，假體依照 ACR 參考之活度濃度比例調配並依照其參數依序在三台儀器造影。造影時間設為四分鐘，皆有進行衰減校正，影像重組條件使用該儀器在臨床全身正子檢查時的常規條件組成五組影像 (MIDR 兩組，SIGNA 兩組，VCT 一組)。將影像使用 AW server 圈選 ROI 並計算 SUV 比較其差異以及找尋相關性。

結果：結果發現兩台新儀器四組影像都與 VCT 的 SUV 有高度的相關性，並找到方程式轉換其數值分別如下： $SUV_{VCT} = 1.34 SUV_{MIDR\ OSEM} + 0.11$ 、 $SUV_{VCT} = 1.3 SUV_{MIDR\ Q350} + 0.06$ 、 $SUV_{VCT} = 1.364 SUV_{SIGNA\ OSEM} + 1.5$ 、 $SUV_{VCT} = 1.299 SUV_{SIGNA\ Q350} + 1.77$ 。

結論：利用本實驗發現新儀器 MIDR、SIGNA 與 VCT 在 SUV 值上的轉換關係，未來可以提供臨床一個參考數值，使新舊儀器銜接能更順利。

PB014

井計數校正 (well-counter calibration) 與標準攝取值 (SUV) 之影響分析

傅雲珠 李冠瑩

長庚醫院北院區核子醫學科暨分子影像中心

背景介紹：一直以來，核醫正子暨電腦斷層掃描在癌症的診斷與分期上扮演著重要的角色。標準攝取值 (SUV) 提供正子影像定量的分析，對於治療前後之成效與腫瘤良惡性之區分上提供了重要的資訊，因此，確保 SUV 值的準確度就顯得相對重要。井計數校正 (well-counter calibration) 的目的是獲取掃描儀效率之數據，用於校正偵檢器非均勻性的採集正弦圖。這些因子用於計算放射性濃度和 SUV，不準確的校正因子會影響影像定量的精確性。

方法：這次我們將以 GE Discovery ST 此機台進行 2D 與 3D 的井計數校正。我們使用 GE 提供的圓柱型假體，在已知體積的假體中灌入純水與 F-18 藥物，同時記錄藥物注入假體前與後的劑量與時間。將藥物跟水充分混和均勻後，即可依照 GE 所制訂的標準程序來進行井計數校正。校正完成後，我們將舊有影像進行重組比較校正前後的 SUV 值之差異。

結果：利用裝有 F-18 藥物的均勻水假體進行井計數校正，可以歸一化 PET 偵檢器、放射性濃度標準和均勻性測試。校正前後的 SUV 值相差 5%~15%。

結論：在 FDG-PET 影像分析中，標準化攝取值 (SUV) 在臨床上普遍被用作半定量的參數。SUV 提供了特定興趣區域 (ROI) 的放射性藥物之活度，該區域根據患者的體重和給藥劑量進行了標準化。SUV 的可變性和偏差可能是由於系統可變性，人為操作錯誤以及用於測定校準放射性劑量的劑量校正儀 (Dose calibrator) 不一致而引起的。為了提供診斷上更精確的數值，依照製造廠商規定的程序與頻率進行井計數校正，藉以提高 SUV 的準確性。

PB015

Evaluation of Validity Period of cGMP-grade [^{18}F]FEPPA by Stability Assay

Shih-Pei Chen^{1,2}, Chi-Wei Chang^{1,2}, Wen-Yi Chang^{1,2}, Chun-Tse Hung^{1,2},
Geng-Ying Li^{1,2}, Wen-Sheng Hwang^{1,2}

¹*Department of Nuclear Medicine, Taipei Veterans General Hospital, Taipei, Taiwan*

²*National PET/Cyclotron Center of Taipei Veterans General Hospital, Taipei, Taiwan*

Introduction: The translocator protein (TSPO) is correlated to a variety of diseases, such as neurodegenerative disorders, heart failure, and cancer. [^{18}F]FEPPA is a radiolabeled imaging tracer of positron emission tomography (PET) for TSPO. The validity period of [^{18}F]FEPPA would be considered not only by the activity amount but also by the stable period. The stability assay should be carried out to evaluate the validity period of [^{18}F]FEPPA.

Methods: [^{18}F]FEPPA was produced in three consecutive batches. According to the specifications of [^{18}F] radiopharmaceuticals: appearance, pH value, radiochemical purity, specific activity, radionuclide identification, radionuclide purity, color spot test for kryptofix 222, residual solvent, bacterial endotoxin test, integrity test and sterility test were included in the general quality control (QC) assays. [^{18}F]FEPPA was kept by incubation with ethanol and saline at room temperature ($22 \pm 0.5^\circ\text{C}$). Product stability was evaluated by appearance, pH value and radiochemical purity (RCP) at different time points (1, 2, 3, 4, 5 and 6 hours) after the QC assays.

Results: The QC results of three batches of [^{18}F]FEPPA were as follows: appearance was colorless and clear, pH value was 7.5 ± 0.5 , radiochemical purity was greater than 99.9%, mean specific activity was 133.2 GBq/ μmol , half-life was 107.77 ± 0.74 minutes, radionuclidic energy was 509.4 ± 1.36 keV, radionuclidic purity was $99.992 \pm 0.009\%$, concentration of kryptofix 222 was less than 50 $\mu\text{g/mL}$, bacterial endotoxins were less than 1.0 EU/mL and integrity test was 22 ± 1 psi. Appearance, radiochemical purity and pH value of [^{18}F]FEPPA met the criteria of QC for 6 hours. The result of stability assay showed that [^{18}F]FEPPA was highly stable in ethanol and saline during 6 hours after the end of synthesis.

Conclusions: The cGMP-grade Pharmaceutical [^{18}F]FEPPA had been successfully established in National PET/Cyclotron Center of Taipei Veterans General Hospital. [^{18}F]FEPPA is ready for clinical research of TSPO-related disease in the future.

PB016

Imaging of Neuroinflammation in a Mouse Model Using [^{18}F]FBAT

Wen-Sheng Huang¹, Chiang Hsuan Lee², Skye, Hsin-Hsien Yeh³, Chi-Wei Chang¹

¹Departments of Nuclear Medicine, Taipei Veterans General Hospital, Taipei, Taiwan

²Department of Nuclear Medicine, Chi Mei Medical Center, Tainan, Taiwan

³Brain Research Center, National Yang-Ming University, Taipei, Taiwan

Purpose: iNOS expression serves a sensitive biomarker for neuroinflammation. The study was to image brain inflammation in a mouse model using a newly developed [^{18}F]FBAT PET tracer and to evaluate its predictive potential for progression of cognition impairment following sepsis.

Methods: [^{18}F]HF was produced via $^{18}\text{O}(p, n)^{18}\text{F}$ using a cyclotron. [^{18}F]Fluoride was incorporated into the nitro precursor at 150°C. [^{18}F]FBAT was synthesized using the automated robotic synthesis system. Mouse models for brain inflammation were induced by i.p. injection of lipopolysaccharide (LPS). Dynamic and static imaging were performed 24 hr after the tracer injection using micro-PET and p-mode software. Data were expressed as mean \pm SD in SUVmean of the interested regions.

Results: After HPLC purification of the reaction mixture, isolated radiochemical yielded the final formulated product of 0.1% (uncorrected for decay) were obtained in a synthesis time of 150 min. The retention time of [^{18}F]FBAT was 29 min which was consistent with the authentic standard of FBAT. The radiochemical purity was greater than 99%.

Conclusions: A robotic, automated method for [^{18}F]FBAT radiosynthesis is feasible. Sufficient radioactivities of [^{18}F]FBAT could be obtained for non-invasive monitoring iNOS expression in vivo with μPET .

PB017

***In Vivo* Long Lasting Alterations of Meth on Serotonin Transporter Activity and Associated Dopamine Synthesis**

Wen-Sheng Huang¹, Guann-Juh Chen^{2,3}, Tung-Han Tsai², Chen-Yi Cheng⁴,
Chyng-Yann Shiue⁵, Kuo-Hsing Ma, Skye⁶, Hsin-Hsien Yeh⁷

¹*Departments of Nuclear Medicine, Taipei Veterans General Hospital, Taipei, Taiwan*

²*Departments of Neurological Surgery, Tri-Service General Hospital, Taipei, Taiwan*

³*Department of Neurological Surgery, Chiayi Branch, Taichung Veterans General Hospital, Chiayi, Taiwan*

⁴*Departments of Nuclear Medicine, Tri-Service General Hospital, Taipei, Taiwan*

⁵*Department of Nuclear Medicine, National Taiwan University Hospital, Taipei, Taiwan*

⁶*Department of Anatomy and Biology, National Defense Medical Center, Taipei, Taiwan*

⁷*Brain Research Center, National Yang-Ming University, Taipei, Taiwan*

Purpose: Reduced availability of serotonin transporters (SERTs) is a primary pathomechanism of serotonergic neurotoxicity for methamphetamine (METH) users. Advanced neuroimaging techniques such as positron emission tomography (PET) using N,N-dimethyl-2-(2-amino-4-[¹⁸F]-fluorophenylthio) benzylamine (4-[¹⁸F]-ADAM), which binds to SERTs, allows the *in vivo* examination of SERT density, location, and binding function. We investigated the potential of SERT imaging using PET 4-[¹⁸F]-ADAM in estimating the chronic effect of METH-induced serotonergic neurotoxicity.

Methods: Male rats were subcutaneously treated with 5 or 10 mg/kg METH for four separate administrations at 1-h intervals. 4-[¹⁸F]-ADAM brain imaging and the specific uptake ratios (SURs) of 4-[¹⁸F]-ADAM were measured 30 days after METH treatment using an animal PET.

Results: In contrast to controls, the SURs of 4-[¹⁸F]-ADAM were significantly reduced in a dose-dependent manner in the midbrain followed by hypothalamus, thalamus, striatum, hippocampus, and frontal cortex. The toxic effects on the varied brain regions were assessed by measuring monoamine levels and tyrosine hydroxylase (TH) immunocytochemistry, which are associated with SERT activity. A significant decrease of the TH immunostaining and integrated optical density (IOD) ratios were seen in the caudate, putamen, and nucleus accumbens, substantia nigra pars compacta, and substantia nigra pars reticulata in the METH-treated rats.

Conclusions: Taken together, the PET 4-[¹⁸F]-ADAM imaging could be suitable for evaluating METH-induced serotonergic neurotoxicity and monitoring withdrawal management and treatment of drug addiction.

PB018

壁報論文發表摘要·基礎組

Using I-123 Single Photon Angiography to Investigate the Effects of Different doses of Potassium Iodide on Thyroid Gland in Rats

Wen-Sheng Huang¹, Kang-Wei Chang², Chiang Hsuan Lee³, Yu-An Chen⁴

¹Taipei Veterans General Hospital, Department of Nuclear Medicine, Taipei, Taiwan

²Taipei Medical University Office of Research Development laboratory Animal Center, Taiwan

³Department of Nuclear Medicine, Chi Mei Medical Center, Tainan, Taiwan

⁴Yuanpei University of Medical Technology, Department of Health and Leisure Management, Taiwan

Introduction: In recent years, the incidence of thyroid abnormalities has increased, which may be related to the intake of iodine-containing foods such as kelp. Especially iodine is one of the most important components in the synthesis of thyroid hormones. Therefore, this experiment is designed to using I123 single photon angiography to investigate the thyroid functions of rat after feeding different doses of potassium iodide.

Methods: 9 Rats were randomly divided into three groups and fed with 25 ug/kg (Low dosage, LD), 166.7 ug/kg (middle dosage, MD), 500.1 ug/kg (high dosage, HD) potassium iodide. In the next day, we took 1.5 c.c. blood from tail vein for T3, T4 and TSH analysis, then inject I123 (0.5 mCi) into tail vein to perform single photon angiography.

Results: After the administration of potassium iodide in rats, the results of I123 single photon angiography showed a trend of decreased thyroid iodine uptake in the rat thyroid. The results of blood analysis showed that the change in T3 was 18.4% (LD), 15% (MD), 2.5% (HD) under different doses of potassium iodide, and the change in T4 was 17.3% (LD), 34.7% (MD), 25.4% (HD), the change in TSH is 128.2% (LD), 160.8% (MD), 8.7% (HD).

Conclusions: Preliminary results show that I123 single photon imaging can detect changes in thyroid iodine intake. Different doses of potassium iodide have different effects on the changes of thyroid hormone. However, due to the small number of experimental animals, T4 and TSH show a large variation, and the degree of thyroid hormone changes after feeding potassium iodide for a period is unknown. Therefore, the changes of thyroid function still need further experimentation to confirm the discussion.

PB019

慢性腦缺血失智動物模式建立與保護劑評估

黃文盛¹ 郭諭燁¹ 李怡萱^{2*}

¹ 臺北榮民總醫院核醫部

² 國立陽明大學生理學研究所

背景介紹：慢性腦灌流不足 (Chronic Cerebral Hypoperfusion, CCH) 為一漸進缺血性腦傷，初期無症狀而被忽略，但為血管性認知障礙及失智症 (Vascular Cognitive Impairment and Dementia, VCID) 的主要病因之一。臨床腦影像發現慢性腦灌流不足會導致腦白質受損與去髓鞘化，但機制不明。本研究旨在建立慢性腦缺血失智症動物模式與療效作為未來核醫分子影像機制探討可能性。

方法：施予短暫缺氧合併單側總頸動脈永久性結紮 (Hypoxia-sensitized Common Carotid Artery Occlusion, 簡稱 HUCCAO) 並以 KBP51 抑制劑 SaFit2 在 HUCCAO 術後第 0 天起每天鼻腔投予 SaFit2 一次，連續七天，之後評估實驗鼠對自發性活動力、新穎事物認知及空間學習記憶行為 (Barnes Maze test) 辨識能力，最後犧牲動物進行腦組織固定切片及免疫染色，檢視其腦白質胼胝體神經軸突蘭氏結完整性及神經膠細胞活化情形。

結果：大鼠術後一週即表現出自發性活動力減少及新穎事物認知能力受損的現象，此急性期的磁振影像和大腦活細胞染色皆無大腦梗塞病灶，而在一週後出現大腦白質的胼胝體與扣帶區在微結構呈現明顯髓鞘受損，並有髓鞘蛋白 MBP 與軸突蛋白 GAP43 表現降低等白質損傷特徵，但神經發炎相關蛋白和基因如 IL6, TNF α , COX2, iNOS 等表達則不明顯，且似乎有髓鞘再生的現象。術後連續七天鼻腔投予 SaFit2 可改善 HUCCAO 造成胼胝體蘭氏結減少的髓鞘受損，並有改善新物體辨識記憶功能的趨勢，對星狀膠細胞活化則無明顯影響。

結論：以 HUCCAO 方式可作為評估 CCH 導致白質損傷及其造成之 VCID 的快速模式平台，可應用於評估具療效白質損傷潛力的藥物，而星狀膠細胞活化誘發神經發炎現象似乎不是其主要機轉。

PB020

壁報論文發表摘要·基礎組

Technetium Tc-99m TRODAT-1 放射化學純度之品質管理與異常事件分析

林欣蕓 張文議 吳元鍾 黃文盛

臺北榮民總醫院核子醫學部

背景介紹：Tc-99m TRODAT-1 為使用於紋狀體區突觸前神經末梢處之多巴胺轉運體之標示，臨床為診斷巴金森症候群與多巴胺轉運體相關神經疾病的重要檢查依據。Tc-99m TRODAT-1 的調製需使用新鮮銻 -99m 淘洗液標幟商業套組 TRODAT-1 kit，於 121°C 加熱 30 分鐘，經放射化學純度分析 (Radiochemical purity, RCP) 合格後調劑。本研究為調劑後放化純度低於 90% 異常事件與後續追蹤。

方法：調製 Tc-99m TRODAT-1 為使用孳生器淘洗之新鮮銻 -99m 溶液與商業套組進行標幟，並監測 RCP 值。異常事件發生當日調製兩批次 Tc-99m TRODAT-1，且 RCP 均 > 90%，但臨床反應病患影像異常，請藥師再次確認藥品 RCP，兩批次藥物經 6~8 小時後 RCP 分別為 43% 與 97%，結果顯示其中一瓶藥物可能有解離現象。隔日調製新一批藥物之 RCP 為 60%，該批藥物不供臨床使用，且該批號套組不再使用，並通報廠商。與廠商更換套組批號後，持續監測 RCP，並提升調劑條件，原調劑條件為，孳生器必須在淘洗前 24 小時內曾經淘洗過，淘洗出之銻 -99m 淘洗液必須在 6 小時內使用，更改為淘洗出之淘洗液在 30 分鐘內使用，並追蹤結果。

結果：原條件之 RCP 自 2017 年起平均為 95.7% (n = 32)，異常事件發生批號的套組平均 RCP 為 80.3% (n = 6)，更換套組批號及提升調劑條件後之 RCP 為 95.8% (n = 20)。

結論：原調製作業按照標準作業程序，歷年之放射化學純度分析均為穩定狀態，本次發生異常事件之批號套組其調製 RCP 並非全部未達標準 (> 90%)，推測可能為藥廠生產套組時凍晶充填不均或 TRODAT-1 kit 純度不夠所致。調劑 Tc-99m TRODAT-1 需要新鮮淘洗之銻 -99m 溶液，於此次異常事件後變更標準作業程序，以提升放射藥品之品質與穩定性。

PB021

Automated Nucleophilic [^{18}F]FDOPA Production with TracerLab MxFDG Synthesiser: A 3-Year Experience at NTUH

Chia-Ling Tsai¹, Ya-Yao Huang¹, Ching-Hung Chiu¹,
Chyng-Yann Shiue¹⁻³, Ruoh-Fang Yen^{1,2}

¹PET Center, Department of Nuclear Medicine, National Taiwan University Hospital, Taipei, Taiwan

²Molecular Imaging Center, National Taiwan University, Taipei, Taiwan

³PET Center, Department of Nuclear Medicine, Tri-Service General Hospital, Taipei, Taiwan

Introduction: In order to satisfy our increasing need for [^{18}F]FDOPA clinical oncological and neurological demand, in 2016 we successfully implemented Martin's method on TracerLab MxFDG module, using disposable cassettes. The aim of this study was to summarize over 3 years, 90 syntheses experience of nucleophilic [^{18}F]FDOPA production at NTUH.

Methods: Briefly, radiofluorination of (S)-N-Trityl-5-formyl-4-methoxy-methylene-2-nitro-phenyl-alanine tert-butyl ester with [^{18}F]TBAF in DMSO at 130°C for ~8 min followed by trapped on C18ec SPE cartridge and oxidized with *m*-CPBA at 55-65°C for 16 min, then hydrolyzed with 30% HCl/EtOH at 50°C for 20 min. The mixture was diluted with phosphate buffer and then passed through HR-P and Plus C18 SPE cartridges. Further the mixture was passed through WAX and AI-N light SPE cartridge and [^{18}F]FDOPA was produced. Quality control tests of [^{18}F]FDOPA were in agreement to USP requirements and specifications established by our site according to literature.

Results: A total of 90 [^{18}F]FDOPA syntheses were performed from March 2016 to Aug 2019. The radiochemical yield (RCY) of [^{18}F]FDOPA was $7.9 \pm 2.5\%$ ($n = 90$) with synthesis time of about 100 min. Based on HPLC measurement of produced [^{18}F]FDOPA, the radiochemical purity was $97.9 \pm 1.6\%$ and the specific activity was $98918.2 \pm 658687.6 \mu\text{Ci}/\mu\text{g}$. The residual [^{18}F]Fluoride content was $0.4 \pm 0.4\%$ from radio-TLC measurement.

Conclusions: In our experience the automated synthesis of [^{18}F]FDOPA performs reliably with a relatively low incident of failures. Our method achieved a consistent and reliable [^{18}F]FDOPA production with USP-compliant quality. Moreover, there was minimal operator intervention and radiation exposure.

PB022

肝纖維化早期診斷分子影像探針之開發

陳俊堂 彭正良 夏建忠

行政院原子能委員會核能研究所

背景介紹：肝臟穿刺切片為肝纖維化診斷的黃金標準方法，但其為侵入式檢查，有出血等併發症的風險，且容易有取樣誤差；然而，傳統影像學的檢查（腹部超音波、電腦斷層掃描或是核磁共振成像）對於早期肝纖維化的診斷率低，臨床應用上仍有相當大的限制。核子醫學分子影像的應用在功能檢測和分子影像方面具有強大的優勢，可提供細胞分子層次的變化。肝纖維化的病理過程中，肝臟星狀細胞的活化與增生扮演重要的角色，因此，發展活化肝臟星狀細胞的分子影像探針有助於早期肝纖維化之診斷。目前已經有許多研究發現活化肝臟星狀細胞的生物標記，且有指出腎素-血管收縮系統 (Renin Angiotensin System) 和肝纖維化相關。肝臟星狀細胞藉由 Angiotensin II (Ang II) 活化 AT1 受體造成細胞收縮與增生，並增加第一型膠原蛋白 (Collagen I) 與轉化生長因子 (TGF- β) 之表現。

目的：發展肝纖維化早期診斷分子影像探針之體外測試平台，建立活化的人類肝臟星狀細胞之細胞模式，測試 AT1 受體拮抗劑 Saralasin 是否有潛力可作為肝纖維化早期診斷分子影像探針之配體。

方法：利用人類肝臟星狀細胞 LX-2 作為細胞模式。首先，細胞以 Ang II 處理後，以 MTT 試驗計算活細胞數目，評估細胞的增生率；再以西方墨點法分析細胞活化標誌的蛋白表現量。接著，細胞以 Saralasin 處理後，以 MTT 試驗計算細胞的存活率，評估 Saralasin 對細胞的毒性。最後，細胞經 Ang II 活化後，在以螢光鍵結的 Saralasin (FITC-Saralasin) 進行作用，並以流式細胞儀、螢光微孔盤分析儀，評估肝臟星狀細胞的活化對 Saralasin 結合力與結合總量之影響。

結果：細胞增生和西方墨點實驗結果顯示，肝臟星狀細胞受到 Ang II 刺激活化後，細胞數、TGF- β 、AT1 受體之蛋白表現量顯著增加，顯示細胞經 Ang II 處理後，細胞大量增生並活化。Saralasin 之細胞毒性測試結果顯示，Saralasin 濃度在 1 mg/mL 以下，不會造成顯著的細胞毒性。流式細胞儀和螢光微孔分析儀的測試結果發現，肝臟星狀細胞的活化雖然不會增加細胞對 Saralasin 之結合力，但是細胞活化後，因細胞大量增生，造成細胞對 Saralasin 之結合總量增加約 1.5 倍。

結論：Saralasin 雖然不是理想的活化肝臟星狀細胞之配體，但本研究成功建立活化的人類肝臟星狀細胞模式，可作為肝纖維化早期診斷分子影像探針之測試平台，未來可將有潛力的配體，搭配螯合劑與放射性同位素，利用強大的核子醫學影像技術，開發肝纖維化早期診斷之非侵入式分子影像探針。

PB023

Automated Production of [^{18}F]NaF with EP Monograph-Compliant Specification

Hsiang-Ping Wen¹, Wei-Hua Kuo¹, Ya-Yao Huang¹, Yu-Rou Yu¹, Yu-Ning Chang¹,
Chia-Ling Tsai¹, Chin-Hung Chiu¹, Chyng-Yann Shiue^{1,3}, Ruoh-Fang Yen^{1,2}

¹*PET Center, Department of Nuclear Medicine, National Taiwan University Hospital*

²*Molecular Imaging Center, National Taiwan University*

³*PET Center, Department of Nuclear Medicine, Tri-Service General Hospital, Taipei, Taiwan*

Introduction: [^{18}F]Sodium fluoride ([^{18}F]NaF) is a high sensitive bone-seeking PET radiopharmaceutical. With $^{99\text{m}}\text{Tc}$ supply around the world is gradually become a crisis due to the shortage of ^{99}Mo -source material, the clinical use of [^{18}F]NaF keeps increasing worldwide. The aim of this study was to validate automated [^{18}F]NaF production with pharmaceutical-grade cassette/reagent kits and FASTlab-2 module. In addition, stability of our produced [^{18}F]NaF injection was further confirmed based on related monograph of European Pharmacopeia (EP).

Method: In this study, [^{18}F]NaF will be radiosynthesized with a cassette-type FASTlab module. Briefly, the [^{18}F]Fluoride trapped on the QMA cartridge was rinsed with the water for injection and then eluted from the QMA cartridge using the 0.9% sodium chloride solution. After transfer and sterile filtration, [^{18}F]NaF injection was obtained and was ready for following QC tests. All QC tests were performed based on EP monograph.

Results: Automated GMP-compliant production of [^{18}F]NaF were successfully validated, resulting in radiochemical yield of $86 \pm 2\%$ (EOS) within 6 ± 0 min ($n = 3$) of synthesis time. For on-site produced [^{18}F]NaF injection at NTUH, all QC criteria listed in EP were fully satisfied. Particularly, radiochemical purity of [^{18}F]NaF was $> 98.5\%$ (EOS, $n = 3$). At periodic times over the 8 hours, the product was measured for radiochemical purity using analytical HPLC.

Conclusion: In this study, we have successfully validated the automated production of [^{18}F]NaF with newly developed pharmaceutical grade cassette/reagent kits and FASTlab-2 module. The use of disposable cassette and cartridge purification significantly simplifies the operation. Finally, the final [^{18}F]NaF injection of NTUH has been prove to meet all of the quality criteria based on the EP monograph of [^{18}F]NaF entitled as “Sodium Fluoride (^{18}F) injection” (No. 2100).

PB024

Characterization and In Vivo Tracking of Mesenchymal Stem Cells Derived Extracellular Vesicles

Cheng-Hsiu Lu¹, Chien-Chih Ke^{1,2}, Yi-An Chen³,
Chao-Cheng Chen¹, Ren-Shyan Liu^{1,2,3,4}

¹Department of Biomedical Imaging and Radiological Sciences, National Yang-Ming University, Taipei, Taiwan

²Biomedical Imaging Research Center, National Yang-Ming University, Taipei, Taiwan

³Institute of Clinical Medicine, National Yang-Ming University, Taipei, Taiwan

⁴Department of Nuclear Medicine and National PET/Cyclotron Center, Taipei Veterans General Hospital, Taipei, Taiwan

Introduction: Mesenchymal stem cells (MSCs) are multipotent stromal cells which show the great potential in tissue engineering, regenerative medicine and the treatment of various diseases. Deep into mechanisms, paracrine effect has been reported to be the major role in MSC therapy.

Further, extracellular vesicles (EVs) are reportedly the major player mediating the therapeutic and paracrine effects of MSCs. With the rapid increase of attention and being of great potential as a future medical regimen for human disease, the information of fate and behavior of EVs in the living subject should be urgently gathered. However, investigators still have not developed an effective method to monitor the in vivo behavior of EVs. Therefore, here in our study, EVs derived from Wharton's jelly MSCs were isolated, characterized and radiolabeled with ¹¹¹In-oxine followed by biodistribution study and in vivo SPECT/CT imaging.

Methods: Conditioned medium was collected followed by exosome isolation using Exo-Prep kit (Hansa BioMed) followed by purification with PD-10 columns and 100 kDa concentration. Expression of EVs specific proteins CD9, CD63 and HSP70 was verified by western blot. Morphology and size were characterized by transmission electron microscopy (TEM) nanoparticle tracking analysis (NTA). For radiolabeling, EVs were incubated with ¹¹¹In-oxine in PBS at 37°C for 1 hr followed by purification and further characterization. Biodistribution and in vivo SPECT/CT imaging of ¹¹¹In-oxine- labeled EVs were performed at 1, 3, 6, 24 hr after intravenous injection into C57BL/6 mice.

Results: CD9 and CD63 expression were observed on EVs as well as ¹¹¹In-oxine-EVs. Radiochemical purity of ¹¹¹In-oxine-EVs as higher than 90% and remained stable for at least 48 hours. Result of biodistribution showed that ¹¹¹In-oxine-labeled EVs accumulated in liver, spleen, bone, and cleared rapidly from the circulation. In vivo SPECT/CT imaging of ¹¹¹In-oxine-labeled EVs showed high accumulation in liver, spleen and kidney, but less in circulation.

Summary/Conclusion: In this study, we have preliminarily demonstrated the feasibility of in vivo tracking of MSC- derived EVs labeled with ¹¹¹In-oxine. Further investigation is still needed and underway to monitor the in vivo fate and behavior of EVs.

PB025

The Efficacy of Biodegradable Drug Delivery System Contained with Diclofenac for the Treatment of Local Osteoarthritis

Ping-Fang Chiang, Ming-Cheng Chang, Cheng-Lian Peng,
Mao-Feng Weng, Ying-Hsia Shih, Yu-Jen Kuo

Isotope Application Division, Institute of Nuclear Energy Research, Taoyuan 325, Taiwan

Introduction: The purpose of this study is to develop biodegradable drug carriers which contained diclofenac therapy for osteoarthritis. By locally and slowly release of diclofenac, it can be extended the effect of local osteoarthritis treatment and reduced side effects.

Methods: In the experiment, two different kinds of drug delivery system were used, one was microparticles and the other was micelles. We used biodegradable and biocompatible polymer Poly(D,L-lactide-co-glycolide) (PLGA) to prepare microparticles through w/o/w double emulsion and the micelles were prepared by lyophilization-rehydration method with a diblock methoxypoly(ethylene glycol)-poly(caprolactone) (mPEG-PCL) copolymer. Due to the much lower encapsulation efficiency of PLGA microspheres, mPEG-PCL micelles were used for drug slow release study and evaluation of treatment efficacy in animal models of arthritis.

Results: The *in vitro* release profile indicated a sustained release manner of diclofenac from the micelles. Meanwhile, *in vivo* therapeutic effect of arthritis animals was evaluated by direct injection of the micelles contained with diclofenac via the ankle joint. The degree of swelling of the joints was measured by four weeks, and the inflammatory state was confirmed by NanoSPECT/CT images in the second and fourth week. The drug micelles do indeed have an effect of suppresses joint inflammation in murine models of acute arthritis.

Conclusions: These results suggest a great potential of the biodegradable micelles as a locally intra-articular injection drug delivery system to improve the bioavailability of the drugs.

PB026

壁報論文發表摘要·基礎組

表面修飾放射性金屬之甲殼素微球體開發 及於荷肝腫瘤動物之生物特性評估

李庚穎¹ 詹惠雯² 李佳哲² 張文議¹ 張智偉¹ 陳昭政² 張鐙元²
陳至豪¹ 黃文盛¹ 王信二²

¹ 台北榮民總醫院核子醫學部正子中心
² 國立陽明大學生物醫學影像暨放射科學系

背景介紹：經肝動脈放射栓塞治療 (transarterial radioembolization, TARE) 被廣泛用於治療無法接受切除手術的肝癌病患。本研究開發放射性金屬修飾的甲殼素微球體 ($^{111}\text{In}/^{177}\text{Lu}$ -DTPA-CMS)，可作為治療肝腫瘤之放射性栓塞製劑。本研究製備 ^{111}In -DTPA-CMS 作為 ^{177}Lu -DTPA-CMS 的放射性替代物，並於荷肝腫瘤大鼠進行其生物特性評估。

方法：甲殼素溶液經乳化交聯反應及篩網 (44 μm 和 25 μm) 二次過濾可製得甲殼素微球體 (CMS)。於 CMS 表面修飾 p-SCN-Bn-DTPA 再標誌 In-111 後獲得具高放射化學產率及純度 (均 > 98%) 的 ^{111}In -DTPA-CMS。分析 ^{111}In -DTPA-CMS 物化特性及體內外穩定度，並於荷原位肝腫瘤 N1-S1 大鼠動物模式進行生物分布及分子造影。

結果：本研究開發之 DTPA-CMS 平均粒徑為 $36.9 \pm 4.9 \mu\text{m}$ ，適用於肝腫瘤放射栓塞治療。將 ^{111}In -DTPA-CMS 置於磷酸鹽緩衝液 (4°C) 及胎牛血清 (37°C) 4 天後，放射化學純度仍維持 > 90%，顯示具有良好體外穩定度。於正常 SD 大鼠經尾靜脈注射 ^{111}In -DTPA-CMS 後進行 SPECT/CT 造影。結果顯示放射活性主要積聚於肺臟，並持續至少 72 小時，顯示體內安定性甚佳。荷原位肝腫瘤大鼠，經肝動脈注射 ^{111}In -DTPA-CMS 後的生物分布結果顯示，大多數放射活性都積聚在肝腫瘤及肝臟中。注射後 24 及 72 小時，肝腫瘤積聚活度從 $12.12 \pm 5.48 \text{ \%ID/g}$ 緩慢降至 $11.78 \pm 2.2 \text{ \%ID/g}$ 。除肝臟外，其他所有正常器官之積聚量均低於 1 \%ID/g 。SPECT/CT 造影結果亦顯示，注射後 72 小時內 ^{111}In -DTPA-CMS 主要積聚於肝腫瘤及部份正常肝葉，與生物分布試驗結果一致。

結論：本研究製備表面修飾放射性金屬之甲殼素凝膠微球體 (^{111}In -DTPA-CMS) 具良好體內外安定性，動物實驗結果指出其於肝腫瘤有高量的積聚，顯示 $^{111}\text{In}/^{177}\text{Lu}$ -DTPA-CMS 具有發展為肝腫瘤栓塞放射治療製劑的潛力。

PB027

Using I123 Single Photon Angiography to Investigate the Effects of Different doses of Potassium Iodide on Thyroid Gland in Rats

Yu-An Chen^{1,3}, Kang-Wei Chang², Wen-Sheng Huang³

¹*Yuanpei University of Medical Technology, Department of Health and Leisure Management, Taiwan*

²*Taipei Medical University Office of Research Development laboratory Animal Center, Taiwan*

³*Taipei Veterans General Hospital, Department of Nuclear Medicine, Taipei, Taiwan*

Introduction: In recent years, the incidence of thyroid abnormalities has increased, which may be related to the intake of iodine-containing foods such as kelp. Especially iodine is one of the most important components in the synthesis of thyroid hormones. Therefore, this experiment is designed to using I123 single photon angiography to investigate the thyroid functions of rat after feeding different doses of potassium iodide.

Methods: 9 Rats were randomly divided into three groups and fed with 25 ug/kg (Low dosage, LD), 166.7 ug/kg (middle dosage, MD), 500.1 ug/kg (high dosage, HD) potassium iodide. In the next day, we took 1.5 c.c. blood from tail vein for T3, T4 and TSH analysis, then inject I123 (0.5 mCi) into tail vein to perform single photon angiography.

Results: After the administration of potassium iodide in rats, the results of I123 single photon angiography showed a trend of decreased thyroid iodine uptake in the rat thyroid. The results of blood analysis showed that the change in T3 was 18.4% (LD), 15% (MD), 2.5% (HD) under different doses of potassium iodide, and the change in T4 was 17.3% (LD), 34.7% (MD), 25.4% (HD), the change in TSH is 128.2% (LD), 160.8% (MD), 8.7% (HD).

Conclusions: Preliminary results show that I123 single photon imaging can detect changes in thyroid iodine intake. Different doses of potassium iodide have different effects on the changes of thyroid hormone. However, due to the small number of experimental animals, T4 and TSH show a large variation, and the degree of thyroid hormone changes after feeding potassium iodide for a period is unknown. Therefore, the changes of thyroid function still need further experimentation to confirm the discussion.

PB028

Study of ^{18}F -FP-(+)-DTBZ (^{18}F -AV-133) PET Imaging in Parkinson's Disease of with Different Sides of Symptom Onset

Ying-Chi Liao¹, Kun-Ju Lin^{1,2}, Yi-Hsin Weng³, Ing-Tsung Hsiao^{1,2}

¹Dept of Medical Imaging and Radiological Science, Chang-Gung University, Taoyuan, Taiwan

²Dept of Nuclear Medicine, Chang-Gung Memorial Hospital at Linko, Taoyuan, Taiwan

³Dept of Neurology, Chang-Gung Memorial Hospital at Linko, Taoyuan, Taiwan

Introduction: Parkinson's disease is a neurodegenerative disease, characterized by dopaminergic neuron loss. ^{18}F -AV-133 is a positron emission tomography (PET) radiotracer targeting the vesicular monoamine transporter type 2 (VMAT2) to detect the reduction of monoaminergic terminal in PD patients. The aim of this study is to investigate the degree of VMAT2 reduction in PD patients of different severity and with different side of symptom onset.

Method: Retrospective ^{18}F -AV-133 PET scans from 70 subjects of 35 left onset (LO) PD and 35 right onset (RO) PD were included in this study. According to the H&Y stage, patients were divided into mild, moderate, and severe group. The standardized uptake value (SUV) and standardized uptake value ratio (SUVR) were calculated using PMOD software. Two sample t-test were used to compare the VMAT2 uptake in different severity group of patients.

Results: In RO PD, there were significant SUVR difference between mild and moderate group, mild and severe group in the regions of caudate ($t = 5.30$, $p < 0.0001$), anterior putamen ($t = 4.45$, $p = 0.0002$), posterior putamen ($t = 4.08$, $p = 0.0005$) and accumbens ($t = 4.60$, $p = 0.0001$). But there was no significant difference between moderate and severe group. In addition, the SUVR of amygdala and hippocampus in the moderate group was higher than those in the mild group. This phenomenon was only found for the LO PD patients.

Conclusion: In mild group, the SUVR in RO PD were significant larger than LO PD in every region. However, in moderate group, the SUVR of accumbens in LO PD was significant larger than RO PD. The future work will focus on using voxelwise analysis to find out spatial distribution of dopaminergic neuron.

PB029

Identification of EMT-derived Cancer Cells and Metastatic CTCs by Using Twist Promoter-driven Reporter Gene

Min-Tzu Ku^{1,4}, Cheau-Ling Ho¹, Luen Hwu², Ren-Shyan Liu^{1,2,3,4*}

¹Department of biomedical imaging and radiological science, National Yang-Ming University, Taipei, Taiwan

²Molecular and Genetic Imaging Core/Taiwan Mouse Clinic, National Comprehensive Mouse Phenotyping and Drug Testing Center, Taipei, Taiwan

³National PET/Cyclotron Center and Department of Nuclear Medicine, Taipei Veterans General Hospital, Taipei, Taiwan

⁴PET/Cyclotron Center and Department of Nuclear Medicine, Cheng Hsin General Hospital, Taipei, Taiwan

Introduction: Epithelial-to-mesenchymal transition (EMT) plays a crucial role in the invasion and metastasis of malignant tumors, which promotes the tumor cells to enter circulation systems and form circulating tumor cells (CTCs). According to the previous studies, overexpression of Twist induces EMT and increase the ability of cancer metastasis and invasion. In order to track this EMT-derived cancer cells, our study transfected SAS head and neck squamous carcinomas cells (HNSCC) with a dual reporter gene (E2-Crimson-P2A::ttksr39) under the control of Twist promoter to characterize the EMT-derived cancer cells.

Methods: Twist promoter was generated from the human genomic DNA by polymerase chain reaction (PCR), and then we established a reporter construct pTwist-E2-Crimson-P2A::ttksr39 and pCMV-E2-Crimson-P2A::ttksr39. We use SAS cells to establish stable clones which express reporter gene. After hypoxia induction, laser confocal microscope and ³H-FEAU uptake were used to detect EMT cells by reporter gene system. In tumor xenograft animal model, we gave an appropriate dose of anti-cancer drug to induce CTCs enrichment and it was observed by IVIS 50 and microPET/CT.

Results: After hypoxia induction, Twist promoter activities overexpressed and could be observed by E2-Crimson (red fluorescent protein) laser confocal microscope, and ³H-FEAU uptake was 2 fold higher than control group in in vitro studies. In animal model, using an appropriate dose of anti-cancer drug to induce CTCs enrichment is workable and can be observed by IVIS 50 and microPET/CT but still need modification to improve the efficiency of detection.

Conclusions: This preliminary results showed that using this Twist reporter gene system is able to detect EMT-derived cells in head and neck cancer - SAS cell line. After induction with an appropriate dose of anti-cancer drug, EMT-derived cells of the tumors can be detected both in vivo and in the blood of mice.

PB030

The Radiosynthesis of [¹⁸F]FEPPA by Eckert-Ziegler Modular-Lab System

Chi-Wei Chang, Chun-Tse Hung, Geng-Ying Li, Shih-Pei Chen,
Wen-Yi Chang, Wen-Sheng Hwang

Department of Nuclear Medicine, National PET/Cyclotron Center, Veterans General Hospital, Taipei, Taiwan

Introduction: A novel [¹⁸F]-radiolabelled phenoxyanilide, [¹⁸F]FEPPA, has been synthesized and evaluated as a potential positron emission tomography imaging agent for the peripheral benzodiazepine receptor (PBR) in our center. [¹⁸F]FEPPA was used for animal imaging study by using microPET/MR in our center. Reliable procedure of [¹⁸F]FEPPA in cGMP conditions was developed by Modular-Lab system.

Methods: For the radiosynthesis, cyclotron-produced [¹⁸F]fluoride (¹⁸O(p,n)¹⁸F) was transferred to the Modular-Lab system and fixed on a QMA cartridge. The activity was eluted from the cartridge with 1.1 mL of a potassium carbonate (12 mg/mL water) and Kryptofix (12.5 mg/mL acetonitrile) solution in water /acetonitrile 1/4 and transferred to the reactor by nitrogen. The complex was azeotropically dried at 120°C by addition of 1.6 mL of acetonitrile. After complete drying, 5 mg of the FEPPA tosylate precursor in 0.6 mL of acetonitrile was added to the activated and dried [¹⁸F]fluoride/K2.2.2 complex and the reaction vessel was heated at 80°C for 10 min. The reaction was quenched with 2 mL of HPLC M.P. (0.5% Phosphoric acid and acetonitrile (1/1)) and the crude product was purified by a semi-preparative HPLC column (YMC-Actus Triart C18 250 X 20 mm I.D S-5 μ m, 12 nm) and eluted with a solution of 0.5% Phosphoric acid and acetonitrile (1/1, flow at 6 mL/min). The fraction containing the product was collected and mixed with 40 mL of water. Subsequently, [¹⁸F]FEPPA was trapped on a pre-conditioned (10 mL ethanol and 20 mL water) tC18plus SepPak cartridge and acetonitrile was washed off by rinsing tC18plus SepPak cartridge with water. The product ([¹⁸F]FEPPA) was eluted with ethanol (0.9 mL) and formulated with normal saline (9 mL).

Results: The sterile [¹⁸F]FEPPA was produced in 80 min with greater than 99% radiochemical purity. The quality control was in accordance to the guidelines of the European Pharmacopoeia with a mean 25% EOS yield and 75 GBq/ μ mol (n = 3).

Conclusions: The routine production of [¹⁸F]FEPPA proved to be reliable and stable. [¹⁸F]FEPPA of the Ph.Eur. quality could be used for clinical study by using PET/MR in the future.

PB031

The Radiosynthesis of [1-¹¹C] Acetate by an Eckert-Ziegler Modular-Lab System

Chi-Wei Chang, Chun-Tse Hung, Geng-Ying Li, Shih-Pei Chen,
Wen-Yi Chang, Wen-Sheng Hwang

Department of Nuclear Medicine, National PET/Cyclotron Center, Veterans General Hospital, Taipei, Taiwan

Introduction: Sodium [1-¹¹C]acetate is the metabolic tracer which regains more and more interest among the oncologists due to its complementary nature to ¹⁸FDG. The catabolic route of acetate is coupled to tricarboxylic acid cycle and is an alternative to the glycolytic pathway of ¹⁸FDG. In our center we have the clinical study for imaging prostate cancer by [1-¹¹C]acetate PET. Reliable and high yield procedure of [1-¹¹C] acetate in cGMP conditions was developed to meet clinical demand by Modular-Lab system.

Methods: [¹¹C]CO₂ was produced by irradiating target gas(N₂+1% O₂)(5.0 N₂ and 5.0 O₂) at 76 Psi target pressure. Beam current 45 μA and current integration 45 μAh were used for routine production of [1-¹¹C]acetate. After irradiation, [¹¹C]CO₂ was trapped in activated charcoal in Modular-Lab system. By heating activated charcoal, [¹¹C]CO₂ was released with a 10 ml/min He and trapped in 1 ml of 0.1 M Magnesium chloride/THF solution. After all [¹¹C]CO₂ was trapped in CH₃MgCl solution, 8 ml of 0.1 M acetic acid was added to quench the reaction. The crude product was passed through Chromafix PS-H⁺ and PS-Ag⁺ and MAXIClean SAX cartridges to the waste. [1-¹¹C]Acetate was retained on MaxiClean SAX cartridge. After rinsing SAX cartridge with water, [1-¹¹C]acetate was washed out by 8 ml of saline through the sterile 0.22 μm filter into the sterile vial equipped with an aeration needle.

Results: The sterile sodium [1-¹¹C]acetate was produced starting from [¹¹C]CO₂ in accordance with criteria of European Pharmacopoeia in 17 min with a mean 50% EOS yield (decay uncorrected).

Conclusions: The production of [1-¹¹C]acetate proved to be reliable in more than 180 times. The procedure provides stable radiochemical yields (50% EOS) of sodium [1-¹¹C] acetate) of the European Pharmacopoeia quality in a short synthesis time (17 min).

PB032

壁報論文發表摘要·基礎組

The Radiosynthesis of [¹¹C]PIB by an Eckert-Ziegler Modular-Lab System

Chi-Wei Chang, Chun-Tse Hung, Geng-Ying Li, Shih-Pei Chen,
Wen-Yi Chang, Wen-Sheng Hwang

Department of Nuclear Medicine, National PET/Cyclotron Center, Veterans General Hospital, Taipei, Taiwan

Introduction: N-methyl-[¹¹C]2-(4'-methylaminophenyl)-6-hydroxybenzo-thiazole([¹¹C]PIB), has been introduced as a highly promising radiotracer for imaging amyloid plaques using positron emission tomography (PET). A large number of [¹¹C]PIB have been synthesized by an Eckert-Ziegler modular system for animal and clinical PET studies in our center. Reliable synthesis procedure of [¹¹C]PIB in cGMP conditions was developed to meet clinical demand by Modular-Lab system.

Methods: [¹¹C]CO₂ was produced by irradiating target gas(N₂+1% O₂)(5.0 N₂ and 5.0 O₂) at 76 Psi target pressure. Beam current 45 μA and current integration 68 μAh were used for routine production of [¹¹C]PIB. After irradiation, [¹¹C]CO₂ was trapped in an activated charcoal. By heating activated charcoal to 60°C, [¹¹C]CO₂ was released through the hydrogenation tube (620°C, He/10% H₂ flow 150 ml/min) into [¹¹C]CH₄ trap (-10°C). After complete trapping of [¹¹C]CH₄ activity, the trap was heated to 90°C and the recirculation system was evacuated by a vacuum pump simultaneously. At 60°C, [¹¹C]CH₄ trap was connected to the evacuated recirculation system and [¹¹C]CH₄ was transferred into the recirculation system with a He flow (50 ml/min). The transfer stopped at the pressure of 0.4 bar within the recirculation system and the recirculation started. The temperature of the bromination oven was set at 640°C and 660°C with the interval of 60 sec. The recirculation was stopped when [¹¹C]CH₃Br was fully trapped in [¹¹C]CH₃Br trap. [¹¹C]CH₃Br was released from [¹¹C]CH₃Br trap at 90°C, by He flow (10 ml/min) and passed through AgOTf/carbograph glass tube (290°C). [¹¹C]CH₃OTf was swept into the HPLC loop coated with precursor solution by a stream of He gas (10 ml/min) at ambient temperature and produced [¹¹C]PIB. When the activity peaked in the loop, the flow of He was stopped and permitted the reaction to proceed for 60s, and then 1.5 ml of HPLC mobile phase (0.01M H₃PO₄/CH₃CN, 3/2) was filled into the LC sample loop. The mobile phase containing raw [¹¹C]PIB were injected into the HPLC column (LUNA 5μ C18 250 X 10 mm, Phenomenex). The fraction containing the product was collected and mixed with 40 mL of water. Subsequently, [¹¹C]PIB was trapped on a pre-conditioned (10 mL ethanol and 20 mL water) tC18plus SepPak cartridge and acetonitrile was washed off by rinsing tC18plus SepPak cartridge with water. The product ([¹¹C]PIB) was eluted with ethanol (0.9 mL) and formulated with normal saline (9 mL).

Results: The sterile [¹¹C]PIB was produced starting from [¹¹C]CO₂ in accordance with requirements of European Pharmacopoeia in 30 min with greater than 99% radiochemical purity and a mean 5% EOS yield (n = 70).

Conclusions: The production of [¹¹C]PIB proved to be reliable in more than 180 patient productions. The procedure provides stable radiochemical yields (5% EOS) of [¹¹C]PIB of the cGMP quality in a short synthesis time (30 min).

PB033

運送短半衰期正子藥物之氣送系統

Chi-Wei Chang, Chun-Tse Hung, Geng-Ying Li, Shih-Pei Chen,
Wen-Yi Chang, Wen-Sheng Hwang

Department of Nuclear Medicine, National PET/Cyclotron Center, Veterans General Hospital, Taipei, Taiwan

Introduction: 由於正子造影檢查用的放射性藥物，其核種半衰期都非常短 (F-18: 110 分鐘，C-11: 20 分鐘，N-13: 10 分鐘，O-15: 2 分鐘)，故需儘快將正子藥物從生產之放射化學實驗室送至注射室，以注射到受檢者體內。大多數正子中心之藥物生產地點 (放射化學實驗室) 與病患受檢地點 (正子中心) 都設在相鄰的區域或者是同一建築物內，但如果兩者設置在不同的建築物內，則藥物的運送會因受到地理位置的限制而衍生運送時間、人力與輻射暴露等問題。

Methods: 由於核醫部的 PET/MR 與 PET/CT 正子造影中心皆設置於本院思源樓一樓，而正子藥物生產地則是在本院正子中心。兩者位於不同的建築物且在不同的樓層，其最短的直線距離約莫有 200 公尺，故參酌本院檢驗部的檢體氣送傳送系統 (翊威公司所代理的荷蘭 Telecom pneumatic tube system) 來建置正子藥物的氣送傳送系統。放射性屏蔽另外請廣陽公司特別設計專屬的氣送筒針劑鉛套筒，以及 PE 材質的針筒固定套組，利用傳送筒每秒 4~8 公尺的傳送速度，傳送於迴旋加速器中心與正子造影中心之間。

Results: 由迴旋加速器中心將正子藥物傳送到正子造影中心花費的時間約莫 20 秒鐘，反過來由正子造影中心回傳到迴旋加速器中心則花費的時間是 40 秒鐘，在相同條件之下，透過人力的方式運送平均所花費的時間則約莫是 5~10 分鐘。

Conclusions: 氣送傳遞系統大幅減少人力傳送時間、減少電梯使用次數、降低人員走動、增加工作空間，同時能有效預防因運送時間而造成藥物活度的損耗，而設計專屬的鉛套筒屏蔽也大幅減少正子藥物在運送時人員的輻射劑量暴露。

PB034

壁報論文發表摘要·基礎組

Novel HDAC Class IIa Selective Radiotracers for PET Imaging of Alzheimer's Disease

Yi-An Chen^{1,3}, Cheng-Hsiu Lu^{2,3}, Chien-Chih Ke^{3,6}, Chi-Wei Chang⁴,
Juri G. Gelovani⁵, Ren-Shyan Liu^{1,2,3,4,7}

¹*Institute of Clinical Medicine, National Yang-Ming University, Taiwan*

²*Department of Biomedical Imaging and Radiological Sciences, National Yang-Ming University, Taiwan*

³*Molecular and Genetic Imaging Core, Taiwan Animal Consortium, Taipei, Taiwan*

⁴*National PET/Cyclotron Center and Department of Nuclear Medicine, Taipei Veterans General Hospital, Taiwan*

⁵*Department of Biomedical Engineering, Wayne State University, Detroit, MI, USA*

⁶*Department of Medical Imaging and Radiological Sciences, Kaohsiung Medical University, Kaohsiung, Taiwan*

⁷*Department of Nuclear Medicine, Cheng Hsin Hospital, Taipei, Taiwan*

Introduction: The clinical symptoms of Alzheimer's disease (AD) include cognitive decline, short-term memory failure, orientation problems and motor abnormalities. Although amyloid- β is considered to play a critical role in AD pathogenesis, epigenetic deregulation is closely associated with synaptic plasticity and memory formation, especially histone deacetylase (HDAC) enzymes. Studies have shown that the level of nuclear HDAC4 is markedly increased in brains of AD patients as well as in AD mouse model. It suggests that HDAC4 may be a promising biomarker for monitoring and prediction of AD progression. Given that HDAC inhibitor treatments restore cognitive performance, novel molecular imaging agents for evaluation of HDACs activity in the brain are urgently needed. This study aims to develop novel HDAC class selective radiotracers, [¹⁸F]TFAHA for monitoring the epigenetic regulation and further to evaluate the therapeutic effect of HDACi treatments on AD.

Methods: To detect the change of brain over time, triple transgenic mouse lines (3xTg-AD) harboring PS1_{M146V}, APP_{Swe}, and tau_{p301L} transgenes and age-matched wild type (WT) mice were used. Each AD mouse and age-matched mouse was injected intravenously with 20 MBq/0.1 ml of [¹⁸F]TFAHA at 8, 11 and 16 month of age. The static images were acquired after injection with the Triumph PET/SPECT/CT imaging scanner (Gamma Medica-Ideas, CA, USA). Regional retention and uptake of these [¹⁸F]TFAHA were processed and analyzed with PMOD 3.5 software package (Pmod Technologies, Zürich, Switzerland).

Results: The uptake of [¹⁸F]TFAHA was higher in 3xTg-AD mice compared with control group at 11 and 16 month of age. The AD-susceptible brain regions were also analyzed. Compared to WT mice, 3xTg-AD mice exhibited significantly higher [¹⁸F]TFAHA uptake in brain regions examined, including hippocampus ($p = 0.0468$), cerebellum ($p = 0.0489$), basal forebrain ($p = 0.0180$), and thalamus ($p = 0.0492$).

Conclusions: The second generation of HDAC class IIa-specific radiotracers, [¹⁸F]TFAHA can be used to distinguish 3xTg-AD mice from wild type mice. It suggests that [¹⁸F]TFAHA PET imaging demonstrates the feasibility in monitoring of AD progression. Further, we anticipate that PET imaging with [¹⁸F]TFAHA can facilitate the development novel HDACs class IIa selective inhibitors for AD therapy.

PB035

探討紋狀體中類澱粉蛋白沉積量 與阿茲海默症疾病嚴重程度的關係

李沛玟¹ 林昆儒² 蕭穎聰^{1,2}

¹長庚大學醫學影像暨放射科學系

²林口長庚醫院核子醫學科

背景介紹：根據以往的研究結果，顯示出類澱粉蛋白 (amyloid- β , A β) 在皮質沉積達一定量後，再增加的量變得不顯著，造成不易判斷疾病嚴重度，無助於臨床上使用，不過有研究發現在紋狀體中類澱粉蛋白的含量還會繼續上升，因此可利用紋狀體來判斷阿茲海默症 (Alzheimer's disease, AD) 疾病的嚴重程度，幫助臨床做出相對應的處理，甚至對疾病做出未來演進的預測。本研究目的是為了找出紋狀體中類澱粉蛋白含量與臨床上嚴重程度的相關性，並且探索是否能夠由此結果來預測發病時間或疾病進程。

方法：使用 50 個臨床判定認知功能正常的受試者 (normal cognition, NC)、50 個臨床判定為輕度認知功能障礙 (mild cognitive impairment, MCI) 的病患以及 50 個臨床判定為 AD 的病患，取得回溯性 AV45 正子掃描造影 (positron emission tomography, PET) 和核磁共振造影 (magnetic resonance imaging, MRI) 影像，再使用 Pmod 軟體進行影像前處理與分析計算。獲得所需要的數據後，根據文獻內容所使用一些統計方法，包括 specificity、sensitivity、accuracy of cognitively impaired versus younger CN 等，找出紋狀體中 A β 含量與疾病嚴重程度的關係。

結果：將受試者的臨床分數 (MMSE、CDR) 分別與皮質和紋狀體中 A β 含量做比較，分析數據後發現紋狀體中 A β 含量與臨床嚴重程度的相關性 ($r = -0.39$) 比皮質區域中 A β 含量與臨床嚴重程度的相關性 ($r = -0.31$) 稍微好一點，但皆與臨床表現有些微相關性。另外，在 MCI 族群中有 38% 的病患其紋狀體的 SUVR 值隨著年紀增加，30% 的病患其皮質的 SUVR 值隨著年紀增加；在 AD 族群中有 59% 的病患其紋狀體的 SUVR 值隨著年紀增加，但只有 40% 的病患其皮質的 SUVR 值隨著年紀增加，所以可以看出確實有較多病患其紋狀體的 SUVR 值隨著年紀而增加。

結論：初步結果發現紋狀體中類澱粉蛋白的含量並沒有明顯跟著疾病嚴重度增加，造成結果不如預期的原因可能為人為圈選感興趣區域產生誤差，或是部分容積效應的影響，導致在計算 SUVR 值時有誤差。另外可能的原因為樣本數量不足，未來將會針對這幾點進行修正。

PB036

壁報論文發表摘要·基礎組

Preclinical Evaluations of a Novel Human Epidermal growth Factor Conjugate on Human Colon Cancer *In Vitro* and *In Vivo*

Mao-Chi Weng¹, Wei-Chuan Hsu¹, Kai-Hung Cheng¹,
Chung-Li Ho¹, Ming-Hsin Li¹, Keng-Li Lan^{2,3}

¹*Institute of Nuclear Energy Research, Taoyuan, Taiwan*

²*Department of Oncology, Taipei Veterans General Hospital, Taipei, Taiwan*

³*Institute of Traditional Medicine, School of Medicine, National Yang-Ming University, Taipei, Taiwan*

Introduction: Epidermal growth factor receptor (EGFR) has been found on multiple cancers, for example, pancreas, colorectal, head and neck, kidney and non-small-cell lung carcinoma. It has also been proved an effective strategy on specific targeting cancer therapy for years. In this research, we have evaluated whether human epidermal growth factor conjugated with albumin binding domain (hEGF-ABD) may provide a novel design of treatment strategies on human colon cancers, *in vitro* and *in vivo*.

Materials and methods: The hEGF-ABD and EGFR related mAb, Erbitux[®], were both radio-labeled with Na¹³¹I; the stability of ¹³¹I-hEGF-ABD in PBS and serum was then analyzed. The binding assay of ¹³¹I-hEGF-ABD and ¹³¹I-Erbitux was evaluated at 10, 20, 30, 40, 50, 60 min, 2, 4, 24 h after incubation with HCT116 cells; the intracellular distribution test of ¹³¹I-hEGF-ABD and ¹³¹I-Erbitux was also investigated by centrifuge. HCT116 cells were incubated with 0.0025, 0.01, 0.04 or 0.16 mCi of free ¹³¹I, ¹³¹I-hEGF-ABD and ¹³¹I-Erbitux for clonogenic assay. The pharmacokinetics in mice was evaluated at 0.5, 1, 2, 4, 8, 24, 48, 72, 96 and 168 h after intravenous (i.v.) injection of ¹³¹I-hEGF-ABD.

Results: The radiochemical purity of ¹³¹I-hEGF-ABD and ¹³¹I-Erbitux was determined > 90% by radio-thin-layer chromatography (TLC); the stability was > 80% at 360 h in serum. The binding of ¹³¹I-hEGF-ABD and ¹³¹I-Erbitux in HCT116 cells was increased within 24 h. The count ratio of 60/10 was 1.52 and 2.17; the count ratio of 24/1 was 1.53 and 1.45, respectively. The intracellular distribution of nucleus/ cytoplasm was 53.01%/46.99% and 8.14%/91.86, respectively. The clonogenic assay showed inhibition on 0.16 mCi groups; the inhibition rate of ¹³¹I-hEGF-ABD was calculated and more significant than ¹³¹I-Erbitux and free ¹³¹I. The pharmacokinetics in mice revealed half-life of ¹³¹I-hEGF-ABD about 27.3 h.

Conclusions: This research has explored the mechanism and effects of human epidermal growth factor conjugated with albumin binding domain (hEGF-ABD) *in vitro* and *in vivo*. The results may provide innovative information for development of treatment strategies on human colon cancers in Taiwan.

PB037

Automatically Synthesis of [^{68}Ga]Macroaggregated Albumin ([^{68}Ga]MAA) with TRACERlab MxFDG Module and a Modified FDG Cassette

Ching-Hung Chiu¹, Ya-Yao Huang¹, Yu-Ning Chang¹, Chi-Lun Ko¹, Ruoh-Fang Yen^{1,2}

¹*PET Center, Department of Nuclear Medicine, National Taiwan University Hospital, Taipei, Taiwan*

²*Molecular Imaging Center, National Taiwan University, Taipei, Taiwan*

Introduction: For pulmonary perfusion imaging agent, [$^{99\text{m}}\text{Tc}$]macroaggregated albumin ([$^{99\text{m}}\text{Tc}$]MAA) SPECT imaging has been used in clinic for a long time. Recently, [^{68}Ga]MAA has been developed for PET/CT imaging in terms of sensitivity, resolution and quantification. In order to fit preclinical and clinical need in near future, we have developed and setup the automated synthetic procedure of [^{68}Ga]MAA with commercial TRACERlab MXFDG module and a modified FDG cassette.

Methods: [^{68}Ga]MAA was automated produced with TRACERlab MxFDG module and an on-site modified cassette. Briefly, [^{68}Ga]GaCl₃ was eluted from $^{68}\text{Ge}/^{68}\text{Ga}$ generator with 0.1 M HCl and then purified with a pre-conditioned SCX cartridge. The SCX cartridge was subsequently eluted to reactor with a mixture of 5.5 M HCl(aq) and 5 M NaCl(aq), and then reacted with precursor and acetate buffer at 90°C for 10 min. Afterwards, the reaction mixture was neutralized with sterile sodium phosphate buffer to achieve final [^{68}Ga]MAA product. The radiochemical purity of [^{68}Ga]MAA was determined with ITLC (0.4 M sodium citrate). Non-decay corrected radiochemical yield is expressed as a percentage of starting activity of [^{68}Ga]GaCl₃.

Results: The RCYs of [^{68}Ga]MAA synthesized by our method were $50 \pm 10\%$ ($n > 3$) with a radiochemical purity of $> 95\%$ and synthesis time of ~ 40 min.

Conclusions: [^{68}Ga]MAA have been successfully synthesized by TRACERlab Mx_{FDG} module and our modified cassette. Preclinical evaluation of [^{68}Ga]MAA as pulmonary perfusion imaging agent is ongoing.

PB038

壁報論文發表摘要·基礎組

以實際偵測值推估適當之人員有效劑量與肢端等價劑量紀錄基準值研究—以南部某醫院為例

陳素英¹ 卓世傑² 陳宜伶¹ 蕭莉茹¹ 林秋美¹ 古琴鳳¹
陳怡如¹ 曾翠芬¹ 劉怡慶¹ 林家揚¹ 張晉銓¹

¹高雄醫學大學附設醫院

²奇美醫院

背景介紹：依據輻防法規定，輻射工作場所之劃定與管制，訂定紀錄基準、調查基準及干預基準。本研究嘗試以單位從事輻射作業工作人員之實際偵測值，推估適當之記錄基準值，希望能提供記錄基準值訂定可行的方法。

方法：收集本單位輻射工作人員佩章劑量記錄由 105 年 2 月至 108 年 7 月止，共 42 個月，其中人員深部有效劑量與肢端等價劑量紀錄有數值者之輻射工作人員前後共有 9 位。並計算各輻射工作人員深部有效劑量與肢端等價劑量記錄之平均值 +3 倍標準差與最大值。

結果：將各輻射工作人員深部有效劑量與肢端等價劑量記錄之平均值 +3 倍標準差設定為本單位之紀錄基準。

結論：我們發現以最大平均值 +3 倍標準差，應可作為本單位輻射工作人員佩章劑量之記錄基準值設定之合理依據。因放射師、調製藥品放射師與護理師工作內容有所不同，雖符合輻防法規，仍應合理抑低 ALARA 集體劑量之規定，需調整彼此工作負擔，以減少曝露。

PB039

Monitoring The Effect Of Personnel Operation In Clean Rooms – Experience In TSGH

Yun-Chih, Wu^{*,1}, Li-Fan Lin^{1,2}, Chuang-Hsin Chiu^{2,#}

¹*PET Center, Department of Nuclear Medicine, Tri-Service General Hospital,
National Defense Medical Center, Taipei, Taiwan*

²*Department of Nuclear Medicine, Tri-Service General Hospital, National Defense Medical Center, Taipei, Taiwan*

Introduction: The production of clinically used PET radiotracer finally needs to be filled and dispensed in a sterile isolator system to ensure the safety for intravenously injection in human. According to PIC/S GMP regulation, aseptic filling and personnel operating area should meet Grade A and Grade B, respectively. However, even if the environments of clean room meet the standard, it is also an important issue whether personnel will affect the environmental cleanliness after a period of dynamic operation. This study was conducted in Grade B clean room of PET Center in TSGH. According to the current PIC/S GMP guideline, contact plates were used to monitor the personnel operation to assure the safety of radiotracer preparation process.

Methods: In order to know whether dressing procedure and dynamic operation affect the clean room cleanliness, the maximum operator in this study were set as three, followed a standardized dressing process with sterilized garments, four time points after entering the clean room were monitored. (0, 1, 2, 3, 4 hours, each labeled as T0, T1, T2, T3, T4). Contact agar were pressed on the surface of clothing for sampling with the maximum surface for ten seconds, then placed in incubator with proper temperature for daily monitoring. After eight days of continuous observation, number of colony growth from 12 positions on personnel gown were recorded and analyzed.

Results: The results showed that the average number of growing colonies in each sampling area at T0 were 0.3 ± 0.1 , T1 for 0.9 ± 0 , T2 for 2.2 ± 0.2 , T3 for 4.5 ± 0.4 and T4 for 5.1 ± 0 , respectively. According to the result, the standardized dressing procedure did not affect the sterility of the protective clothing.

Conclusions: We confirmed that by appropriate dressing procedure, three operators in a three hours operation did not significantly affect the environmental cleanliness of the Grade B clean room. Operation above three hours to four hours did not meet PIC/S GMP regulation for the Grade B. Therefore, our standard routine operation time in PET Center should be less than three hours to ensure that the operating process is fully in compliance with the regulations and ensure the safety of clinical use.

PB040

壁報論文發表摘要·基礎組

Experience Of ^{18}F -FDG Synthesis And Quality Control With GE FASTlab Synthesizer In TSGH

Fan-Chieh Meng¹, Li-Fan Lin^{1,2}, Chuang-Hsin Chiu²

¹*PET Center, Department of Nuclear Medicine, Tri-Service General Hospital, National Defense Medical Center, Taipei, Taiwan*

²*Department of Nuclear Medicine, Tri-Service General Hospital, National Defense Medical Center, Taipei, Taiwan*

Introduction: 2- ^{18}F fluoro-2-deoxyglucose (^{18}F FDG) is the most widely used radiotracer for clinical positron emission tomography (PET) scan. Commercially available GE FASTlab automated synthesizer is routinely used for the production of ^{18}F FDG in TSGH. However long-term monitoring of ^{18}F FDG production is important because the production process must comply with good manufacturing practice (GMP) and the final product must conform to the required quality specifications to ensure the safety for clinical use.. In this work, we share our experience of GMP-compliant automated synthesis ^{18}F FDG and quality control.

Method: 778 batches of ^{18}F FDG were produced using GE FASTlab and analyzed retrospectively. The monitoring issue consisted of uncorrected radiochemical yield (RCY), appearance, radiochemical purity (RCP), pH value, radionuclidic identity, half-life, chemical purity and residual solvent including ethanol and acetonitrile, sterility and bacterial endotoxin level.

Result: The FASTlab cassette installation was convenient and the average synthesis time of ^{18}F FDG was 22.8 ± 0.2 min. The mean value of RCY for 778 batches of ^{18}F FDG production was $71 \pm 7.7\%$, average RCP value were $99.9 \pm 0.36\%$, pH value were 5.66, radionuclidic purity were 100%, half -life were 109.52 ± 0.9 min and the residual solvent of ethanol and acetonitrile among these batches were $0.14 \pm 0.05\%$ and $< 0.001\%$, the bacterial endotoxin level of final product were below 175 EU/V and no bacteria growth.

Conclusion: In this study we present our experience in using FASTlab for routine production of ^{18}F FDG. FASTlab is uncomplicated and easy to use for production of ^{18}F FDG which met the acceptance criteria. Since the pharmaceuticals production is a strongly regulated process, corrective and preventive actions and statistical methodologies is very important. According to regular monitoring of daily ^{18}F FDG production, our process is GMP-compliant and reliable to offer clinical use.

PB041

Optimizing the Radio-chemical Yield of Radio-iodinated Doxorubicin

Wen-Yi Chang¹, Wen-Sheng Huang¹, Hsin-Ell Wang²

¹*Department of Nuclear Medicine, Veterans General Hospital, Taipei, Taiwan*

²*Department of Biomedical Imaging and Radiological Sciences, National Yang-Ming University, Taipei, Taiwan*

Introduction: Nuclear medicine imaging is a method of producing images by detecting radiation signals from radiolabeled tracers or medicine. Iodine-131 is widely used in clinical for diagnosis and therapy. Doxorubicin is a DNA inter-chelator that inhibits topoisomerase II thereby inhibiting cancer cell proliferation. Radio-iodinated doxorubicin may have the potential to diagnosis and treatment cancer.

In this study, radio-iodinated doxorubicin was performed with several radiolabeling parameters.

Methods: Synthesis of radio-iodinated doxorubicin was carried out by direct electrophilic substitution with iodine-131 using chloramine-T (CAT) as an oxidizing agent. In addition to its desirable half-life time ($t_{1/2} = 8$ days), iodine-131 affords the ability to use high specific activity iodide no carried added iodine. Various reaction parameters, including the chloramine-T amount, doxorubicin amount, reaction pH and reaction time, were optimized to obtain the maximum radiochemical yield.

Results: Radioiodination of doxorubicin was optimized through studying chloramine-T (CAT) amount, doxorubicin amount, pH and reaction time parameters to obtain the maximum radiochemical yield. A maximum radiochemical purity ($95 \pm 0.8\%$) was obtained using 2 mg of CAT amount, 50 μg doxorubicin amount, at pH 6 and for 30 min reaction time.

Conclusions: In this study, we optimized the radio-labelling yield of radio-iodinated doxorubicin. Biological evaluation of radio-iodinated doxorubicin will perform in the future.

PB042

壁報論文發表摘要·基礎組

Study on Deep Learning Based Differential Diagnosis of Parkinson's Disease and Atypical Parkinsonian Disorder on PET ^{18}F -FP-(+)-DTBZ Imaging

Sheng-Yao Huang¹, Kun-Ju Lin^{1,2}, Yi-Hsin Weng³, Ing-Tsung Hsiao^{1,2}

¹Dept of Medical Imaging and Radiological Science and Healthy Aging Research Center, Chang Gung University, Taoyuan, Taiwan

²Dept of Nuclear Medicine, Chang Gung Memorial Hospital at Linkou, Taoyuan, Taiwan

³Dept of Neurology, Chang Gung Memorial Hospital at Linkou, Taoyuan, Taiwan

Introduction: Early differential diagnosis of different parkinsonism is usually difficult. ^{18}F -FP-(+)-DTBZ is a positron emission tomography (PET) radiotracer for imaging the vesicular monoamine transporter type 2 (VMAT2). Deep learning has potential to improve medical diagnosis for providing more classification accuracies. The aim of this study is to investigate the use of deep learning method on PET VMAT2 images for differential diagnosis of Parkinson's disease (PD) and atypical Parkinsonian, progressive supranuclear palsy (PSP).

Method: Retrospective ^{18}F -FP-(+)-DTBZ PET scans from 85 subjects of 30 PD, 25 PSP and 30 normal controls (NC) were included in this study. To reduce the computation, four slices at the level of striatum, substantia nigra, and mid brain from each original 3D ^{18}F -AV-133 image were extracted and merged into one 2D image of 312 x 312. Data augmentation is used to expand the training and testing data for the 2D-CNN (convolutional neural network) model. For the simple deep learning model, there are 11 layers including input images, 4 convolutional layers with batch normalization and ReLU layers, 3 maxpooling layers, one full connected layer, soft max layer and output layers. After augmentation, the dataset includes 540 images. All images were classified with 2D-CNN using leave-one-out cross-validation.

Results: The deep learning CNN model was trained for 50 epochs and 4 iterations per epoch. The curve of accuracy function in CNN converged quickly, and so did the loss function. The result indicates that the deep learning CNN model was able to discriminate among the three groups of NC, PD and PSP with training accuracy 100% and testing accuracy over 95%.

Conclusion: The initial result shows that the deep learning method on the ^{18}F -FP-(+)-DTBZ images can achieve differential diagnosis accuracy over 95% for NC, PD, and PSP. Future work will include more sample size and more atypical Parkinsonism groups.

PB043

探討轉速、溫度、時間對 RIA 實驗的影響 —以 CIS Ca199 為例

王安美

馬偕紀念醫院核子醫學科

前言：放射免疫分析的方法和一般自動化的免疫分析方法最大差異在於發報告的時間。放射免疫分析優勢在於一次可以操作大批次量 (Batch run) 的檢體，一次可以發出大批次的報告。而自動化免疫分析儀的優勢在於它可以短時間內發出單一報告，如果大批次量的檢體對自動化免疫分析是無法一次消耗完。此結果是優於放射免疫分析系統。然而雖說如此，如果放射免疫分析的檢驗步驟愈是簡單更是可以加速發報告時間，如此一來更是可以增加放射免疫分析優勢。本文所探討的就是利用溫度、轉速的改變，改變實驗的反應時間，以驗證結果值是否和原廠提供的步驟所得之結果值一致，如此也可提供原廠確效並改進，以提升 RIA 的競爭優勢。

材料方法：CIS Bio Ca199，CA199：採用原廠提供的標準 overnight 步驟：並依此選出 70 支檢體 (含蓋低中高的濃度)，原廠提供之 short time 標準步驟，原廠建議改良之 short time 步驟，本實驗室設計之 short time 步驟。

結果：原廠建議改善之方法，因須 37°C 200 rpm 之水浴箱，因本實驗室無 37°C 200 rpm 之水浴箱，故選擇改變程序。先使用原廠說明書之標準作業步驟操作實驗後，共選 70 支檢體，所選用之檢體含蓋低中高之數據，再與本實驗室自行設計的方法比對，經數據分析結果，二組數據之 R 值為 0.91 與 0.92，主因高值的數據，較低於原步驟之數據。可能因為標準曲線高值處結合率太高，造成曲線斜率過於陡峭，因而影響高值數據，低值、中間值之數據較無明顯差異。依數據分析，本實驗室所設計的方法是可行的，只是室溫 400 rpm 2 小時可以再縮短時間，對於高值之數據差異已與原廠討論，並請原廠的驗證，以期能成為原廠正式的標準作業步驟。

結論：放射免疫分析的原理，不論是競爭或非競爭的原理，其最終所需要的是抗原抗體結合的複合物，且於 37°C 時反應最為穩定，而這個複合物可以因溫度、轉速、反應時間受到影響，但是如果選擇適當的條件，改變原來的設計有時得到的效果是比原廠的設計更有優勢，更可提升 RIA 的效率及 TAT，並期待原廠之驗證成為正式之步驟提申 RIA 之優勢。

PC001

Detection of Sentinel Lymph Node by Lymphoscintigraphy in Contralateral Axilla at Initial Presentation of Breast Cancer

Jih-Fang Hsieh¹, Chiang-Hsuan Lee^{1,2}, Chih-Shun Wu²

Department of Radiology, Section of Nuclear Medicine

¹Chi Mei Medical Center, Yongkang Dist., Tainan, Taiwan

²Chi Mei Foundation Hospital, Liuying Dist., Tainan, Taiwan

Purpose: The aim of this study was to determine in our institution the incidence of contralateral axilla sentinel lymph nodes (SLNs) by lymphoscintigraphy at initial presentation of breast cancer.

Methods: We reviewed retrospectively initial pre-operative lymphoscintigraphy of 457 consecutive female patients with biopsy proved breast cancer. Lymphoscintigraphy was performed after intradermal injection of 1 mCi Tc-99m phytate in 0.4 ml volume. Planar images of anterior and lateral views were obtained routinely.

Results: SLNs were demonstrated in 457 patients of which 2 had both ipsilateral and contralateral axillary SLNs. One of the two patients had positive malignancy in both ipsilateral and contralateral axillary SLNs. The second patient had a positive malignancy ipsilateral axillary SLN but negative malignancy in the contralateral axillary. The incidence of extra-axillary SLNs in this study is 0.04% (2 out of 457).

Conclusion: Metastases to the contralateral axillary lymph nodes in breast cancer patients are uncommon. Involvement of a contralateral axillary lymph node denote an M1 (stage IV). Identification of a contralateral sentinel lymph node may change the multi-disciplinary management of breast cancer to include a contralateral axillary dissection, chemotherapy, and/or radiotherapy to the contralateral axilla.

PC002

Combined Use of BMD and FRAX for the Prediction of Fracture Risk in Low Bone Density Patients

Pao-Liang Chen^{1,2}, Shih-Chin Chou¹, Tzyy-Ling Chuang^{1,3},
Jian-Guo Liao¹, Yuh-Feng Wang^{1,3}

¹Department of Nuclear Medicine, Dalin Tzu Chi Hospital, Buddhist Tzu Chi Medical Foundation, Chiayi, Taiwan

²Department of Medical Research, Dalin Tzu Chi Hospital, Buddhist Tzu Chi Medical Foundation, Chiayi, Taiwan

³School of Medicine, Tzu Chi University, Hualien, Taiwan

Background: The FRAX screening tool is used to estimate the 10-year probability of hip fracture and the 10-year probability of a major osteoporotic fracture (spine, forearm, hip, or shoulder) in patients with osteoporosis. This study aims to determine whether patients with low bone density without osteoporosis are at greater risk of fracture that could be identified using FRAX.

Methods: This retrospective study was a cross-sectional design. Patients who underwent outpatient examination including DXA from September 2017 to May 2019 were further screened; those with the history of spinal surgery, total hip replacement, or incomplete medical records were excluded. A total of 2613 patients were included in the final cohort, 430 males (16%) and 2183 females (84%). Demographic information and clinical histories, including age, height, weight, BMI, were collected. Factors associated with a ten-year probability of fracture (previous fracture, parental hip fracture, current smoking, glucocorticoids use, rheumatoid arthritis, secondary osteoporosis and alcohol intake 3 or more units daily) were also recorded.

Results: DXA and FRAX results differed significantly between patients with normal bone density, low bone density, and osteoporosis. DXA and FRAX results of bilateral hips differed significantly between patients with high risk (major osteoporotic fracture, > 20%; hip fracture, > 3%) and low risk (major osteoporotic fracture, < 20%; hip fracture, < 3%) of fracture. High fracture risk was identified by FRAX results as hip fracture > 3% in patients with bone loss not yet progressed to osteoporosis. But in our study low bone density group of high risk major osteoporotic fracture, > 20% and hip fracture > 3% total 562 (22%).

Conclusions: Patients with bone loss not yet progressed to osteoporosis would benefit from FRAX determination of 10-year risk of fracture. While both DXA and FRAX can be used to determine the 10-year probability of fracture in patients with bone loss, we recommend the use of FRAX in the clinical setting.

PC003

Discussion on Screw Breakage of Scintillating Camera Detector

Chia-Hao Chang¹, Ya-Lian Chang¹, Jin-Yen Wang¹, Yu-Sheng Hung¹,
Chih-Shun Wu¹, Chiang-Hsuan Lee^{2*}

¹*Division of Nuclear Medicine, Department of Medical Imaging, Chi Mei Medical Center, Liouying, Tainan, Taiwan*

²*Division of Nuclear Medicine, Department of Medical Imaging, Chi Mei Medical Center, Tainan, Taiwan*

Purpose: The scintillation camera is the most commonly used machine in the nuclear medicine department. Due to the relationship between optical imaging principle and spatial resolution, detectors moved closer to patients, we can get more clear image. Besides, when we take Single-Photon Emission Computed Tomography technology (SPECT), detectors will rotate around over the patient. Whether the detectors and accessory components are well-fixed, it would be related to patient safety directly. Scintillation Camera in our division maintained regularly, but one screw behind the detector disappeared was found by radiographer in daily check before nuclear study. This article will explore this event.

Material and method: Scintillation Camera in our division (Siemens, E.CAM) was installed in 2005 and maintained by Siemens Healthineers. This machine was maintained every two months, and radiographer perform safety inspection around camera before nuclear medicine exam everyday.

Result: One day morning, we found that screw was disappeared. After inspection by the Siemens Healthineers engineer, he found that screw was fractured on the detector (Collimator Clamp), but the screw can't be replace by himself immediately. There are no safety concerns in performing daily nuclear medicine exam. Only when replacing electronic component in the detector, the screw on the lock plate on the rear of the c-frame would be removed. But based on the reasons of patient safety, we ask engineers arranging time to replace the related components as soon as possible.

Conclusion: Only 19 days since the last maintenance, we found that screw was fractured, and this item included in maintenance subject (12-Month Maintenance). It's very important that engineers perform maintenance following the maintenance procedure. The service life of screws related to patient safety must be discussed, preventive replacement strategy should be considered. Daily inspections of imaging room before nuclear medicine exam by radiographers would be helpful for patient safety.

PC004

Common Daily Radiation Sources and Pollution Detection Principles

Chien-Hua Lu¹, Chih-Shun Wu¹, Chiang-Hsuan Lee^{2*}

¹*Division of Nuclear Medicine, Chi Mei Medical Center, Liouying, Tainan, Taiwan*

²*Division of Nuclear Medicine, Chi Mei Medical Center, Tainan, Taiwan*

Objective: Occasionally, a doctor will encounter a patient with a radiation injury.

In addition to radiation professionals, Usually, the average person has a smattering of the types of nuclear species and their radiation characteristics. Therefore, the radiation sources and their characteristics that may be encountered in industry and life are sorted and classified. Allowing physicians to be exposed to such radiation-contaminated patients with radiation can give proper control and treatment.

For those who use radioactive materials in industrial and people's livelihoods:

Lightning rod: In the process of manufacturing lightning rod, the cavity will be coated with a layer of ²⁴¹Am (Americium) radioactive material, ²⁴¹Am will release α particles, which can enter the bone surface of the body by ingestion, inhalation, puncture wound, skin contamination, ²⁴¹Am The α activity is three times that of ²²⁶Ra and there is a significant risk of ingestion or inhalation.

Smoke Detector: A fire detector for smoke detection with a low-activity ²⁴¹Am source.

Watches, clocks and compasses: Old-style watches and clocks use ²²⁶Ra (Radium) as the light source of the night light. When these watches are to be repaired, ²²⁶Ra may be touched or ingested into the body, causing radiation damage. Now use ³H (helium) and ¹⁴⁷Pm (Promethium) as the light source. The $T_{1/2}$ of ³H is 12.43 years. When it decays into ³He, low-energy β rays are released. The $T_{1/2}$ of ¹⁴⁷Pm is 2.6 years, and low-energy β rays are also released during decay.

Glass: Uranium-containing glass can be made into yellow or green antique utensils, which emits attractive light in the dark; even ordinary glass contains ⁴⁰K (potassium) or ²³²Th (Thorium) high enough to be detected by the detector. In the early 1960s, camera lenses were often painted with ²³²Th to change their refractive index. ⁴⁰K spontaneously generated ⁴⁰Ar (argon) and ⁴⁰Ca (calcium) by β decay, releasing β and γ rays with a $T_{1/2}$ of 1.248×10^9 years. The $T_{1/2}$ of ²³²Th is 14.05 billion years, emitting α particles.

Welding electrode: The electrode used in welding is about 2%, which contains about 30 μ Ci of radiation activity.

Radiation injury pollution inspection principle: The radiation patterns of radioisotopes are α , β and γ -ray. Both α and β do not need to worry about the radioactivity in vitro. The plastic or skin is enough to block, but pay attention to the damage in the body. γ has a penetrating ability to the substance, and the damage is strong, which requires more attention. When the People to the clinic and complains about the above-mentioned radiation pollution or injury, The physician should isolate the patient in the clinic. first determine the radiation source, and immediately notify the radiation protection personnel to perform radiation detection at the clinic. If the detection result is radiation The dose rate greater than 0.2 μ Sv/h should be immediately reported to initiate the radiation strain procedure. If the radiation dose rate of the detection result is less than 0.2 μ Sv/h, that is, there is no radiation pollution or injury, it should be treated according to the general medical treatment process.

PC005

To Detect and Evaluative Therapy Response of Intrapulmonary Right-to-left Shunt by Tc-99m MAA Scintigraphy

Ya-Ju Tsai, Hsin-Yung Chen

Department of Nuclear Medicine, Taipei Medical University Hospital

Introduction: Pulmonary arteriovenous malformation (PAVM) is abnormal communication between pulmonary artery and vein resulting in a right-to-left shunt to allow systemic venous blood to bypass gas exchange and pulmonary capillary bed. PAVM can cause a variety of complications including stroke, cerebral abscess, pulmonary hemorrhage and hypoxemia with substantial morbidity and mortality. We used Tc-99m MAA scintigraphy to evaluate the shunt ratio and assessment therapy effect in two cases.

Method: Patient was in supine position and right-to-left shunt scintigraphy was acquired following the intravenous injection of 2.5-5 mCi Tc-99m MAA (about 100k-200k particles). A dynamic flow imaging of chest at 2 seconds per image for 60 seconds was obtained followed by anterior and posterior whole-body images using a dual-head camera at a speed of 10 cm/min. Regions of the interest (ROIs) were drawn on the both lungs and whole-body area on composed whole-body image by geometric mean. The right-to-left shunt ratio is calculated by the following formula: $[(\text{Total body counts} - \text{Total lung counts}) / \text{Total body counts}] \times 100$. The normal cutoff value of scintigraphic shunt ratio ranged from 3-10% with variable sensitivity and specificity according to previous literatures. Brain and renal uptakes of Tc-99m MAA are suggestive of right-to-left shunt. It has been reported that brain visualization might be a more reliable sign in consideration of free Tc-99m pertechnetate.

Case reports:

#Case 1: 45-yr-old female is a case of exertional dyspnea and chest discomfort for years. Chest CT showed a 4.3 cm PAVM and a 0.8 cm PAVM in the right lower lobe. Tc-99m MAA shunt scintigraphy showed brain & renal uptakes of MAA with a right-to-left shunt ratio of 20%. After transcatheter arterial embolization, the scintigraphic shunt ratio was declined to 8% and no more visualization of brain & renal uptakes of MAA. Mild degree of free Tc-99m pertechnetate was noted in both initial and post-treatment scans.

#Case 2: 46-yr-old female suffered from right anterior chest pain on and off for months. A 0.3 cm PAVM at right middle lung was noted by chest CT. Tc-99m MAA shunt scintigraphy showed brain & renal uptakes of MAA with a scintigraphic shunt ratio of 9.5%. The patient received wedge resection of right middle lobe.

Conclusion: Tc-99m MAA scintigraphy for right-to-left shunt is a simple and useful method to evaluate the shunt percentage and assessment therapy effect by calculating scintigraphic shunt ratio and analyzing brain and renal uptakes.

PC006

An Unusual Case of Altered Gallium-67 Citrate Distribution with Multiple Red Blood Cell Transfusions

Yung-Chieh Tsai, Jr-Jian Juan*

Department of Nuclear Medicine, Ministry of Health and Welfare Fengyuan Hospital, Fengyuan, Taiwan

Introduction: Gallium-67 (Ga-67) scintigraphy (GS) is a well-established procedure for diagnosing inflammation or infection. However, Ga-67 citrate is a nonspecific inflammation imaging agent. The distribution of Ga-67 citrate in the body is influenced by a number of pharmaceuticals, treatments, interventions, and iron metabolism. Saturated iron-binding sites are associated with an abnormal biodistribution of Ga-67 citrate after repeated red cell transfusions. An increase in red cell production with marrow extension causes a diffusely increased uptake of radiogallium in the skeleton. This unusual case of GS's mimicking a bone scan is described herein.

Methods: A 59-year-old male with colon cancer developed progressively worsening fatigue, nausea, and fever. He had undergone several surgical procedures, targeted therapy, and radiation therapy. The patient had a history of symptomatic anemia and leukemia. Then, GS had been used to assess the fever of unknown origin. He received multiple red blood cell transfusions within two weeks before GS. GS was conducted performed 24 hours following the intravenous injection of Ga-67 citrate (185 MBq).

Results: Whole-body gallium-67 scintigraphy anterior and posterior revealed increased gallium uptake in the axial skeleton, proximal parts of the appendicular skeleton, and the liver. Focal tracer was taken up by the left anterior pelvis. The alteration of the Ga-67 citrate distribution might have been caused by a change in iron metabolism brought on by the red blood cell transfusions.

Conclusions: Incidental findings of GS's mimicking bone scan have been reported elsewhere. The detailed history of the patient must be understood. Adequate patient preparation before scintigraphic procedures is essential. Various drugs and biological products interfere with binding sites of the Ga-67 citrate by saturating the receptor sites. Accordingly, more attention should be paid to these scintigraphic procedures before GS.

PC007

胸腔積液中攝護腺特異性抗原 (PSA) 升高之病例報告

林淑靜¹ 張素雲¹ 薛仔婕¹ 廖建國¹ 王昱豐^{1,2}

¹ 佛教慈濟醫療財團法人大林慈濟醫院核子醫學科

² 慈濟學校財團法人慈濟大學醫學系

簡介：攝護腺癌根據國民健康署統計資料顯示，發生率在男性癌症中排名第 5 位，而死亡率則是男性癌症中第 7 位，其重要性可知。攝護腺癌好發於 65 歲以上的男性。攝護腺特異性抗原 (又稱前列腺特異性抗原, prostate specific antigen, PSA) 是攝護腺製造的一種物質。PSA 大多存在於精液中，但血液中也發現微量的 PSA，大多數男性的血液含量 < 4 ng/mL。攝護腺癌會導致濃度上升，如果濃度介於 4-10 ng/mL，表示有四分之一的機率罹患攝護腺癌；如果超過 10 ng/mL，機率就超過 50%，且會隨 PSA 濃度上升而提高。但 PSA < 4 ng/mL 的男性也可能罹患攝護腺癌。PSA 可用於攝護腺癌診斷及分期，亦可用來偵測及追蹤治療效果。此外，PSA 會隨著年齡升高而升高。根據攝護腺癌的研究，診斷攝護腺癌時，大約會有 10% 的病患會併發骨轉移，而轉移病患通常會有較差的預後。

病例報告：77 歲男性因呼吸困難，骨頭多處疼痛入院，進行胸部電腦斷層掃描，CT 影像發現右側肺葉有一結節及雙側胸腔內有中度的胸腔積液，醫師由此處進行胸腔穿刺術抽取積液送檢，送檢右肺肋膜積液檢驗 PSA，同時抽血液檢體，經實驗室化驗後，血液 PSA 949.0 ng/mL，肺肋膜積液 PSA 277.4 ng/mL。實驗室數據 Hb 由 15.4 mg/dL (三月) 降到 8.6 mg/dL (四月)，顯示貧血且患者亦有排尿困難及血尿情況。攝護腺組織切片經過免疫組織化學檢測診斷為 Gleason 4 級攝護腺腺癌；另外核醫骨骼掃描 Tc-99m MDP 骨掃描發現全身瀰漫性骨骼轉移 (diffusely metastases) 包括顱骨 (特別是枕骨)、脊椎骨、兩側肋骨、骨盆、兩側肩胛骨和左股骨均有放射性藥物攝取，診斷為原發性癌症骨轉移。最終診斷為攝護腺癌 (腺癌) 伴有淋巴結和骨轉移合併惡性胸腔積液。

結論：後期攝護腺癌容易發生肺轉移 (46%)，而有 21% 的機率會發生胸膜轉移。攝護腺腺癌的惡性胸腔積液 (PMPE, paramalignant pleural effusion) 在臨床並不常見，有研究指出，只有 1% 發生胸膜腫塊 / 結節或積液。PSA 是一個特異性很高的免疫標誌，鮮少會在其他體液中發現其蹤跡。此病例在肋膜積液中發現高值 PSA，證實是攝護腺癌經由腹膜轉移胸腔及骨骼。PSA 是用於攝護腺癌篩檢和治療監測的最常使用的生物標誌。胸腔積液中 PSA 的檢測是轉移性攝護腺癌診斷中有用的輔助試驗，但目前仍需進一步研究確定 PSA 在積液中的敏感性和特異性。血清 PSA 是否用來作為攝護腺癌篩選目前仍有爭議，但有研究指出血清 PSA 的篩檢可減少轉移性攝護腺癌的發生。期許能在尚可治療的階段找出癌症，可提高治療成功的機會，也能改善患者未來生活品質。

PC008

Techetium-99m Ethyl Cysteinate Dimer Brain Perfusion SPECT in the Logopenic Variant of Primary Progressive Aphasia: A Case Report

Yu-Erh Huang¹, Chung-Wen Chen², Chih-Feng Chen³, Hung-Yi Hsu²

¹*Department of Nuclear Medicine*

²*Department of Neurology, Tungs' Taichung MetroHarbor Hospital, Taichung, Taiwan*

³*Department of Radiology, China Medical University Hospital, Taichung, Taiwan*

Abstract

Introduction: Primary progressive aphasia (PPA) is a slowly progressing language disorder resulting from neurodegenerative diseases and is now divided into the following three categories: non-fluent variant, semantic variant, and logopenic variant. Clinical findings of specific variants are associated with relatively distinct neuroimaging patterns on magnetic resonance imaging (MRI), single photon emission computed tomography (SPECT) or positron emission tomography.

Case: We report the case of a 75-year-old woman who presented with gradually progressive speech disorders and memory impairment. Brain MRI revealed a senile change of the brain without asymmetrical atrophy. Technetium-99m ethyl cysteinate dimer brain perfusion SPECT with semiquantitative analysis revealed hypoperfusion in the left hemisphere, predominant on the posterior temporal lobe extending to the posterior parietal lobe. After considering the clinical presentation and SPECT findings, we established a diagnosis of logopenic variant of PPA.

Conclusions: Although MRI provides accurate localization, earlier perfusion abnormalities may precede the atrophy and allow SPECT for early PPA variant classification. This case highlights the significance of brain perfusion SPECT with quantitative analysis for imaging-supported PPA variant diagnosis.

PC009

壁報論文發表摘要·臨床組

提升對低碘飲食認知之台中某教學醫院經驗分享

劉宛茹 林娜宜 陳慶元

佛教慈濟醫療財團法人台中慈濟醫院

背景介紹：甲狀腺癌是國內十大死因之一，有逐年攀升的趨勢，手術是治療甲狀腺癌的最主要的方式，手術後方可確立腫瘤的型態與基因序列。依據美國甲狀腺協會 (ATA V2015) 發表的治療指南指出，甲狀腺腫瘤在手術治療後，依低、中、高度復發風險群指標來評估碘-131 治療的必要性和劑量風險，低度風險者無須採用放射碘治療，如果是中、高度風險者：頸部淋巴結轉移、淋巴結包膜侵犯、腫瘤顯著侵犯到甲狀腺外、不完全切除腫瘤有顯著殘存腫瘤、淋巴結轉移大於 3 公分的腫瘤症狀，即需要進行放射碘的治療。放射性碘 131 治療是利用甲狀腺癌細胞可以攝取碘的特性，以放射線來殺死甲狀腺癌細胞。一般安排在手術後 4-6 週施行，作為輔助性治療。在安排放射碘治療的前 2 週，需先採取「低碘飲食」，並且停用甲狀腺素 4 週或是不停藥搭配人工合成甲狀腺促素使用，再進行放射碘的掃描和治療。此外，甲狀腺癌每年定期皆須利用放射性碘 131 追蹤，因此衛教低點飲食格外重要。

方法：許多剛發現癌症患者，擔心低碘飲食不夠徹底，會影響放射性碘 131 治療，所以除了護理人員衛教外，自己還會上網查詢哪些食物不行吃，雖然 2 週低碘飲食不長，但也造成患者對低碘飲食有恐懼感。為了降低患者對低碘飲食的迷思及提高患者每年對碘 131 追蹤，故由一位專門的護理人員收集初次發生甲狀腺癌的 15 名患者對低碘認知 (前測)，再給予這 15 名患者一對一口頭衛教及增加圖示解說 (後測)，分別以 1. 無碘飲食與低碘飲食一樣嗎？ 2. 營養成分含鈉是指含碘嗎？ 3. 正常人可以吃無碘鹽嗎？ 4. 十字花科可以吃嗎？ 5. 治療完畢後可以吃海帶類嗎？五項是非題前後測驗及統計。

結果：收集初次發生甲狀腺癌的 15 名患者，給予低碘飲食衛教前後測驗，統計發現：1. 無碘飲食與低碘飲食一樣嗎？前後測皆 100% 2. 營養成分含鈉是指含碘嗎？由 80% 提升到 100% 3. 正常人可以吃無碘鹽嗎？由 26.67% 提升到 100% 4. 十字花科可以吃嗎？由 46.67% 提升到 100% 5. 治療完畢後可以吃海帶類嗎？由 20% 提升到 100%。發現患者可以分辨低碘與無碘是不同的，但因為食物含碘成分不同，造成患者在食物挑選及份量拿捏上無所適從。治療過後的患者自覺自己跟正常人不同，對自己會過份要求飲食上跟正常人有所不同，造成身心上的壓力，透過衛教及持續心理支持可以讓患者慢慢適應及接受現在的自己，就算在低碘飲食碘 131 追蹤時，吃飯時也能跟家人一同共享，不會造成患者費心思考下一餐要吃什麼的困擾，因此提高患者碘 131 追蹤的意願。

結論：發現門診護理人員要兼顧跟診及衛教，無法仔細詳訴低碘飲食內容及傾聽患者問題，由一位專門的護理人員一對一口頭衛教，能提升患者對低碘飲食的認知及降低患者的焦慮，但相對耗時及耗人力，因此，後續將增設海報及影音檔案提供患者重複觀看，提高對低碘飲食了解進而提升患者碘 131 追蹤的意願。

PC010

Accidentally Found Radioactive Iodine Uptake in Distant Metastases from Differentiated Thyroid Carcinoma in a Patient Who had not Undergone Complete Surgical Resection

Ya-Wen Chuang, Ying-Fong Huang, Chin-Chuan Chang, Chia-Yang Lin,
Chih-Ting Liu, Hsiu-Lan Chu

Department of Nuclear Medicine, Kaohsiung Medical University Hospital, Kaohsiung, Taiwan

Introduction: Thyroidal radioactive iodine (RAI) accumulation is mainly contributed by Na⁺/I⁻ symporter (NIS)-mediated iodide influx. Since NIS expression is often reduced in malignant thyroid tissues, a total or at least subtotal thyroidectomy is routinely recommended before cancer worked-up for distant metastases in RAI scintigraphy. Preoperative RAI scanning will not reveal any metastases, and all iodine will be concentrated in the thyroid glands.

Case Report: The authors demonstrate the unusual presentation of a case with disseminated metastatic thyroid cancer, without complete surgical resection of the thyroid gland, showing multiple hot spots in the whole-body ¹³¹I scan.

Discussion: This case illustrates potential unexpected RAI accumulation in distant metastases from differentiated thyroid cancer before thyroidectomy. This patient had decreased serum TSH level, and suppression of the radioiodine uptake in thyroid gland tissue should be considered.

PC011

正子斷層掃描 使用安全針具靜脈留置針餘藥影像比較及評估

楊鶴廷 鄭如金 余雅惠 王淑芳 朱麗蓉 陳世欣

基隆長庚紀念醫院核子醫學科

背景介紹：近十幾年來，正子斷層掃描 (PET/CT) 在癌症分期、轉移、治療後評估扮演著重要的角色，已為臨床上不可或缺的利器。以前正子中心執行靜脈注射 F-18 FDG 前，先預埋靜脈留置針，並鎖上間歇注射帽，再以 18 號頭皮針穿刺間歇注射帽，另一端接妥三路活塞進行注射 F-18 FDG 及 10~15 ml 的生理食鹽水沖洗，降低藥物殘留於間歇注射帽的比例，但依然有藥物殘留的情形，影響該區域影像判讀與定量。本實驗響應安全針具推廣政策，改用螺旋式間歇注射帽、T 型延長管與三路活塞三種免針式安全型針具，比較哪一種免針式安全型針具殘餘 F-18 FDG 藥量較低。

方法：本研究取 36 位使用安全針具靜脈留置針的個案 (12 位三路活塞、12 位螺旋式間歇注射帽與 12 位 T 型延長管) 執行全身 18F-FDG PET/CT 造影。病人注射 $10 \text{ mCi} \pm 1 \text{ mCi}$ 18F-FDG，休息 50~90 分鐘後進行攝影。利用 ROI 圈選安全針具靜脈留置針殘餘餘藥影像位置，並圈選同側手臂肌肉區域為背景值，比較三種安全針具餘藥影像數值與背景值的比值。

結果：由圖一比較三種不同安全針具的靜脈留置針，明顯看出使用 T 型延長管的靜脈留置針，在影像上有較低顯影的餘藥殘留影像。使用 ROI 圈選殘留餘藥影像數值與背景值的平均比值分別為，三路活塞 5.16 ± 3.56 ，螺旋式間歇注射帽 4.52 ± 2.79 ，T 型延長管 1.77 ± 0.72 。

結論：上述證明使用 T 型延長管有最低殘留藥物，能改善影像品質與較準確 SUV 定量，又符合工作人員使用免針式安全針具的原則。

PC012

神經鞘瘤在骨骼掃描的表現

葉馨潔 陳慶元

台中慈濟醫院

背景介紹：神經鞘瘤又名許旺氏細胞瘤 (Schwannoma)，為生長緩慢的腫瘤，源自於週邊神經的髓鞘細胞，包覆於神經外的許旺氏細胞大多為良性，可能會復發，但惡性轉移的機會很小，大部分發生於頭頸部。患者通常無症狀，腫脹是最常見的抱怨。

方法：靜脈注射 20 mCi 的 Tc-99m MDP 後，等待 2-4 小時進行全身骨骼掃描，再針對手指處進行 SPECT 掃描。

結果：本病例為 35 歲女性病患，左手無名指有一 2.5 公分大小的腫塊，皮膚外觀平滑，形狀固定，壓不會痛。骨骼掃描顯示在左手無名指有放射性示蹤劑攝取增加，組織切片結果為良性神經鞘瘤。

結論：手部的神經鞘瘤在臨床上是很罕見的，在 SPECT 影像上有明顯的藥物攝取。回顧了幾篇神經鞘瘤的論文，有加作三相骨掃描，建議之後如果有遇到神經鞘瘤的例子，可改做三相骨掃描，以獲得更多的資訊有助於醫師做判讀。

PC013

RIA 分類之廢棄物重量與輻射劑量之相關性研究 —以南部某醫院 RIA 為例

張朝鈞 卓世傑 曾宜玲 顏吉龍 張淑芬 廖淑娟 段淑薰 李將瑄 顏玉安

奇美醫療財團法人奇美醫院核子醫學科

背景介紹：RIA 因作業產生含微量輻射劑量之廢棄物處理，依台灣現有法令，係放射免疫分析實驗室的重要工作之一。現雖可依分類之方式，將殘存較低輻射劑量之試管等廢棄物，偵測低於外釋劑量標準後，予以記錄後外釋。但基於保守原則，外釋之低輻射劑量廢棄物仍需限制在一定重量以下。因此，如廢棄物重量與輻射劑量並非相關即可使外釋作業更有彈性。本文即為探究 RIA 分類之廢棄物重量與輻射劑量之相關性研究。

方法：

1. 收集南部某醫院 RIA 自 106 年 10 月至 108 年 3 月之分類廢棄物重量及其 5、100 公分之輻射劑量率測量紀錄為一筆資料，分別為 106 年 33 筆，107 年 133 筆，108 年 26 筆。
2. 將上述資料，依 106、107、108 等 3 年份，分別歸類製表。
3. 分別計算各年份資料之平均數、標準差，以及重量與 5、100 公分輻射劑量之相關係數。

結果：

1. 106、107、108 年，RIA 分類廢棄物平均重量為 4.38、4.42 及 4.92 公斤，重量似有稍增之情形，標準差則分別為 1.02、1.05 和 0.93 公斤。
2. 106、107、108 年，廢棄物平均 5 公分之輻射劑量率分別為 0.57、0.54 及 0.58 $\mu\text{Sv/h}$ ，標準差則為 0.08、0.11 和 0.08 $\mu\text{Sv/h}$ ，各年度變化不大。
3. 廢棄物平均 100 公分之輻射劑量率，106、107、108 年各為 0.13、0.13 及 0.12 $\mu\text{Sv/h}$ ，標準差則為 0.02、0.02 和 0.01 $\mu\text{Sv/h}$ ，接近背景值。
4. 在相關係數方面，最高的為 106 年 5 公分劑量率的 0.29，最低的為 108 年 100 公分處劑量率之 0.01，依 5 及 100 公分順序，106 年為 0.29、0.09，107 年為 -0.10、0.25，108 年為 -0.04、0.01。

結論：南部某醫院 RIA 之 106、107 及 108 年之分類廢棄物，依本文之計算結果，其重量與其 5 公分及 100 公分之輻射劑量率之相關係數，最高僅為 0.29，最低則為 0.01，甚至 107 及 108 年度之重量與 5 公分輻射劑量率分別為 -0.10、-0.04 之負相關。顯示分類後之 RIA 廢棄物其重量與輻射劑量率，不論是於 5 公分處或 100 公分處，均無顯著相關。因此，分類後之 RIA 廢棄物於外釋時，不需特別考慮重量會增加輻射劑量之問題。

PC014

健康檢查陪同服務人員接受輻射劑量之研究 —以南部某醫院高階健康檢查為例

卓世傑¹ 田玉萍² 張虹麗¹ 梁育雅¹ 鄭揚霖¹
陳懿貞¹ 李將瑄¹ 顏玉安¹ 張南雄¹

¹ 奇美醫療財團法人奇美醫院核子醫學科

² 奇美醫療財團法人奇美醫院健康管理中心

背景介紹：健康檢查，是現代社會極為重要且常見的疾病預防方式。而為了協助民眾流暢受檢，通常會安排服務人員在健檢過程進行引導與陪同。不過健檢通常會包含各類利用輻射進行診斷的檢查儀器，例如 CT、X 光等。因此，健康檢查服務人員也可能接受到非必要之輻射劑量，值得探討。本研究即為探究，健康檢查陪同之服務人員，實際接受多少輻射劑量之研究。

方法：

1. 自 107 年 1 月 8 日至 2 月 9 日，請南部某醫院之陪同服務人員，佩戴劑量筆。
2. 收集每次陪同進行 CT 高階健檢之服務人員，其起始、結束劑量與總陪同時間，共 17 次。
3. 將每次之結束劑量減起始劑量，分別計算每次之實際接受劑量。
4. 將實際接受劑量除總陪同時間後，即得到每小時接受劑量率。
5. 每小時劑量率，再減除背景值 (0.06 $\mu\text{Sv/h}$) 後，即為實際接受之輻射劑量率。

結果：

1. 17 次資料中有 8 次起始及結束劑量相同，故實際接受劑量均為 0 μSv ，另外 9 次資料中，實際接受劑量最高為 4 μSv ，餘 8 次均為 1 μSv 。
2. 實際接受劑量除總陪同時間，再減除背景值之劑量率部分，9 次資料中最高為 1.082 $\mu\text{Sv/h}$ ，最低則為，0.267 $\mu\text{Sv/h}$ ，平均為 0.421 $\mu\text{Sv/h}$ 。

結論：依本研究之結果顯示南部某醫院健康檢查陪同服務人員，所額外接受之輻射劑量，應屬可忽略之輻射劑量。理由如下：

1. 健康檢查陪同服務人員 17 次紀錄中，接受之輻射劑量最高雖為 1.082 $\mu\text{Sv/h}$ ，但其實際接受劑量僅為 4 μSv ，且只有 1 次，遠低於每人 1 年 1000 μSv 之規定。
2. 所有 17 次紀錄中有 8 次，佔 47% 並無接受到輻射劑量，表示輻射劑量並非恆常出現。
3. 其餘 9 次有輻射劑量之記錄，平均亦僅 0.421 $\mu\text{Sv/h}$ ，仍低於本院記錄基準之 0.5 $\mu\text{Sv/h}$ 。

惟因本研究之樣本較少，且實驗設計仍有不足，如需確認健康檢查陪同服務人員所接受之輻射劑量究為多少，恐需更進一步的研究。

PC015

以 Herfindahl-Hirschman Index 探究檢查開單 是否集中個別醫師之研究 —以南部某醫院核醫心肌灌注掃描檢查為例

卓世傑 張虹麗 梁育雅 鄭揚霖 陳懿貞 李將瑄 顏玉安 張南雄 林凡珍

奇美醫療財團法人奇美醫院核子醫學科

背景介紹：臨床醫師開立的檢查單分布情形，對於檢查單位有極大之意義。一方面，較為均勻之開單情形，可避免檢查單位的作業安排波動過大，浪費人力及資源。另一方面如能掌握臨床醫師開立檢查單是否有集中或偏差顯著之狀況，則更可提供檢查單位極大之改善依據。本研究即以常用來測量產業集中度的 Herfindahl-Hirschman Index (HHI) 為方法，計算南部某醫院核子醫學心臟檢查的開單情形，探究檢查開單情形是否有集中個別醫師之研究。

方法：

1. 收集南部某醫院 107 年 7-12 月，所有開立之核醫心肌灌注掃描檢查單數量及其開單醫師。
2. 將上述資料，以各醫師每個月之開單數量，分別歸類製表。
3. 剔除未完整開立 7-12 月檢查單之醫師，以有完整開立醫師之每月開單數量，分別計算每月之 HHI。
4. HHI 公式如下：

$$HHI = \sum_{i=1}^N (X_i/X)^2 = \sum_{i=1}^N S_i^2$$

X- 完整開立醫師的病人加總 Xi-i 醫師的病人數 Si = Xi / X- 第 i 個醫師的病人占有率
n- 完整開立醫師的人數

結果：

1. 開單之醫師共有 32 位，內含心臟科醫師 17 位，完整開立 7-12 月檢查單之醫師則為 11 位，其每月開單數佔病人數之比例。
2. 經計算 7-12 月之 HHI 分別為 0.121，0.115，0.123，0.112，0.102，0.130。

結論：一般來說 HHI 越大，表示集中程度越高，也就是各醫師開單的偏差較大。依照本研究之結果來看，南部某醫院核醫心肌灌注掃描檢查之開單情形，其 107 年 7-12 月之 HHI 值最大僅 0.130，最小為 0.112，平均則為 0.117，低於通常視為有集中情形之 0.180。因此，南部某醫院核醫心肌灌注掃描檢查之開單情形 並無偏差或集中之狀況。

PC016

洗腎病人接受門診碘 131 治療劑量後之輻射劑量率研究

卓世傑 鄭揚霖 陳懿貞 張虹麗 李將瑄 顏玉安 陳興隆 梁育雅

奇美醫療財團法人奇美醫院核子醫學科

背景介紹：依據 MIRD 第 5 號報告，一般病人接受碘 131 治療 24 小時後，約有 76% 的放射活性會隨尿液、汗、唾液、排遺等排出體外。由於洗腎病人之尿液排放量通常較正常人為少，因此甚難期待洗腎病人 24 小時後放射活性之排出率與一般病人相同。但究竟其排出率為多少，國內之討論與紀錄則似相當稀少。本文即為南部某醫學中心一位洗腎病人接受 30 mCi 碘 131 治療後 7 日之輻射劑量率量測研究記錄。

方法：本文由輻防師以 S. E. 公司之 INSPECTOR 型手提輻射偵檢器 (序號 07890，校正日期 2014.12.3，校正單位：行政院原子能委員會輻射偵測中心)，分別於病人接受 30 mCi 碘 131 治療後之 D + 2 日、D + 5 日及 D + 7 日，至血液透析室之病人床邊距離 1 公尺處，進行量測。

結果：病人接受 30 mCi 碘 131 治療後之 D + 2 日 0810 及 1130 時，測量病人之輻射劑量率分別為 34.72 與 21.28 uSv/h。D + 5 之 0810、1130 時則為 9.74、6.05 uSv/h。D + 7 日 1130 時之測量結果則為 3.92 uSv/h。若以 1 mCi 之碘 131 於 1 公尺處之劑量率為 2.2 uSv/h 換算，則 D + 2 日 0810、1130 時病人剩餘之活度為 15.78、9.67 mCi。D + 5 日 0810、1130 時病人剩餘之活度則為 4.43、2.75 mCi。至 D + 7 日 1130 時測量之病人活度則為 1.78 mCi。

結論：根據本文測量結果換算，則該洗腎病人於接受 30 mCi 碘 131 至尚未洗腎之 D + 2 日 08:10 時排出之活度僅約為 47.4% 與依據 MIRD 第 5 號報告期待之 76% 排出率有相當之差距。但 11:30 時洗腎完畢後之剩餘活度則降至 9.67 mCi，排出率提高為約 67.8%。至洗腎 3 次後之 D + 7 日，病人剩餘活度僅為 1.78 mCi，排出率高達約 94.1%。

PC017

Indium-111 Octreoscan Detected Large Cell Neuroendocrine Carcinoma Presenting with Ectopic Adrenocorticotrophic Hormone Syndrome

Tse-Hao Lee¹, Cheng-Pei Chang¹, Shih-Chieh Lin², Wen-Sheng Huang¹

¹*Department of Nuclear Medicine, Taipei Veterans General Hospital, Taipei, Taiwan, R.O.C.*

²*Department of Pathology and Laboratory Medicine, Taipei Veterans General Hospital, Taipei, Taiwan, R.O.C.*

Introduction: A 70 year-old male patient was diagnosed of ectopic adrenocorticotrophic hormone syndrome (EAS). He initially presented with ACTH-dependent hypercortisolism but Cushing's disease was excluded due to negative result of inferior petrosal sinus sampling test. Chest CT revealed several nodular lesions in the mediastinum but it failed to further characterize the nature of these nodules.

Methods: Indium-111 (In-111) whole body Octreoscan with single photon emission computed tomography/computed tomography (SPECT/CT) was performed after intravenous administration of In-111 labeled octreotide.

Results: In-111 Octreoscan with SPECT/CT accurately detected nodular lesions in the mediastinum with high somatostatin receptor expression. Surgical removal of these nodules was performed and histopathological diagnosis was large cell neuroendocrine carcinoma. Immunochemical staining for ACTH revealed positive result, confirming the ectopic ACTH secretion by large cell neuroendocrine carcinoma. Besides, positive immunochemical staining for somatostatin receptor 2 (SSTR2) expression was compatible with positive In-111 Octreoscan result.

Conclusions: Nuclear medicine image by targeting somatostatin receptor expression, such as In-111 Octreoscan, may be a useful tool for accurate diagnosis of EAS, localization of neuroendocrine tumor and guiding surgical approach.

PC018

Predicting PD-L1 Expression on Lung Cancer Cells Using Different Wavelet Decomposed Radiomic Features of F-18 FDG PET Image

Yu-Hung Chen¹, Shu-Hsin Liu^{1,2}, Sung-Chao Chu³, Sheng-Chieh Chan¹

¹Department of Nuclear Medicine, Hualien Tzu-Chi Hospital, Buddhist Tzu-Chi Medical Foundation, Hualien, Taiwan

²Department of Medical Imaging and Radiological Science, Tzu Chi College of Technology, Hualien, Taiwan

³Department of Hematology and Oncology, Hualien Tzu-Chi Hospital, Buddhist Tzu-Chi Medical Foundation, Hualien, Taiwan

Introduction: PD-L1 expression can guide immune modulation therapy in advanced-stage lung cancer. However, the methods of quantification vary, and sometimes, different staining results contradict each other.

Methods: We conducted a retrospective study investigating 26 patients with lung cancer. Biopsy specimens from all subjects were stained with PD-L1 22C3 Assays (DAKO IHC 22C3 pharmaDx kit), and the expression level was either $\leq 1\%$ (low expression) or $\geq 50\%$ (high expression). All patients received F-18 FDG PET as well. We extract image features of the primary tumor from the original radiomics and eight different wavelet decompositions (LLL, LHL, LHH, LLH, HLL, HHL, HLH, and HHH). We used ROC curve analysis to examine the predictive value of these image features. The results were expressed as area under the curve (AUC) and p -value.

Results: Among all these 230 image features, primary tumor Run Length Matrix high-intensity run emphasis (RLMhire) and primary tumor HLL Texture Feature Coding Matrix coarseness (HLL-TFCcoarseness) were significantly associated with high PD-L1 expression ($p = 0.023$, AUC = 0.785 and $p = 0.017$, AUC = 0.799, respectively). In addition, SUV histogram skewness and kurtosis showed marginal statistical significance ($p = 0.059$, AUC = 0.736 and $p = 0.052$, AUC = 0.743, respectively).

Conclusions: Radiomic features derived from the original as well as wavelet decomposed F-18 FDG PET image may be associated with PD-L1 expression. A larger and longitudinal cohort is warranted to study the association of image features with PD-L1 expression and the response to immune modulation therapy.

PC019

Incorporating Radiomics Into Survival Prediction Model Improves Prognostic Stratification in Patients with EGFR-mutated Lung Adenocarcinoma

Yu-Hung Chen¹, Shu-Hsin Liu^{1,2}, Tso-Fu Wang³, Sheng-Chieh Chan¹

¹Department of Nuclear Medicine, Hualien Tzu-Chi Hospital, Buddhist Tzu-Chi Medical Foundation, Hualien, Taiwan

²Department of Medical Imaging and Radiological Science, Tzu Chi College of Technology, Hualien, Taiwan

³Department of Hematology and Oncology, Hualien Tzu-Chi Hospital, Buddhist Tzu-Chi Medical Foundation, Hualien, Taiwan

Introduction: Most of the patients with EGFR-mutated lung adenocarcinoma are responsive to tyrosine kinase inhibitors (TKI). However, the time to drug failure varies widely. Thus, a more sophisticated prognostic model is warranted.

Methods: We conducted a retrospective study investigating 51 patients with EGFR-mutated lung cancer. All subjects received F-18 FDG PET for staging and then treated primarily with TKI. Twenty-two radiomic features of the primary tumor were extracted from F-18 FDG PET. The radiomic features were dichotomized with median value. The association of radiomic with overall survival (OS) were first analysed using Kaplan-Meier curve (Log rank test). COX regression analysis was used to seek independent predictors of OS. The independent prognosticators were used to devise survival prediction model. We test the model with OS and PFS data and the model was validated by bootstrap internal validation process.

Results: One traditional F-18 FDG PET feature and 5 textural features were selected for COX regression analysis. A primary tumor SUV histogram entropy ≥ 3.71 ($p < 0.001$, HR = 4.143), and pleural effusion ($p = 0.002$, HR = 2.963) were independently associated with poor OS. These two survival prognosticators were used to construct a scoring system (score 0-2), and this model was superior to the traditional TNM staging system ($p < 0.001$ versus $p = 0.019$ for OS; $p = 0.005$ versus $p = 0.422$ for PFS). The c-index of this model for OS and PFS were 0.69 and 0.63, respectively. The results of internal validation showed similar predictive capability in both training and testing sets.

Conclusions: Higher tumor heterogeneity and the presence of pleural effusion indicate poor OS and early disease progression. Our prediction model enables better risk stratification in EGFR-mutated lung cancer and may be used to select candidates for add-on therapy for other targeted gene mutations or immune modulation.

PC020

Exploiting Proliferative Marker F-18 Fluorocholine PET and Radiomics of F-18 Fluoride Image to Improve Detecting Metastasis from Prostate Adenocarcinoma

Yu-Hung Chen¹, Shu-Hsin Liu^{1,2}, Hann-Chorng Kuo³,
Yuan-Hong Jiang³, Jing-Liang Chen³

¹Department of Nuclear Medicine, Hualien Tzu-Chi Hospital, Buddhist Tzu-Chi Medical Foundation, Hualien, Taiwan

²Department of Medical Imaging and Radiological Science, Tzu Chi College of Technology, Hualien, Taiwan

³Department of Urology, Hualien Tzu-Chi Hospital, Buddhist Tzu-Chi Medical Foundation, Hualien, Taiwan

Introduction: F-18 fluoride and F-18 fluorocholine (FCH) PET showed similar sensitivity for prostate cancer metastasis. Yet, fluoride uptake is non-specific. We thus study the added value of FCH PET and radiomics of fluoride image.

Methods: We conduct a prospective study from Jan. 2018 and this study has been approved by local Institutional Review Board and Ethics Committee. All subjects with a diagnosis of prostate adenocarcinoma received F-18 fluoride PET and F-18 FCH PET. Main interpretation of both images was qualitative. We also extract radiomic features from fluoride PET. The reference standard was a combination of pathology, images, and clinical follow-up. ROC curve analysis (corrected by Benjamini Hochberg false discovery rate (FDR)) and logistic regression were used to analyze radiomic features.

Results: We recruited 32 patients. There were 19 fluoride-avid osseous metastases and were all FCH avid. Eleven fluoride avid lesions (3 curvilinear rib lesions, 4 skull, 2 spinal, 1 pelvic and 1 tibial lesions) were determined to be equivocal and FCH PET correctly categorized the entity (1 skull metastasis whereas others benign). The FDR-corrected ROC curve analysis showed 4 radiomic features (SUVmax, SUVmean, SUV SD and SULpeak) were associated with osseous metastasis ($p < 0.05$). After logistic regression, only SULpeak ($p = 0.001$, OR = 1.31) was independent predictor. We applied a SULpeak cutoff of 14.5 with sensitivity and specificity of 80% and 93.6%, respectively. SULpeak correctly categorized 90.9% (10/11) equivocal fluoride avid lesions. Furthermore, F-18 FCH PET identified 8 extra-skeletal cancerous lesions in 7 patients (4 lymph node metastases, 2 cases with pulmonary metastases, one with pleural metastases and one with hepatoma.)

Conclusions: FCH PET is useful in determining the disease nature for equivocal fluoride avid lesions. SULpeak on fluoride PET, although less powerful than FCH PET, may also help to differentiate benign from malignant fluoride avid lesion. F-18 FCH also has the added value of detecting extra-osseous cancerous lesions. However, our results warrant larger cohort to verify the authenticity.

PC021

Intra-adrenal Pheochromocytoma Negative on CT and MRI Detecting by I-123 MIBG SPECT

Ya-Ju Tsai, Tzu-Hua, Lee

Department of Nuclear Medicine, Taipei Medical University Hospital

Introduction: We reported a case with left adrenal pheochromocytoma that is not identified on CT and MRI but detected by I-123 MIBG SPECT.

Case report: 78-yr-old male is a case of hypertension and suspected coronary artery disease. The patient complained episodic hot sensation of trunk and legs with dyspnea and high blood pressure up to 180 mmHg. Rising level of urinary fractionated catecholamines was noted (vanillylmandelic acid is 80.90 mg/24hr). But both abdominal CT and MRI didn't show adrenal or extra-adrenal lesion in the scan field. I-123 MIBG SPECT/CT revealed increased MIBG uptake in left adrenal gland suggest pheochromocytoma without corresponding anatomic adrenal lesion identified on CT. No MIBG-avid tumor was noted in right adrenal gland or extra-adrenal site in whole body survey. The patient received laparoscopic adrenalectomy of left adrenal gland. Pathology revealed a lobulated tumor lesion within the medulla of adrenal gland, measuring 2.5 x 2.4 x 1.0 cm in size. Microscopically, it shows a picture of pheochromocytoma composed of polygonal epitheloid cells arranged in nests, solid sheets, and focal trabecular patterns with rich vasculature within the adrenal medulla.

Discussion: Pheochromocytoma is the tumor arising from sympathetic chromaffin tissue in the adrenal medulla. Measurement of plasma or 24-hour urinary fractionated metanephrines is the best biochemical diagnostic test. The anatomical and functional imaging are critical to guide treatment decisions. For biochemically suspected pheochromocytoma, CT and MRI have high sensitivity and specificity (> 90%) in localizing pheochromocytoma. Radionuclide imaging such as MIBG scintigraphy, FDG-PET and somatostatin receptor (SSTR) imaging provide functional information. The specificity of MBG is high although physiologic adrenal uptake may result in false-positives. Variable sensitivity of MIBG scintigraphy to detect adrenal or extra-adrenal pheochromocytoma has been reported. The sensitivity of MIBG is lower than that of CT, MRI, FDG, and Ga-68 somatostatin analogs because false negatives may occur in small and extra-adrenal pheochromocytomas, and pheochromocytomas with pseudohypoxic gene mutations. Different gene mutations are reported in 32–79% of cases. In our case, the intra-adrenal pheochromocytoma appears a rare imaging pattern that it is not identified on CT and MRI, which have high sensitivity, but detected by I-123 MIBG SPECT.

Conclusion: It could be suggested that the high specificity and positive predictive value of MIBG SPECT provide strong evidence of the presence of pheochromocytomas or paragangliomas in patients with biochemically suspected catecholamine-secreting tumors, even though anatomic imaging is negative.

PC022

複合式單光子電腦斷層掃描儀 (SPECT/CT) 之全身骨頭掃描案例分享

黃信慈 陳慶元

佛教慈濟醫療財團法人台中慈濟醫院

背景介紹：骨骼掃描是目前唯一可以進行全身骨骼癌症轉移的篩檢工具，其敏感度比 X 光高 30-40%，且發現病灶的時間可以比 X 光提早 3-6 個月。X 光必須要骨密度改變 50% 左右才會顯示出異常，而全身骨骼掃描則在疾病早期血流增加或成骨活動增強時就可以清楚看到，是各種癌症骨轉移的最佳篩檢工具。

案例報告：該案例為女性 (65 歲) 有子宮頸癌病史 (100.1)，已手術、放療、化療完成，後續自行吃中藥治療；今年因喘掛急診後發現右胸積水疑似轉移性肺病，給予豬尾巴導管引流肋膜積水，電腦斷層掃描後確診為肺癌合併肝轉移。肺癌患者約有三成至五成有骨骼轉移，所以病患在治療之前的疾病分期，或是在治療後的追蹤過程中，常會進行全身骨骼掃描，檢查是否有骨骼轉移的情形。

結果：骨骼掃描靜脈注射 Tc-99m MDP 20 mCi 放射性追蹤劑後 3 小時，掃描顯示右側額骨、第 1.9.10 胸椎、第 4 腰椎以及右側第 7.9.10 肋骨放射攝取相對增加；但意外在腹部發現有很高的放射攝取，執行腹部掃描的 SPECT / CT 後顯示大量放射活性聚集處為在結腸的乙狀結腸和下行段。由於之前病史發現子宮頸腫瘤侵犯膀胱和直腸結腸，懷疑有膀胱結腸造瘻。

結論：「複合式單光子電腦斷層造影儀」結合單光子電腦斷層造影儀 (SPECT) 及電腦斷層儀 (CT)，除了可執行傳統核醫所有造影功能外，並附加低功率 X 光電腦斷層，能獲得融合核醫與電腦斷層的立體影像，提供清楚的解剖位置，增強醫師判讀的信心與報告的正確性。除了用在提升解剖定位精確性外，還可以廣泛用在特定檢查的衰減校正，以達到更符合真實的影像品質與診斷結果。

PC023

壁報論文發表摘要·臨床組

腦質斷層灌注掃描 (Cerebral Perfusion SPECT Scan) 之案例分享

黃信慈 陳慶元

佛教慈濟醫療財團法人台中慈濟醫院

背景介紹：隨著社會結構的高齡化導致人口急速老化，腦部相關疾病也與日俱增，核子醫學在這方面檢查優勢，功能性腦血流灌注檢查，利用放射性示蹤劑，可了解病患腦部血流分佈圖譜，臨床上可以用來協助腦血管病變、癲癇病灶、失智症等之診斷，再結合影像醫學科系資料 (MRI)，達到更全面化影像 (分子與功能性影像)，提高診斷效率與精準性。臨床上常見中風或腦傷患者，醫師多半注重在患者肢體癱瘓或麻木等活動上的問題，對於神經系統病變引起的語言障礙經常忽略。本案例失語症 (Aphasia) 是指後天性腦傷所導致的語言障礙，最常見的病因是由中風 (CVA) 所引起的；神經心理學測驗是一種大腦功能性的檢查，主要在測驗病患是否有大腦認知功能的缺損，也可以測量心智功能，注意力，語言障礙，記憶功能，視覺空間功能與大腦高級認知功能。

案例報告：該案例為男性 (59 歲) 有中風病史 (107.12)，後續出現失讀及記憶等相關問題，經由神經心理學檢查鑑別有明顯語言問題、可能的視空間知覺及記憶能力缺損。其中語言問題，尤其表現在其命名物品，閱讀及書寫表現較差 (Pure Alexia)，且幾乎無法念讀文字，書寫上僅部分正確；但在生活一般溝通上語言的表達及理解未出現明顯困難，這類群過去的報導多概述是受損部位在 L't Temporo-Occipital Lobe 部分，該個案有施行腦血流灌注掃描 (Cerebral Perfusion Scan ECD) 及磁振造影 (MRI)，均發現在左側顳葉及枕葉部分有異常缺損。

結論：利用核醫工作站 (Xeleris 3)，進行影像融合 (SPECT/MRI)，可以提高影像達到分子與功能性目的，進而提供臨床科系最佳診斷訊息，本案例經由融合後發現，腦血流灌注缺損與磁振造影發現異常部位極為一致，神經心理學檢查也經評估後推測可能是該部位受損。

PC024

利用閉氣肺部電腦斷層來降低呼吸假影

沈淑禎¹ 曾柏銘² 呂建璋¹ 門朝陽² 林雅婷¹ 蕭聿謙³

¹天主教中華聖母修女會醫療財團法人天主教聖馬爾定醫院核子醫學科

²天主教中華聖母修女會醫療財團法人天主教聖馬爾定醫院正子造影中心

³亞東紀念醫院核子醫學科

背景介紹：現在 PET/CT 的電腦斷層因掃描速度快，病人在掃描過程中閉氣或做較淺的吸呼運動所得的影像，在執行衰減校正時常因和正子影像處於不同的呼吸時期而出現影像錯位 (misalignment)。假影無法精確地找出病灶之所在，故此次利用肺部閉氣之方法，來降低呼吸假影之產生。

方法：我們收集了十位位人，在照完第一套的正子全身掃描後，如發現病患肺部有病變或因其它影像導致無法有效判斷肺部是否有病變時，均加做一套閉氣電腦斷層掃描。

結果：做完發現閉氣的電腦斷層掃描可明顯的改善因閉氣帶來的肺部影響。其中一位病人在 early view 做完，被懷疑為肺部轉移，再作一套閉氣之電腦斷層掃描後，確定該病灶是由下方的極左肝葉所造成的影像錯位，而肺部本身則是無任何病灶，此案例則為因吸呼的錯位而造成得誤判。

結論：為了解決呼吸所帶來的假影問題，有研究團隊提出使用呼吸閥控 (Respiratory Gated) 裝置來配合取像來解決呼吸假影的問題，但目前一般商業化的 PET/CT 造影並未搭載呼吸閥控裝置，流程麻煩且造價昂貴，並不是每家醫院都能負擔，故對於肺部懷疑有轉移的病患，建議增加一組閉氣之電腦斷層攝影，不但可提高診斷的準確性，又可降低吸呼所帶來之假影實為經濟又實惠之方法。

PC025

降低因注射所引起藥物堆積之經驗分享

曾柏銘¹ 呂建璋² 沈淑禎² 門朝陽¹ 林雅婷² 蕭聿謙³

¹天主教中華聖母修女會醫療財團法人天主教聖馬爾定醫院正子造影中心

²天主教中華聖母修女會醫療財團法人天主教聖馬爾定醫院核子醫學科

³亞東紀念醫院核子醫學科

背景介紹：核子醫學的檢查是使用診斷用藥物，標記在非穩定之放射性同位素上(以下簡稱核醫藥物)，使得造影劑在進入身體後，能依據各種不同診斷藥物進行不同之分佈。然而，在臨床上，注射核醫藥物同時卻很有可能將一部份之藥物殘留在留置針或病人之血管內，進而造成影像品質及醫師之診斷率下降，此情況以全身性檢查如骨骼掃描更為明顯，故降低因注射所引起之藥物堆積，為我們此次之研究重點。

方法：本次研究所稱之藥物堆積造成之影像不良，包含病人之留置針及血管所造成之影像堆積，其藥物堆積之程度需靠手動方式來調整影像品質，或需將因堆積所造成之核醫藥物屏蔽掉才可進行影像調整之案例。調查 108 年 01-03 月骨骼掃描因注射核醫藥物造成之影像不良數共有 16 例，佔所有骨骼掃描檢查 6% (16/264)，所有病人皆由護理師確認管路暢通。經數次開會討論後，決議將於每位病人於留置針設定完之後，先給予 3 c.c. 生理食鹽水進行管路測試以確定留置針是否通順。待注射完核醫藥物之後，再另給予 7 c.c. 之生理食鹽水，以「壓 - 停 - 壓」之間歇性方法進行沖洗；若為住院病人，則於病人打藥前前回抽觀察留置針有無回血，再使用 3 c.c. 之生理食鹽水測試是否順暢，若住院病人使用 T-connect 留置針，則避開較長管路，直接由留置頭頭部，亦進行『壓 - 停 - 壓』之間歇性方法進行沖洗。

結果：我們統計了 108 年 05-06 月之骨骼掃描造影人數為 188 位，因注射核醫藥物造成之影像不良片數僅 1 例，佔所有骨骼掃描 0.5%，與 01-03 月相比，降低了 5.95%，研究結果非常成功，可做為未來科內之建議實施改善流程。

結論：本次研究發現大部份的核醫藥物堆積都來於漏針及留置針堆積所造成，藉由此次研究，能消除大部份因漏針或留置針所帶來藥物堆積之問題。但仍有些因血管壁所造成之核醫藥物堆積仍無法有效解決，與護理師討論後亦無太大之改善空間，護理師於注射當下亦無感到任何異常。故如何降低因血管壁造成之藥物堆積，則是我們下期之研究重點。

PC026

降低骨骼掃描病患於檢查前解尿不完全件數

曾柏銘¹ 陳昭芸³ 沈淑禎² 門朝陽¹ 呂建璋² 林雅婷² 蕭聿謙⁴

¹天主教中華聖母修女會醫療財團法人天主教聖馬爾定醫院正子造影中心

²天主教中華聖母修女會醫療財團法人天主教聖馬爾定醫院核子醫學科

³天主教中華聖母修女會醫療財團法人天主教聖馬爾定醫院管理科

⁴亞東紀念醫院核子醫學科

背景介紹：骨骼掃描為全身性骨骼檢查，需要一段檢查時間掃描且需要患者配合。如遇病患解尿不完全則會造成影像不良之情形，醫事放射師需等待至全身掃描結束後，進入攝影室排除影像不良原因，並再次進行局部掃描，將會影響現有病人及下一位病人檢查等待時間，使整體之醫病關係下降，而影像品質下降之結果亦無法供臨床醫師判讀，且影響病人疾病診斷之時效性。

本院統計 2019 年 1 月至 3 月因解尿不完全導致骨骼掃描影像不良共計 13 件，故運用 FOCUS-PDCA 手法進行改善，降低病患骨骼掃描檢查前解尿不完全件數，以提升骨骼掃描影像品質。

方法：為瞭解病患骨骼掃描檢查前解尿不完全之原因，由醫師、醫事放射師及管理師共 6 人組成 FOCUS-PDCA 改善小組，經原因樹 (why tree) 方法確認根本原因為以下二點：(一) 未明確提醒並說明解尿時間、(二) 未依規定解尿。

根據上述 2 點根本原因擬定改善對策行動計畫：

- (一) 利用 QC 手法愚巧法之提示法，製作叮嚀卡片於核子醫學科櫃檯，提示行政助理在病人報到時【提醒病人於檢查前五分鐘解尿】。
- (二) 利用 QC 手法愚巧法之提示法，製作解尿重要性之衛教海報貼於檢查室門口，提醒醫事放射師確認病患使否以解尿及讓病人了解檢查前解尿之重要性。
- (三) 進行核子醫學科 2 位護理師及 2 位醫事放射師執行確認病患是否解尿之教育訓練及稽核。

討論：經製作叮嚀小卡、衛教海報、教育訓練實施後，統計 2019 年 5 月至 6 月解尿不完全導致骨骼掃描影像不良共計 4 件 (平均 2 件 / 月)，較改善前每月平均減少 5 成。

結論：隨著造影設備、放射性製藥等多方面迅速發展，骨骼掃描對於骨骼病變能更早的被偵測出來，對於患者能早期診斷並施以相應之治療，能增加治癒之機會。

藉由改善骨骼掃描前置準備流程，明顯減少骨骼掃描影像不良件數，有效提升影像品質，有助於提升診斷之時效性及正確性，對於醫療品質之提升及患者就醫即時性皆是不可或缺。

PC027

利用鼓氣可順利分辨舌頭及口腔黏膜之 FDG 攝取

曾柏銘¹ 呂建璋² 沈淑禎² 門朝陽¹ 林雅婷² 蕭聿謙³

¹天主教中華聖母修女會醫療財團法人天主教聖馬爾定醫院正子造影中心

²天主教中華聖母修女會醫療財團法人天主教聖馬爾定醫院核子醫學科

³亞東紀念醫院核子醫學科

背景介紹：PET/CT 為結合功能性及解剖學影像的一台儀器，利用其功能性影像及全身性掃描，可探究人體組織或器官內細胞的代謝情況。但由於頭頸部構造，舌頭於掃描中會因為肌肉的不自主收縮而呈現 FDG 攝取，如此狀況發生於口腔部腫瘤之患者，會呈現影像混淆不清的狀況而影響臨床醫師診斷，故此次是利用了患者鼓氣的方式進行掃描，來評估頭頸部患是否能將舌頭與口腔黏膜部之空間分開，以利分辨不同部位的病灶。

方法：我們收集了十位口腔癌之患者進行掃描，在正常（無特別鼓氣）的情況下進行 Early 與 Delay view 掃描後，於最後加照口腔部鼓氣照，藉此來比對患者鼓氣前後的影像差異。

討論：在文獻中，很少有 PET/CT 在評估口腔癌的方法，而評估口腔癌原發病灶及後續追蹤的最佳技術現今也仍有爭論，其中 FDG 無法給予準確之定位，且原發病灶也會因附近之肌肉、發炎、唾液腺、開刀、放射、化學治療、以及腫瘤與腫瘤分化的差異也有所限制。目前 MRI 已被證實在評估舌癌分期是較具優勢的。而舌頭為口腔中可見之器官，於臨床中用肉眼即可進行診斷，如 PET/CT 能分辨 FDG 之攝取為舌頭或口腔黏膜，對病患的後續治療則會有很大的幫助。

結論：與沒閉氣的 PET/CT 頭頸部患者相比，有鼓氣的病患確實可改善口腔癌患者的腫瘤定位，評估腫瘤範圍，並檢測附近結構的腫瘤侵犯情況。鼓氣掃描可與病人在約定時間內進行掃描，在掃描完頭部之後即可請患者放鬆口腔部位肌肉以降低病患之不適。病人在接受口腔鼓氣攝影之後，即使病人鼓氣的幅度不是很大，但仍能將一部份口腔部及舌頭之 FDG 吸收分開。

PC028

由於膈神經麻痺導致對側橫膈膜 FDG 之不正常顯影 — 案例報告

曾柏銘¹ 呂建璋² 沈淑禎² 門朝陽¹ 林雅婷² 蕭聿謙³

¹ 天主教中華聖母修女會醫療財團法人天主教聖馬爾定醫院正子造影中心

² 天主教中華聖母修女會醫療財團法人天主教聖馬爾定醫院核子醫學科

³ 亞東紀念醫院核子醫學科

背景：在進行正子造影檢查時常常會看到肺部肌肉有 FDG 攝取，通常是因不自主的肌肉收縮所造成，常見於運動、過度呼吸或壓力引起的肌肉痙攣，或是轉移性病變。

案例報告：一名 74 歲男性病患，被診斷為左側肺癌併發左側肋膜積水，主要症狀為呼吸急促，該病患於 PET/CT 顯示肺左上葉 (LUR) 腫瘤、左側肋膜積水，及橫膈膜淋巴結轉移外，特別的是單側右邊橫膈膜具有 FDG 瀰漫性的吸收，在仔細對照肺部電腦斷層 (Computed Tomography)，右側肺臟在解剖結構上並無異常。

結果：單側之橫膈膜吸收增加，主要的原因乃橫膈麻痺 (diaphragmatic paralysis) 導致肺部體積縮小而塌陷 (atelectasis) 所造成；另一項則可能為肺部惡性轉移。但這位患者為左側肺癌，經仔細比對後發現肺臟右側之電腦斷層 (Computed Tomography) 影像並無異常，最可能的原因是左側大量肋膜積水引起呼吸頻率急促，導致右側橫膈膜過度使用所造成的。

結論：肺部肌肉的 FDG 攝取增加常見於不自主的肌肉收縮、胰島素分泌增加、以及開刀等影響；而單側橫膈膜 FDG 攝取增加則可能是因為病理性因素如原發性惡性腫瘤轉移，而生理性因素大都是對側病灶引發補償性對側呼吸肌肉增加，導致呼吸肌肉過度用力而造成，故此類之病患應仔細比對其它影像以免導致誤判。

PC029

Does Administration of Tc-99m Bone Radiopharmaceutical Interfere with the Bone Mineral Density Measurement Using Dual-Energy X-ray Absorptiometry?

Ching-Lin Sung^{1,3}, Yu-Hung Chen¹, Shu-Hsin Liu^{1,2}, Kun-Han Lue^{1,3,4}

¹Department of Nuclear Medicine, Hualien Tzu-Chi Hospital, Buddhist Tzu Chi Medical Foundation, Hualien, Taiwan

²Department of Medical Imaging and Radiological Sciences, Tzu Chi University of Science and Technology

³Hualien Hsien Association of Radiological Technologists

⁴Department of Biomedical Engineering and Environmental Sciences National Tsing Hua University Hsinchu Taiwan

Introduction: Literatures studying the interference of bone tracers on Dual-Energy X-ray Absorptiometry (DXA) measurement has shown conflicting results. In addition, most of the studies were small-scaled and retrospective. Therefore, we conducted a prospective study to evaluate the effect of Tc-99m bone tracer on bone mineral density (BMD) measurement.

Materials & Method: We prospectively enrolled 46 patients scheduled for Tc-99m MDP scan. Patient received DXA measurement before and after (when imaging bone scan) tracer injection. The DXA system was GE lunar Prodigy Primo. We measured central DXA including lumbar spine, total hip and femoral neck. Paired t-test was used to compare BMD before and after tracer injection. Least significant change (LSC) was also calculated using another cohort (30 volunteers). We used logistic regression model to seek possible independent risk factor of significant BMD reduction after tracer injection (BMD reduction exceeding LSC).

Results: There were 43 lumbar spine BMD, 91 total hip BMD and 91 femoral neck BMD analyzed. The mean changes of L-spine BMD, total hip BMD and femoral neck BMD after Tc-99m MDP injection were 0.192 ± 0.036 , 0.002 ± 0.016 , and 0.003 ± 0.024 , respectively. We found significant reduction of BMD measurement after tracer injection in lumbar spines ($p = 0.001$), but not in total hip or femoral neck ($p > 0.05$). The logistic regression analysis revealed that Body Mass Index (OR = 1.209, $p = 0.001$) and measuring Lumbar spine (OR = 13.438, $p = 0.000$) were independent risk factors of significant BMD reduction after tracer injection (BMD reduction exceeding LSC).

Conclusion: Hip BMD measurement was not significantly interfered by Tc-99m bone tracer. However, measuring lumbar spine and larger body size are associated with significant BMD reduction after bone tracer injection. Therefore, after bone tracer injection, we should avoid measuring lumbar spine BMD, especially for those with a higher BMI.

PC030

以田口實驗法探討核子醫學骨頭掃描之最佳攝影參數

劉宛茹^{1,2} 潘榕光²

¹ 台中慈濟醫院核子醫學科

² 中台科技大學醫學影像暨放射科學系

背景介紹：核子醫學骨骼掃描有反映局部血流量及骨骼代謝活躍程度，因其靈敏度高、輻射劑量低並能檢查全身骨骼，臨床應用日益普遍。參照其它影像檢查，可進一步提昇骨骼掃描的診斷特異度。

^{99m}Tc-MDP 是骨骼掃描的常用藥物，經由靜脈注射後隨血流運送到全身組織，靜脈注射後約 2~4 小時後進行全身造影。

此次實驗利用田口方法尋找核子醫學骨頭掃描之最佳攝影參數，利用假體驗證找出最佳化條件組合，有助於影像的空間解析度與對比度的提升，未來可應用於臨床上，以達提升臨床骨骼掃描的影像品質。

方法：此實驗根據常用的造影條件，選擇可能會影響影像解析度的條件六個因子：準直儀、距離、掃描時間、能窗、矩陣大小、放大倍率，進行田口 L18 的實驗。將因子帶入田口 L18 直交表，設定不同的掃描條件，使用 GE Infinia Hawkeye 4 SPECT/CT，將 100 c.c. 的水加入 4 mCi 的 ^{99m}Tc-MDP，並將其染色後，注入壓克力假體，並進行攝影。攝影條件所得出之影像，共十八張，請三位工作同仁進行排序評分，影像品質最好為 18 分，最差為 1 分，進行評分。

結果：利用田口 L18 直交表做核子醫學骨頭掃描影像最佳化，發現影響影像解析度因子最主要為準質儀及距離。得出最佳化的條件設定準質儀 (LEHR)、距離 (20 cm)、掃描時間 (300 sec)、能窗 (16%)、矩陣大小 (256 x 256)、放大倍率 (1.00)。

結論：在核子醫學科的檢查中，骨骼掃描由於具有高敏感度及早期偵測骨骼病灶的能力，在臨床上應用的很廣泛，是核醫檢查中最重要之項目之一。執行骨骼掃描檢查時，會先掃描患者全身，若在全身掃描的影像中有發現部分區域有異常吸收時，則會針對該區域進行靜態的照影。此次實驗目的為了能在靜態照影時，提供更清晰的影像，因此利用田口方法找出影像解析度最佳之條件進行攝影，期望可輔助醫師進行影像判斷。

PC031

Reverting Iodine Avidity of Radioiodine Refractory Differentiated Thyroid Cancer with Anaplastic Dedifferentiation: A Case Report

Yi-Chen Wu^{1,2,3}, Huei-Yong Chen¹, Jyum-Ying Huang¹

¹Department of Nuclear Medicine, E-DA Hospital, Kaohsiung, Taiwan

²Department of Medical Imaging and Radiological Sciences, I-Shou University, Kaohsiung, Taiwan

³Department of Information Engineering, I-Shou University, Kaohsiung, Taiwan

Introduction: Although most differentiated thyroid cancers show excellent prognosis, treating radioiodine refractory differentiated thyroid cancer (RR-DTC) is challenging. Redifferentiation followed by radioiodine therapy is a promising alternative therapy for RR-DTC. Beside, radioactive-iodine (RAI) therapy is also typically unprevailing as anaplastic thyroid cancer (ATC) management, owing to the decrease in the endogenous sodium iodide symporter (NIS) expression. Therefore, new strategies for NIS re-induction are required to improve the efficacy of RAI therapy in ATC. Targeted molecules are used as redifferentiation agents in recently. We report a case of radioiodine refractory papillary thyroid cancer with anaplastic dedifferentiation shows reverting iodine avidity after the target therapy by the Sorafenib and followed by radioiodine therapy.

Case report: A 56 years-old man with history of nasopharyngeal cancer, AJCC stage II (cT2N1M0), status post definitive concurrent chemoradiotherapy on 2008 and cervical esophageal cancer, cT3N1Mx, status post concurrent chemoradiotherapy on 2012 with residual tumor. Papillary thyroid carcinoma with anaplastic dedifferentiation was found in Aug, 2017. He received bilateral total thyroidectomy and then, esophagus invasion with tracheal margin and peritracheal soft tissue invasion were founded. Total esophagectomy and elongated gastric tube pull-up, lymph node dissections, feeding jejunostomy, total laryngectomy, left neck dissection and permanent tracheotomy were done at that time. Radioactive iodine ablation therapy with 150 mCi was given on Nov, 2017. The post therapeutic I-131 whole body scan showed negative finding. ¹⁸F-FDG PET/CT was arranged and multiple metastatic lesions at lung, mesentery and rectus abdominis muscle were founded. As the radioiodine refractory differentiated thyroid cancer was found, he started the target therapy by Sorafenib on Feb, 2018 and showed partial response. A second radioactive iodine therapy with 200 mCi was given on May, 2018. The post therapeutic I-131 whole body scan with SPECT/CT showed a radioiodine avid lesion at the mesentery, which was corresponding to the lesion seen on the previous ¹⁸F-FDG PET/CT scan. A follow up ¹⁸F-FDG PET/CT was arranged. In despite of the disease showed progression, the lesion at the mesentery showed regression. Unfortunately, as the disease progressed, he was expired on May, 2019.

Conclusion: Radioiodine is the most effective therapy for patients with residual DTC after surgery, unresectable disease, or distant metastasis. For patients whose tumors are either resistant to radioiodine or become refractory to radioiodine over time, new therapies are needed. Redifferentiation therapy followed by I-131 therapy is an alternative option for RR-DTC patients. Treatment with these targeted molecules, like MEK/ERK inhibitors, including Sorafenib, resulted in increased radioiodine uptake by enhanced NIS expression in DTC, as this case we showed. It might enhance efficacy of radioiodine therapy and improve outcome of RR-DTC, which is refractory to conventional radioiodine treatment.

PC032

A Case of Periaortic Inflammation at the Iliac Bifurcation on ^{18}F -FDG PET/CT and Radionuclide Venography

Chun-Yin Huang, Huei-Yong Chen, Yi-Chen Wu

Department of Nuclear Medicine, E-DA Hospital, Kaohsiung, Taiwan

Introduction: Although ^{18}F -FDG PET/CT is mostly used in the workup for malignancy, FDG accumulation can also be instigated by inflammation. We report a case of periaortic inflammation at the iliac bifurcation detected by ^{18}F -FDG PET/CT. Furthermore, ilio caval venous obstruction is proven by radionuclide venography.

Case report: A 39 year-old man had rupture of mycotic aneurysm at aortic bifurcation and received surgical management including resection, debridement of infected tissues, and graft replacement about three years ago. He has suffered from chronic non-healing wounds on the bilateral feet caused by fall from height since ten months ago. Because of the foot wounds, he was admitted to the hospital for surgical debridement and antibiotics. Gallium-67 scintigraphy would have been arranged for application of hyperbaric oxygen therapy. However, a shortage of supply of Gallium-67 made us turn to ^{18}F -FDG PET/CT. The whole body PET/CT images demonstrated significant ^{18}F -FDG uptake not only in the regions of bilateral feet, but also the bifurcations of abdominal aorta and inferior vena cava. Contrast-enhanced CT disclosed thrombosis and obliteration of the abdominal aorta from the infrarenal level to common external iliac arteries. Radionuclide venography of lower extremities showed poor visualization of bilateral common iliac veins with collateral circulation in the bilateral lumbar veins and bilateral ascending lumbar veins. Hyperbaric oxygen therapy and apixaban, an anticoagulant, were added. The foot wounds improved gradually and antibiotics therapy was continued in outpatient department.

Conclusions: In this case we report the findings of ^{18}F -FDG PET/CT and radionuclide venography, which support abdominal vascular occlusion. Chronic non-healing wounds on the bilateral feet may be attributed to poor blood supply for this patient. We also prove the value of ^{18}F -FDG PET/CT for inflammation workup.

PC033

The Importance of Optimal ROIs Delineation in FBPA-PET and Correlation of Tumours' Response After BNCT

Ko-Han Lin¹, Yi-Wen Lo¹, Jia-Cheng Lee², Yong-Sin Hu^{3,4}, Chien-Ying Li¹,
Yi-Lun Chen¹, Chi-Shuo Lin², Wen-Sheng Huang¹, Yi-Wei Chen^{2,4}

¹Integrated PET/MR Imaging Centre, Department of Nuclear Medicine,
Taipei Veterans General Hospital, Taipei, Taiwan

²Division of Radiotherapy, Department of Oncology Medicine, Taipei Veterans General Hospital, Taiwan

³Department of Radiology, Taipei Veterans General Hospital, Taipei, Taiwan

⁴School of Medicine, National Yang-Ming University, Taipei, Taiwan

Introduction: The boron neutron capture therapy (BNCT) is a high selective treatment with FBPA-PET pre-treatment survey. In the past decade, the patients were recruited to implement the BNCT treatment by the tumour-to-normal ratio (T/N) of FBPA-PET with standardized uptake values ratio (SUVr) > 2.5. However, there is no specific study for the region-of-interests (ROIs) selection for FBPA-PET about the specific normal region. This study would like to reveal the optimal ROIs assessment within reasonable time and precise information for the BNCT planning to achieve with better tumour response. Thus, to find consistent and practical ROIs with standard-operating-procedure (SOP) is the critical purpose of this study.

Methods: In this retrospective study, overall 25 subjects (15 males and 10 females) with age from 7 to 70-years-old were referred through the compassionate therapy application of BNCT in the Taipei Veterans General Hospital from February 2017 to May 2018. The FBPA-PET/CT performed 40 ~ 60 minutes after intravenous injection of ¹⁸F-FBPA with 5.2 ± 0.82 mCi (194.99 ± 30.34 MBq). The optimal ROIs determinations were implemented by four readers by double-blind test and data were analysed by the weighted algorithm which can benchmark with the commercial planning software. The tumour response assessment was conducted by two medical physicians to determine the differences between the pre-treatment and post-treatment gross tumour volume (GTV) for the tumour shrinkage rate (TSR) and evaluated by RECIST (version 1.1).

Results: After the statistics by intraclass correlation coefficient (ICC) (n = 25), the tumours' SUV ICC by weighted algorithm and the tumours' SUV ICC by Eclipse™ were strong agreement by 0.812 to 0.889 (p < 0.001). The SUV of the normal tissue at cerebrum between data from department of nuclear medicine and four readers were ICC from -0.023 (p = 0.522) to 0.439 (p = 0.082). The SUV of the normal tissue following with the new protocol were perfect agreement by ICC from 0.807 to 0.894 (p < 0.05). The tumour-to-cerebellum ratio (T/Ncere) and the SUV of the cerebellum as the normal baseline have substantial to perfect agreement by ICC of T/Ncere from 0.679 (p < 0.05) to 0.84 (p < 0.05) and ICC of Ncere from 0.909 to 0.921 (p < 0.05) respectively. The tumour-to-brain stem ratio (T/NBS) and the SUV of the brain stem as the normal tissue have ICC of T/NBS from 0.296 (p = 0.198) to 0.772 (p < 0.05); the ICC of NBS were by 0.316 (p = 0.179) to 0.853 (p < 0.05). Regarding tumour response (n = 20), the Pearson's correlations (r) of TSR for T/NNM, T/NPlan, T/Ncere and T/NBS were 0.35 (p = 0.13), 0.12 (p = 0.60), 0.44 (p < 0.05) and 0.65 (p < 0.05). The Pearson's correlations (r) of RECIST in four T/Ns were 0.20 (p = 0.40), 0.03 (p = 0.90), 0.48 (p < 0.05) and 0.50 (p < 0.05).

Conclusion: Regarding a successful BNCT, the optimal ROI selections for FBPA-PET are crucial not only in the metabolic tumour volume (MTV) measurement but also in the normal tissue baseline. Our measurements revealed that if we select the cerebellum and Pons precisely, the correlation between T/N and tumour response is close to excellent agreement. Regarding the feasibility in clinic, the cerebellum as the normal referencing tissue is the optimal baseline to improve the treatment response efficiently.

PC034

比較不同造影角度及分析軟體 在多門控取像法的左心室射出分率

魏文祺 徐景龍 黃文盛

臺北榮民總醫院核子醫學部

背景介紹：多門控取像法 (Multiple Gated Acquisition, MUGA) 常用於評估左心室的射出分率 (Ejection Fraction, EF)。為了準確地獲得射出分率，必需調整探頭的取像角度，將左、右心室清楚分開。然而，每位病人心臟角度的差異及不同放射師在造影角度的選擇上可能不相同。本研究的目的是比較同一病人在不同造影角度及使用不同分析軟體在多門控取像法的左心室射出分率。

方法：59 位病人 (10 男，男 / 女：55±11/71±14 歲)，採用紅血球體內標誌技術，於注射 20 mCi ^{99m}Tc 20 分鐘後用 Siemens E-cam 造影儀執行造影。先以 ECT (Emission Computer Tomography) 採像模式收集胸部左側至正面的影像 (10 秒 / 影像，1 幀影像 / 3 度，矩陣大小為 64×64)，將影像中，左、右心室分離最大，心中膈最清楚的定義為角度 1，最小可分辨影像定義為角度 2。在這些病人中，此兩角度差異從 6 到 15 度之間。分別執行此兩角度的多門控取像。使用 Siemens E-soft 及 GE Xeleris 計算左心室的射出分率，統計分析使用 PSPP 統計軟體。

結果：Siemens E-soft 軟體計算所得角度 1 及角度 2 的射出分率分別為 62.11±8.27% 與 62.28±8.65%， $P = 0.74$ ；GE Xeleris 為 61.45±7.90% 與 61.01±9.08%， $P = 0.43$ 。角度 1 及角度 2 所得的射出分率並無顯著性差異。使用 Siemens E-soft 及 GE Xeleris 軟體計算出的左心室射出分率也近似。

結論：在執行多門控取像前，使用 ECT 採像模式可協助放射師找出最佳的造影角度。只要左、右心室能清楚分開，即使造影角度不同，其射出分率也無顯著差異。不同廠商提供的分析軟體所計算出的結果是近似的。

PC035

Association Between High-Sensitivity Cardiac Troponin I Levels and Myocardial Ischemia

Li-Hua Tang^{1,2}, Jei-Yie Huang^{1,3}, Ruoh-Fang Yen¹

¹*Department of Nuclear Medicine, National Taiwan University Hospital and
National Taiwan University College of Medicine, Taipei, Taiwan*

²*School of Nursing, College of Medicine, National Taiwan University, Taipei, Taiwan*

³*Institute of Epidemiology and Preventive Medicine, College of Public Health,
National Taiwan University, Taipei, Taiwan*

Introduction: Cardiac troponin I (cTroI) is a specific and sensitive biomarkers for cardiac injury. Prior studies reported the diagnostic performance of sensitive cTroI, which could improve early diagnosis of myocardial infarction. Recent reports also indicated that high-sensitivity cTroI can released in myocardial ischemia, even in the absence of necrosis and could be associated with outcomes.

The aim of this study is to find the association between hs-cTnI and myocardial ischemia and the predictive value of hs-cTnI. Myocardial ischemia is defined by radionuclide myocardial perfusion imaging (MPI).

Methods: We prospectively enrolled patients with suspected CAD and was referred to nuclear medicine department for MPI from April, 2018 to October, 2018. All patients underwent standard exercise thallium-201 MPI with bruce protocol. Plasma hs-cTnI was measured at rest and at peak stress (reach of 85% maximal hear rate). MPI were interpreted blindly using a 17-segment model and summed stress scores (SSS) and total perfusion deficit (TPD) were calculated.

Results: A total of 125 (mean age: 60.56 + /- 8.84), 88 (70.4%) men) were enrolled in this study. There was a strong and significant correlation between post-stress hs TroI and rest hs TroI. There were also significant correlation between hs Tro I and SSS, which indicated myocardial injury. However, there was no significant correlation between hs Tro I and TPD, which implied ischemic burden. A trend of elevated hs Tro I in the abnormal SSS group and abnormal TPD group was noted.

Conclusions: High sensitivity TroI is a stable biomarker in the human body, regardless of stress or rest status. A trend of elevated hs Tro I was noted in ischemic patients. Further evaluation and follow-up should be done to evaluate the predictive value of hs Tro I in the future.

PC036

Effect of Medical Therapy in A Patient with Stable Ischemic Heart Disease Demonstrated by Myocardial Perfusion Scan

Tzyy-Ling Chuang^{1,2}, Chih-Wei Chen^{3,4}

¹Department of Nuclear Medicine, Dalin Tzu Chi Hospital, Buddhist Tzu Chi Medical Foundation, Chiayi, Taiwan

²School of Medicine, Tzu Chi University, Hualien, Taiwan

³ChenChihWei Clinic, Chiayi, Taiwan

⁴Department of Cardiology, Dalin Tzu Chi Hospital, Buddhist Tzu Chi Medical Foundation, Chiayi, Taiwan

Introduction: We present a case of stable ischemic heart disease under medical therapy and with interval improvement demonstrated by myocardial perfusion scan (MPS).

Case report: A 51-year-old male had effort dyspnea and chest tightness since two months ago in April 2016. His chest tightness may be associated with left arm radiation. His first visit in outpatient department showed blood pressure 146/105 mmHg and heart rate 76 bpm. Aspirin 300 mg loading was given. Then, aspirin 100 mg, bisoprolol 1.25 mg and amlodipine 2.5 mg per day were prescribed. Sublingual nitroglycerin was recommended to be used while chest discomfort. MPS was arranged and showed high likelihood for significant stress-induced myocardial ischemia in apicoseptal and septal walls (partial reverse). At the second visit, his blood test was within normal limit, except higher LDL-C (167 mg/dl). So Vytorin (Ezetimibe & Simvastatin) 10 & 20 mg/tab HS was added. Cardiac echo showed left ventricular ejection fraction 78.5% with borderline dilated LV and without regional wall motion abnormality. Because the patient hesitated to have cardiac catheterization, the cardiologist kept medical control for the patient. Till July 2016, he was angina free, and LDL-C measured 58 mg/dl. MPS in October 2016 only showed small perfusion defect with total reverse in the mid-anteroseptal wall. Under optimal medical treatment for more than 2 years, he remained angina free even under regular exercise and MPS in August 2018 showed homogeneous distribution of radiotracer in stress and rest tests at all myocardial walls.

Discussion: The COURAGE trial followed 2287 patients with stable ischemic heart disease. The patients were randomized to two groups, and received optimal medical therapy with or without PCI. After a mean 4.6-year follow-up period, there was no difference in survival between two groups. Among 1211 patients (53%) with follow-up of 15 years, there revealed 284 (25%) deaths in the PCI group, and 277 (24%) deaths in the medical-therapy group. The authors concluded that compared with medical therapy along, PCI did not improve long-term survival in patients with stable ischemic heart disease. Angina history for 2 months seems to be stable angina. Medical control was prescribed based on stable angina and patient's refusal of cardiac catheterization. Treatment strategy was anti-angina and risk factor modification, especially LDL-C reduction. Using high-potency cholesterol lowering agent (Vytorin) is for LDL-C treatment goal of less than 70 mg/dl. Aspirin can reduce thrombosis and will achieve the therapeutic effect one week later under daily dose of 100 mg. So 300 mg Aspirin as a loading dose was given while starting treatment. Not only anti-hypertension effect, amlodipine, which is a long-acting calcium channel blocker, is also a potent anti-angina medication. Bisoprolol, which is a beta blocker,

can reduce oxygen demand which is also a standard anti-angina medication. For the dramatic improvement of angina symptom, follow up MPS was arranged six months later and also showed massive improvement of the perfusion defect. As a result, coronary angiography was no more recommended and medical treatment was kept for two years when MPS showed totally normal. Among patients with stable ischemic heart disease and significant coronary artery disease, there was no difference in rate of long-term survival with an initial strategy of optimal medical therapy plus PCI as compared with optimal medical therapy alone. MPS can provide objective evidence of change in myocardial ischemia and is a good modality for disease monitoring during the medical treatment and follow up.

PC037

Gallium Scintigraphy of Pericarditis

Tzyy-Ling Chuang^{1,2}, Feng-Jung Yang^{3,4}

¹*Department of Nuclear Medicine, Dalin Tzu Chi Hospital, Buddhist Tzu Chi Medical Foundation, Chiayi, Taiwan*

²*School of Medicine, Tzu Chi University, Hualien, Taiwan*

³*Department of Internal Medicine, National Taiwan University Hospital Yun Lin Branch, Douliu, Taiwan*

⁴*Graduate Institute of Clinical Medicine, College of Medicine, National Taiwan University, Taipei, Taiwan*

Introduction: We present a case of pericarditis without other focus demonstrated by gallium scintigraphy with SPECT/CT.

Case report: A 92-year-old female had 1) end stage renal disease under hemodialysis, 2) thoracic aortic aneurysm without operation, 3) congestive heart failure, New York Heart Association Functional class III, diastolic dysfunction. She suffered from conscious change on 2019/03/25. In emergency department, initial temperature was 37.9°C and pulse rate showed 111/min. The laboratory data revealed leukocytosis (WBC 17.29 K/ μ L), procalcitonin (5.78 ng/mL), elevated CRP (18.89 mg/dL), hyperkalemia and mild hyponatremia. Urine analysis showed pyuria. CXR showed right neck PermCath. Brain CT showed multiple old insults without intracranial hemorrhage. Chest CT showed irregular pericardial thickening, mediastinal lymphadenopathy, small pleural effusion, and gallstones. Her conscious change was suspected to be infection related. Gallium scan with SPECT/CT was arranged due to still intermittent fever after antibiotic treatment and showed increased radiouptake to pericardial region (cardiac silhouette) with pericardial effusion and right pleural effusion. Hematologic disease is unlikely by hematologist consultation. Septic shock developed latter, but the patient passed away because her family refused the further invasive treatment.

Discussion: Infection is one differential diagnosis of conscious change. Pericarditis is a life-threatening illness necessitating prompt diagnosis and treatment. Gallium is recognized as an effective non-invasive localizer of tumors and of either infectious or inflammatory regions. The CT of our case showed pericardial irregular thickening with effusion; different diagnosis included pericarditis or tumor seeding. Ga-67 uptake by the heart has been demonstrated in a number of different diseases, including: pericarditis in infective (viral, bacteria, tuberculosis, and fungus) (halo cardiac silhouette), idiopathic (solid cardiac silhouette) and secondary to constrictive pericarditis (extensive myocardial uptake) or IgG4-related disease (enhanced uptake around the heart); myocardial abscess (patchy or focal uptake); bacterial endocarditis (uptake in endocardium); myocarditis (diffuse myocardial uptake); sarcoidosis (less intense than liver and localized to myocardium); primary/secondary cardiac malignancy (often intense and irregular with other lymphadenopathy, only one case surrounding heart shadow); Kawasaki disease (doughnut-shaped pattern in the left ventricle); myocardial infarction (often focal over the left ventricle). In the patient's gallium scan, the isotope was localized to the cardiac silhouette as a "halo" of increased uptake. SPECT/CT confirmed that the gallium activity appears to lie within the pericardium or pericardial effusion, making differentiation between these diseases more easily. Pericardial localization of gallium-67 may be useful for diagnosing the cause of fever and evaluating the efficacy of treatment in pericarditis.

PC038

Gallium SPECT/CT Facilitate Early Diagnosis of Encapsulating Peritoneal Sclerosis

Tzyy-Ling Chuang^{1,2}, Chen-Sen Huang³, Shih-Chin Chou¹, Yuh-Feng Wang^{1,2}

¹Department of Nuclear Medicine, Dalin Tzu Chi Hospital, Buddhist Tzu Chi Medical Foundation, Chiayi, Taiwan

²School of Medicine, Tzu Chi University, Hualien, Taiwan

³Department of Nephrology, Dalin Tzu Chi Hospital, Buddhist Tzu Chi Medical Foundation, Chiayi, Taiwan

Introduction: We present a case that Gallium SPECT/CT facilitated early diagnosis of encapsulating peritoneal sclerosis (EPS).

Case report: A 54-year-old female had end-stage renal disease under peritoneal dialysis since 2009/06. She had abdominal fullness, poor appetite, and malnutrition in 2018/07. She had epigastric pain, and esophagogastroduodenoscopy with biopsy (2018/08) showed duodenal melanosis. On 2019/01/24, she developed general weakness, dizziness, and malaise for days; body temperature measured 37°C. Ascites routine showed clear clarity, RBC 0-2/HPF, WBC 0/HPF. Ascites culture latter showed no growth for Mycobacterium. Ceftibuten was given. Hemoglobin (Hb) dropped from 11.1 g/dl (2018/11/27) to 7.2 g/dl (2019/02/01), favor chronic occult infection, cause to be determined. She was treated with NESP (Darbepoetin alfa) for low Hb. The blood data showed WBC $12.16 \times 10^3/\text{ul}$ 、N.seg. 74.9%、CRP 2.19 mg/dl. She was treated first with Amoxicillin-Clavulanic Acid and Ciprofloxacin. Gallium scan with SPECT/CT (2019/02/13) show that some mild uptake in the mesentery region and peritoneum was suggestive for checking up the possibility of EPS. However, low abdominal pain and persist gastrointestinal problem were complained. CT was performed under the suggestion of nuclear medicine physician. CT (2019/03/14) showed long segmental mural swelling/thickening of the small and large bowel, bowel tethering and peritoneal calcification, suggesting EPS. Tamoxifen was prescribed since 2019/04/02. She visited emergency department due to epigastric pain and nausea sensation without diarrhea or constipation in 2019/04/24.

Discussion: EPS is a rare but serious complication of peritoneal dialysis characterized by fibrotic encapsulation of the bowel due to a progressive intraabdominal inflammatory process, as a response to peritoneal irritation, causing by proliferation and hyperplasia of peritoneal mesothelial cells and peritoneal capillary angiogenesis, resulting in ultrafiltration failure, and bowel obstruction. The inflammation is presumed to be related to the chronic exposure to bioincompatible dialysate, an initial step for the fibrotic process, that may evolve until EPS. EPS is a slowly progressive, frequently asymptomatic disorder that occurs after many years on peritoneal dialysis. The prevalence of EPS increased from 1.9% at longer than two years to 19.4% at longer than eight years on PD. Symptoms includes anorexia, nausea, diarrhea, and intermittent abdominal pain, latter becomes constipation, and vomiting. Anemia and high CRP can be found in case of EPS. The duration of time on peritoneal dialysis and intraperitoneal inflammation triggered by repeated episodes of peritonitis are major risk factor for EPS. The diagnosis of EPS is often delayed, and many patients with mild or early cases of EPS are not diagnosed. The contrast-enhanced CT may have a sensitivity of 100% and a specificity of 94% for diagnosing EPS. Peritoneal thickening, calcification, bowel tethering, thickening and dilatation were significantly more

commonly reported in the EPS group and can differentiate EPS from peritoneal changes associated with duration of PD therapy. Treatment primarily consists of medical therapy with tamoxifen and prednisone (both improving survival), surgery, and resting the peritoneum. Mortality associated with EPS was very high, about 35-50%, from 20% to 90%. In our case, bacterial or tuberculous peritonitis is not likely due to clear ascites and only mild uptake of mesentery and peritoneum in Gallium scan, and the EPS symptoms were not obvious initially. Not only CT, but also Gallium SPECT/CT, which reveals peritoneum inflammation, can provide diagnostic help in detecting early cases of EPS. A high index of suspicion can help in the early diagnosis of EPS and in early intervention for management of EPS, which currently offers the only hope for a better outcome.

PC039

比較使用閃爍攝影機計算腎絲球過濾率與與估計來自 MDRD 公式的血清肌酐清除率間的關係

許文齡 張淑敏 張晉銓 許玉春 李岱恩

高雄醫學大學附設中和紀念醫院核子醫學部

目的：本研究目的是在 ± 4 週的區間內，找出使用閃爍攝影機 Gate's 方式計算腎絲球過濾率及使用血清肌酐 MDRD 公式計算腎絲球過濾率間的相關性。

材料與方法：使用回顧性病例查找方式收集 2019 年 1 月到 2019 年 8 月，在本科接受腎動態掃描並同時接受血清肌酐此項血液生化檢驗的病人，將其接受檢查時間與抽血檢驗時間區間不同分成 ± 3 天 (Group 1)； $\pm 4-7$ 天 (Group 2)； $\pm 8-14$ 天 (Group 3)； $\pm 15-28$ 天 (Group 4)，使用線性回歸分析方式，找出腎動態掃描參考 modified Gate's 方式進行腎絲球過濾率的計算與使用血清肌酐 MDRD 公式計算腎絲球過濾率間的關係。

結果：總共 35 位病人納入本研究，其中男女生比例約 1:1，年齡介於 19-80 歲之間。身高為 159.7 ± 8.12 cm (Mean \pm SD)，體重為 64.6 ± 12.9 kg，血清肌酐 (Plasma creatinine) 為 1.41 ± 1.06 mg/dl，GFR (Glomerular filtration rate) 為 50.9 ± 21.86 ml/min，MDRD 公式所得之 GFR (eGFR) 為 70.2 ± 37.7 ml/min。

在 Group 1 之 GFR 與 eGFR 相關係數為 0.91 (p 值 < 0.05)；Group 2 之 GFR 與 eGFR 相關係數為 0.91 (p 值 < 0.05)；Group 3 之 GFR 與 eGFR 相關係數為 0.87 (p 值 < 0.05)；Group 4 之 GFR 與 eGFR 相關係數為 0.67 (p 值 < 0.05)。

結論：在 Group 1-3 的病人中，其 GFR 與 eGFR 間的相關性皆呈現高度相關，而 Group 4 的病人中，其相關性明顯下降，表示當兩項檢查的區間拉長，疾病可能正在發展亦或是病人使用藥物等影響其結果。

PC040

壁報論文發表摘要·臨床組

緩瀉劑的使用是否影響 ^{18}F -FDG-PET/CT 在腸道系統中的判讀

張雅玲 陳賢淑 梁佐安

高雄阮綜合醫院核子醫學科

背景介紹： ^{18}F -FDG 經常會蓄積在腸道當中，在正子斷層影像上經常造成腸道系統的判讀困難，本實驗希望利用飲食的衛教與瀉劑的使用來幫助減少因腸道收縮而造成的 ^{18}F -FDG 在腸道上的蓄積而造成誤判的情形，以探討是否對於臨床的判讀是否有幫助。

方法：本研究共計收受共 202 位，依受檢的次序分成未服用瀉劑與服用瀉劑兩組，未服用瀉劑的人共計 109 位；服用瀉劑的人共計 93 位，經由有經驗之核子醫學專科醫師判讀後，依腸道分別統計升結腸、橫結腸、降結腸、乙狀結腸、直腸五段腸道的 SUV 值，分別統計，1、性別與各腸道 SUV 值是否有影響，2、年齡與各腸道 SUV 值間是否有影響，3、其 SUV 值來判斷未服用瀉劑與服用瀉劑腸道 SUV 值是否有差異。利用正子掃描的生理功能影像加上電腦斷層提供的人體解剖影像，判讀 ^{18}F -FDG 在人體的代謝分佈，與瀉劑 (Klean-prep) 的使用，減少因便秘所引起的腸道平滑肌的收縮或蠕動增加所造成的腸道 ^{18}F -FDG 藥物活性攝取的增加，以減少腸道生理上的攝取，由統計軟體 SPSS2 以描述性統計分析各變項之分布情形。最後以無母數分析 Kruskal Wallisru、Mann-Whitney U 進行相關檢定。

結果：結果顯示有遵守飲食衛教與配合服用瀉劑者比未遵守飲食衛教與配合服用瀉劑者，其顯示出的影像中的 ^{18}F -FDG 攝取的活性強度值有較下降，故由此可知有遵守飲食衛教與瀉劑的使用是可以有效改善腸道的收縮所造成的 ^{18}F -FDG 在腸道中蓄積的情形。

結論：瀉劑的使用降低葡萄糖正子斷層掃描檢查影像中 FDG 追蹤劑在腸道中的聚積，以利於腸道中的病灶判讀，在檢查的前一天給予緩瀉劑的使用與低渣飲食的衛教，可減少因便秘或宿便的累積造成腸道中的 FDG 追蹤劑攝取量，提升了對於腸道的疾病影像判讀的品質。經過本研究證實使用緩瀉劑確實可以減少腸道的攝取量，減少因為正常腸道生理攝取而造成誤判。另外，病史的收集、理學檢查及實驗室的檢驗數據等資料，都是 FDG PET/CT 影像判讀上很重要、不可或缺的參考依據。

PC041

Quantitative Analysis of ^{99m}Tc -TRODAT-1 SPECT by Ratio of 3D Location Variances

Chao-Yu Chen¹, Chin-Chiu Cheung¹, Tzu-Ting Huang¹, Po-Wei Tu²

¹Department of Nuclear Medicine, Yuan's General Hospital, Taiwan

²Department of Nuclear Medicine, E-DA Hospital, Taiwan

Purpose: The ^{99m}Tc -TRODAT-1 Single Photon Emission Computed Tomography (SPECT) was often used to diagnosis brain function. The study was focused to find image features to analyze the risk of Parkinson's Disease (PD).

Materials and Methods: The retrospective study was successfully collected 212 subjects. The experimental groups were involved 200 cases. The control group was 12 negative cases. The seven novel features including UpperSum, UperMean, UpperSD, LowerSum, LowerMean, LowerSD, ratio of 3D location variances (F-Ratio) were extracted from SPECT image. The Mann-Whitney U test was used to test significant features. The logistic regression (LR) were applied to analysis the groups of PD.

Results: According to Mann-Whitney U test, the result was shown statistical significant in UpperSum, UpperSD, LowerSum, F-Ratio ($P < 0.05$). Among building logistic regression model including UpperSum, UpperSD, LowerSum, F-Ratio. AUC = 82.5% ($P < 0.05$).

Conclusion: F-Ratio was a novel and useful significant features which was considered whole 3D information to classify groups. In the future, the more negative cases should be added into the study in order to improve the variation of false positive rate.

PC042

^{99m}Tc -MAA SPECT/CT 顯示腫瘤所導致之肺灌注缺損之案例報告

游宜芳¹ 張瀚² 余品嫻² 郭俊良¹ 張鈺弘¹ 羅雅芬^{3,4*}

¹ 新竹馬偕紀念醫院核子醫學科

² 新竹元培科技大學放射系

³ 新竹馬偕紀念醫院呼吸治療中心

⁴ 亞洲大學健康產業管理學系長照組

背景介紹: 一位 68 歲男性因呼吸急促與疑似肺栓塞 (PE) 進而住院診療。此外，他還罹患左扁桃腺癌、聲門上型癌、開放性肺結核 (TB) 與慢性腎病 (CKD) 等病史。由於腎功能不良，該病人無法使用注射顯影劑之電腦斷層血管攝影掃描 (CTA)，且因開放性肺結核，所以我們單純使用灌注相之 SPECT/CT 代替傳統的平面通氣 / 灌注 (V/Q) 掃描來診斷 PE。

方法: 使用 185 MBq (5 mCi) 的 ^{99m}Tc -MAA 進行肺灌注掃描。注射前先將放射性示踪劑搖晃均勻，病人平躺於檢查檯上靜脈注射，然後利用 GE Discovery NM/CT 670 (使用低劑量方案的 CT) 來獲取平面與斷層等影像。

結果: ^{99m}Tc -MAA SPECT/CT 斷層影像清楚地顯示右下肺葉有大面積灌注缺損，其懷疑癌症相關。故將病人轉至放射科使用 128 切電腦斷層掃描 (CT)，顯示右下葉有大體積之腫塊，並伴有右下葉支氣管和右下肺靜脈侵犯，且其腫塊已與右下葉之血管和支氣管等融合。此外，SPECT/CT 也顯示左肺頂端有灌注缺損對應於 CT 中的空洞病變，這可能是由 TB 引起的。

結論: 肺栓塞的正確診斷是很重要的，不論未診斷或誤認為是肺栓塞皆對病人造成傷害或死亡等可能。因此，若病人有 CT 檢查之禁忌症時， ^{99m}Tc -MAA SPECT/CT 是 CT 可行替代方案，並提供比傳統平面 V/Q 掃描來得更多的信息，可提高診斷正確率。

PC043

Pneumoconiosis on F-18 FDG PET/CT: A Case Report

Chao-Jung Chen¹, Cheng-Hsieh Hsiao²

Departments of ¹Nuclear Medicine, ²Infectious Disease, Yuan's General Hospital, Kaohsiung, Taiwan

Introduction: Pneumoconiosis is caused by the accumulation of inhaled particulates and involves a reaction of tissue in the lung. There is limited data in patients with pneumoconiosis on F-18 fluorodeoxyglucose (FDG) positron emission tomography/computed tomography (PET/CT), we herein present a rare case of pneumoconiosis on F-18 FDG PET/CT.

Case report: A 53-year-old male patient is a road worker for more than 20 years. He was diagnosed as pneumoconiosis for many years without regular follow-up. He was referred for F-18 FDG PET/CT to exclude extra-pulmonary malignancy and multiple tiny pulmonary nodules with mildly increased FDG uptake were found (the largest one, 0.7 cm in greatest dimension, SUVmax: early 3.25, delayed 4.18). Multiple reactive lymph nodes in the mediastinal and bilateral pulmonary hilar regions were detected (SUVmax: early 5.57, delayed 7.33). In a summary, pneumoconiosis is compatible and no extra-pulmonary FDG-avid malignancy can be identified.

Discussion: Progressive massive fibrosis (PMF) of the lung is a type of late-stage pneumoconiosis of an aggregation of silicotic nodules fused by connective tissue. It appears rapidly and tends to increase in size. Solitary PMF lesion is frequently confused with lung cancer, and biopsy is often needed to determine whether the lesion is malignant or benign. FDG PET scanning could be a sensitive screening test for lung cancer among patients with pneumoconiosis. The difference in glucose metabolic rate between lung cancer and PMF was clearly demonstrated by PET image in some reports.

Conclusion: In conclusion, we demonstrated the rare case of pneumoconiosis on F-18 FDG PET/CT scan. It showed mild FDG uptake in the bilateral pulmonary tiny nodules. This case emphasizes that F-18 FDG PET/CT can exclude not only the primary lung cancer but also the extra-pulmonary malignancy in patients with pneumoconiosis. Furthermore, it can point out the location of the potential pulmonary lesion as a guide for biopsy.

PC044

The Effect of Caffeine in Myocardial Blood Flow and Myocardial Flow Reserve on Dynamic SPECT/CT: A Case Report

Wen-Chun Lin, Hung-Pin Chan

Department of Nuclear Medicine, Kaohsiung Veterans General Hospital, Kaohsiung, Taiwan

Introduction: The aim of this report is to evaluate the effect of caffeine on MBF and MFR on Dipyridamole pharmacologic stress. We recent presents a new method to achieve SPECT flow quantitation from dynamic SPECT /CT images and a compartment flow model for flow calculation comparable to the established PET methods.

Methods: One day Rest/Dipyridomale-stress dynamic SPECT with ECG-gated studies will be performed on a dedicated Siemens Symbia-T2 SPECT/CT system.

Results: Caffeine reduced myocardial blood flow and myocardial flow reserve by Dipyridamole-induced coronary hyperemia on Dynamic SPECT/CT that may yield false positive results.

Conclusions: These findings suggest that abstinence for caffeine before Dipyridamole stress testing may be needed for preventing false positive on Dynamic SPECT/CT. However, prohibited caffeine for only 12 hours may not enough.

PC045

Texture Analysis of Pretreatment NaF PET Image Predicts Histologic Response to Neoadjuvant Chemotherapy in Patients with Osteosarcoma

Kuan-Yin Ko¹, Chia-Ju Liu², Ruoh-Fang Yen¹

¹Department of Nuclear Medicine, National Taiwan University Hospital, Taipei, Taiwan

²Department of Nuclear Medicine, National Taiwan University Hospital Yun-Lin branch, Yunlin County, Taiwan

Introduction: The aim of the study was to evaluate whether the texture features derived from NaF and FDG PET images performed before chemotherapy can predict the histologic response of osteosarcoma.

Methods: A retrospective analysis of the pretreatment NaF and FDG PET images of the patients with newly diagnosed osteosarcoma from 2012 to 2018 was conducted. All patients were treated with neoadjuvant chemotherapy and underwent surgery. Histologic tumor necrosis rate was the main outcome measure. Primary tumor was segmented by using semi-automatic tool (3D slicer) and 100 imaging features were extracted from shape, histogram analysis, gray level co-occurrence matrix, gray level size zone matrix, gray level run length matrix, neighbouring gray tone difference matrix, and gray level dependence matrix. Regression model was used for feature selection. Performance of the texture features was evaluated by receiver operating characteristic curve analysis (ROC).

Results: In total, 14 patients were enrolled, among whom 5 showed good histologic response (tumor necrosis rate $\geq 90\%$). After univariate analysis, four features (2 from gray level co-occurrence matrix, 2 from gray level size zone matrix) from NaF PET had significant association with histologic tumor necrosis. Multivariate regression analysis revealed the value of zone entropy as the independent differentiator. ROC analysis yielded a cutoff of 4.4 with an area under the curve of 0.90 for identification for good responder. However, statistic analysis didn't not highlight prognostic role on histologic response of all the considered FDG PET features.

Conclusions: In patients with osteosarcoma, texture analysis of NaF PET image has the potential to differentiate histologic response; zone entropy in particular is an independent predictor.

PC046

^{99m}Tc-pyrophosphate Cardiac Scintigraphy Can Differentiate The Severity of Heart Failure in Patients with Transthyretin Cardiac Amyloidosis

Tse-Hao Lee, Chih-Yung Chang, Wen-Sheng, Huang

Department of Nuclear Medicine, Taipei Veterans General Hospital, Taipei, Taiwan. R.O.C.

Introduction: Cardiac scintigraphy with ^{99m}Tc-pyrophosphate (PYP) has been one of the diagnostic image for amyloid cardiomyopathy. Heart failure is the most common manifestation of amyloid cardiomyopathy and echocardiography is the most available tool for evaluation of heart failure. The aim of our study was to find the correlation between the severity of heart failure (especially left ventricular diastolic dysfunction), which is evaluated by echocardiography, and the uptake of ^{99m}Tc-PYP in the myocardium.

Methods: Fifteen patients with clinically suspected or diagnosed of amyloid cardiomyopathy were retrospectively studied between May 31th, 2017 and December 11th, 2018. Each patient underwent planar cardiac images (anterior, lateral and left anterior oblique views) one and three hours, respectively after intravenous injection of ^{99m}Tc-PYP (740 MBq). For semi-quantitative analysis of cardiac images in the 1st hour, regions of interest (ROI) were drawn over the heart on the planar images and were mirrored over the contralateral chest. A heart to contralateral ratio in the first hour image (H/CL-1st hour) was calculated as the fraction of heart ROI mean counts to contralateral chest ROI mean counts with cut-off value: 1.5 (≥ 1.5 was regarded positive for amyloid cardiomyopathy). We could also semi-quantitatively analyze the 3rd hour image and calculate (H/CL-3rd hour) with the same method as for the 1st hour image. The (H/CL-3rd hour) to (H/CL-1st hour) ratio for every patient could also be calculated. Left ventricular diastolic function was evaluated by echocardiography

Results: In 9 of all 15 patients, (H/CL-1st hour) was ≥ 1.5 . Only three of these 9 patients had left ventricular diastolic dysfunction and the other 6 patients did not. (H/CL-3rd hour) to (H/CL-1st hour) ratio was higher (cut-off value: 0.95) in these two patients with left ventricular diastolic dysfunction. For patients with (H/CL-1st hour) < 1.5 (6 patients), two of these 6 patients had left ventricular diastolic dysfunction and higher (H/CL-3rd hour) to (H/CL-1st hour) ratio (≥ 0.95) than other 4 patients without left ventricular diastolic dysfunction.

Conclusions: Semi-quantitative analysis of ^{99m}Tc-PYP cardiac images in the 1st hour and 3rd hour post injection with calculation of (H/CL-3rd hour) to (H/CL-1st hour) ratio may correlate the left ventricular diastolic function.

PC047

Comparison of Clinical Tools for Measurements of Myocardial Blood Flow and Flow Reserve Assessed with ^{99m}Tc -MIBI CZT SPECT

Chuang-Hsin Chiu¹, Ta-Wei Tseng¹, Ing-Jou Chen¹

¹Department of Nuclear Medicine, Tri-Service General Hospital, National Defense Medical Center, Taipei, Taiwan

Introduction: Several tools for the quantitative analysis of myocardial blood flow (MBF) at stress and rest and myocardial flow reserve (MFR) with ^{99m}Tc -MIBI dynamic SPECT have been implemented for clinical use. The aimed of this study was to compare quantitative results obtained from two software tools (MyoFlowQ and 4DM).

Methods: Dynamic SPECT/CT image data sets of 21 patients referred for MBF and MFR for the evaluation of coronary artery disease (CAD) were included in this study. All patients were divided in to 2 groups: group 1 comprised 9 subjects (8 men and 1 women, age: 65 ± 5 yrs) with known obstructive CAD, and group 2 comprised 12 subjects (8 men and 4 women, age: 63 ± 10 yrs) with low-to-intermediate probability of CAD. All dynamic data were rebinned into 18 frames (ten 10-s, five 5-s, two 60-s, and one 280-s frames). Global and regional stress and rest MBF and MFR values were obtained with each tool. Left ventricular contours and the region of input function were obtained automatically in each tools.

Results: Rest MBF (ml/min/g) (0.85 ± 0.21 in MyoFlowQ vs. 0.46 ± 0.10 in 4DM, $P < 0.001$ in group 1; 0.77 ± 0.26 vs. 0.51 ± 0.10 , $P < 0.001$ in group 2; 0.79 ± 0.24 vs. 0.49 ± 0.10 , $P < 0.001$ in all patients), stress MBF (ml/min/g) (1.25 ± 0.52 vs. 1.34 ± 0.53 , $P = 0.445$ in group 1; 1.87 ± 0.48 vs. 2.32 ± 0.72 , $P < 0.05$ in group 2; 1.64 ± 0.57 vs. 1.96 ± 0.81 , $P < 0.05$ in all patients) and MFR (1.55 ± 0.54 vs. 3.01 ± 1.27 , $P < 0.001$ in group 1; 2.70 ± 1.03 vs. 4.61 ± 1.18 , $P < 0.001$ in group 2; 2.28 ± 1.03 vs. 4.02 ± 1.42 , $P < 0.001$ in all patients) were significantly different between each tools.

Conclusion: Different reconstruction and analysis methods in MyoFlowQ and 4DM lead to different MBF and MFR. In resting MBF, 4DM is lower than MFQ, and in stress MBF, 4DM is higher than MFQ, resulting in 4DM MFR higher than MFQ MFR.

Quantitative assessment of MBF and MFR is dependent on the software. Clinical use for follow-up and treatment assessment should be used with the same software and method.

PC048

壁報論文發表摘要·臨床組

The Usefulness of F-18 NaF and F-18 FDG PET in Detecting Coronary Atherosclerotic Plaques – A Case Report

Pei-Ju Chuang¹, Jei-Yie Huang^{1,2}, Ya-Yao Huang¹, Wei-Hua Kuo¹,
Yen-Hung Lin³, Yen-Wen Wu^{4,6}, Ruoh-Fang Yen¹

¹*Department of Nuclear Medicine, National Taiwan University Hospital and
National Taiwan University College of Medicine, Taipei, Taiwan*

²*Institute of Epidemiology and Preventive Medicine, College of Public Health,
National Taiwan University, Taipei, Taiwan*

³*Department of Internal Medicine, National Taiwan University Hospital and
National Taiwan University College of Medicine, Taipei, Taiwan*

⁴*Department of Nuclear Medicine*

⁵*Cardiology Division of Cardiovascular Medical Center, Far Eastern Memorial Hospital, New Taipei City, Taiwan*

⁶*National Yang-Ming University School of Medicine, Taipei, Taiwan*

Introduction: Atherosclerosis is the primary disease process of cardiovascular disease, such as myocardial ischemic disease and stroke. Acute cardiac event, including myocardial infarction and sudden cardiac death, often resulted from complications of vulnerable plaques, rather than coronary artery stenosis. Positron emission tomography (PET) using F-18 sodium fluoride (NaF) targeting micro-calcification and F-18 fluorodeoxyglucose (FDG) targeting inflammation, might be able to help us identifying these high-risk plaques. Here, we demonstrate the PET images of a patient with coronary artery disease and atherosclerotic plaque proved by angiography and intravascular ultrasound (IVUS).

Case Presentation: This 69-year-old gentleman, who had diabetes mellitus, dyslipidemia, and history of cerebral infarction, experienced aggravated intermittent chest tightness. Percutaneous coronary intervention (PCI) was indicated for significant stress-induced ischemia at left anterior descending artery (LAD) territory noted on dipyridamole-stress myocardial perfusion images. He received NaF and FDG dual-tracer, cardiac and respiratory dual-gated PET two weeks before PCI. Diagnostic coronary angiography revealed 3-vessel-disease with 70% to 90% stenosis at LAD, 50% to 70% stenosis at left circumflex artery (LCx), and hypoplastic right coronary artery (RCA) with diffuse stenosis up to 70% degree. A vulnerable plaque was noted at proximal LAD by IVUS, which showed NaF avidity and FDG non-avidity on PET. PCI with stent implantations at LAD and LCx was performed smoothly. He was angina free thereafter.

Discussion: Vulnerable plaques are known to correlate with potential cardiac events, which most often caused by acute rupture of plaques and occlusion of coronary artery. Invasive coronary angiography combining IVUS or optical coherence tomography (OCT) to characterize plaque core is the standard technique to detect vulnerable plaques in previous studies. PET tracers including NaF and FDG offer non-invasive evaluation of atherosclerotic lesions. We also performed cardiac and respiratory dual-gated PET to overcome difficulty among coronary lesions, due to their small size and inevitable motion artifacts from heart beats and breathing. In the presented case, focal uptake of NaF over proximal LAD showed good registration to the vulnerable plaque on

IVUS, as the interpretation of coronary FDG remained challenging due to high background activity.

We believe dual-tracers, dual-gated PET with NaF and FDG is able to detect vulnerable coronary plaques as presented, targeting different physiology of different stages within the heterogeneous lesions. NaF might show advantages comparing FDG with better lesion-to-background ratio regarding cardiac region, which will be further evaluate in the ongoing study now under patient recruitment.

PC049

多巴胺轉運體活性分佈及活性體積之 ^{99m}Tc -TRODAT-1 單光子電腦斷層影像合理分類模型

涂博偉¹ 許耘萱¹ 陳輝墉¹ 陳昭宇² 許士彥³ 陳泰賓³

¹義大醫療義大醫院核子醫學科

²阮綜合醫療社團法人阮綜合醫院核子醫學科

³義守大學醫學影像暨放射科學系

背景介紹： ^{99m}Tc -TRODAT-1 單光子電腦斷層造影技術，已成為臨床常規評估腦部多巴胺傳導物質系統相關疾病之檢查。文獻上經常採用感興趣區域 (Region of Interest, ROI) 比值方式，量化紋狀體特異性攝取率，評估腦部神經傳導物質相關疾病，此方法仍有改善之空間。

方法： 本研究採用回顧性分組實驗設計，共收集 202 筆 ^{99m}Tc -TRODAT-1 SPECT 影像及診斷報告，包括正常腦部 6 筆及帕金森氏病 (Parkinson's Disease, PD) 196 筆。根據帕金森氏病嚴重程度又分為帕金森氏病 HYS (Hoehn and Yahr Scale) I、II、III 組 (102 筆) 及帕金森氏病 HYS IV、V 組 (94 筆)。利用三維方式估算活性分佈及紋狀體活性體積之影像特徵共六個，採用統計無母數檢定找出具有顯著性之特徵值，再經由 Support Vector Machine (SVM) 分類方法進行建模，並評估合理單光子電腦斷層影像之帕金森氏病分類模型。

結果： 結果顯示 SVM 分類模型於解釋變數中使用偏態值、峰度值及多巴胺轉運體活性體積三個特徵值，分辨正常腦部及帕金森氏病之靈敏度、特異性、陽性預測率、陰性預測率、準確度及 Kappa 值皆高達 99%。分辨正常腦部、帕金森氏病 HYS I、II、III 組及帕金森氏病 HYS IV、V 組之靈敏度、特異性、陽性預測率及準確度均高於 80% 且 Kappa 值為 68%。

結論： 此模型能有效判定不同嚴重程度之帕金森氏病，期能提供臨床醫師診斷帕金森氏病嚴重程度之參考依據。目前仍須更多無異常影像之案例，以了解分類模型之偽陽性變化情形。未來能將此研究方式考量套用於 SPECT/CT 之影像，更可有效評估活性體積之大小，並建立 ^{99m}Tc -TRODAT-1 SPECT/CT 影之合理分類模型。

PC050

Colon Cancer with Bone Metastasis: A Case Report

Pei-Jung Li, Po-Ling Chang

Department of Nuclear Medicine, Changhua Christian Hospital

Introduction: The incidence of bone metastasis with colon cancer is relatively rare. Most patients with colon cancer suffered from bone metastasis also with other distant metastasis. The 5-year survival rate is very low for the colon cancer patient with bone metastasis.

Methods: A 41-year-old man was diagnosed with colon cancer diagnosed bone metastasis in a follow up bone scan.

Results: The first bone scan in 2017-11, there were increased uptake areas in the right 6th, left 4th ribs, third lumbar vertebra and left sacroiliac joint. The picture is more likely suggestive of benign lesions such as traumatic fracture or degenerative change. The FDG-PET scan for initial staging workup revealed distant metastases involving the liver, right supraclavicular, bilateral hilar regions and mediastinum 7 months ago, but no obvious evidence of bone metastasis was noted. However, the follow up bone scan in 2019 showed the typical pattern of bone metastasis with disseminated lesions in the spine, ribs, pelvic bones, sternum, left scapula, right humerus and bilateral femurs. The old lesions in the right 6th rib, third lumbar vertebra and left sacroiliac joint were more extensive and intense compared to the bone scan in 2017.

Conclusions: The most powerful tool for detection of bone metastasis of patients with colon cancer is FDG-PET scan. In this case, the first image revealed bone metastasis was the CT scan in 2018-03 and it was 4 months later. A Whole Body FDG-PET scan or a MRI scan may confirm bone metastasis sooner.

PC051

壁報論文發表摘要·臨床組

Dosimetry Based on Bremsstrahlung Imaging After Yttrium-90 Embolization – Experience from Taipei Veterans General Hospital

林可瀚¹ 羅翊文¹ 李家誠² 黃品逸² 劉晉昇² 黃文盛¹ 李潤川³

¹ 臺北榮民總醫院核醫部

² 臺北榮民總醫院腫瘤醫學部

³ 臺北榮民總醫院放射線部

Introduction: 本研究的目的希望能利用 Y-90 微球體產生的制動輻射信號，透過核醫的 SPECT/CT 來進行確認造影，偵測微球體在肝臟腫瘤與正常肝臟的分佈，與治療前的模擬檢查影像進行比較。並希望藉由制動輻射 SPECT/CT 影像產生放射治療所需的劑量分布圖，進而計算 Y-90 放射栓塞的體內劑量分佈。

Methods: 自 105 年 11 月 1 日至 106 年 12 月 31 日，共計 60 位接受 Y-90 放射栓塞治療的患者被收案。由於 Y-90 制動輻射的信號微弱，且 SPECT/CT 的解析度受限，故肝內最大的腫瘤直徑不超過 1.5 公分，或者單一次治療注射活度不超過 1.0 GBq 的患者無法進行進一步分析，必須排除在外。總計共有 21 位患者，包括 13 位原發肝腫瘤，含 11 位肝癌、1 位肝內膽管癌、1 位 epithelioid hemangioendothelioma；以及 8 位轉移性肝腫瘤，含 3 位大腸癌、2 位神經內分泌腫瘤、1 位胃癌、1 位腎細胞癌、1 位胸腺癌，被收案進行後續的影像分析。

Results: 總計本研究共計有 21 位患者，包括 13 位原發肝腫瘤，含 11 位肝癌、1 位肝內膽管癌、1 位 epithelioid hemangioendothelioma；以及 8 位轉移性肝腫瘤，含 3 位大腸癌、2 位神經內分泌腫瘤、1 位胃癌、1 位腎細胞癌、1 位胸腺癌，被收案進行後續的影像分析。治療給予的 Y-90 活度： 2.0 ± 1.1 GBq (median: 1.9 GBq)，Range: 0.95 – 6 GBq。治療前計畫的腫瘤劑量為： 121.6 ± 70.4 Gy (median: 114 Gy)，Range: 56.5 – 401.4 Gy。治療前計畫的正常肝臟計量為： 40.6 ± 22.9 Gy (median: 35.6 Gy)，Range: 18.7 – 107 Gy。治療後根據 SPECT/CT 制動輻射影像計算之實際腫瘤劑量： 133.9 ± 53.8 Gy (median: 123.9 Gy)，Range: 28.6 – 236.1 Gy。實際正常肝臟劑量： 65.4 ± 42.8 Gy (median: 57.1 Gy)，Range: 19.5 – 230.9 Gy。術前影像與術後影像顯示的腫瘤劑量方面並無明顯差距 (121.6 Gy versus 133.9 Gy; $p = 0.23$)，但在正常肝臟劑量方面則有顯著差異 (40.6 Gy versus 65.4 Gy; $p = 0.0009$)。

Conclusion: 本研究顯示在接受 Y-90 放射栓塞的患者上，使用 SPECT/CT 偵測 Y-90 制動輻射能成功轉換出 Y-90 的劑量圖，進而產生出 dose-volume histogram。並且可以與術前 Tc-MAA 的模擬結果進行比較。然而，在部分患者上，特別是注射活度較小，或者是腫瘤界線不清晰的患者上，SPECT/CT 的制動輻射影像效果並不理想。

PC052

使用 Camera-Based Clearance 法量測放射性藥品計數時 不同衰減物質對有效腎血漿流量計算的影響

魏文祺 徐景龍 黃文盛

臺北榮民總醫院核子醫學部

背景介紹：以 Camera-Based Clearance 法來評估有效腎血漿流量 (Effective Renal Plasma Flow, ERPF)，其需要在注射前、後利用造影探頭距離 30 公分處量測注射針筒內放射藥品的計數。本研究的目的是比較藥品在量測時使用不同衰減的針筒支撐物對 ERPF 的影響。

方法：31 位受檢者 (18 男, 55±13 歲) 注射 8 mCi Tc99m-MAG3 使用 GE Infinia 以 Camera-Based Clearance 方法執行腎臟功能造影。未注射前含藥針筒分別放置於造影探頭上方 30 公分處之碳纖維檢查床板上、30 公分高空瓦楞紙箱上及上方 30 公分處空氣中量測藥品的計數。造影後依同樣方法量測注射後針筒及注射處之計數。影像後處理使用 ERPF Modified Gates 法，將注射藥品置於碳纖維檢查床板、瓦楞紙箱上及空氣中量測所得計數來計算受檢者的 ERPF。

結果：瓦楞紙箱與碳纖維檢查床板兩者的 ERPF 分別是 338.77±82.82 ml/min 與 357.64±87.3 ml/min, $p < 0.001$ 。此外，比較空氣與碳纖維檢查床板所計算出的 ERPF 分別是 321.87±78.25 ml/min 與 357.64±87.3 ml/min, $p < 0.001$ ，兩者同樣有顯著的差異。結果顯示，使用比造影床板衰減低的針筒支撐物會低估 ERPF。

結論：使用 Camera-Based Clearance 法來評估腎臟功能時，不同的物質如碳纖維、瓦楞紙箱或空氣，因衰減的不同，如置於含放射性藥品針筒與造影探頭間，會量測到不同的計數而造成 ERPF 的差異。因此，置於造影探頭與針筒間的針筒支撐物應使用與造影床板具同樣衰減的物質為宜。

PC053

The Correlation between Tc-99m MAG3 Effective Renal Plasma Flow (ERPF) and Estimated Glomerular Filtration Rate (eGFR)

Wan-Chen Chen, Guang-Uei Hung

Department of Nuclear Medicine, Show Chwan Memorial Hospital, Changhua, Taiwan

Introduction: Tc99m MAG3 ERPF was commonly used for quantitation of renal function in nuclear medicine department by evaluating MGA3 clearance on dynamic renogram. eGFR is a clinical routine for evaluation of renal function by a simple formula of calculating serum creatinine level. This study is aimed to investigate the correlation between the value of normalized ERPF and eGFR.

Methods: we retrospective enrolled twenty-six subjects (12 males and 14 females), aged 13-79 years old, with a mean age of 58 ± 18 y. All subjects underwent Tc-99m MAG3 dynamic renogram for calculating normalized ERPF ($\text{mL}/\text{min}/1.73 \text{ m}^2$). All of them also received blood test for eGFR (mL/min) within 2 weeks of scintigraphy.

Results: Pearson's correlation test showed a significantly positive correlation ($r = 0.83$, $p < 0.0001$) between MAG3 ERPF and eGFR. The approximated value of MAG3 ERPF may be generated from eGFR by the following formula: $\text{normalized MAG3} = 116.1383 + 3.4138 * \text{eGFR}$.

Conclusions: Our study suggested that the normalized MAG3 ERPF was significantly correlated to eGFR. However, the case numbers of our study were limited and further study is needed for further clarifying the influence of gender and age.

PC054

Does Routine Triple-time-point F-18 FDG PET/CT Imaging Improve the Detection of Liver Metastases?

Li-Chun Wu, Chiang Hsuan Leec*

Department of Nuclear Medicine, Chi Mei Medical Center, Tainan, Taiwan

Introduction: This study aimed to evaluate whether routine triple-time-point fluorine-18 (^{18}F) fluorodeoxyglucose (FDG) positron emission tomography/computed tomography (PET/CT) imaging improves the detection of liver metastasis. Our investigation focused on liver metastases detected only on delayed imaging, but not visible on initial images.

Methods: Total 310 patients with various malignancies who underwent modern PET/CT scans were included. Triple-time-point imaging was obtained, all imaging including the liver. The maximum standardised uptake value, tumour-to-normal liver ratio and comparison between negative- and positive-liver lesions on delayed imaging for patients with an initial negative imaging were analysed.

Results: Among the 310 patients, liver lesions in 286 patients were not detected on initial imaging. Liver lesions in six of them were detected on delayed imaging. No liver lesions were detected on further delayed imaging. All the lesions were subsequently pathologically or radiologically confirmed metastases. The analysis showed a significant difference in the percentage of colorectal cancer (66.67%) and liver lesions before the PET scan (50.00%), compared with unchanged results (22.14% and 3.93%, respectively). The other 24 liver lesions identified on initial imaging were still visible on delayed and further delayed imaging.

Conclusions: Although triple-time-point imaging did not improve the detection of liver metastases, delayed imaging (dual-time-point imaging) of the liver obtained at 100–120 min may be recommended in patients with colorectal cancer and with liver lesions before the PET scan. However, triple-time-point imaging still might have some advantages to confirm liver lesions or to observe whether increased image contrast of the liver lesions.

PC055

哺乳期女性接受碘 131 治療停止哺乳時程之探討

賴佳玟¹ 陳雅鳳¹ 黃兆駿¹ 李柏葦¹ 張哲璋¹ 吳彥雯¹ 汪姍瑩^{1,2*}

¹ 亞東紀念醫院核子醫學科

² 陽明大學生物醫學影像暨放射科學系

背景介紹：碘 131 釋放出貝他射線及伽瑪射線，被甲狀腺組織吸收後，可藉以達到治療及造影之功能。因此在臨床上之使用相當廣泛，其適應症包括治療甲狀腺機能亢進、分化型甲狀腺癌術後偵測及消融其殘存或轉移病灶。分化型甲狀腺癌治療為主，病患男女比例為 1:3，且好發於中年育齡女性，所以女性病患在接受碘 131 治療前必須確認有無懷孕及哺乳，以確保胎兒及母親因輻射劑量所帶來的考量。

案例報告：一位 39 歲女性，進行甲狀腺癌追蹤掃描，口服劑量 2 mCi 之碘 131 膠囊後並於 48 小時後進行全身掃描，利用 GE Infinia Hawkeye 4 進行造影，影像呈現前頸部及甲狀腺有明顯攝取；雙側乳房有中度攝取；鼻腔、口腔、結腸和膀胱與生理攝取一致，且沒有偵測到遠端有轉移之熱區。全身造影後當下詢問病患是否有哺乳，她回覆在口服碘 131 之前還有哺乳之行爲。隨後即叮嚀病患務必停止哺乳行爲以避免嬰兒喂養具有碘 131 之乳汁。

討論：口服碘 131 之多項禁忌當中女性病患除了懷孕還有即是哺乳，因為碘 131 會通過乳腺泌乳而濃縮在乳房中造成乳房接受到輻射劑量。SNM Guideline 及美國食品藥物管理局 (FDA) 建議哺乳期婦女在給予碘 131 之前至少 6 週停止母乳喂養，以留出足夠的時間進行乳腺分泌退化，並避免乳房組織中有過量濃度的碘 131。另外也可以考慮使用藥物來抑制泌乳。若嬰兒喂養碘 131 之乳汁會有發生甲狀腺功能減退的風險。

結論：SNM Guideline 建議在給藥前須停止哺乳至少 6 週，對正在哺乳中的女性病患使用碘 131 時，應謹慎思考是否建議乳腺退化後再投藥。若必須立即治療，可考慮增加藥物以抑制泌乳，減低對乳房的輻射劑量。投藥後切不可再哺乳，避免對嬰兒甲狀腺低下之後遺症。

PC056

探討 PETMR 與 PETCT 在頭頸部上 SUV 值的相關性

李建穎 陳奕倫 張嘉容 楊邦宏 黃文盛

臺北榮民總醫院核醫部暨全方位正子磁振造影中心

背景：新型 GE SIGNA PET/MR 配置更高效能的晶體與演算技術，並結合 MRI 較佳的軟組織對比影像，可以使 PET 得到更高訊號源與更佳的影像解析力資訊。然而腦部 PET/MR 組像的衰減校正 (AC) 的準確性，仍然是一個眾所皆知的問題所在，因此本研究目的在探討比較 PET/CT 與 PET/MR 在頭頸部上 SUV 值的相關性。

方法：我們選擇了 12 位受檢者 (7 位男士、5 位女士；年齡範圍 40-77 歲)，於商售的 PET/CT (GE Discovery VCT) 與 PET/MR (GE SIGNA) 進行造影，所有的受檢者皆先靜脈注射 5.29 MBq/kg 的 F^{18} -FDG 後休息 60 分鐘進行 PET/CT 造影，結束後立即至 PET/MR 造影。PET/CT 影像經過標準的 CTAC 重建後，當作金標準值；PET/MR 則使用 Dixon 波序，產生 Atlas-AC 衰減校正影像。兩組影像皆由同一位放射師圈選六個選定的 ROI (小腦、橋腦、視丘、鼻咽、胸鎖乳突肌、額葉灰質區)，分別記錄其 SUV_{max} 、 SUV_{ave} ，並分析兩台造影儀器 SUV 之相關性。

結果：我們觀察到頭頸部 PET/MR 的 SUV_{max} 或者 SUV_{ave} 值都小於 PET/CT，且在額葉灰質區、視丘、小腦以及胸鎖乳突肌四個 ROI 中，兩台造影儀器 SUV_{ave} 線性回歸中呈現高度的相關性 (額葉灰質區 $R^2 = 0.63$ ，視丘 $R^2 = 0.81$ ，小腦 $R^2 = 0.81$ ，胸鎖乳突肌 $R^2 = 0.77$ ， $P < 0.05$)，且可透過線性公式轉換；相較在剩下鼻咽部與橋腦兩各區域的 SUV_{ave} 卻沒有很高的相關性 (橋腦 $R^2 = 0.39$ ，鼻咽 $R^2 = 0.28$)。

結論：由於 PETMR 使用 Dixon 波續 MRAC (Atlas-based) 對於空氣與骨骼結構之校準能力較差 (乳突和鼻腔)，造成顱底結構 SUV 值受影響較大，有明顯高估之疑慮，且較無相關性；其餘的腦部區塊部分，PETCT SUV 值可以透過回歸方程式轉換來推測得知。在未來將使用 MRI 之 ZTE-based 波序來補強 Atlas-based 缺點的部分，可能是下一步研究的重點。

PC057

比較不同 MUGA 造影條件之 EF 計算數值

林智偉 徐景龍 黃文盛

臺北榮民總醫院

背景介紹：核醫多頻道心室功能攝影 (Multiple-Gated Acquisition, MUGA) 乃是評估左心室射出分率 (Ejection Fraction, EF) 的黃金準則。臨床造影條件設定可使用總計數值或是規律心跳數為基準，再將累計的影像資料進一步分析，計算出 EF 數值。

方法：總計 32 位病患 (平均年齡 57 ± 12 歲) 進行 MUGA 造影，運用體內標誌技術 (in-vivo technique)，施打 20 mCi ^{99m}Tc pertechnetate 後，使用 Siemens Symbia E 進行造影，每位病患各收集三組 MUGA 資料，Beat Window 皆設定為 30%，造影條件分別為 8M (preset count: 8000K)、4M (preset count: 4000K) 與 500B (preset heartbeat: 500 beats)，最後計算 EF 數值。

結果：三組 MUGA 造影資料中，平均 accepted heartbeat 與造影時間分別為 8M (1024 ± 315 , 14.26 分鐘)、4M (526 ± 173 , 7.36 分鐘)、500B (500, 7.14 分鐘)。經 Repeated measures ANOVA 分析，Wilks' Lambda = 0.969, $F(2,30) = 0.481$, $P = 0.623$ ，三組不同 MUGA 造影條件之 EF 計算數值無顯著差異。在各組資料中，EF 值與病患年齡、最後納入計算的心跳數、造影角度皆無相關，而 EF 值與背景值具正相關 (8M, $p = 0.001$ ；4M, $p < 0.001$ ；500B, $p = 0.019$)。

結論：本研究中 8M、4M、500B 三組 MUGA 造影條件所估算的 EF 無顯著差異。因此，對於無法久躺或是心律不整的病患，可將造影條件調整為 4M (preset count: 4000K) 或 500B (preset heartbeat: 500 beats)，藉以縮短造影時間。

AFP 和 PIVKA-II 檢測值之比較及探討

張素雲¹ 薛仔婕¹ 林淑靜¹ 廖建國¹ 王昱豐^{1,2}

¹ 佛教慈濟醫療財團法人大林慈濟醫院核子醫學科

² 慈濟學校財團法人慈濟大學醫學系

背景：臨床常用的血清甲型胎兒蛋白 (alpha-fetoprotein, AFP) 對肝癌的敏感度並不高，相關研究指出有 30~40% 的肝癌患者無 AFP 升高情形，因此 AFP 並不是早期診斷肝癌的完美指標；而腹部超音波檢查準確度也會因檢查者而異。在 1984 年首次被稱為肝癌標誌物之 PIVKA-II (Protein induced by Vitamin K absence or antagonists-II)，為維生素 K 缺乏或阻抗劑 -II 所誘導蛋白，是一種異常的凝固因子 factor II，會出現於肝癌患者的血清中，在肝細胞癌病人的血液中會呈現特異性上昇。本研究目的為初步比較 AFP 和 PIVKA-II 之檢測值，並探討 PIVKA-II 應用於肝癌診斷的角色。

材料方法：2019/04/25 至 2019/07/25 間，篩選肝膽胃腸科追蹤之病患，共收集 20 支血液檢體，其中 11 支為肝癌患者，9 支為非肝癌患者。離心取上清液，使用 ADVIA Centaur 全自動化學冷光免疫分析儀檢測 AFP (量測區間 1.3~1000 ng/mL，參考值 8 ng/mL)，另以 Lumipulse® G 化學冷光酵素免疫測定法 (CLEIA) 檢測 PIVKA-II (參考值 9.1~27.8 mAU/mL)。分析比較兩者之檢測結果，觀察檢測值是否皆正常或異常，以了解其於診斷上的一致性，並比較兩者應用於肝癌診斷之敏感度。

結果：AFP 和 PIVKA-II 數值皆異常有 2 人，AFP 和 PIVKA-II 數值皆正常有 5 人，AFP 異常和 PIVKA-II 數值正常有 3 人，AFP 正常和 PIVKA-II 數值異常有 10 人，顯示 AFP 和 PIVKA-II 檢測結果之一致性並不高 (7/20)。進一步比較肝癌檢體之檢測結果，發現 PIVKA-II 之敏感度為 81.82% (9/11)，而 AFP 之敏感度則僅為 18.18% (2/11)，也就是 81.82% 的肝癌患者無 AFP 升高情形，此結果明顯高於其他相關研究之結果 (30~40%)，這應與本研究收集之樣本數較少有關。實際臨床應用上，PIVKA-II 與 AFP 可作為肝細胞癌 (hepatocellular carcinoma, HCC) 互補的腫瘤標記，PIVKA-II 可結合傳統影像學輔助 HCC 診斷，評估療效與疾病再發的評估。另外，PIVKA-II 的血清半衰期比 AFP 短很多 (40~72 小時 vs. 5~7 天)，這與肝癌的分期和生存情況相關，因此 PIVKA-II 更能協助判斷肝癌患者的治療效果和預後。

結論：初步比較結果，AFP 和 PIVKA-II 檢測結果之一致性並不高，PIVKA-II 應用於肝癌診斷的敏感度高於 AFP。PIVKA-II 與 AFP 雖無直接相關性，來源機轉亦不相同，但臨床上若能同時一起檢測，則有相輔相乘的效果，比兩者單獨使用準確率更高。

PC059

放射免疫分析實驗室改善試劑庫存管理——個案報告

薛仔婕¹ 張素雲¹ 林淑靜¹ 廖建國¹ 王昱豐^{1,2}

¹ 佛教慈濟醫療財團法人大林慈濟醫院核子醫學科

² 慈濟學校財團法人慈濟大學醫學系

背景：檢驗服務品質基於良好的實驗室供應品，特別是直接影響檢驗品質之關鍵性試劑耗材，而庫存管理是實驗室日常運作穩定的基礎，良好的庫存管理可確保試劑耗材品質、減少浪費、控制成本、避免試劑短缺，故應從實驗室試劑之種類及採購量等進行管理。庫存過多可能使試劑過期浪費成本，若庫存不足試劑短缺將直接影響報告時效，導致報告逾時，間接影響臨床醫師之診斷。2018 年本科實驗室曾發生試劑短缺而導致報告逾時之事件，因此將此事件改善之過程與結果，整理後提出個案報告。

個案報告：2018 年 10 月本科實驗室發生因醫檢師無法有效控管試劑庫存量，導致試劑短缺而報告逾時之事件，經檢討其原因主要為實驗室平均使用量未適時更新及調整，以致當作業量增加時庫存試劑量無法供應實驗室的正常運作。為避免試劑短缺事件再次發生，擬訂改善措施如下：(1) 重新分析過去 1 年每月各檢驗項目試劑平均使用量及實際訂貨量，並計算其安全庫存量以及最高庫存量，以適當調整每月訂貨量。訂藥時依據每月平均使用量以及訂藥時的庫存量，評估該月的訂貨量。另外，因 RIA 試劑有效期限較短，訂藥時以不低於每月平均使用量的最低訂貨量為原則，以避免訂貨量過多造成過期。(2) 當每月收到試劑時，負責各檢驗項目的醫檢師立即評估是否足夠臨床檢驗業務量使用，且於使用中隨時評估庫存量是否足夠，如發現庫存量可能不足或檢驗業務量有明顯增加趨勢時，及早向技術主管提出反應，以利向廠商或其他實驗室調試劑使用。改善措施自 2018 年 11 月開始執行後，追蹤至 2019 年 8 月底為止，未再發生類似異常，證明改善措施可有效防止斷藥事件。

結論：試劑的庫存管理攸關實驗室的正常運作與品質，透過此異常個案的檢討與改善，可提醒實驗室同仁定期檢視平均使用量與訂貨量的合理性，並適時進行調整，以避免因庫存量不足而影響正常作業。

PC060

胸腔 - 腹膜腔分流核醫掃描病例報告

呂建璋¹ 林雅婷¹ 曾柏銘² 沈淑禎¹ 門朝陽² 蕭聿謙³

¹ 天主教中華聖母修女會醫療財團法人天主教聖馬爾定醫院核子醫學科

² 天主教中華聖母修女會醫療財團法人天主教聖馬爾定醫院正子造影中心

³ 亞東紀念醫院核子醫學科

背景介紹：腹膜透析 (PD) 用於治療末期腎臟病 (End stage renal disease, 簡稱 ESRD)。腹膜透析可能產生併發症，腹膜透析併發透析液滲漏為較不常見的一種，透析液滲漏可能的路徑有兩個，向上滲漏至肋膜腔，向下經腹股溝滲漏至外生殖器。利用放射性核醫藥物 (示蹤劑)，可幫助診斷確認透析滲漏的路徑及位置，本文介紹二則病例報告。

病例報告一：一位 49 歲男性 ESRD 患者，於 105 年 2 月初次接受腹膜透析治療後約 4 個月，因呼吸困難入院，胸部 X 光顯示兩側肋膜積水。由於病患在腹膜透析後發生呼吸急促，懷疑透析液向上滲漏進入肋膜腔，試圖藉由核醫掃描確認腹膜透析液是否滲漏。進行胸腔 - 腹膜腔分流掃描前，將示蹤劑 Tc-99m DTPA 混合透析液後，經導管注入腹膜，先收集一組動態造影 (1min/frame, 共 10 分鐘)，再收集延遲影像，觀察胸部是否有放射活性的累積。核醫檢查結果顯示兩側皆有放射活性累積 (右側 > 左側)，亦即透析液自腹膜腔滲漏進入肋膜腔之證據。病患於檢查後並未接受手術治療，而以減低壓力的方式進行 PD，之後再增加透析液的體積。後續追蹤至目前為止，並未再發生滲漏。

病例報告二：一位 65 歲男性 ESRD 患者，於 108 年 7 月年初次接受腹膜透析治療後 16 天，發生腹股溝及陰囊水腫入院接受檢查，超音波顯示兩側陰囊皆有積水的情形，懷疑是否因腹股溝疝氣導致透析液滲漏。患者接受胸腔 - 腹膜腔分流掃描，發現右側腹股溝及兩側陰囊異常放射活性的累積，證實有滲漏的情形。病患後續接受疝氣修補手術，傷口復原後，再次接受 PD，持續觀察，目前未發生水腫之情形。

結論：胸腔 - 腹膜腔分流核醫掃描用於診斷腹膜透析併發透析液滲漏，可幫助診斷確認滲漏的路徑及位置。相較於其他診斷工具，如 CT 或 MRI，雖然解析度不高，但核醫掃描的特性，在於即使滲漏的量不高，亦可藉由多次收集延遲影像的方式，追蹤滲漏路徑，而不會增加病患輻射劑量，是一項很有價值的診斷工具。

PC061

壁報論文發表摘要·臨床組

比較數位 CZT 半導體偵檢器 與傳統 NaI 偵檢器在影像上的表現

陳苓仕 陳至豪 黃文盛

台北榮民總醫院核子醫學部

目的：數位時代的來臨，促使核子醫學偵檢器也進入半導體數位化，GE Healthcare NM/CT 870 CZT 是新設計的代表機型之一。本實驗嘗試透過四象限條狀假體來觀察比較 NM/CT 870 CZT 與 Discovery NM/CT 670 (NaI) 新舊設計機型在影像上的表現。

材料與方法：利用四象限條狀假體與鈷 -57 均勻平板射源在 Discovery NM/CT 670 與 NM/CT 870 CZT 的每個偵檢器頭各收集 10,000,000 個計數量，再透過 Xeleris 影像分析工作站計算並比較各偵檢器頭的對比度 (Contrast) 及訊雜比 (SNR)。

結果：比較結果發現在 Contrast 及 SNR 表現上，NM/CT 870 CZT 在四象限假體的每一個象限 (鉛柵間距：6.35 mm、4.77 mm、3.97 mm、3.18 mm) 都優於 Discovery NM/CT 670。且當鉛柵間距越小，兩者的 Contrast 及 SNR 差異越大。

結論：根據實驗結果，我們觀察到在大組織間距時，兩者都能得到理想的影像表現，且 NM/CT 870 CZT 略優於 Discovery NM/CT 670；而當組織間距漸趨細小時，NM/CT 870 CZT 在影像上的 Contrast 及 SNR 表現明顯優於 Discovery NM/CT 670，足見 CZT 半導體偵檢器對影像解析度的提升有明顯的幫助。

PC062

Huge Uterine Cavity Mass Lesion Mimicking Lymphoma on ^{18}F FDG PET/CT Scan – A Case Report

Shu-mei Lu, Yu-Ling Hsu

Department of Nuclear Medicine, Ditmanson Medical Foundation Chia-Yi Christian Hospital, Chia-Yi, Taiwan

Case: A 63y female has symptoms of sorethroat and fever off and on for 1 month, referred form LMD due to suspected left tonsil tumor. Differential diagnoses including bilateral tonsil enlargement with mucopus , tonsillitis, or malignancy. During OPD follow up in the following week, she was suggested biopsy. Therefore billateral tonsillectomy was done; patholohy revealed malignant lymphoma. PET-CT scan was performed and found low grade FDG avid lymph nodes at left parotid, cervical level 2-4 regions. A mass lesion with intensive FDG avidity was noted at uterine cavity with enlarged para-aortic lymph nodes, highly suggested malignancy. (figure). After pelvis MRI with contrast was done, leiomyosarcoma from uterus or other etiology was suspected. Metastatic lymphadenopathy and pelvic seeding lesions also cannot be excluded. After surgery, however, the intramural tumor show a picture of leiomyoma, composed of proliferation of smooth muscle cell in fascicular arrangement without cellular atypism and atypical mitosis, which is benign.

Discussion: ^{18}F -FDG PET-CT is used extensively for staging and monitoring patients with uterine cervical cancer. Because of high glucose metabolism, FDG generally accumulates in malignant lesions. FDG uptake, however, is not specific for cancer cells and, therefore, sometimes it leads to false-positive conclusions for benign inflammatory lesions. Despite this, FDG-PET have radically changed the management of lymphoma. Growing evidence supports its incorporation into clinical decision algorithms, negative interim and end of treatment PET being strong predictors of good outcome in most lymphoma subtypes. As a result of its widespread use, false PET positivity became a common challenge. Examples include infection, post chemo- or radiotherapy inflammation and not uncommonly secondary tumors with benign entity, as in our case.

PC063

A Case of Gout Stone Mimics Urine Contamination Detected by ^{99m}Tc -MDP Whole-Body Bone Scan

Shih-Fu Wang, Dom-Gen Tu, Yu-Ling Hsu

Department of Nuclear Medicine, Ditmanson Medical Foundation Chia-Yi Christian Hospital

Case Report: A 38-year-old male patient has multiple emergent visits due to recurrent episodes of idiopathic chronic gout with cellulitis of the right lower extremity. Bone scan was scheduled because of suspicious lung cancer.

There are multiple abnormal activities in bilateral thigh in bone scan. In the process of eliminating urine contamination, many hard masses were found at the posterior aspect of the thigh.

Previous computerized tomography of the patient showed multiple solid masses at the posterior side of the thigh, which proved to be tophi. Therefore we suspect that multiple focal abnormal activities in thigh in bone scan are caused by tophi, too.

Discussion: Tophi often occurs in the finger and toe joints. Rare in the trunk and thighs. Therefore, with similar imaging pattern, in addition to eliminating contamination, we should also consider whether it is gout stone or masses of other nature.

PC064

運用失效模式與效應分析 (HFMEA) 進行核醫造影時間延遲原因之分析

陳雅鳳 賴佳玟 黃兆駿 李柏葦 張哲瑋 汪姍瑩 吳彥雯

亞東紀念醫院核子醫學科

背景介紹：核子醫學檢查種類及項目繁多，施打的放射性同位素其半衰期較短，在執行核子醫學檢查的過程中，時間的掌握相對重要。運用失效模式與效應分析 (HFMEA) 針對會影響核子醫學造影檢查時間延遲的各項原因，進行分析及改善措施，以有效提高造影檢查的效率。

方法：針對 2018 年 7 至 12 月核子醫學檢查項目，運用失效模式與效應分析 (HFMEA) 針對「病人報到」、「衛教並給予放射性藥物」及「執行核醫檢查」三個主流程，利用危害指數矩陣 (Hazard Scoring Matrix) 及決策樹分析 (Decision Tree) 進行失效原因評估及危害風險分析，其中針對 13 項失效原因進行改善，擬定改善措施並於改善後重新進行危害風險分析。

結果：針對 13 項失效原因進行改善，擬定改善措施並於改善後重新進行危害風險分析，其風險計分均有顯著下降，有效改善造影時間延遲之發生機率，提高核子醫學造影檢查的執行效率。

結論：利用失效模式與效應分析 (HFMEA) 可針對流程做完整性的失效原因評估及風險危害分析，針對失效原因進行改善並有效減少危害的發生機率或降低危害指數，以達到有效提高核子醫學造影檢查的執行效率。

PC065

壁報論文發表摘要·臨床組

Evaluation of LV EF Prediction Accuracy and Benefit Obtained from ^{201}Tl Myocardial Perfusion Scan by CZT Cardiac Camera

Hsiao-Ling Chiang, Bang-Hung Yang, Cheng-Pei Chang,
Lee-Shing Chu, Wen-Sheng Huang

Department of Nuclear Medicine, Taipei Veterans General Hospital, Taipei, Taiwan

Introduction: The shorter imaging time with better imaging quality using CZT detectors compared to conventional ones makes it feasible to perform the left ventricular ejection fraction (LVEF) in the meantime of doing ^{201}Tl Myocardial perfusion imaging (MPI). The study was to compare LVEF from ^{201}Tl MPI using a CZT with that from first-pass radionuclide angiography (FPRA) using a NaI camera, and Evaluated the LVEF Prediction Accuracy of that, and the assistance for myocardial quantitative results.

Methods: A total of 117 patients (aged 81 ± 13 years old) were collected. All underwent ^{201}Tl MPI using a CZT camera (Discovery NM530c) and FPRA using a conventional camera (Symbia E Signal Head System) in 2 wks. Correlations of LVEF obtained from these two examinations were evaluated by SPSS 20.0 statistical software.

Results: The $\text{LVEF} \geq 50\%$ was 76 cases in MPI group and 74 cases in FPRA group. Observed agreement of both groups was 92.3%. Chance agreement representing the expected probability of both test results was 53.7%. The KAPPA coefficient κ of the chi-square test was 0.83 ($p < 0.0001$). The stress defect score, rest defect score and stress defect percentage of Polar Map were defined by the LV EF less than 50. The receiver operating characteristic curves (ROC) of the three quantitative value were derived, and the AUC values were 0.70, 0.83, and 0.75, respectively.

Conclusions: The KAPPA coefficient of the chi-square test showed almost perfect in consistency between both tests ($\kappa = 0.83$, $p < 0.0001$), indicating LVEF using ^{201}Tl Myocardial Perfusion Scan (MPS) was highly accurate in predicting heart dysfunction. The AUC values (0.70, 0.83, and 0.75, respectively) defined by the LV EF less than 50 showed that all three quantitative values had good predictive rates. Thus, the three thresholds 8, 5, and 18 of defect scores can be derived, and the results can help Clinical diagnosis of myocardial ischemia.

PC066

評估不同衰減校正法在 FDG PET/MR 正常腦部影像定量之差異

姜振豪 張嘉容 楊邦宏

臺北榮民總醫院核醫部

背景介紹：光子衰減校正在正子影像之判讀扮演著重要的角色，根據病人的體型以及體內軟組織、脂肪、骨頭分布上的差異，透過正確的衰減校正可以呈現體內正子藥物實際吸收分布狀況，並提供精準的 SUV 值協助臨床診斷，隨著儀器的進步，PET/MR 在臨床上也開始嶄露頭角，相較於 PET/CT 之 CT 提供的 μ map，目前 MR 具有的衰減校正方法較多（包括 Dixon-based、Atlas-based、ZTE-based 等），本研究目的為探討以 PET/MR 收集頭部影像中，比較以 Atlas-based 與 ZTE-Based 做衰減校正時定量上的差異。

方法：本研究造影儀器採用 GE SIGNA PET/MR，將 15 位正常腦部受試者（ 52.75 ± 12.98 歲；8 位男性、7 位女性），注射 ^{18}F -FDG（活性 247.53 ± 90.28 MBq），於 60 分鐘後蒐集腦部 PET/MR 影像，透過不同影像衰減校正：1) Atlas-Based 及 2) ZTE-Based 重組影像，以 CortexID (GE Healthcare) 將腦部影像標準化並將大腦皮質分成 26 個區域，將各區 SUV 與參考基準相除，得到 SUVR ($\text{SUV}_{\text{ratio}}$)。參考基準分別為橋腦 (pons)，小腦 (cerebellum) 及全腦皮質 (global)，並比較 Atlas-Based 及 ZTE-Based 之衰減校正法在各區域 SUVR 的差異。

結果：以 CortexID 分析 ^{18}F -FDG 腦部各區皮質吸收，得到以橋腦、小腦及全腦皮質為參考基準之 SUVR，且這三組在 ZTE-Based 與 Atlas-based 間皆有非常好的相關性 ($R^2 > 0.99$)。當以全腦皮質為參考基準時，SUVR 在 Atlas-Based 及 ZTE-Based 的衰減校正下皆有較小的標準差，並且在以下區域（內側顳葉、小腦、橋腦）經過 ZTE-Based 校正後的影像 SUVR 有顯著增加 ($p < 0.05$)；而在以下區域（左感覺運動區、後扣帶皮層、楔前葉、下頂葉、側枕葉）經過 Atlas-Based 校正後的影像 SUVR 有顯著增加 ($p < 0.05$)。

結論：對在正常 FDG PET/MR 腦部影像定量時，利用 ZTE-Based 可以獲得與 Atlas-based 相似的結果，代表 ZTE 也適合於臨床應用，其中參考區為全腦皮質相比之 SUVR 有比較穩定的表現。

PC067

氟化去氧葡萄糖在 PET/MR 與 PET/CT 的全身正子造影 SUV 值之比較

張嘉容 李建穎 楊邦宏 黃文盛

臺北榮民總醫院核醫部

背景：在臨床上常使用氟化去氧葡萄糖的 PET/CT 全身正子造影來評估是否癌症轉移、復發或是病情分期，PET/MR 是近年來是很創新的技術發明，除了對受試者有較少的輻射暴露，在解剖構造上也提供更多資訊，其正子影像衰減校正方式有別於 PET/CT。因此本研究之目的在於比較 PET/CT 及 PET/MR 氟化去氧葡萄糖全身造影中正常器官組織的 SUV 值之關係。

材料與方法：本研究中共有 13 位受試者 (55.64 ± 12.06 歲；7 位男性、6 位女性)，注射氟化去氧葡萄糖後 60 分鐘造影，進行常規 PET/CT 全身造影，接著再做 PET/MR 全身造影。針對肺部，肝臟，腰椎，腰大肌，股骨頭，臀大肌等六區圈選 VOI (1cm³)，比較在各區域 PET/CT 及 PET/MR 之 SUV (Max/Average) 的差異。

結果：在 PET/CT 及 PET/MR 影像中，正常器官組織中肺臟 ($SUV_{Max}/SUV_{Average}$ ， $R^2 = 0.45/0.80$) 及肝臟 ($SUV_{Max}/SUV_{Average}$ ， $R^2 = 0.27/0.52$) 的 $SUV_{Average}$ 有良好的相關性。腰椎 ($SUV_{Max}/SUV_{Average}$ ， $R^2 = 0.76/0.52$) 及股骨頭 ($SUV_{Max}/SUV_{Average}$ ， $R^2 = 0.65/0.63$) SUV_{Max} 及 $SUV_{Average}$ 有良好的相關性。在腰大肌 ($SUV_{Max}/SUV_{Average}$ ， $R^2 = 0.03/0.05$) 及臀大肌 ($SUV_{Max}/SUV_{Average}$ ， $R^2 = 0.0/0.17$) 則無顯著相關。此外，在 PET/CT 的 SUV_{Max} 及 $SUV_{Average}$ 皆略高於 PET/MR。

結論：在 PET/CT 與 PET/MR 的氟化去氧葡萄糖全身正子造影中，正常器官組織除了腰大肌與臀大肌外， $SUV_{Average}$ 皆有良好的相關性，所以 PET/MR 在定量上可以提供與 PET/CT 相似的結果，可適用在臨床造影。

PC068

¹⁸F-FDG PET/CT Imaging Unexpectedly Discovered “Collision Tumors” in Thyroid

Yi-Hsun Chen, Dom-Gen Tu

Department of Nuclear Medicine, Ditmanson Medical Foundation Chia-Yi Christian Hospital

Case report: A 65-year-old woman who had loss of appetite and weight loss 19 kgs in half a year was referred to ¹⁸F-FDG PET/CT imaging. Her medical history included hypertension and systemic lupus erythematosus. The ¹⁸F-FDG PET/CT images showed two FDG uptake nodules, one at left superior (SUVmax of 3.2) area and another at left inferior (SUVmax of 8.7) thyroid lobes. Biochemical investigations showed TSH of 1.68 μ IU/ml (normal range 0.25-4 μ IU/ml), Free T4 of 1.37 ng/ml (normal range 0.7-1.8 ng/ml), Ab-thyroglobulin < 10 IU/ml (normal range < 115 IU/ml), Thyroglobulin of 118.9 ng/ml (normal range 1.6-59.9 ng/ml), Anti-Tg of 1.94 IU/ml (normal range 0-4.11 IU/ml), Anti-TPO Ab of 0.14 IU/ml (normal range 0-5.61 IU/ml), and TSH receptor Ab < 5% (normal range < 14%). The patient was admitted for surgery. Radical thyroidectomy and unilateral neck lymph node dissection were performed. Histopathological examination confirmed the lesions at left superior and inferior thyroid lobes were papillary carcinoma and Hurthle cell adenoma, respectively.

Discussion: Papillary carcinoma is the most frequently encountered thyroid gland malignancy including different histologic variants with different patterns of biological behaviors. Papillary differentiated thyroid cancer is associated with a tumor showing low glucose affinity. Hurthle cell adenoma is defined as a rare, benign thyroid neoplasm composed of Hurthle cells that comprise more than 75% of adenoma cell population. Hurthle cell adenomas show significantly higher focal FDG uptake as compared to follicular lesion and should always be considered in the differential diagnosis of FDG-PET positive thyroid nodules.

The occurrence of any neoplasm in thyroid is usually of a single type. The presence of two intimately associated but morphologically distinct neoplasm in thyroid is an unusual phenomenon. These tumors can occur as mixed tumors, composite tumors, or collision tumors. Collision tumors refer to coexistent but independent tumors that are histologically distinct. Collision tumors involving the thyroid gland and/or neck region are especially uncommon, with most reported cases involving papillary thyroid carcinoma in coexistence with medullary thyroid carcinoma, follicular carcinoma, and metastatic disease. We present collision tumors being a combination of Hurthle cell adenoma and papillary carcinoma occurring in a female. The case of collision tumors in thyroid has only one been reported so far in the literature to the best of our knowledge.

PC069

The Appearance of Tc-99m MDP Bone Scintigraphy in Chondroblastic Osteosarcoma: A Case Report

Shih-Chin Chou¹, Tzyy-Ling Chuang^{1,2}, Yuh-Feng Wang^{1,2}

¹Department of Nuclear Medicine, Dalin Tzu Chi Hospital, Buddhist Tzu Chi Medical Foundation, Chiayi, Taiwan

²School of Medicine, Tzu Chi University, Hualien, Taiwan

Introduction: Tc-99m MDP Whole Body Bone Scan is a useful tool for detecting bony metastases in many kinds of malignancy, occult fracture and prosthesis failure. We report a case of chondroblastic osteosarcoma detected by Tc-99m MDP Whole Body Bone Scan.

Case Report: A 76-year-old woman was a case of uterine cervical cancer post irradiation therapy 20 years ago, then lost to follow-up. She received right total hip replacement for right hip avascular necrosis three months ago. This time, she suffered from persistent right hip pain after falling from bed last night. Pelvic x-ray showed right pubic ramus fracture. Tc-99m MDP three phases study and whole-body bone scan with SPECT/CT to pelvic area was arranged for evaluation of prosthesis loosening and other occult bony lesions. The increased radioactivity along the prosthesis, right pubic bone and diffusely radioactivity in the swelling soft tissue of right thigh consisted with prosthesis loosening, right pubic fracture and soft tissue edema. However, diffusely and heterogeneously increased vascularity and perfusion of tracer over the right hip with intensely and heterogeneously increased metabolism in the right iliac bone and the nearby swelling calcified muscles were also noted. Debridement and synovectomy were done, and the pathologic report from excisional tissue showed high-grade epithelioid to spindled tumor cells with areas of cartilaginous matrix and malignant osteoid production and focal cellular sheets. Immunohistochemical study showed CK(-), P40(-), S100(+), CDK4(-), MDM2(-), loss of H3K27me3 and no mutation of IDH1/2 sequencing. Chondroblastic osteosarcoma was diagnosed.

Conclusions: In this case we report the scintigraphic findings in chondroblastic osteosarcoma with heterogeneously increased blood flow, perfusion and intense and heterogenous radioactivity. Primary malignant neoplasm should be listed into the differential diagnosis if only single lesion detected by bone scintigraphy in cancer patient.

PC070

F-18 FDG PET/CT Helps Primary Tumor Detection and Further Planning in Metastatic Axillary Lymphadenopathy with Occult Breast Primary Origin: A Case Report

Shih-Chin Chou¹, Tzyy-Ling Chuang^{1,2}, Yuh-Feng Wang^{1,2}

¹Department of Nuclear Medicine, Dalin Tzu Chi Hospital, Buddhist Tzu Chi Medical Foundation, Chiayi, Taiwan

²School of Medicine, Tzu Chi University, Hualien, Taiwan

Case Report: A 57-year-old woman had underlying disease of hypothyroidism under medicine control. She suffered from right axillary mass for few weeks. No breast or other lesions were detected by physical examination, breast sonography or chest CT. Pathology from excision of right axillary mass revealed metastatic carcinoma with suspicious breast origin. F-18 FDG PET/CT (PET) was arranged for primary tumor and systemic cancer survey, which showed several hypermetabolic processes in the lower inner quadrant of right breast (SUVmax: 3.9 → 4.7, 1.8 → 2.1), right axillary lymph nodes (SUVmax: 3.5 → 3.7, 3.1 → 3.5, 4.7 → 4.9), liver at S6 (SUVmax: 6.8 → 7.3) and bones at T1 (SUVmax: 4.7 → 4.7), L3 (SUVmax: 2.5 → 3.0) and right sacrum (SUVmax: 3.3). An about 0.6 cm tiny lesion in accordance of the hypermetabolic process in the right breast was then identified by breast sonography. Echo-guided core needle biopsy was done and pathologic report revealed carcinoma. She received right partial mastectomy and right axillary lymph nodes dissection. Pathology confirmed right breast invasive carcinoma with right axillary lymph nodes metastases, pT2(2)N3a (AJCC 8). Immunohistochemistry studies showed ER (positive, 100% tumor nuclei stained); PR (positive, 1% tumor nuclei stained); HER2/neu (equivocal, 2+); E-Cadherin (+); Ki-67 index up to 60%. Liver and bone metastases were confirmed by the abdominal MRI. Further adjuvant chemotherapy, radiotherapy, hormone therapy and denosumab for disease control would be arranged for her.

Conclusions: Breast cancer patients rarely present with isolated axillary lymph node metastasis without any clinical or radiological evidence of primary tumor, which only account for 0.1% to 0.8% of all the cases of breast cancer in females. The role of PET was still not been evaluated in cases of occult primary breast carcinoma. In this case, PET not only helps in guiding biopsy of primary tumor but also detecting liver and bone metastases which has definite impact on appropriate management. PET should be considered in this situation.

PC071

核醫造影檢查單開立不當之分析及探討

廖建國¹ 許幼青¹ 朱湘蓮¹ 莊紫翎^{1,2} 王昱豐^{1,2}

¹ 佛教大林慈濟醫院核子醫學科

² 慈濟大學醫學系

背景：核醫造影檢查前，檢查單開立不當的個案並不少見。本科醫師例行於造影檢查前審查各項檢查單開立之正確性，並適時的與開單醫師溝通。2018年6月起，本科也開始每月收集檢查單開立不當的個案，並進行分析及檢討。本研究目的即為分析近2年檢查單開立不當的比率，以了解是否有所進步，並作為持續改進之參考。

方法：回溯性收集2018年6月至2019年8月，例行造影檢查之檢查單開立資料，分析各月份之檢查單開立不當的比率，並歸納其開立不當之項目及原因，進行探討。另外，由於經常發現臨床醫師開立檢查單時，開錯檢查項目，因此探討開立不當之項目時，也重新檢視本院醫囑系統中臨床醫師之開單畫面，檢討其中是否有讓臨床醫師開錯單的因素，例如骨骼掃描誤開立為骨髓掃描、心肌灌注掃描誤開立為心肌梗塞掃描，以及是否仍有臨床醫師不知如何開立之項目。

結果：總計收集7557件開單個案，其中開單不當之個案計34件。整理結果發現，2018年6月至2019年8月之間，開單異常率皆維持在1%以下，2019年(1-8月)之平均異常率(0.30%)與2018年(6-12月)(0.59%)比較，有明顯的進步。其中開單異常發生件數較多的仍為檢查量較多的項目，前3名分別為BMD、骨骼掃描及心肌灌注檢查。至於發生原因，則依序分別為開錯項目(佔50%)、近期做過檢查(佔33%)、重覆開單(佔17%)。由於開單不當之原因，以開錯項目佔最大宗，因此我們在醫囑系統的開單畫面，將部份可能造成臨床醫師誤開之項目刪除(例如骨髓掃描、心室射出檢查(ventricular ejection)等)，也減少了部份的誤開件數。

結論：研究結果顯示，本科近2年之開單異常率平均為0.45%，其中2019年較2018年有明顯的改善。透過核醫醫師每日審查檢查單的機制，並每月針對開單異常率及其原因，進行分析及檢討，可有效降低開單異常率，提升整體作業品質。

PC072

核醫造影住院病人排檢成效分析

廖建國¹ 許幼青¹ 朱湘蓮¹ 莊紫翎^{1,2} 王昱豐^{1,2}

¹ 佛教大林慈濟醫院核子醫學科

² 慈濟大學醫學系

背景：排檢作業為核醫造影檢查前重要的一環，排檢等候天數的長短對於檢查報告的完成時間以及病人滿意度也有相當的影響。一般而言，住院病人的排檢應更急迫，需要被優先處理。然而，我們發現仍有少數個案，並不如預期，因此 2019 年起我們開始進行監控與改善。本研究目的即為分析近 2 年住院病人排檢天數以及排檢逾時個案，以了解初步改善成效，並作為持續改進之參考。

方法：回溯性收集 2018 年 1 月至 2019 年 6 月，例行造影檢查之門診排程報到資料，分析各月份之住院病人排檢天數及其逾時個案，並探討其發生因子。排檢天數以開單時間至排定檢查時間之天數計算。逾時件數以超過 4 天之個案為計算依據。另外，針對需連續多天造影之檢查項目，為作業方便常安排在周 1 至周五檢查（不跨周休日），因此計算時也排除 Ga-67 炎症或腫瘤檢查、腎上腺檢查等檢查。

結果：總計收集 1273 件住院個案，其中逾時個案計 20 件。整理結果發現，2018 年住院病人平均等候天數為 1.6 天，而 2019 年上半年之平均等候天數為 1.5 天，與 2018 年相近。而在住院病人排檢逾時率方面，2018 年平均逾時率為 2.9%，2019 年上半年則為 2.3%，顯示 2019 年開始監控後，排檢天數超過 4 天之個案已大幅降低。因此造影室利用每月品保會議，例行監控住院病人的排檢天數與排檢逾時率，並根據逾時個案之發生原因（例如病房送單時間太晚、單位排檢因素、醫師醫療處置因素、病人病況變化因素），進行檢討與改善，可提升排檢成效與管理品質。

結論：研究結果顯示，本科近 2 年之排檢平均等候天數均維持在 1.6 天以內，2019 年排檢逾時率較 2018 年大幅降低約 2 成，造影室透過每月例行的監控與檢討，可有效改善住院病人的排檢效率。

PC073

核醫影像檢查認證文件撰寫——經驗分享

廖建國¹ 許幼青¹ 張素雲¹ 莊紫翎^{1,2} 王昱豐^{1,2}

¹ 佛教大林慈濟醫院核子醫學科

² 慈濟大學醫學系

背景介紹：全國認證基金會於 2016 年 4 月公告影像醫學 (Medical Image) 之核子醫學影像檢查項目開放認證申請後，至今已有 4 家核醫造影之認可單位，本科即為其中 1 家。近期全國認證基金會為回應許多有意參加認證之核醫造影單位詢問有關文件撰寫的問題，於 2019 年 4 月邀請目前已通過認證之核醫造影單位管理階層擔任講師，共同舉辦核醫影像檢查認證文件撰寫之訓練課程。本文即為參加此次文件撰寫訓練並擔任講師後，整理認證文件撰寫之相關資料，提出經驗分享，期望對於有意參加認證的單位有所幫助。

文件架構：一般而言，核醫造影單位皆為區域級以上之大型醫院，因此文件架構建議可以四階文件的架構進行撰寫，四階文件包括一階文件 (品質手冊)、二階文件 (品保作業程序)、三階文件 (標準操作手冊或程序)、四階文件 (表單紀錄) 等。然而，四階文件架構並非一定的架構，核醫造影單位可依據自己的規模，制定適合自己的文件架構。若是規模較小之核醫造影單位，可將文件分為三階，包括品質文件 (將品質手冊與品保作業程序合併)、技術文件 (依檢驗項目或依文件屬性分類)、表單 (含品質與技術表單等)。

準備作業：由於核醫影像檢查之認證系統，其依據之國際規範為「ISO 15189 醫學實驗室 - 品質與技術要求」及「醫學領域之核子醫學影像檢查技術規範」，因此有意參加認證之單位應於文件撰寫前至少規劃 2 位同仁負責文件撰寫的工作 (例如品質主管與技術主管)，並請其先了解認證規範之相關內容，最好參加全國認證基金會辦理之相關訓練，在有一定的基本認知下，再進行撰寫，才能事半功倍，寫出符合認證要求並能有效執行的理想文件。

撰寫順序：依據本科的經驗，認證文件撰寫的重點在二階文件 (品保作業程序)，可先完成二階文件之撰寫後，再依據二階文件的內容大綱撰寫一階文件 (品質手冊)。而二階文件的撰寫可先撰寫文件管制作業程序，因為所有文件的撰寫必須在符合認證要求的文件管制架構下進行，因此文件管制作業程序為最優先撰寫的文件。至於其他各項二階文件則可依 ISO 15189 的章節分別撰寫，例如在管理要求 15 個章節以及技術要求 10 個章節，應分別對應撰寫出相關的管理文件。另外，撰寫時應再搭配「醫學領域之核子醫學影像檢查技術規範」的要求事項，於相關文件中撰寫管理程序，以符合認證要求。至於三階文件 (標準操作手冊)，一般而言各單位應已有相關作業標準，不須另外撰寫，只須依認證相關要求加以補強即可，而四階文件 (表單)，則可依各文件中的執行需求，訂定相對應的表單，以便進行紀錄。

結論：依據本科的經驗，認證文件的撰寫並不困難，但有意參加認證的單位，應先選定負責撰寫文件的人，並接受相關訓練，以了解認證相關規範，再依重點文件的撰寫順序逐一進行，相信一定可以制定屬於自己並符合認證要求的文件。

PC074

放射免疫分析報告逾時率之分析及探討

廖建國¹ 張素雲¹ 莊紫翎^{1,2} 王昱豐^{1,2}

¹ 佛教大林慈濟醫院核子醫學科

² 慈濟大學醫學系

背景：檢驗報告逾時可能造成臨床醫師診斷或治療上的延遲，因此報告逾時率一直為實驗室例行監控的重要指標之一。在放射免疫分析的日常作業中，報告的逾時也並不少見。本研究目的即為分析近年報告逾時之檢驗項目，並探討其原因，以作為持續改進之參考。

方法：回溯性收集 2018 年 1 月至 2019 年 6 月，實驗室每月例行檢討之品質指標資料，分析每月報告逾時項目、逾時率之變化，並探討其發生因子。報告逾時之定義，以報告發出之時間超過收件時間 7 天者計算。逾時個案之收集，由品質負責人每月自檢驗系統中撈取檢驗報告超過 7 天之件數，進行分析。

結果：總計收集 102699 件檢驗個案，其中報告逾時之個案計 64 件。整理結果發現，2018 年平均報告逾時率為 0.04%，而 2019 年上半年則為 0.03%，顯示 2019 年略有進步。而 2018 年 1 月至 2019 年 6 月之間，報告逾時之個案，皆以 2 月份最高，其原因為每年春節期間因放假天數較長所導致。進一步分析報告逾時之項目，發現逾時項目中委外項目佔 68%，而自行檢驗之項目佔 32%，顯示自行檢驗的部份仍有改進的空間。而其中逾時件數居前 6 名者，分別為 CA-125、GH (Growth hormone)、Thyroglobulin、PRA (Plasma renin activity)、Vit.B12、PTH-i (Intact parathyroid hormone) 等項，探討其原因，皆因為這些項目皆為荷爾蒙檢查項目或檢驗操作時間較長之項目 (例如步驟中需要培育過夜 (incubation over night))。

結論：本科 2019 年之報告逾時率較 2018 年略為降低，但其中自行檢驗的部份佔總數的 32%，仍有改進的空間，未來可針對件數較多的項目，加強監控與管制，以持續改善報告效率，提升作業品質。

PC075

放射免疫分析實驗室電子簽章完成率成效分析

廖建國¹ 張素雲¹ 莊紫翎^{1,2} 王昱豐^{1,2}

¹ 佛教大林慈濟醫院核子醫學科

² 慈濟大學醫學系

背景：由於國內各大醫院幾乎皆已實施電子病歷，因此實驗室發出之檢驗報告目前均以電子簽章的方式進行報告簽署，電子簽章的完成率，也成為各大醫院例行監控的項目之一。本科於 2018 年監控電子簽章完成率時，發現 5 月份之 24 小時簽章完成率未達 90%，因此針對此問題進行檢討與改善。本研究目的即為分析近 2 年電子簽章完成率之結果，以了解持續改善之成效。

方法：回溯性收集 2018 年 1 月至 2019 年 6 月，實驗室每月由醫院資訊系統例行收集之電子簽章資料，分析每月電子簽章總完成率以及 24 小時電子簽章完成率，並比較 2019 年與 2018 年之表現情形，以了解改善措施是否持續有效。由於造成電子簽章完成率未達 100% 的主要原因皆為同仁忘記簽章所致，因此 2018 年 6 月起本科以 TRM 手法實施同仁間守望相助、彼此支援、互相提醒之改善策略。

結果：整理結果發現，在電子簽章總完成率方面，2018 年總完成率為 99.54%，而 2019 年上半年則為 100%。而在 24 小時內完成率方面，2018 年平均為 99.15%，而 2019 年上半年的平均值則為 99.16%，雖然兩個年度之平均值相近，但 2019 年每月的完成率皆在 94% 以上，且僅有 1 位同仁 24 小時內完成率未達 100%，與 2018 年之 2 位同仁相較，仍有進步。顯示 2018 年 6 月實施同仁間守望相助之改善策略，可有效持續提升簽章完成率。

結論：研究結果顯示，本科 2019 年之電子簽章總完成率及 24 小時內完成率較 2018 年持續進步，顯示本科實施電子簽章的改善措施，確實已有成效，但是其中電子簽章 24 小時內完成率，仍有改進的空間，期望未來可再提升至 95% 以上，持續改善品質。

PC076

RIA 實驗室更新生物安全查核基準——個案報告

廖建國¹ 張素雲¹ 莊紫翎^{1,2} 王昱豐^{1,2}

¹ 佛教大林慈濟醫院核子醫學科

² 慈濟大學醫學系

背景：近年來，疾病管制署對於實驗室生物安全的要求，愈來愈嚴謹。2018 年疾病管制署又修訂 BSL-2 實驗室生物安全暨生物保全查核基準，因此本科 RIA 實驗室針對新頒訂之查核基準修訂實驗室生物安全自我查核表。本案例即為整理修訂實驗室自我查核表之過程，並比較新舊版基準之差異，提出分享。

個案報告：由於 2018 年疾病管制署修訂之 BSL-2 實驗室生物安全暨生物保全查核基準與之前頒訂之版本差異頗大，其中查核所要求的單位主要包括生物安全會及實驗室，因此修訂前須逐一比對其差異，由其中選擇實驗室的查核項目進行整理，並刪除有關生物安全櫃、滅菌器及生物感染性材料等不適用的查核項目，項次的排列也依照新版基準的項次，因此可說是大改版。改版後之主要查核項目有 5 大類，包括實驗室（保存場所）管理與維護（14 項）、實驗室消毒滅菌措施與感染性廢棄物處理（11 項）、持續性教育訓練與資源應用（1 項）、實驗室人員安全防護與健康措施（12 項）、緊急應變與意外事件（7 項）等。而原版基準有 7 大類（A-G 類），包括 A. 營造實驗室人員安全且合格的工作環境（19 項）、B. 實驗室之消毒滅菌與感染性廢棄物處理符合規定（16 項）、C. 感染性生物材料之管理與運送符合規定（14 項）、D. 鼓勵員工在職教育並提供相關資源（7 項）、E. 人員具備適當的健康防護及操作符合安全規範（17 項）、F. 緊急應變與意外事件（7 項）、G. 化學品及放射性物質（12 項），合計 75 項。新舊版本之編排明顯不同，但其中絕大多數的查核項目並無改變，僅在文件管理方面有新增一些要求，例如建立文件管理制度或程序、建立文件總覽表、訂有機敏文件保全措施、具機敏性之文件紀錄落實文件保全管理等。另外，根據本科的經驗，當 RIA 實驗室不再操作肝炎項目後，在實驗室生物安全等級的認定上仍歸屬於 2 級實驗室，其中主要因為依疾管署的認定「醫療院所之非微生物實驗室（血庫組、鏡檢組、生化組、血液組等），無法排除可能針對傳染病病人檢體進行非微生物學之檢驗」的判定原則。

結論：本科 RIA 實驗室依據 2018 年新頒訂之查核基準修訂實驗室生物安全自我查核表，透過修訂的過程逐一檢視新舊版的差異，並將修訂結果於品保會議中提報，讓所有同仁都了解，有助於持續改善實驗室之生物安全。

PC077

股骨頭軟骨下透亮硬化造成骨質密度異常增加 ——個案報告

陳保良^{1,2} 莊紫翎^{1,3} 周詩瑾¹ 廖建國¹ 王昱豐^{1,3}

¹ 佛教慈濟醫療財團法人大林慈濟醫院核子醫學科

² 佛教慈濟醫療財團法人大林慈濟醫院醫學研究部

³ 慈濟學校財團法人慈濟大學醫學系

簡介：目前臨床上診斷骨質疏鬆症疾病大多使用 DXA 來診斷，診斷方式只要整體 T 分數大於 -1.0 即判讀為正常。但有時會因骨頭相關疾病而使 T 分數遠大於正常值常多，或兩側髖關節差異非常大，此時我們就要留意患者是否有其他特殊其病造成骨質密度異常增加。

個案報告：一位 50 歲男性，至本院預防醫學中心執行健康檢查，身高 167 公分，體重 81.3 公斤，身體質量指數 29.2 kg/m^2 (輕度肥胖)，體脂肪 26.8 (偏高)，血壓 129/83 mmHg，抽血驗鹼性磷酸酶 76 (正常範圍 46-166)，鈣離子 2.29 (正常範圍 2.29-2.52)，甲狀腺刺激素 0.283 (正常範圍 0.55-4.78)，低於正常值，過去曾因左手肘韌帶斷裂手術，過去並無其他病史或家族病史。X 光診斷胸椎下段及腰椎輕度退化性關節疾病，及腰椎部分有骨刺。左側髖關節 X 光診斷有軟骨下透亮硬化及中度骨關節炎。骨質密度報告結果腰椎及兩側髖關節，數值皆判斷為正常，但是左側股骨頭骨質密度 1.393 g/cm^2 及 T 分數 4.4。

結論：當放射師做完檢查時，確認數據差異甚多時，除了確認分析是否有誤外，也需要進一步確認過去影像報告臨床醫師是否有診斷骨頭有特殊疾病。有時候數值上看似正常，其實隱藏許多問題。我們必須多方確認，才可提供臨床醫師及患者一份正確的報告。

PC078

高劑量碘 -131 輻射病房預防火災發生之應變程序

張桂蘭 黃南傑 張晉銓 趙莉琪

高雄醫學大學附設中和紀念醫院核醫科

摘要

目的：高劑量碘 -131 治療甲狀腺癌的病人需獨立自主於病房內 2-3 天，在發生火災的緊急狀況下醫院會集醫療團隊、保安隊、防災中心、滅火團隊…等，能夠在預防輻射暴露下，建立對病人的救助，安置及滅火等應變措施，熟悉火災發生之應變程序，期使住院期間病人及救助團隊於輻射環境災害應變流程進行救災，能確保病人之住院安全。

研究方法：病房除了設有急救拉鈴，煙霧偵測器外，硬體設備先架設好火災緊急拉鈴，此警鈴須連動防災中心，保安室，更重要的是病人自救離開時，進出管控之自動門同時打開，配合病人移方便性況設定離開時間並自動關門，以防火勢蔓延。

因此，輻射病房火災救助人力團隊，1. 病人拉病室火警拉繩後，穿著鉛衣，離至安全處等待支援人力。2. 防災中心接獲病室火警報知器或偵煙器警報，聯絡 2 間碘 131 病室確認是否誤報。若為火警，通報保安組、119、工務室。若病房火，通報鄰近滅火團隊。3. 保安接獲防災中心通報，立刻前往碘 131 病房支援。若病房火警報知器未警報，按下病房火警報知器，通報鄰近放射腫瘤科。

病房火警報知器鳴響或接獲火警通知進行 RACE 應變：A. 啟動自衛消防編組。通報班通知 119、總機及收治單位（內分泌科病房分機 7381 及核醫科分機 7152）。總機接獲放射腫瘤科通報後，啟動紅色零號廣播，並通報零階支援人力。

結論：輻射住院病房之危機管理於演練結果及缺失改善，提升監視設備畫質及功能並瞭解到整合呼叫鈴及對講機功能，改善病室內通訊設備，以利病人與內分泌科病房即時通訊。並且每年辦理碘 131 病房自衛消防編組，加強應變流程熟悉度，確保病人之住院安全。

PC079

Impacts of Vegetarian Diet and Physical Activity on Slowing Down the Bone Mineral Density Loss - A Pre-Post Study

Yuh-Feng Wang^{1,2,3}, Mei-Hua Chuang^{4,5}, Tzyy-Ling Chuang^{1,3},
Pao-Liang Chen¹, Malcolm Koo⁶

¹Department of Nuclear Medicine, Dalin Tzu Chi Hospital, Buddhist Tzu Chi Medical Foundation, Chiayi

²Center of Preventive Medicine, Dalin Tzu Chi Hospital, Buddhist Tzu Chi Medical Foundation, Chiayi

³Department of Radiology, School of Medicine, Tzu Chi University, Hualien

⁴Faculty of Pharmacy, National Yang-Ming University, Taipei

⁵Department of Pharmacology, School of Medicine, Tzu Chi University, Hualien

⁶Graduate Institute of Long-term Care, Tzu Chi University of Science and Technology, Hualien

Objective: Factors such as gene, physical activity, diet, and hormone are the primary causes for bone mineral density (BMD) loss in aging people. Previous researches had concluded that people on long-term vegetarian diets might consequent BMD changes. In this study, we explored the potential impacts of physical activity being the volunteers at the recycling station on their BMD alterations in Taiwanese women.

Material and Methods: This is a pre-post study on the relationship between the effects of both diet and physical activity and the BMD changes. From January to July 2019, age of 55 to 65 years old female subjects, who underwent routine examination at a regional teaching hospital in Taiwan were recorded. Furthermore, only subjects who had received BMD studies three to five years prior this study were eligible to enroll to this study. Subjects who had vertebral problems, post internal fixation, or total hip replacement were excluded.

Dual-energy X-ray absorptiometry (DEXA) was used to determine BMD for L2 to L4 vertebrae. The difference of BMD value of the pre-post DXA study (Δ) was documented. Participants that neither vegetarian nor doing recycling activity are defined as the control group. In contrast, the observed group is subjects who are vegetarian and doing recycling activity. Based on their total working periods for recycling activity, the subjects in observed group were further divided into subgroup: A (0-5 years), B (> 5-10 years), C (> 10 years), respectively. In addition, according to the frequency of doing recycling activity per week, the observed group was allocated into the subgroup: a (≤ 3 days a week) and b (> 3 days a week).

Results: The female BMD was declined rapidly after the 5th decade ($\Delta = 0.0483$), which is consistent with the normal tendency of postmenopausal women. However, in females with doing > 10 years recycling activity (subgroup C), the BMD change ($\Delta = 0.0095$) was statistically mild-mannered decline compared with the control group. The similar result was noted in subgroup b ($\Delta = 0.0051$) with significant differences compared with control group. For subjects who are vegetarian and doing recycling activity for >10 years and > 3 days a week, the significant difference of mild-mannered decline of BMD was also noted ($\Delta = 0.0097$).

Discussion: Bone remodeling is a continuous and complex process. Vitamin D, thyroid hormone, parathyroid hormone, sex hormones, dietary protein, calcium, caffeine, alcohol, cigarette and physical activity are possible imperative factors in modulating the rate of bone remodeling. Our results showed that women who are on vegetarian diet and continued daily physical activity could maintain BMD better and milder the slope of bone mineral loss.

人工血管術後在骨骼掃描的顯影

張秀瑛¹ 莊紫翎^{1,2} 王昱豐^{1,2}

¹ 佛教大林慈濟醫院核子醫學科

² 慈濟大學醫學系

背景介紹：全身骨骼掃描所利用的親骨骼放射性同位素製劑 (Tc-99m MDP) 是經由靜脈注射後隨血流運送到全身組織，所以局部血流增加的病灶會有 Tc-99m MDP 活性聚積隨之增加的現象，在此，我們介紹一位在全身骨骼掃描中發現因人工血管剛手術後的充血或發炎反應而導致活性攝取異常增加的案例。

影像報告：一名 70 歲女性患者於 2019 年 7 月被診斷出罹患左側腎盂輸尿管惡性腫瘤第四期，因患者主訴有骨頭疼痛的情形，故轉介至核醫科進行全身骨骼掃描。全身骨骼掃描結果發現其骨骼方面並無任何異常，但其前胸部右上側區域有一處非骨骼的小型線性放射活性聚積，加照舉肩的局部影像之後發現該處的放射活性聚積隨即消失，經詢問患者近期內有無相關受傷或開刀病史之後，得知該患者在進行全身骨骼掃描的前一日於該位置進行了植入人工血管手術，且本科同仁也確定並非經由人工血管注射放射性同位素，由此可知該處的放射活性聚積應是前一日的人工血管手術後導致的充血或發炎反應所形成。

結論：人工血管是經由皮下植入方式，將導管與靜脈血管相接，藉此傳輸系統，用來執行靜脈注射給藥。接受化學治療的患者大多會放置人工血管手術，以減少對人體組織的傷害，雖放射性同位素多由一般靜脈所注入，但不排除會有因患者靜脈不易注射而直接從人工血管注入的可能，如此一來極有可能會在人工血管管壁造成活性殘留，因此相關病史的詢問對於此次介紹的案例就相當重要，因可幫助對從人工血管注入放射性同位素的活性殘留或因近期人工血管手術後所的充血發炎反應產生活性聚積進一步加以鑑別診斷。

PC081

全身骨骼掃描加照 SPECT/CT 之效益

許幼青¹ 廖建國¹ 陳薇璇¹ 莊紫翎^{1,2} 王昱豐^{1,2}

¹ 佛教慈濟醫療財團法人大林慈濟醫院核子醫學科

² 慈濟學校財團法人慈濟大學醫學系

背景介紹：全身骨骼掃描產生出前位像和後位像，但有時在異常時很難區分真實的位置，執行 SPECT/CT 可正確定位和解釋病變並幫助區分良性和轉移性病變。但通常是否需要執行 SPECT/CT 的評估一般而言是由核子醫學科醫師來進行，往往醫師在做出這樣的決定時，大多是在忙碌其他臨床事宜，但若由核子醫學科的醫事放射師按照醫師提供的加照 SPECT/CT 之準則、並經過訓練後來判斷執行，可以減少等待醫師決定的時間，可以增加整體流程的效益。

影像報告：從別家醫院轉檢一名 53 歲女性，左側乳腺浸潤癌，於 2019 年 5 月 10 日執行改良型乳癌根治手術；右側乳頭狀瘤乳頭狀瘤，同天執行右部分乳房切除術。醫師安排全身骨骼掃描並常規接受單光子電腦斷層掃描檢查，於全身骨骼掃描影像中呈現右大轉子有活性攝取增加的情形，懷疑有轉移的現象，醫事放射師按照醫師提供的加照 SPECT/CT 之準則判斷，執行單光子電腦斷層掃描，在影像中卻呈現右大轉子附近的右臀中肌附著處有活性攝取增加，骨骼未發現其他潛在疾病的明確異常。加照 SPECT/CT 之準則判斷如表。

結論：全身骨骼掃描是一項快速且準確的檢查，其影像卻只有正位像和後位像的平面影像，需要進一步執行 SPECT/CT 才能得到立體的影像，但往往醫事放射師需要花費時間於等待核子醫學科醫師前來判斷是否需要執行 SPECT/CT。若醫事放射師遵照醫師提供的加照 SPECT/CT 之準則，可以減少患者及醫事放射師等待時間，同時可以提高檢查流程的效率。

網膜蛋糕

陳薇璇¹ 許幼青¹ 張秀瑛¹ 莊紫翎^{1,2} 王昱豐^{1,2}

¹ 慈濟醫療財團法人大林慈濟醫院核子醫學科

² 慈濟學校財團法人慈濟大學醫學系

背景介紹：卵巢癌發現都是以晚期居多，因此病人大多會接受手術治療以及術後化學治療。腹膜轉移癌 (Peritoneal Carcinomatosis, PC) 為非源自腹膜本身的癌症在腹膜內擴散，導致腹膜表面癌化，最常來自於腹腔內惡性腫瘤，如卵巢癌、大腸癌、胰臟癌等。網膜 (Omentum) 被侵蝕、消融凝成一團厚厚的網膜蛋糕 (Omental cake)。而高溫腹腔化療灌注術 (Hyperthermic Intraperitoneal Chemotherapy, HIPEC) 主要用於治療腹膜轉移癌，為目前治療腹膜轉移癌最有效的方法。

影像報告：一名 60 歲女性，G4P3A1，有糖尿病病史，患有卵巢癌，因腹水造成不適而入院，醫師安排全身骨骼掃描檢查，影像結果顯示雙側恥骨有骨破壞，腹腔有瀰漫性活性攝取，懷疑為腹膜轉移癌，進而執行單光子電腦斷層掃描 (SPECT/CT)，並且由影像發現為網膜蛋糕 (Omental cake)。後經電腦斷層結果亦能證實，另發現多處淋巴結轉移，而後病患接受 HIPEC，除了緩解症狀外，也希望能延長病患生命。

結論：全身骨骼掃描是一項可用來追蹤癌症是否有骨骼轉移的檢查，具有高敏感度及早期偵測骨骼病灶的能力，對於產生鈣化的軟組織也有活性攝取，再搭配上 SPECT/CT 輔助，就可以更加確定病灶位置，並且幫助鑑別診斷是否為惡性腹水或者是軟組織上的病灶，而網膜蛋糕則是因為轉移性鈣化而有活性攝取，總而言之，SPECT/CT 不僅能提供更多病灶的資訊，對於非骨骼的軟組織病灶也有相當好的診斷結果。

PC083

Use Dual Energy X-ray Absorptiometry to Examination Bone Mineral Density to Discovery Lumbar Spine Image Abdominal Aortic Calcification – A Case Report

Pao-Liang Chen^{1,2}, Tzyy-Ling Chuang^{1,3}, Shih-Chin Chou¹, Yuh-Feng Wang^{1,3}

¹Department of Nuclear Medicine, Dalin Tzu Chi Hospital, Buddhist Tzu Chi Medical Foundation, Chiayi, Taiwan

²Department of Medical Research, Dalin Tzu Chi Hospital, Buddhist Tzu Chi Medical Foundation, Chiayi, Taiwan

³School of Medicine, Tzu Chi University, Hualien, Taiwan

Introduction: Vascular and skeletal diseases are both chronic age-related disease that share many common dietary and lifestyle risk factors and cause considerable morbidity and mortality. Atherosclerotic lesions in the abdominal aorta (AA) generally begin around the major vessel bifurcations and branching arteries such as the inferior mesenteric artery (IMA) and the lumbar arteries that supply blood and nutrients to the lumbar spine (L-spine). Occlusion of these vessels may causes ischaemia in the L-spine and may result in intervertebral disc degeneration and asymptomatic vertebral fractures.

Case report: A 82-year-old female, weighted 54 kg, and height 143 cm, main low back pain to our hospital emergency department patient chief complaint unable to stand, pain score is 7 (between moderate to worst possible pain), oxygen saturation concentration 99%, her heart rate (HR) is 73 beats per minute (bpm), systolic blood pressure (SBP) and diastolic blood pressure (DBP) is 174 mmHg and 85 mmHg and body temperature is 36.2°C. Low back pain without limbs numbness and weakness. Patient she had Lumbar spine 2 to 4 compression fracture, no surgery. X-ray show mild kyphosis, degenerative changes with spur formation and narrowed intervertebral disc spaces. Other physical evaluation no neurologic sign, conscious clear. Head, eyes, ears, nose, and throat (HEENT) is supple, chest nontender, symmetric and abdomen is soft. Straight leg raising test (SLRT) > 70. Final use morphine 10mg/1ml/amp intramuscular (injection) (I.M.) for pain control after to orthopedics outpatient department (OPD) follow up.

The first return visit orthopedics OPD by physician examination, for bone mineral density (BMD) to evaluation bone quantity by dual-energy X-ray absorptiometry (DXA). The BMD report show according to the WHO criteria and normal reference curves for BMD study of the same area, the bone mineral condition of this patient is osteoporosis. Final for drug treatment osteoporosis and pain control (e.g. Tramacet (TraMADo/Acetaminophen), Dimethicone (Gaslan), Estazolam (Eurodin), Denosumab (Prolia)). In addition, in lumbar spine BMD image serendipity abdominal aortic calcification.

Conclusion: Our result suggest AAC will affect BMD and diagnostic result in clinically. In future AAC patients of the lumbar spine region unable to interpretation.

PC084

Imaging Evident Striatal Loss of Dopamine Transporter Activity with Aging

Wen-Sheng Huang¹, Cheng-Yi Cheng², Meei-Shyuan Lee³,
Jiann-Chyun Lin⁴, Younn-Hsiau Chian⁵, Ying-Kai Fu⁶

¹*Departments of Nuclear Medicine, Taipei Veterans General Hospital, Taipei, Taiwan*

²*Departments of Nuclear Medicine, Tri-Service General Hospital, Taipei, Taiwan*

³*School of Public Health, National Defense Medical Center*

⁴*Departments of Neurology and*

⁵*Neurosurgery, Tri-Service General Hospital, Taipei, Taiwan*

⁶*Institute of Nuclear Energy Research, Luntan, Taiwan*

Purpose: Loss of dopamine transporters (DAT) in the presynaptic terminal membrane as part of normal aging has been demonstrated in post-mortem studies. This study was undertaken to observe the changes of striatal DAT uptake in healthy adults in our community using Tc-99m TRODAT-1, a radioligand for DAT single photon emission tomography (SPECT).

Methods: Fifty normal subjects (mean age \pm SD, 63 ± 12 y; age range, 36 – 80 y) were studied. Tc-99m TRODAT-1 was prepared from a lyophilized kit. Brain DAT SPECT imaging was acquired between 165-195 min post-injection (740 MBq), using a dual-head camera equipped with fan-beam collimators (Helix SPX; GE). Specific uptake in striatum (ST), putamen (PU) and caudate nucleus (CA) were calculated from reconstructed transaxial slices at the level of maximal striatal activity. Occipital cortices were used as reference areas.

Results: The decrease of specific uptake in the ST was significantly correlated with increasing age ($r = -0.6$; $p < 0.001$), declining by approximately 23% over the age studied, or 5.9% per decade. There was also a negative correlation with age for PU uptake ($r = -0.64$; $p < 0.001$) but only weak relationship for CA uptake ($r = -0.29$; $p = 0.04$). Greater decrease of uptake in PU than in CA with advancing age was found (7% vs. 3.8% per decade).

Conclusions: The decline of DAT binding in ST and its sub-regions with increasing age was in line with previous image observations and post-mortem data, implying that age-related degeneration of DAT in the ST and its sub-regions might be uneven involvement during aging process.

PC085

A Compromising use of PET/CT and PET/MR in Practice

Yu Kuo^{1,2}, Chia-Jung Chang², Chien-Ying Lee², Bang-Hung Yang²,
Chien-Hsin Ting², Ko-Han Lin², Wen-Sheng Huang²

¹Departments of Radiology, Taipei Veterans General Hospital, Taipei, Taiwan

²Departments of Nuclear Medicine, Taipei Veterans General Hospital, Taipei, Taiwan

Both PET/CT and PET/MR are clinically used facilities, while PET/CT is familiar to clinicians in practice, PET/MR is one of the most attractive field in medical research and applications which has reflected by growing research publications with years as shown by number of publication per-averaged month).

Based on different institutional circumstances and patient requirements, both PET/CT and PET/MR own its advantages and disadvantages in terms of patient centered medical cares. It is believed that PET/CT and PET/MR should be compromised rather than confronted in real clinical scenarios.

Herein, we presented two cases illustrating optimization of imaging uses in practice.

Case 1. A 54 years-old female who experiences papillary thyroid cancer (PTC) 10 years ago, the follow-up sonography showed an enlarged lymph node with cytologically proved metastatic PTC that was very close to the right common carotid artery. Surgical removal was suggested first. However, it is difficult to determine if there is invasion to the wall of common carotid artery and its metastatic status and biological behavior solely on ultrasonography. F-18 FDG PET with CT and MR were performed on the same day. It revealed a solitary FDG positive in the right neck, level III region. Notably, the PET/MR showed preserved fat plane between the lesion and adjacent carotid sheath on T1-weighted image, indicating no attachment or invasion of the lesion to common carotid artery. This finding was hard to clarify on PET/CT images. The case revealed that PET/MR might be more useful in charactering soft tissue features than PET/CT.

Case 2. A 56 years-old female who was told to have a pulmonary nodule measuring about 2 cm in the right upper lobe. CT guided biopsy was not performed due to personal considerations. Under the impression of malignancy, she was then referred for further F-18 FDG PET examination and staging. The PET/CT showed high uptake foci in the lesion, with clear morphological patterns such as irregular and spiculated margin, presence of air-bronchogram, sign of pleural tractions. However, these structural details cannot be appreciated on PET/MR images.

PC086

Simultaneous Time-of-Flight PET/MR Identifies the Hepatic ^{90}Y -resin Distribution After Radioembolization

Chien-Hsin Ting¹, Ko-Han Lin¹, Chuang-Hsin Chiu²,
Rheun-Chuan Lee³, Wen-Sheng Huang¹

¹*Departments of Nuclear Medicine, Taipei Veterans General Hospital, Taipei, Taiwan*

²*Departments of Nuclear Medicine, Tri-service General Hospital, Taipei, Taiwan*

³*Departments of Radiology, Taipei Veterans General Hospital, Taipei, Taiwan*

A female patient with multiple hepatic metastases from uterus cervical cancer received ^{90}Y radioembolization. The simultaneous time-of-flight (TOF) PET/MR clearly identified the untreated tumor parts on the post-therapeutic ^{90}Y internal pair-production imaging. After another boosted ^{90}Y injection, the metastatic hepatic tumors were well-covered. The follow-up PET/MR revealed tumor shrinkage. The one-stop-shop TOF PET/MR provided useful follow up information in patients receiving ^{90}Y radioembolization.

Our case illustrated the clinical usefulness of simultaneous PET/MR with time-of-flight (TOF) in the evaluation of hepatic distribution of microspheres and the correlation with target tumor lesions that might be not achievable from a traditional SPECT/CT or PET/CT. The limitation of a SPECT/CT Bremsstrahlung scan comes from low resolution, high scatter caused by wide-energy-window acquisition, and lack of tumor boundary of CT. The small abundance of 511 KeV energy emitted from ^{90}Y IPP could be detected superiorly with TOF-PET/CT than the non-TOF PET/CT and SPECT/CT. However, the IPP TOF-PET/CT can only provide well functional but suboptimal anatomic information.

With the state-of-the-art simultaneous PET/MR with TOF function, the ^{90}Y IPP signals could be obtained within an acceptable time period (20 minutes). meanwhile, the simultaneous MR could provide various anatomic and diffusion sequences, allowing more detailed images for accessing the efficacy and response after ^{90}Y radioembolization. In conclusion, the new model of simultaneous PET/MR equipped with TOF function is feasible for ^{90}Y radioembolization in clinical use, including post-treatment strategy and response evaluation.

PC087

Comparison of Clinical and Imaging Staging in Parkinson's Disease

Wen-Sheng Huang¹, Yo-Tsen Liu², Chih-Hao Chen¹,
Bang-Hung Yang¹, Din-E Shan²

¹*Departments of Nuclear Medicine, Taipei Veterans General Hospital, Taipei, Taiwan*

²*Departments of Neurology, Taipei Veterans General Hospital, Taipei, Taiwan*

Purpose: ^{99m}Tc-TRODAT-1 SPECT (TRODAT) has been used to evaluate striatal dopamine transporter (DAT) activity in practice. The study sought to observe consistency of disease staging between TRODAT visual inspection and classical clinical scoring in patients with Parkinson's Disease (PD).

Methods: From July 2016 to September 2019, forty-five patients with clinically confirmed PD referred for TRODAT scanning. The unified Parkinson's rating scale, part 5 (UPDRS-5), i.e. the modified Hoehn-Yahr scale was applied to rate patient severity by experienced neurologists and the TRODAT was performed within 1 yr. interval. Imaging patterns (EANMMI 2004; 31: 155) were interpreted by experienced NM physicians using visual inspection. The resulting scales were thus compared each other. The imaging protocol routinely utilized 45 min scan time at 4 h post 20 mCi TRODAT injection using a dual-head camera equipped with ultra-high resolution fan-beam collimators. Data were reconstructed using the filtered back-projection method with both Metz and Butterworth filters and the modified-Chang method for attenuation correction.

Results: Of the 45 patients, 12 were rated as the same stage, 12 with 0.5-point difference, 17 with 1 point, 2 each with 1.5 and 2 points difference. No case with different rating greater than 2 points. Those with 2- point difference (n = 2, Clinical vs. imaging staging = 1 vs. 3 and 2 vs. 4) were aged 82 and 83 years old.

Conclusions: Visual inspection of TRODAT SPECT might provide a useful reference for disease severity of PD patients. Aging might be a possible source for inconsistent rating between clinical and imaging criteria. More data to clarify this are warrant.

PC088

Comparison of ^{18}F -BPA and ^{18}F -FDG Activity in Head and Neck Cancers Using a Novel PET/MR

Chien-Yin Lee, Ling-Wei Wang, Bang Hong Yang,
Ko-Han Lin, Yi-Wei Chen, Wen-Sheng Huang*

Departments of Nuclear Medicine and Radiation Oncology, Taipei Veterans General Hospital, Taipei, Taiwan

Background: 4-borono-2- ^{18}F -fluoro-phenylalanine (^{18}F -BPA) PETMR and ^{10}B -BPA boron neutron capture therapy (BNCT) are merging theranostics. However, the ^{18}F -BPA production is hard to fulfil clinical demand. We observed if ^{18}F -FDG was able to be a screening means for further ^{18}F -BPA examination using a novel PET/MR.

Material and methods: Ten patients with head and neck cancers were recruited.

All underwent ^{18}F -BPA and ^{18}F -FDG PET/MR in 2 wks. SUVmean and tumor-to-normal ratio (TNR) of both radioligands were measured using a time-of-fly PET/MR 1 h after injection of the radioligands. The tumor uptake expressed as SUVmean in a 3D auto-segmented volume of interest with a 50% threshold of the highest tumor uptake. TNRs of ^{18}F -BPA and ^{18}F -FDG were calculated as tumor SUVmean divided by that of contralateral or adjacent normal soft tissue. Both TNR and SUVmean SUV data were compared using paired *t*-test and were correlated using Pearson's correlation. $p < 0.05$ served as statistically significant.

Results: The averaged SUVmean and TNR for ^{18}F -BPA vs. ^{18}F -FDG were 4.32 ± 2.40 vs. 7.35 ± 2.39 and 3.85 ± 2.62 vs. 6.39 ± 2.93 , $p < 0.05$ respectively; Significantly positive correlation of SUVmean and TNR between the two radioligands were found ($r^2 = 0.48$ and 0.56 , $p < 0.05$ respectively; ^{18}F -BPA SUVmean = $0.69054 \times ^{18}\text{F}$ -FDG SUVmean - 0.753 , while ^{18}F -BPA TNR = $0.6713 \times ^{18}\text{F}$ -FDG TNR - 0.436). A ^{18}F -FDG TNR of 4.38 was equivalent to 2.5 of ^{18}F -BPA SUVmean.

Conclusions: ^{18}F -FDG PET/MR might serve as a clue to select candidate for ^{18}F -BPA PETMR, however the false positive of ^{18}F -FDG due to inflammation, a contraindication for BNCT remains to be considered.

PC089

Potential Errors in Semi-quantitative Analysis of ^{99m}Tc -TRODAT-1 SPECT

Chih-Hao Chen^{1,2}, Ling-Shih Chen¹, Cheng-Pei Chang¹,
Bang-Hung Yang^{1,2}, Wen-Sheng Huang¹

¹Department of Nuclear Medicine, Taipei Veterans General Hospital, Taipei, Taiwan

²Department of Biomedical Imaging and Radiological Sciences, National Yang-Ming University

Introduction: Parkinson's disease (PD) has been one of the most common diseases in the elderly since the late 20th century. In clinical practice, diagnosis of PD mainly relies on clinical criteria yet problems remain, especially in its early stage. ^{99m}Tc -TRODAT-1, a radioligand that selectively binds to dopamine transporter has been applied in clinical evaluation of PD using both visual and semi-quantitative analysis. The "TRODAT Tool" can provide normalized quantitative data to assist diagnosis of PD and its progression. However, an improper operation will result in an unexpected error diagnosis. In this study, we discuss the improper manipulations that may lead to incorrect diagnosis.

Material and Methods: (1) A striatal phantom with 370 MBq ^{99m}Tc inside was scanned using routine TRODAT-1 SPECT/CT protocol to demonstrate the effects of various tilt angle mismatches between the SPECT image and the ROI template. (2) Approximately 400 retrospective TRODAT-1 clinical cases were collected using Metz and Butterworth filter reconstructions to demonstrate the effects of different filter reconstructions on semi-quantitative analysis.

Results: (1) The TRODAT-1 SPECT misalignment (≥ 5 degrees) with the ROI template may interfere the asymmetrical index measurements of idiopathic Parkinson's disease patients. (2) The TRODAT-1 SPECT with different filter reconstructions will cause different specific uptake ratio (SUR) in caudate, putamen and striatum, but the asymmetry trend of these three is similar.

Conclusions: The factors, which will affect the semi-quantitative results of ^{99m}Tc -TRODAT-1 SPECT, includes erroneous head position and misalignment and different reconstruction parameters. Carefully checking imaging parameters will make better images.

PC090

^{18}F -L-boronphenylalanine (^{18}F FBPA) for PET Imaging Analysis of Recurrent Head and Neck Carcinoma by Bayesian Penalised Likelihood Reconstruction (Q. Clear)

Geng-Ying Li, Ling-Shih Chen, Bang-Hung Yang, Wen-Sheng Huang

Department of Nuclear Medicine, Taipei Veterans General Hospital, Taiwan

Introduction: A role for fluoride-18-labeled L-boronophenylalanine (^{18}F FBPA) is an amino acid PET radiotracer approved for recurrent head and neck carcinoma patients and evaluation of boron neutron capture therapy (BNCT) in clinical. We investigated the use of Bayesian penalised likelihood (BPL) reconstruction for L- ^{18}F FBPA in GE SIGNATM PET/MR.

Methods: L- ^{18}F FBPA images were reconstructed using ordered subset expectation maximization (OSEM) with time-of-flight (TOF) modeling. All images were reconstructed with BPL using β -values 100、300、500、1000、2000, respectively. We retrospectively analyzed data accumulation of ^{18}F FBPA as the ratio of maximum and average radioactivity counts to that of normal tissue (Tmax/N and Tmean/N ratios, respectively) from 10 patients.

Results: Comparing the image data of ^{18}F FBPA BPL to OSEM + TOF, there were increase in Tmean/N ratio of BPL. As the β -value decrease, the imaging showed that the region of interesting was close to the actual size. The ratio of BPL to OSEM + TOF raised approximately 5-10%, and it raised up to 10% while β -value is 300.

Conclusions: The Tmean/N ratio of ^{18}F FBPA-PET/MR imaging reconstructed by BPL can be observed increments.

PC091

核子醫學檢查住院病人各科別尿布分布之研究 —以南部某醫院全身骨骼掃描檢查病人為例

張虹麗 鄭揚霖 陳懿貞 梁育雅 陳興隆 張南雄 李將瑄 顏玉安 卓世傑

奇美醫療財團法人奇美醫院核子醫學科

背景介紹：由於社會之要求並因應行政院原子能委員會之宣導，核子醫學檢查住院病人之尿布收集，現已成為台灣各醫院核子醫學科的日常業務之一。因此，如能掌握各科別尿布之產出分布，即能針對主要產出科別病房之工作人員，主動與事先加強收集尿布之衛教指導，以避免遺漏。另一方面，也可以瞭解醫院內放射性廢棄物之分布情形，以做為全院公共安全與輻射風險管制的參考。不過，現在台灣對於各科別病人產生尿布分布情形之研究，卻極為缺乏。本研究即是以核子醫學檢查經常施行的全身骨骼掃描檢查為例，針對南部某醫院住院病人各科別尿布分布統計之研究。

方法：

1. 收集南部某醫院 106 年 3 月至 108 年 8 月止，共 100 人次，所有接受子醫學全身骨骼掃描檢查住院病人之尿布資料。
2. 將上述資料，分別將各病人之開單科別，尿布包數，尿布總重，分別歸類整理。
3. 先分別統計，內、外、婦、兒科病房產出之尿布總重量與包數及佔全體之比例，再就各科之次專科各自統計其尿布總重量與包數和佔全科之比例。

結果：

1. 100 個病人中，內科系佔 83 人，外科系 16 人，婦科系 1 人，兒科系則沒有病人尿布。全體總重量之比例，內、外、婦科系各別為 83.5、16.1 與 0.4%，全體包數方面，內、外、婦科系之比例，則為 84.7、14.7 與 0.6%。
2. 內科系部分，佔比例最高的為血液腫瘤科，其人次、總重與包數比例，分別為 42.2、44.7、39.9%，再來依序是胸腔內科的 27.7、29.2、29.7%，一般內科 15.7、15.8、15.9%，腎臟內科之 6.0、5.8、5.8% 與其他內科的 8.4、4.5、8.7%。
3. 外科系部分，最多的是一般外科，該科的人次、總重和包數比例，是 31.3、26.6 以及 29.2%，其次則是骨科 25.0、24.5、25.0%，泌尿外科的 18.8、28.4、25.0%，胸腔外科的 12.5、1.8、8.3%，與其他外科之 12.5、18.7、12.5%。

結論：依南部某醫院，接受子醫學全身骨骼掃描檢查住院病人之尿布資料顯示。1. 尿布產出主要集中在內科系，佔了全體尿布重量的 83.5，全體包數的 84.7%。2. 內科系內則以血液腫瘤科為產生尿布的最主要科別，佔了內科系重量的 44.7%，包數的 39.9%。3. 血液腫瘤科、胸腔內科、一般內科、腎臟內科、一般外科、泌尿外科等 6 科即涵蓋了全體人次的 84.0%，重量的 88.5% 與包數之 85.3%。因此有關衛教的宣導與場所之輻射安全設計考量應以內科系為主，尤其是血液腫瘤科之病房。但是有關衛教的宣導與場所之輻射安全設計考量，如能再擴展至、胸腔內科、一般內科、腎臟內科、一般外科、泌尿外科等科別，則必能更有效的達成管制與增進安全的目標。

PC092

Creatinine 指數對住院病人尿布重量影響之研究 —以南部某醫院全身骨骼掃描檢查病人為例

杜珠理 陳興隆 鄭揚霖 張南雄 陳懿貞 梁育雅 李將瑄 顏玉安 卓世傑

奇美醫療財團法人奇美醫院核子醫學科

背景介紹：為促進輻射安全，在主管機關的宣導與鼓勵下，台灣各醫院亦將接受核子醫學檢查住院病人之尿布收集，列為需執行的工作之一。因此，如能對尿布產生之各種來源加強掌握，將可更妥適的規劃尿布收集的途徑，並可針對重點來源別進行較為仔細的衛教與監測，從而使尿布的收集更為完善。而 creatinine 指數則是評估腎功能的有效指標之一，當腎臟功能變差，creatinine 指數也會異常。所以如病人有使用尿布的情形，其 creatinine 指數是否正常，將會影響排尿之多寡，進而導致使用後之尿布重量產生變化。本研究即以住院病人之 creatinine 指數做為探究其對尿布重量影響之研究。

方法：

1. 收集南部某醫院 106 年 3 月至 108 年 8 月止，共 100 人次，所有接受核子醫學全身骨骼掃描檢查住院病人之尿布資料。
2. 將上述資料，先依男、女分開，然後將男、女組病人，依照 Creatinine 指數正常值之內與正常值之外，再各分為兩組，即得到男異常、男正常與女異常、女正常共四組資料，分別歸類整理。
3. 將四組資料各病人之尿布總重、平均重量、尿布包數及單包平均重量，分別加總統計，再統計各組資料之尿布總重、平均重量、尿布包數及單包平均重量，佔全體之比例。

結果：

1. 100 人中男性為 56 位，女性為 44 位，其中男異常組有 34 人、男正常組 22 人，女異常組為 15 人、女正常組則為 29 人。
2. 尿布總重量部份，各組重量 %/ 人數 % 之比值，最高的為女性異常組的 1.4、其次依序為男異常組 1.06、女正常的 0.9 與男正常組的 0.77。
3. 尿布包數部份，各組包數 %/ 人數 % 之比值，最高的仍為女性異常組的 1.07、再來則為女正常組的 1.07，男正常組 1.05 及男異常組 1.03。
4. 平均重量與單包重量部份，異常組顯著高於正常組，男、女異常與男、女正常的數據，平均重量與單包重量分別是，1838、2383、1309、1543 與 1054、1391、809、942 g。
5. 男性異常病人較正常病人之平均重量與單包重量分別重 529、245 g，女性異常之病人其平均重量與單包重量則更高於正常病人 840 與 449 g。

結論：依本研究之結果顯示 Creatinine 指數對住院病人尿布重量之影響主要有以下 3 點：1. creatinine 指數異常的男、女性病人尿布平均重量與單包重量均較正常的病人，顯著為高。2. 男性異常病人較正常病人之平均重量與單包重量分別重 529、245 g，女性異常之病人其平均重量與單包重量更分別高於正常病人 840 與 449 g。2. 尿布總重量 %/ 人數 % 之比值與尿布包數 %/ 人數 % 之比值部份，女性

均高於男性。因此，接受核子醫學檢查之住院病人，如有 creatinine 指數異常的情形，則尿布的重量即可能較指數正常之病人為重，尤其是女性之病人。所以針對女性病人，特別是 creatinine 指數異常的病人，有關衛教的工作應特別加強。

PC093

Detection of Recurrent Cervical Cancer with Serum SCC-Ag and FDG PET/CT

Nan-Jing Peng^{1,2}, Chin Hu¹, Yu-Li Chiu¹, Chang-Ching Yu¹, An-Jen Chiang³

¹Department of Nuclear Medicine, Kaohsiung Veterans General Hospital, Kaohsiung, Taiwan

²National Yang-Ming University, School of Medicine, Taipei, Taiwan

³Department of Gynecology and Obstetrics, Kaohsiung Veterans General Hospital, Kaohsiung, Taiwan

Introduction: Serum squamous-cell carcinoma antigen (SCC-Ag) was associated with tumor stage and nodal involvement in squamous-cell carcinoma (SqCC) of uterine cervix. The aim of this study is to evaluate the usefulness of serum SCC-Ag and 2-[¹⁸F]fluoro-2-deoxy-D-glucose-positron emission tomography/computed tomography (FDG-PET/CT) in the detection of recurrent cervical cancer and patient survival.

Methods: FDG-PET/CT was performed on patients with elevated serum SCC-Ag levels > 1.5 ng/mL (Group 1) or suspicious recurrences without rise in serum SCC-Ag levels (Group 2). The results were analyzed on the basis of histological data, disease progression, and/or clinical follow-up. Recurrence was defined as evidence of recurrent lesions within 6 months of the FDG-PET/CT scan. The outcome was calculated based on medical records.

Results: Eighty-eight consecutive cervical SqCC cancer patients with suspected recurrence (62 in Group 1 and 26 in Group 2) were enrolled. Recurrences were proven in 55 [77.4% (48/62) in Group 1 vs. 26.9% (7/26) in Group 2, $p < 0.001$]. The overall sensitivity, specificity, and accuracy of FDG-PET/CT were 98.2%, 90.9%, and 95.5%, respectively, and were 97.9%, 92.9%, and 96.8% in Group 1 and 100% and 89.5% and 92.3% in Group 2, respectively. Surgical resections were performed in 16 patients. After a follow-up, 40.3% (25/62) of Group 1 patients and 88.5% (23/26) of Group 2 patients was survival at the end of study ($p < 0.001$). The survival in patients with surgical resection of recurrent tumors was higher than those without [62.5% (10/16) vs. 17.9% (7/39), $p = 0.001$].

Conclusions: Serum SCC-Ag could predict tumor recurrence and survival in patients with SqCC cervical cancer. The surgical resection of limited recurrent disease, as determined by FDG-PET/CT, might improve the survival of cervical cancer patients.

PC094

手術室施行同位素前哨淋巴結 探索輻射劑量偵測分析

鄧仁淡¹ 劉仁賢^{1,2,3}

¹ 振興醫療財團法人振興醫院核子醫學部

² 國立陽明大學生物醫學影像暨放射科學系

³ 台北榮民總醫院核子醫學部

背景介紹：前哨淋巴結同位素造影及手術中以輻射偵檢探針偵測聚積同位素的淋巴結，是探索前哨淋巴結的常規方法之一。檢查時，於患側乳房乳暈皮內注射 0.2 毫升含 0.5 毫居里 (mCi) 同位素藥劑 Tc-99m phytate 的生理食鹽水，旋即於 15 分鐘完成前哨淋巴結核醫造影。前哨淋巴結同位素造影完成後，病患轉送至手術室進行前哨淋巴結探索手術。本文探討在手術過程中工作人員的輻射曝露劑量是否符合輻射安全標準。

方法：本次檢查使用 0.5 mCi 之放射性同位素銻製劑 (Tc-99m Phytate)。注射之同位素藥物局限於乳房注射處及附近之淋巴結，不會經血液循環遍及全身。使用 Thermo SCIENTIFIC 型號：RADEYE PRD-ER 輻射偵檢器，依各醫護人員 (外科醫師、刷手護理師、麻醉護理師及手術助理) 工作位置現場實測。手術時間約 60-90 分鐘，本次量測採最長時間 90 分鐘計。探索手術每週約 1-4 台，每年以 100 台計。

結果及結論：參與同位素前哨淋巴結探索手術工作人員的年輻射曝露量以手術時間 60 分鐘估算，均不會超過一般人 (非輻射工作人員) 年劑量限度。工作人員可以安心執行探索手術。如手術時間以 90 分鐘估算，除手術醫師年輻射曝露 (1.26 毫西弗) 略高於一般人員 1 毫西弗的年劑量限度外，其他工作人員的年輻射曝露亦未超過 1 毫西弗。如手術時間大多數達 90 分鐘，則建議手術醫師應視同輻射工作人員，接受原能會認可之 18 小時以上輻射防護訓練，考試及格，取得結業證書。佩帶人員劑量佩章，每年接受輻射防護教育 3 小時，每年定期作輻射工作人員健康檢查。本院目前 Tc-99m phytate 注射劑量調整為 0.2 mCi，並建議：如非必要，探索手術請安排在核醫檢查 4 小時以後施行，亦可降低約一半的輻射曝露劑量。懷孕的女性工作人員，參與探索手術，因輻射曝露劑量未超過一般人之曝露劑量限值，仍可放心正常工作。為謹慎起見，參與手術時，建議佩帶人員劑量佩章。監控輻射曝露量，一旦發現有超過一般人之年劑量限度之虞，立即由輻射防護管理委員會評估是否可繼續參與手術並給與健康照護建議。

PC095

SPECT/CT – 異常軟組織與骨骼鑑別之利器

楊承領¹ 許幼青¹ 莊紫翎^{1,2} 王昱豐^{1,2}

¹ 佛教慈濟醫療財團法人大林慈濟醫院核子醫學科

² 慈濟學校財團法人慈濟大學醫學系

背景介紹：全身骨骼掃描是目前常見的核子醫學檢查項目之一，其平面影像在正常影像上會出現骨骼系統和泌尿系統。通常骨骼上出現較高之攝取或是骨骼系統以外的異常攝取，就會讓人產生病灶轉移之疑慮，若是沒有加入其他的檢查項目，將導致醫師無法更精準的做出判斷。

病例報告：一位 65 歲患有左側乳癌 (pT1cN1a, stage IIA) 之女性患者 (病人 A)，與一名 80 歲患有肺腺癌 (cT1cN3M1c, stage IVB) 之女性患者 (病人 B)，分別於本院進行全身骨骼掃描檢查 (^{99m}Tc-MDP, Dose: 20-28 mCi) 時，結果於病人 A 右側肩胛骨與病人 B 右後側肋骨皆發現異常線性活性攝取狀況，爲了對該病灶進行詳細的了解，故執行 SPECT/CT 檢查。檢查結果發現這兩例異常攝取皆來至骨骼之外，經後續的電腦斷層追蹤後，發現病人 A 右側肩胛骨之攝取爲鈣化腫塊，而病人 B 右後側肋骨之攝取則爲腎臟鈣化。

結論：全身骨骼掃描檢查一般會出現骨骼與泌尿系統的影像，而這兩例患者的影像起初皆讓人以爲是骨骼上之異常攝取，實則爲軟組織之鈣化，若單憑平面前後像的影像，便無法清楚判斷出異常軟組織與骨骼重疊處之狀況，然而在 SPECT/CT 與其他檢驗單位的協助之下，成功地克服種種的問題，並且清楚的顯示出這兩例異常攝取皆非來自於骨骼，由此我們便得知若是在全身骨骼檢查的平面影像上出現疑慮時，再進一步進行 SPECT/CT 或是其他角度之影像有其絕對的必要性。

PC096

An Application Error Case for Semi-quantitative Analysis of ^{99m}Tc -TRODAT-1 SPECT

Chih-Hao Chen, Jing-Long Hsu, Lee-Shing Chu,
Bang-Hung Yang, Wen-Sheng Huang

Department of Nuclear Medicine, Taipei Veterans General Hospital, Taipei, Taiwan

Introduction: Dopamine transporter imaging utilizing ^{99m}Tc -TRODAT-1 SPECT provides a convenient tool to detect the degenerative function of pre-synaptic dopaminergic neurons which cause by the pathology of Parkinson's Disease (PD). The TRODAT Tool is an automatic semi-quantitative analytical tool for ^{99m}Tc -TRODAT-1 SPECT. It is based on MATLAB SPM software conjugated MRI-based template to normalize all brain DICOM file from clinical scanning instruments. The specific uptake ratio (SUR) and the asymmetric index (ASI) of the striatum and its sub-region, i.e. the caudate and putamen nuclei were calculated to obtain high accurate and reproducible data to assist clinical availability of movement disorders including PD.

Case Presentation: A 38-year-old female visited our hospital in July 2019. Her clinical manifestations showed progressive bilateral arms and neck dystonia. Under the impression of Parkinsonism, cause unknown, she was referred for ^{99m}Tc -TRODAT-1 SPECT. The SPECT was performed 4 hours after intravenous administration of 740 MBq ^{99m}Tc -TRODAT-1 using a SIEMENS Symbia-E SPECT scanner. The brain image was routinely preprocessed, such as reconstruction, attenuation correction, and reorientation, prior to TRODAT Tool semi-quantitative analysis. The initial visual results showed a decreased uptake on the left putamen but not unusual uptake on the right putamen and bilateral caudate nuclei. However, the TRODAT Tool analyses showed almost equal SUR over bilateral striatum and its sub-regions which appeared discordant with visual inspection. After backtracking imaging procedures, the patient's head was found to be tilted forward on the sagittal view, resulting in a false semi-quantitative SUR report. Therefore, after re-adjusting the head image orientation, the semi-quantitative result showed Rt. Caudate = 1.90, Lt. Caudate = 2.06; Rt. Putamen = 1.78, Lt. Putamen = 1.62; Rt. Striatum = 1.76 and Lt. Striatum = 1.71; The ASI for caudate, putamen and striatum were 8.10%, 9.57% and = 2.69%, respectively which were consistent with those of visual inspection.

Discussion: Generally, coronal azimuth error and axial elevation error are easily found in brain SPECT images. However, sagittal roll errors are often ignored or incorrectly adjusted. In this case study, the incorrectly reorientation adjustment (sagittal roll error) in preprocessing of the brain SPECT image is the main cause of errors in semi-quantitative analysis. Although automated semi-quantitative analysis can provide quantitative data that is intuitive and helpful for diagnosis. But proper image preprocessing is essential. Therefore, in clinical practice, we recommend that image pre-processing parameters should be carefully examined and that the original visual and semi-quantitative results must be consistent to ensure a better clinical diagnosis.

PC097

Evaluation of Lung Deposition of Tc-99m DTPA Aerosol Delivered by a Novel Vibrating Mesh Nebulizer in Healthy Subjects

Chih-Yung Chang^{1,2}, Bang-Hung Yang^{1,2}, Wen-Yi Chang¹,
Rong-Hong Jhou¹, Yu-Yeh Ko¹, Chien-Chih Ke³, Jing-Long Hsu¹,
Wen-Sheng Huang^{1,2}, Ren-Shyan Liu^{2,4}

¹Department of Nuclear Medicine, Taipei Veterans General Hospital, Taipei

²Department of Biomedical Imaging and Radiological Sciences, National Yang-Ming University, Taipei

³Department of Medical Imaging and Radiological Sciences, Kaohsiung Medical University

⁴Department of Nuclear Medicine, Cheng-Hsin General Hospital, Taipei

Introduction: This study aimed to evaluate the performance of a novel vibrating mesh-type nebulizer for the intrapulmonary delivery of radioaerosols in healthy subjects.

Methods: Six healthy subjects (mean age of 28.7 ± 6.2 y) inhaled 2 mL of Tc-99m diethylenetriaminepenta-acetic acid (DTPA) and normal saline solution (20 mCi) via vibrating mesh nebulizer (DK010, DELBio, Taipei, Taiwan). The nebulizer's mass median aerodynamic diameter (MMAD) is between 2.3 μm and 5.0 μm (3.47 ± 0.37 μm) and the nebulization rate is greater than 0.2 ml/min. Scintigraphy was performed to count radioaerosols in the regions of interest to determine the total and regional lung deposition and extrathoracic airway deposition of aerosols, penetration of aerosols, and radioactivity count balance.

Results: The total lung deposition of aerosols was $21.2 \pm 5.2\%$ (% ex-valve dose), $27.4 \pm 8.0\%$ (% ex-device dose) and $13.8 \pm 4.1\%$ (% initial dose) in nebulizer. The extrathoracic airway deposition was $4.8 \pm 1.1\%$. The radioactivity count balance was $5.4 \pm 3.0\%$. The ratio of outer vs inner lung deposition (O/I ratio, or penetration index) was 1.89 ± 0.55 .

Conclusions: The delivery efficiency of DELBio DK010 vibrating mesh-type nebulizer is comparable with the jet-type nebulizer. The penetration of aerosols to the peripheral lung is better achieved by the DELBio DK010 nebulizer than the commercialized jet-type and vibrating mesh-type nebulizer. The DELBio DK010 nebulizer is also feasible for radionuclide lung ventilation scintigraphy.

PC098

Comprehensive PET/MR and PET/CT System for Better Health Care in TVGH

Wen-Sheng Huang, Wan-Yuo Guo, Bang-Hung Yang,
Ko-Han Lin, Chih-Yung Chang, Tun-Wei Hsu

¹*Departments of Nuclear Medicine and Radiology, Taipei Veterans General Hospital, Taipei, Taiwan*

Background: Positron emission tomography (PET) integrated with CT or MR are clinical tools for molecular imaging although the use of PET/MR is exploring in practice. The running expense, professionals, relatively complicated operation techniques and imaging time-line further make it hesitate to be purchased for health care. We reported status of a comprehensive PET/MR and PET/CT system in a governmental hospital.

Material and methods: The running expense and professionals were analysed (using Hospital and departmental data) and dispatched by Radiological and Nuclear Medicine (NM) departments, respectively. The operating techniques (sequences) and imaging time-line (patient arrangement) were compromised based on radiopharmaceutical availability and patient centered considerations. Both clinical and research applications are targets of the imaging system.

Results: Finance appeared to be supported with daily 3 PET/MR (on regular working hrs) and 15 MR imaging (including off-hrs) based on the current health care system. It also shortened MR waiting list of skeletal and abdomen sections about 1 wk. For PET, NM staff only appeared enough. For both PET/MR characterized imaging, co-worked technicians and physicians from both departments, however were crucial. Except for lung lesions, PET/MR provided appropriate imaging details, especially in brain, liver, breast and pelvic lesions that need frequent follow-up in youngsters. In terms of complimentary, comparative and radiation controlling purposes, allocating PET/MR and PET/CT at an area closed to the cyclotron site appeared convenient to daily practice.

Conclusions: Facing an era of sophisticated molecular medicine, combined high-end PET, MR and CT together including professionals as a team appeared needed for better utilization of the advanced NM machines.

PC099

Salivette[®] Cortisol 採集唾液皮質醇之使用情形

邱祖廷¹ 方雅潔¹ 余景陽¹ 韓璞¹ 陳芄嘉¹ 林慶齡^{1,2}

¹ 國泰綜合醫院放射免疫實驗室

² 國泰綜合醫院內分泌新陳代謝科

背景介紹：皮質醇是主要甾性皮質賀爾蒙，由腎上腺皮質分泌，為生命中必需，在應付壓力中扮演重要角色，例如：控制碳水化合物、蛋白質、脂質代謝、維持正常血壓、抑制過敏及炎症反應。皮質醇是由腎上腺皮質合成及分泌其間經過下視丘、腦下垂體等分泌之 CRH、ACTH 等激素控制。在一健康個體，皮質醇之值會有固定的上下伏的型態，最高值於早晨醒後，最低值於夜晚。皮質醇的測量常常結合動態功能測試為判定甾質皮質醇不足或過盛的疾病提供診斷工具。因此需要一個低壓力、低干擾、可靠、精確且便利於病患的採檢方式來做進一步的檢驗。

方法：文獻指出夜間唾液皮質醇診斷 Cushing's Syndrome 之敏感性 (sensitivity) 與特異性 (specificity) 分別為 92% 及 96%，和半夜血清皮質醇 (midnight serum cortisol) 相當。然而，二十四小時尿液診斷 Cushing's Syndrome 雖有 95-100% 之敏感性，但其特異性只有 40-50%。目前臨床上以抽血、二十四小時尿液檢驗皮質醇為主要方式，為了避免抽血造成病人壓力而影響檢驗數據與收集檢體不便，且同時考慮到高敏感性及特異性，實驗室利用唾液來檢測皮質醇。採集唾液之方法有：Expectoration (咳)、Passive drool (被動流口水) 及 Salivette[®] Cortisol。唾液皮質醇檢驗結果會因採集方式不同而有所差異，目前最佳的採集方法為 Salivette[®] Cortisol，所測得的結果與血液的最一致且不受 cortisol binding globulin 之影響。Salivette[®] Cortisol 專門設計用於從體積小或皮質醇表現非常低的檢體中，獲得精確的分析值。從 Salivette[®] 取出拭子放入口中咀嚼 60 秒後，將拭子放回 Salivette[®] 並蓋上蓋子，送回實驗室離心，1000 xg，2 分鐘。乾淨的唾液檢體會於錐形管底部，再將拭子及 column 取出。

結果：目前實驗室已使用 Salivette[®] Cortisol 採集到十位病人的唾液檢體。檢驗前會遇到的問題為 Salivette[®] 是否適用於所有年紀之病人？由於 Salivette[®] 拭子之大小為可吞嚥，所以並不建議給三歲以下孩童做採檢。咀嚼 Salivette[®] 拭子取代傳統直接吐口水的優點在於能清潔衛生採集唾液，並百分之百離出唾液 cortisol。使用初期由於病房護理人員尚未清楚 Salivette[®] 採集之步驟，將 Salivette[®] 內的 column 丟棄，導致送回實驗室離心後無唾液檢體。因唾液皮質醇之檢測多用於診斷 Cushing's Syndrome，採集時間應於夜間十一點。發生多次採檢時間點錯誤、夜間病人疲憊及活動式假牙配戴與卸除不便使唾液檢體量不足。上述原因導致退件，需重新採集唾液檢體。此外，採檢人員常常詢問採集後之 Salivette[®] 保存方式。經過實驗室討論後，每次採集兩管相同唾液之檢體，附上 Salivette[®] 採集步驟之衛教單並註明確切採檢時間及採集後檢體需冷藏，進而降低因時間點錯誤或檢體量不足之退件率，提升採檢之效率。

結論：使用 Salivette[®] Cortisol 採集唾液檢測皮質醇為非侵入性、簡單、方便且精確之採檢方式，對於病患及醫護人員都能達到最大效益。

PC100

Differentiation of Osteosarcoma Recurrence Based on PET-CT Radiomics

Chien-Yi Liao¹, Chia-Feng Lu¹, Bang-Hung Yang^{1,2}, Ren-Shyan Liu^{1,2}

¹*Department of Biomedical Imaging and Radiological Sciences, National Yang-Ming University, Taiwan*

²*Department of Nuclear Medicine and National PET/Cyclotron Center, Taipei Veterans General Hospital*

Introduction: The Positron Emission Tomography-Computed Tomography (PET-CT) imaging has been used to diagnosis osteosarcoma (OS) recurrence, but the accuracy of conventional PET prognostic factor (SUVmax) would be influence by inflammation or attenuation correction artifact. This study aim to develop a PET-CT-based radiomics signature and test its ability for recurrent diagnosis of OS.

Methods: A total 38 PET-CT images from postoperative OS patients were enrolled in this study. All images were divided into two groups: tumor and non-tumor. Radiomics features were extracted from whole body PET-CT images. Furthermore, we used two independent radiomic cohorts for training (70% of patients) and validation (30% of patients). An optimal radiomics signature was chosen using support vector machine (SVM). A multivariate radiomics and a maximum standard uptake value (SUVmax) model were built, and the area under the curve (AUC) of operating characteristics (ROC) was used to compare their performance to differentiate OS recurrence.

Results: 30 radiomics features were chosen from 71 candidate features to build a radiomics signature that was significantly associated with tumor, and they presented good performance to differentiate OS recurrence. The AUC of multivariate radiomics and SUVmax models were 0.97 and 0.89, respectively, with the sensitivity being 0.8 and 0.75, and the specificity being 1.0 and 0.86, respectively. Adding radiomics signatures into conventional PET image prognostic factor (SUVmax) can improve the accuracy of the postoperative model in differentiate OS recurrence.

Conclusions: The radiomics signature was an effective factors for differentiate the recurrence. In the future, incorporating radiomics signature into conventional PET-CT prognostic factors will improve the accuracy of osteosarcoma recurrence diagnosis.

PC101

The Evaluation of Caffeine Effects in Myocardial Blood Flow and Myocardial Flow Reserve by Tc-99m MIBI Dynamic SPECT/CT

Hung-Pin Chan^{1,3}, Chin-Chang Cheng², Chin Hu¹,
Chang-Ching Yu^{1,3}, Nan-Jing Peng^{1,4}

¹Department of Nuclear Medicine, Kaohsiung Veterans General Hospital, Kaohsiung City, Taiwan

²Division of Cardiology, Department of Internal Medicine, Kaohsiung Veterans General Hospital, Kaohsiung City, Taiwan

³Department of Medical Imaging and Radiology, Junior College of Medicine and Management, Kaohsiung City, Taiwan

⁴School of Medicine, National Yang-Ming University, Taipei city, Taiwan

Introduction: Cardiovascular Disease is the 2nd cause of death in Taiwan. The main reason of coronary artery disease is caused by atherosclerosis. When unstable plaque formation is noted in coronary arteries, it may cause coronary stenosis, myocardial ischemia, acute myocardial infarction, and even leading to death. In nuclear medicine, quantitative coronary blood flow could be collected by dynamic single-photon emission computed tomography/ computed tomography (Dynamic SPECT/CT) for CAD diagnosis. Previous cardiac PET articles revealed that caffeine decreased myocardial blood flow (MBF) and myocardial flow reserve (MFR) by dipyridamole-induced stress in whole left ventricle. However, it is little known about the relationship between caffeine and Dynamic SPECT/CT. The purpose of this study is to investigate the role of caffeine on Dynamic SPECT/CT in the diagnosis of CAD.

Methods: The patients who suspected CAD or with abnormal CT angiography (CTA) were referred by cardiologists. They were divided into 3 groups, caffeine abstinence for 3 days before Dynamic SPECT/CT test Intake of one caffeine tablet (about 200 mg) < 24 hours before rest study; and > 24 hours before rest study. Statistical analysis was performed with commercially available soft ware (SPSS) and P < 0.05 was considered statistically significant.

Results: In our 1 year research program, we had the following result showed:

1. We have developed the caffeine test model. The level of serum theophylline has positive correlation to the serum caffeine level. The theophylline level rose to the peak at 24 hour after caffeine intake.
2. Caffeine reduced hemodynamic effects (heart rate response, HRR) during dipyridamole pharmacologic stress.
3. Caffeine reduced stress MBF and MFR by dipyridamole-induced coronary stress in Dynamic SPECT/CT. Interesting, caffeine has no influence in rest MBF.

Conclusions: Caffeine reduces hemodynamic effects, stress MBF and MBR. Therefore, caffeine should be prohibited at least 24 hours before Dynamic SPECT/CT to avoid false positive result. In addition, since the high cost of caffeine test, it is also possible to replace the caffeine test by serum theophylline level.

PC102

Xanthogranulomatous Mastitis Incidentally Detected by FDG PET/CT

Sin-Di Lee¹, Nan-Jing Peng^{1,2}

¹*Department of Nuclear Medicine, Kaohsiung Veterans General Hospital, Kaohsiung, Taiwan*

²*School of Medicine, National Yang-Ming University, Taipei, Taiwan*

Introduction: We present a case of xanthogranulomatous inflammation incidentally detected by F-18 FDG PET/CT.

Case report: This is an 83-year-old woman has history of hypothyroidism. She received F-18 FDG PET/CT due to pericardial effusion and pleural effusion. F-18 FDG PET/CT revealed a 0.6 cm FDG-avid nodule in 7.3 cm/1:00 axis of right breast. Core needle biopsy on the same day showed foamy histocytes infiltration mixed with foreign-body type giant cells, pigmentation, cholesterolclefts and chronic inflammatory infiltration, indicated xanthogranulomatous mastitis. CK AE1/AE3 immunostain were negative, which means no evidence of malignancy.

Discussion: Xanthogranulomatous inflammation is a rare condition, characteristic with mixture of foamy macrophages and activated plasma cells, multinucleate giant cells, empty cholesterol clefts and yellow hematoidin pigment. Xanthogranulomatous inflammation in gall bladder, kidney, stomach and spinal epidural space has been reported as FDG-avid. It could involve various organ systems, including bone, gall bladder, kidney, pancreas, appendix, eyes, female genital tracts, colon, and urachus. In breast core biopsy, xanthogranulomatous mastitis could be distinguished from malignancy by using cytokeratin stain.

PC103

The Role of FDG PET-CT in Evaluation of Patients with Advanced Head and Neck Cancer After Curative Treatment

Dung-Ling Yu, Shu-Fen Chen

Department of Nuclear Medicine, Mennonite Christian Hospital, Hualien, Taiwan

Introduction: There is high recurrence rate in patients with advanced head and neck cancer (AHNC) after curative treatment. The purpose of this study is to investigate the role of follow-up PET-CT after curative treatment of patients with AHNC.

Methods: There were 31 patients (M:F = 29:2, mean age = 60.1 y/o) had curative treatment for AHNC collected for study. All of patients had PET-CT scan during their follow-up period (range 3.1-5.6 years, mean = 4.1 years) without any symptoms or evidence of recurrence. PET-CT results were interpreted visually. The final diagnosis is based on histopathological findings or clinical follow-up.

Results: There were 9 out of 31 patients (29.0%) showing positive findings of PET-CT, with 7 true-positive and 2 false-positive. There were 22 out of 31 patients (71.0%) showing negative findings of PET-CT, with 19 true-negative and 3 false-negative. Overall, the sensitivity, specificity, positive predictive value, negative predictive value and accuracy were 70.0%, 90.5%, 77.8% 86.4% and 83.9% respectively.

Conclusions: In this limited study, PET-CT has potential role in detection of recurrent lesion in patients with AHNC after curative treatment without clinical evidence of recurrence during follow-up. The study suggests PET-CT is a useful surveillance tool during follow-up period of patients with AHNC after curative treatment.

PC104

評估乳腺癌前哨淋巴結攝影與術前淋巴結切片術之影像特徵關聯性分析

俞長青^{1,2} 詹宏彬^{1,2} 丁健益² 詹繕合² 丁慧枝⁴ 彭南靖^{1,3}

¹ 高雄榮民總醫院核子醫學科

² 樹人醫專醫學影像暨放射技術科

³ 陽明大學醫學系

⁴ 義守大學醫學影像暨放射科學系

目的：在乳癌的治療中，腋下淋巴結是否轉移扮演著重要的角色。核醫中術前淋巴結攝影 (Lymphoscintigraphy) 可幫助外科醫師精確定位前哨淋巴結進行切片。本研究的重點在於發展一套電腦輔助檢測系統 (computer-aided detection, CAD) scheme，探討如何正確找出注射點位置並有效濾除注射點以及擴散藥物，並可自動檢測出每張淋巴影像中 SLN 的方法。藉由分析電腦輔助檢測術前淋巴結攝影之結果與乳腺癌前哨淋巴結切片手術 (Sentinel lymph node biopsy, SLNB) 中的臨床應用比較。

材料與方法：回溯 2015 年 1 月至 2017 年 12 月本院收治之 92 例乳腺癌患者，於乳腺腫塊處、乳暈 6 點、12 點位置各注射 Tc-phytate 0.3 mCi 後分別於 10 min, 30 min, 1 hr, 2 hr 進行前哨淋巴結攝影，比較術中用 r 探針探測“熱點”淋巴結，分析術前淋巴結攝影與電腦輔助檢測乳腺癌 SLNB 的結果。本論文採 (1) 以色調映射 (tone mapping) 的方法：包括 (線性方式直接映射、取對數映射、影像分段映射) 後將高動態範圍的淋巴影像轉換成低動態範圍。(2) 訓練分段影像及合成：包括 (自動分割參考影像、計算權重值)。(3) 探討如何有效取得注射點位置，並利用 Otsu 的方法自動找出適當的門檻值。(4) 形態學運算：包括 Dilation (膨脹) 及 Extraction of Connected Components (連通成分抽取)。(5) 濾除並取得淋巴結點位置，將淋巴影像進行切割，濾除低像素值以及二值化以便進行淋巴影像之 FROC 曲線分析。P < 0.05 做為具有統計顯著性差異。

結果：術前前哨淋巴結攝影成功確定 79 例患者 (85.86%) 前哨淋巴結，13 例患者發現腋窩以外之前哨淋巴結。(1) 淋巴結攝影與注射同位素之照相時間有顯著性相關 (P < 0.05)。(2) SLNs 顯像結果：92 例乳腺癌患者，SLN 顯像 79 例 SLN 檢出率 85.86% (79/92)。(3) SLNB 結果：92 例有 89 例術中成功探測到 SLN，SNB 的成功率為 96.74% (89/92)。(4) 電腦輔助檢測結果：SLNs 的正確率為 98.22%，錯誤率為 1.78% (P < 0.05)。

結論：電腦輔助檢測淋巴結攝影對於乳腺癌 SLN 術前具有高度檢測率，評估在乳腺癌前哨淋巴結切片術中有高度臨床價值。

PC105

Potentially Improving Interpretation of Spine Imaging Using an Advanced PET/MR

Wen-Sheng Huang, Wan-You Kuo, Bang Hung Yang,
Ko-Han Lin, Chih-Yung Chang, Tun-Wei Hsu

Departments of Nuclear Medicine and Radiology, Taipei Veterans General Hospital, Taipei, Taiwan

Background: Integrated positron emission tomography (PET) and magnetic resonance (MR) imaging provides certain imaging characteristics that might be not acquirable from that of PET/CT. We reported differences of spine imaging between these 2 modalities from a hospital's data base.

Material and methods: Thirteen subjects were recruited for evaluating vertebral bone (marrow) FDG uptake and its variety of MR sequences to provide a better confidence to interpret bony abnormalities, e.g. metastatic lesions. The SUVmax and SUVmean were calculated from PET/MR and PET/CT to observe both differences and correlations. Useful MR sequences were applied to investigate the possible gain in differentiating diagnosis of the lesions.

Results: There were 13% SUVmax and 20% SUVmean decrease of bone marrow uptake seen on PET/MR compared to that of PET/CT (2.81 ± 0.58 vs. 2.48 ± 0.62 and 2.10 ± 0.38 vs. 1.75 ± 0.41 , $P < 0.0001$ each). Good correlations between the 2 parameters were found ($\text{SUVmax (PET/MR)} = 0.9351 \text{ SUVmax (PET/CT)} - 0.1477$, $r^2 = 0.7648$; while $\text{SUVmean (PET/MR)} = 0.732 \text{ SUVmean (PET/CT)} - 0.1156$, $r^2 = 0.5201$). The useful MR sequences, such as T1 and T2 (propeller or FSE with FS) for imaging bony loss and lesion features which could be easily fused with the corresponding PET imaging and enabled nuclear physicians confidently interpreted the lesions.

Conclusions: Normally, bone marrow uptake seen on PET/MR appeared significantly lower than that on PET/CT, whether the lower background in conjunction with the application of useful MR sequences provided a better discrimination of bony pathologies, e.g. metastatic lesions needs further explored.

PC106

壁報論文發表摘要·臨床組

Left Atrium Lymphoma Follow-up by F-18 FDG PET/CT for Further Treatment: A Case Report

Yu-Chien Shiau, Ya-Huang Chen, Chia-Wen Lai, Fang-Shin Liu,
Yen-Wen Wu, Shan-Ying Wang

Division of Nuclear Medicine, Far Eastern Memorial Hospital, New Taipei, Taiwan

Introduction: Primary cardiac lymphoma is a relatively rare malignancy which affects more often the right atrium. Several authors reported PET/CT to be useful for evaluation of the disease. Atrium lymphoma is an even rarer disease. We report a case with left atrium high-grade B cell lymphoma followed-up by PET/CT for further staging and treatment.

Case report: The 83 year-old man suffered from short of breath, dizziness and chest tightness for 3 days. He went to ER at other hospital and then was referred to our hospital, and echocardiography with M-mode showed a large myxomatous left atrium mass, nearly obliterating left atrial chamber, attached to AML, highly suspecting myxoma, without protrusion to LV, and concurrent severe TR, moderate MR, mild to moderate AR, and probable severe pulmonary hypertension. Chest to abdominal CT showed ascites, bilateral pleural effusion, and ascending aortic dilated 4.1 cm. Under the impression of LA tumor, he received MV and TV repair, excision of LA tumor, and repair of ASD with autologous pericardial patch. Pathology showed high-grade B cell lymphoma, favor diffuse large B cell lymphoma. PET/CT was arranged for further staging and treatment, which showed suspicious residual malignancy or postoperative change in anterior wall of left atrium, and suspicious lymphoma involvement in paraesophageal lymph nodes at T9-10 level. With the findings of PET/CT, chemotherapy with R-COP was arranged and the patient was followed-up in OPD.

Conclusions: We report the findings of F-18 FDG PET/CT of a case with left atrium high-grade B cell lymphoma. PET/CT findings helped more accurate and postoperative staging and further treatment decision making for the patient. In the future, we hope to gather more cases for more detailed statistical analysis.

PC107

Diffuse Liver Metastases of Postoperative Breast Cancer Detected by F-18 FDG PET/CT And Correlated with CT Images: A Case Report

Yu-Chien Shiau, Chia-Wen Lai, Ya-Huang Chen, Fang-Shin Liu,
Yen-Wen Wu, Shan-Ying Wang

Division of Nuclear Medicine, Far Eastern Memorial Hospital, New Taipei, Taiwan

Introduction: Liver metastasis of breast cancer is not a rare condition. But diffuse liver metastases of breast cancer is a relatively rare disease condition, which could be more difficult for detection by traditional CT images. F-18 FDG PET/CT could be useful for evaluation of this disease condition. We report a case with diffuse liver metastases of postoperative breast cancer detected and followed-up by F-18 FDG PET/CT and correlated with CT images.

Case report: The 56 year-old female had a history of L't breast cancer s/p total excision in 2016 at other hospital. She suffered from abdominal fullness, nausea, fatigue, mild shortness of breath, and tea colored urine. During admission, a huge hepatic tumor was noted. CT reported 1. A 8.3*7.7*8.4 cm irregular and hypodense mass in the right hepatic lobe, with differential diagnoses of focal nodular hyperplasia, huge hemangioma, cholangiocarcinoma; 2. a 2.0 cm nodule in the right hepatic dome and a 2.5 cm mass in the S6/7 of liver, with differential diagnoses of focal nodular hyperplasia, metastasis; and 3. A 7.1 mm ground-glass nodule in the RLL. Tumor marker showed AFP 8.04 ng/mL, CEA25.1 and CA-19930.29 U/mL. PES and CFS showed no tumor lesion. Because of unclear diagnosis of the examinations, PET/CT was arranged for further staging and treatment, which showed suspicious metastatic lymph node in left internal mammary region, diffuse liver metastases, multiple bone metastases in C5, T2, right posterior rib, T10, L5, S1, left iliac bone, and suspicious right shoulder, and suspicious thyroid tumor in left lobe. Under the impression of breast cancer with diffuse liver metastases and multiple bone metastases, the patient was recommended and decided to receive hospice combined care.

Conclusions: We report the findings of F-18 FDG PET/CT of a case with diffuse liver metastases of postoperative breast cancer. PET/CT findings helped staging and further treatment decision making for the patient. Although hospice combined care was recommended after PET/CT findings, the decision should be better for the patient's condition. In the future, we hope to gather more cases for more detailed statistical analysis.

PC108

Experience of I-123 mIBG Sympathetic Activity Image in Taiwan and its Additional Adrenal Medullary Scan for Pheochromocytoma Evaluation

Ming-Hsien Lin^{1,2,3}, Szu-Man Yu¹, Jui-Ning Lee², Ren-Shyan Liu¹

¹Department of Nuclear Medicine, Cheng Hsin General Hospital, Taipei Taiwan

²Division of Nuclear Medicine, Taipei City Hospital Zhongxiao branch, Taipei Taiwan

³Department of Biomedical Imaging and Radiological Sciences, National Yang Ming University, Taipei Taiwan

Introduction: The I-123 mIBG sympathetic activity imaging is for chronic heart failure & Lewy body-related disorder (DLB). It is amazing that take I-123 mIBG heart image can predict whether dementia or not. Degenerative process of cardiac sympathetic nerve is concordant as brain due to alpha-synuclein aggregated. The I-123 mIBG heart-to-mediastinum ratio (HMR) all decreased & can be as a potential biomarker for DLB, PD (Parkinson disease) & PDD (Parkinson disease dementia). Scintigraphy with I-123 mIBG, was reported to have a sensitivity of 83%-100% and specificity of 95%-100% for detecting pheochromocytoma (PHEOs). We report first three subjects in Taiwan referred for dementia evaluation & additional images to rule out the possibility of PHEOs.

Methods: Three subjects (M: F = 1:2, age 59-83 y/o) suspect dementia were enrolled. Withheld nasal decongestants, cocaine, anti-hypertension drug (labetalol), anti-depressants & anti-psychotics for 3 days before image was advised. The HMR & HMR standardized by conversion coefficient (CC, for GE 530 LEHR collimator, the CC is 0.55) at 3 hrs post injection of 3 mCi I-123 mIBG were obtained (planar image 800K). The HMR (N: mean 2.5, range 1.9-3.1) & HMR standardized (HMR-S) (N: 2.1) lower than normal limit indicating DLB, PD or PDD. When patient was a victim of hypertension, serial planar adrenal scan at 3, 6, 24 and/or 72 hrs post injection were performed. The 48hrs post injection was not available due to Sunday condition. Asymmetrically focal area of increased I-123 mIBG uptake at 24, 72 hrs post injection defined as PHEOs.

Results: All subjects' HMR & HMR-S lower than normal limits & high probability of DLB, PD or PDD were suggested. The additional adrenal scan showed no evidence of pheochromocytoma.

Conclusions: The procedures of I-123 mIBG scan were well established in Taiwan. For those dementia associated with hypertension and suspect PHEOs, I-123 mIBG HMR may as a potential biomarker for DLB, PD & PDD and provide additional information of PHEOs.

PC109

甲狀腺癌分類及男女發生率之統計

呂建璋¹ 林雅婷¹ 曾柏銘² 沈淑禎¹ 門朝陽² 蕭聿謙³

¹ 天主教中華聖母修女會醫療財團法人天主教聖馬爾定醫院核子醫學科

² 天主教中華聖母修女會醫療財團法人天主教聖馬爾定醫院正子造影中心

³ 亞東紀念醫院核子醫學科

背景介紹：甲狀腺結節指發生於甲狀腺之腫塊，經常是單一的，也有多發性的。95% 的甲狀腺結節時無害的（良性），5% 為惡性（甲狀腺癌）。甲狀腺癌的分類大致為五種：(1) 乳突癌 (2) 濾泡細胞癌 (3) 何氏細胞癌 (4) 髓質癌 (5) 未分化癌，發生率較高者為乳突癌及濾泡細胞癌。根據國民健康署 2016 統計數據顯示，甲狀腺癌居國人十大癌症第 7 位，標準化發生率為 12.0（每十萬人口），女性標準化發生率 18.1，男性標準化發生率為 5.9，男性發生率比女性發生率為 1:3。本研究分析本院甲狀腺癌患者分類及男女發生率之差異。

方法：本研究收集 96 年至 107 年 147 位曾於本院接受治療或追蹤之甲狀腺癌患者病歷資料，先分析男女病患之比率，再逐筆查閱病理報告資料，統計患者甲狀腺癌之分類。

結果：147 位曾於本院接受治療或追蹤之甲狀腺癌患者，男性比女性為 1:4。由於部分患者之病歷不完整，147 位中僅有 108 位得以查詢病理報告，統計結果如下：(1) 乳突癌 95 位 /88% (2) 濾泡細胞癌 10 位 /9% (3) 何氏細胞癌 1 位 /1% (4) 髓質癌 1 位 /1% (5) 未分化癌 1 位 /1%。

結論：台灣的甲狀腺癌發生率逐年上升，特別是甲狀腺癌已居女性癌症發生率第五位，本院甲狀腺患者之比率男性比女性為 1:4，大部分患者為分化良好之乳突癌及濾泡細胞癌，經甲狀腺切除術，再配合碘 131 治療，達到最佳的治療效果。

PC110

壁報論文發表摘要·臨床組

Improved Accuracy of Quantitative Myocardial Blood Flow Derived by Dynamic MPI Using an Ultrafast Cardiac SPECT in Patients with Multi-vessel Coronary Artery Disease

Fang-Shin Liu¹, Shan-Ying Wang^{1,4}, Yu-Chien Shiau¹, Yen-Wen Wu^{1,2,3,4*}

¹Department of Nuclear Medicine and

²Division of Cardiology, Cardiovascular Medical Center, Far Eastern Memorial Hospital, New Taipei City, Taiwan

³National Yang-Ming University School of Medicine, Taipei, Taiwan

⁴Department of Nuclear Medicine, National Taiwan University Hospital and
National Taiwan University College of Medicine, Taipei City, Taiwan

Introduction: SPECT myocardial perfusion imaging (MPI) is a clinical mainstay with static imaging protocol and semi-quantitatively assessed for perfusion abnormalities. However, extensive ischemia with multi-vessel disease is difficult to diagnose. Dynamic cardiac SPECT provides quantitative estimation of stenosis severity and ischemic burden by the assessment of myocardial flow reserve (MFR) and myocardial blood flow (MBF). Our aim is to evaluate the incremental value of dynamic SPECT in the detectability of multi-vessel coronary artery disease (CAD).

Methods: Patients with suspected CAD who underwent dynamic ECG-gated dipyridamole MPI using a cardiac-dedicated ultrafast CZT camera (D-SPECT) and invasive/or computed tomography coronary angiography within 6 months were retrospectively reviewed. Subjects with history of coronary interventions in the past 90 days, frequent arrhythmia or intense extra-cardiac activity on static MPI were excluded. Dynamic imaging data were analyzed using commercial Corridor 4DM software package, and static perfusion and volumetric data were analyzed utilizing QPS/QGS software, which provided automatically plots according to the 17-segment model, and subsequently divided into three main vascular territories (LAD, LCX, RCA). Significant stenosis was defined as $\geq 50\%$ luminal stenosis. The performance of static perfusion data, including summed stress, rest and difference scores (SSS, SRS and SDS), and dynamic perfusion data, namely post-stress and resting MBF (MBFs, MBFr) and MFR were compared at both patient level and vessel level. The statistical significance was $P < 0.05$.

Results: A total of 55 patients with 152 stenotic vessels were analyzed, 23 with three-vessel disease (42%), and 10 patients (18%) with myocardial infarction (MI). Globally increased SSS and impaired MBFs were significantly associated with significant CAD at patient level ($P < 0.001$ in both), but SDS and MFR didn't. In vessel-based analysis, regional SSS failed to detect LAD disease and SDS was only significant in detecting LCX disease. Importantly, MBFs successfully detected ischemia in 3-vessel territories ($P = 0.009, 0.005, 0.002$, respectively), whereas MFR did not. Using receiver operating characteristic (ROC) curve analysis, the best cutoff value of regional MBFs to detect significant stenosis was 3.5 ml/g/min (area under the curve: 0.758, $P < 0.001$). The sensitivity, specificity, accuracy, positive and negative predictive value were 81, 55, 70, 70, 70%, respectively. Yet, the optimal cut-off value of MFR was not found using a ROC curve analysis.

Conclusions: A clinically available method for MFR quantification by dynamic ^{99m}Tc -perfusion SPECT utilizing a CZT camera has been validated in the current study. It improves the detectability of multi-vessel CAD, and MBFs is superior to MFR or other static MPI parameters.

PC111

Uptake of I-131 on a Post Thyroid Ablation Whole Body Scan Due to Renal Stones, Mimicking Metastases

Shiou-Chi Cherng^{1,2}, Yu-Hsiang Chou¹, Tsung-Han Yang¹

¹Department of Nuclear Medicine, Taipei Tzuchi Hospital, Buddhist Tzuchi Medical Foundation, Taiwan

²School of Medicine, Buddhist Tzuchi University, Hualien, Taiwan

Abstract: A 35 years old female with papillary thyroid carcinoma (PTC) status post (s/p) total thyroidectomy, I-131 ablation therapy (4,440 MBq) was performed due to suspicion of recurrence with regional lymph nodes metastases. A focal increased uptake in the right kidney was shown on the whole body (WB) post-therapeutic scan. Computed tomography (CT) of abdomen revealed a right renal stone. After antibiotics treatment, follow-up I-131 WB post-ablation (1,110 MBq) scan showed complete disappear of the kidney uptake.

Case Report: A 35 years old female had the left PTC s/p total thyroidectomy. Four rounds of small-dose I-131 ablation treatment (4,440 MBq in total) were administrated after then, and the last one post-ablation WB scan showed complete response to the treatment. Four months later, neck sonogram, however, revealed several lymph nodes in the anterior neck and the left supraclavicular fossa, with suspicion of recurrence with regional lymph nodes metastases. Large-dose I-131 ablation therapy (4,440 MBq) was performed; post-therapeutic WB scan with single photon emission computed tomography (SPECT) of chest and upper abdomen showed almost no uptake in the lymph node regions, but there was a focal area of increased I-131 uptake in the right kidney. The urinary activity of I-131 might suggest an unusual condition of renal metastasis of PTC. Abdomen CT revealed a right renal stone. Antibiotics treatment for infection was, therefore, given because her urine routine showed bacteria 3+. Follow-up I-131 WB post-ablation (1,110 MBq) scan showed complete disappear of the kidney uptake.

Conclusion: Nuclear medicine physicians may keep in mind asymptomatic renal stone when focal increased kidney uptake is seen on the I-131 WB post-ablation scan in patient with PTC.

PC112

膽道攝影診斷新生兒膽道閉鎖的價值 ——馬偕經驗

林安蓉¹ 呂坤達¹ 曹勤和² 吳明聰¹

¹ 台東馬偕紀念醫院

² 台北馬偕紀念醫院

背景介紹：新生兒膽汁滯留的主要病因是新生兒肝炎引起膽汁淤積和膽道閉鎖。二者早期臨床表現相近，鑑別困難。但是二者有截然不同的治療方法，前者通過內科藥物治療，後者只能通過肝門腸道吻合手術 (Kasai 手術) 治療，而且在出生 60 天之內愈早接受開刀治療，其預後會愈好。因此及早診斷是否為膽道閉鎖是非常重要的。本研究的目的是回顧馬偕醫院膽道攝影檢查在新生兒膽汁滯留的準確性，並且與其他抽血檢驗數值做分析，希望能更有效區分新生兒肝炎與膽道閉鎖。

方法：本研究採回溯性方法，收集馬偕醫院台北及台東院區新生兒膽道攝影檢查。使用藥物為 Tc-99m mebrofenin，注射後收集 5，15，30，45，60 分鐘的影像，視膽汁排出情形加照 2 至 24 小時延遲相。比較影像診斷結果與手術紀錄其檢查靈敏度與特異性。此外，也統計病患的抽血數值，例如：直接膽紅素 (DB)、總膽紅素 (TB)、天門冬胺酸轉胺酵素 (AST)、血清麩胺酸丙酮酸轉氨基酵素 (ALT)、 γ - 谷氨轉胺酶 (γ -GT) 的數值分析與新生兒肝炎或膽道閉鎖的相關性。

結果：本研究總共收錄近五年來疑似膽道閉鎖的新生兒膽道攝影共 41 例 (女性 19 例男性 22 例，平均年齡 52.9 天)。其中檢查為陽性有 10 例、陰性 31 例。10 例陽性中手術確診為膽道閉鎖有 6 例。診斷膽道閉鎖的靈敏度跟特異性分別為 100% 和 88.6%。31 例陰性的患者，平均掃描時間為 4.8 小時，平均看到腸道活性的時間為 88.7 分鐘。6 例膽道閉鎖的患者，平均掃描時間為 23.6 小時，而 4 例偽陽性患者 (其中 3 例掃描時間為 8 小時，1 例掃描時間為 24 小時)。統計膽道閉鎖患者與非膽道閉鎖患者的直接膽紅素數值分別為 5.1 mg/dl 與 3 mg/dl ($P < 0.001$)， γ -GT 數值分別為 661.3 IU/L 與 127.3 IU/L ($P < 0.001$)。此兩者的結果發現膽道閉鎖患者的數值均高於非膽道閉鎖患者。

結論：由上述可知核醫膽道攝影檢查在診斷膽道閉鎖有很高的靈敏度跟特異性 (100% 和 88.6%)，在診斷與排除膽道閉鎖很有幫助。雖然有 3 例偽陽性病患，但是病理學為不明原因膽汁滯留。另外，我們發現在一個陰性的案例中，掃描時間到 8 小時未發現腸道活性，加做 24 小時延遲相後發現了腸道活性，由此可知 24 小時延遲相有其必要性。因此我們建議掃描時間到 4 小時若未見腸道活性，可請患者隔天再來加照 24 小時延遲相即可，可以減少新生兒的檢查時間與鎮定藥物的劑量。此外，直接膽紅素 (DB)， γ - 谷氨轉胺酶 (γ -GT) 的數值有助於膽道閉鎖的鑑別診斷。然而因為 Tc-99m Mebrofenin 在衛生署的藥物查驗登記過期，每次使用都需要專案申請，目前全台灣並不是所有醫院在做這項檢查，誠屬可惜。

PC113

壁報論文發表摘要·臨床組

FDG PET-CT in Patients with Increasing Serum Tumor Marker after Complete Treatment of Ovarian Cancer

Dung-Ling Yu, Shu-Fen Chen

Department of Nuclear Medicine, Mennonite Christian Hospital, Hualien, Taiwan

Introduction: This study aimed to assess role of FDG PET-CT in patients with treated ovarian cancer with increasing serum level of CA125 but negative results on conventional studies.

Methods: There were 26 patients (age range 36-88 y/o, mean 64.7 y/o) with ovarian cancer after complete treatment collected for study. The patients had high serum level of CA125 but negative on conventional studies. FDG PET-CT scan was performed within a month after laboratory test of serum CA125. FDG PET-CT was interpreted as positive on the basis of visual analysis. Final diagnosis was established by histopathological results or clinical follow-up and /or imaging findings.

Results: The level of CA125 was range of 45-959 U/mL with mean of 127.5 U/mL. FDG PET-CT was positive in 18 out of 26 patients (69.2%) with mean CA125 of 147.5 U/mL, and negative in 8 out of 26 patients (30.1%) mean CA125 of 48.9 U/mL. There is statistic significantly ($p < 0.01$).

Conclusions: Our study suggests FDG PET-CT is useful in detection of recurrence in patients with increasing serum level of CA125 but negative results on conventional studies after treatment of ovarian cancer.

PC114

Fully Automatic Respiratory Motion Correction Improves the Diagnostic Performance of Treadmill-stressed Myocardial Perfusion Imaging with CZT Cameras

Chi-Lun Ko, Pei-Yao Lin, Ruoh-Fang Yen

Department of Nuclear Medicine, National Taiwan University Hospital, Taipei, Taiwan

Objectives: Myocardial perfusion imaging (MPI) sometimes suffered from motion artifacts, especially in treadmill-exercised studies. The motion artifacts can cause image blurring and may degrade the diagnostic accuracy. Data-driven motion correction can be performed on list-mode enabled CZT cameras, and this may reduce the artifacts. We have developed a fully automatic motion correction algorithm with the aid of deep-learning technique. In this study, we applied the algorithm on clinical scans to evaluate the effects of motion correction on the diagnostic accuracy of coronary artery disease (CAD).

Methods: We unselectively recruited 8731 consecutive subjects referred for routine treadmill-exercise TI-201 myocardial perfusion imaging between June 2011 and June 2017. Among them, 1021 subjects with subsequent coronary angiography within 180 days were analyzed. The images were automatically segmented and rotated with the aid of a trained deep-learning model for further analysis. The emitted photon events were binned into five respiratory gates and were reconstructed into motion-corrected images. The original and corrected images were independently scored on the AHA 17-segment model with manual verification. The summed scores were used to predict obstructive CAD (70% or more luminal stenosis). A p -value of less than 0.05 was considered significant.

Results: The heart excursed more in post-stress images (10.0 ± 4.0 mm, range 1.2-34.3 mm) than in redistribution images (7.6 ± 3.1 mm, range 0.8-26.5 mm, $p < 0.01$). Based on the Youden's J-statistic, the optimal cut-off point was 7 for summed stress score (SSS) to predict obstructive disease. The diagnostic specificity (0.740 vs. 0.610, $p < 0.01$) and accuracy (0.753 vs. 0.706, $p = 0.019$) were significantly increased with motion correction, while the sensitivity remained the same (0.764 vs. 0.783, $p = 0.478$). One-third (59 out of 177) of the falsely positive studies can be avoided with motion correction.

Conclusions: The diagnostic specificity and accuracy of MPI can be improved with fully automatic motion correction. This technique can reduce significant amount of falsely positive studies.

PC115

The Prognostic Value of Tc-99m ECD SPECT in Patients with Out-of-Hospital Cardiac Arrest Receiving Therapeutic Hypothermia: A Prospective Cohort Study

Yi-Chieh Chen¹, Wei-Tien Chang², Yih-Hwen Huang¹, Yen-Wen Wu^{3,4},
Rouh-Fang Yen¹, Mei-Fang Cheng¹

¹Department of Nuclear Medicine, ²Emergency Medicine, National Taiwan University Hospital and National Taiwan University College of Medicine, Taipei, Taiwan

³Department of Nuclear Medicine and ⁴Cardiology Division of Cardiovascular Medical Center, Far Eastern Memorial Hospital, New Taipei City, Taiwan

Introduction: Therapeutic hypothermia (TH) is recommended in non-traumatic patients with out-of-hospital cardiac arrest (OHCA) aiming to improve neurological outcome. Our study aims to prospectively evaluate whether specific brain perfusion patterns shown in Tc-99m ECD SPECT can predict neurological recovery in successfully resuscitated OHCA patients receiving hypothermia.

Methods: This is a prospective cohort study done at a tertiary referral hospital. Consecutive adult non-traumatic OHCA patients received TH between January 2010 and December 2015 were recruited. Tc-99m ECD SPECT were performed in all subjects on day 7th to 10th after OHCA, and SPECT images were analyzed using PMOD software. After automatic MR-based atlas normalization, brain image segmentation was applied to acquire mean count uptake in each volume of interest (VOIs) in different regions of brain. The VOIs were then normalized to the mean count of the entire cerebral cortex to obtain an adjusted ratio for each brain region. The primary outcome was favorable neurological status at hospital discharge (Cerebral Performance Category (CPC) score of 1 or 2). CPC score of 3 to 5 conferred to moderate to severe neurological disability (“poor outcome”). Student’s t-test was used to evaluate the brain perfusion differences in each region of brain between the two groups. Patients presented with no cerebral perfusion seen in SPECT images were excluded for analysis.

Results: A total of 85 patients (54 men and 31 women, mean age: 64.2 ± 16.0) were included. Subjects were dichotomized into “good” (CPC 1–2, n = 27) versus “poor” (CPC 3–5, n = 58) neurological outcome. In subjects with poor neurologic outcome, significant lower uptake was noted in the central region (“good” group: 0.87 ± 0.08 vs. “poor” group, 0.77 ± 0.10 ; $P < 0.0001$) and insula (“good” group: 1.02 ± 0.10 vs. “poor” group: 0.95 ± 0.10 ; $P < 0.001$) compared to those showing favorable neurologic recovery. Combined perfusion in thalamus and brainstem can successfully predict neurological outcome in OHCA patients (“good” group: 0.87 ± 0.08 vs. “poor” group: 0.82 ± 0.10 ; $P < 0.018$).

Conclusions: Tc-99m ECD SPECT may be a useful tool for early neuroprognostication in successfully resuscitated OHCA patients receiving TH.

PC116

Catheter Kinking and Microleakage Diagnosed by Tc-99m DTPA Cisternography with SPECT/CT: A Case Report

Lien-Hsin Hu¹, Chien-Ying Lee¹, Kan-Du Liu^{2,3}, Tsui-Fen Yang⁴, Wen-Sheng Huang¹

¹*Department of Nuclear Medicine, Taipei Veterans General Hospital, Taipei, Taiwan*

²*Neurosurgery, Taipei Veterans General Hospital, Taiwan*

³*National Yang-Ming; University Medical School, Taipei, Taiwan*

⁴*Department of Physical Medicine and Rehabilitation, Taipei Veterans General Hospital, Taipei*

We reported a case of hereditary spastic paraplegia who suffered from difficult gait for years and received baclofen infusion pump implantation (Medtronic SynchroMed II Infusion Pump[®]) for symptoms control. He was able to walk without assistance after the infusion system implanted.

However, baclofen withdrawal syndrome as exaggerated rebound spasticity occurred twice after this infusion system implanted and malfunction of the infusion system was suspected. Tc-99m DTPA cisternography was used to confirm the diagnosis of malfunctioning infusion system and to clarify the causes of the two episodes of malfunction. The first episode was diagnosed as catheter microleakage which had not been diagnosed under serial X-ray examination and myelography. Patient's symptoms relived after catheter revision. Similar symptoms recurred several months later, and this second episode was diagnosed as catheter kinking also by radionuclide cisternography. A second time of catheter revision was performed and patient's symptoms subsided. In both studies, SPECT/CT was employed and added great anatomical information which facilitate the diagnoses and provide confidence of surgical intervention.

The procedures and the imaging protocol for this indication is very different from a routine cisternography and should be designed individually. Nevertheless, the application of radionuclide cisternography in this scenario is seldom discussed but its great value in diagnosing intrathecal infusion system malfunction is clear in experiences learned from this case.

PC117

Extrastriatal Uptake of Tc-99m TRODAT-1 in Brain SPECT: An Atlas from A Case Series

Lien-Hsin Hu, Chien-Ying Lee, Wen-Sheng Huang

Department of Nuclear Medicine, Taipei Veterans General Hospital, Taipei, Taiwan

Tc-99m TRODAT-1 is known to bind specifically to the dopamine transporter (DAT) and may provide a marker for the functional integrity of the dopamine neuron. Unexpectedly extrastriatal localization of Tc-99m TRODAT-1 in a variety of physiological and pathological conditions is rarely mentioned in the literatures. We report the fortuitous occurrence in a case series referred for evaluation of the DAT brain imaging. Among these cases, certain degree of reduced striatal activity with concurrent extrastriatal accumulation of Tc-99m TRODAT-1 were presented including uptake in pituitary, oculomotor muscles, midbrain, nasal septum, eyes, and pons. The causes of extrastriatal accumulation of this novel complex remain to be investigated. However, the occurrence of these extrastriatal uptake should be kept in mind because most of the current striatal TRODAT uptake ratio quantitation software involves a normalization of the whole image dataset to the hottest spot in the skull which is usually the caudate nucleus. Whether the visual and quantitative results of striatal uptake is biased by these extrastriatal uptake is to be determined.

PC118

Based on the Reinforcement Learning DCGAN Small Data Model Training, Improve the Prediction Accuracy of MPI Polarmap for CAD Deep Learning Model

Tawei Tseng, Ingjou Chen, Lifan Lin, Chuang-Hsin Chiu

Department of Nuclear Medicine, Tri-Service General Hospital, Taipei, Taiwan

Introduction: This study collected Polarmap images of the T1-201 myocardial perfusion imaging (MPI) and focused on cardiac catheterization as a training target for coronary artery stenosis. A deep convolution generation against the network (DCGAN) was performed and convolution was performed. The Convolutional Neural Network (CNN) establishes and predicts the extent of coronary artery stenosis and compares it with CNN training results to assess whether DCGAN can improve predictions.

Methods: The study collected 411 sets of stress polarograms (normal: 91 myocardial defects: 320), trained images using a 3-layer convolutional neural network architecture (without hyperparameter optimization), and estimated accuracy and AUC based on Out-off-sample data. Then use deep convolution to generate the inverse network DCGAN enhanced learning method. First, the data is divided into three categories: normal 46, defect: 167, Equivocal: 213 (where Equivocal is subdivided into two subcategories, normal: 181, Defect: 32 pens). Then, using DCGAN to generate 3000 “pseudo-polar map images”, classify the markers, then train the images through a 3-layer convolutional neural network, and then use the additional sample data to predict the data to obtain accuracy and AUC.

Results: The 3-layer CNN model training is due to data imbalance and insufficient data. The model accuracy rate was 63% and the AUC was 0.61. After the second method of DCGAN + CNN training, the accuracy of the out-of-sample data prediction model was 81%, and the AUC was 0.76. The accuracy and AUC parts have been significantly improved.

Conclusions: The training of CNN modeling with MPI Strss PolarMap image can effectively predict the degree of coronary artery stenosis, but it is also easy to cause bias due to data imbalance and insufficient data.

Using the DCGAN reinforcement learning method can improve the learning accuracy of small data in deep learning, and use this model for clinical assistant diagnosis.

PC119

案例報告： 葡萄糖正子造影於一名 抗合成酶抗體症候群患者的臨床應用

陳迺傑 張雁翔

高雄長庚紀念醫院核子醫學科

背景介紹：抗合成酶抗體症候群是一種自體免疫疾病，其特徵為自體抗體攻擊體內 tRNA 的合成酶。典型的臨床表徵包含肺間質性病變、肌炎、關節炎、雷諾氏症、不明原因發燒、以及技工手。本次報告案例為葡萄糖正子造影於一名抗合成酶抗體症候群患者的臨床應用。

案例報告：患者為 63 歲女性，曾有子宮頸癌的病史，主訴為關節腫脹疼痛以及下肢無力。抽血檢查發現血中肌酸激酶以及肌紅蛋白增高。肌電圖檢查顯示有四肢肌肉病變的情形。胸部斷層掃描發現兩側下肺葉有瀰漫性浸潤。抗體檢測發現抗 Jo-1 以及抗 PL-12 抗體陽性。本案例接受了葡萄糖正子造影，排除了體內潛在的癌病變的可能性。同時，正子造影顯示氟化去氧葡萄糖的攝取值在肌肉、關節、以及肺部病灶有上升的情形，與抗合成酶抗體症候群的典型特徵相符。

結論：使用葡萄糖正子造影可以幫助診斷肌炎以及肺間質性病變，其為抗合成酶抗體症候群的重要特徵，同時也可以排除合併有癌病變的可能性。我們認為葡萄糖正子造影於抗合成酶抗體症候群的患者臨床應用上具有相當的價值。

PC120

Beyond Malignancy for FDG PET: SLE Presented with FUO with Lymphadenopathies

Jui-Hung Weng¹, Pan-Fu Kao^{1,2}

¹*Department of Nuclear Medicine, Chung Shan Medical University Hospital, Taichung, Taiwan*

²*School of Medicine, Chung Shan Medical University, Taichung, Taiwan*

Introduction: Fever of unknown origin (FUO) is a commonly encountered clinical entity. The etiologies may be infection, malignancy or inflammatory/connective tissue disease.

We reviewed the image manifestation of SLE on FDG PET and what angiolymphoid hyperplasia with eosinophilia (ALHE) is.

Case report: A 39 year-old lady without history of systemic disease before presented with FUO. FDG PET after other clinical survey identified symmetrical lymphadenopathies on both sides of diaphragm and increased uptake in spleen. Although certain differential diagnoses including lymphoma were suggested by the reporting physician, no specific diagnosis could not be made by FDG PET finding alone. The biopsy of a lymph node reported to be ALHE, which seemed not to be the answer. Finally, SLE was diagnosed by meeting the clinical criteria. Her fever subsided after adequate management.

Discussion: The role of FDG PET for surveying the etiology of FUO has been established. However, oncologic indications still have been the most well-known to nuclear specialists. In addition, our knowledge to FDG PET finding of benign diseases should keep expanding.

PC121

Left Adrenal Abscess: A Rare Complication of Injection Sclerotherapy for Gastric Varices in a Cirrhotic Patient Revealed by Gallium SPECT/CT Scan

Chun-Che Lo¹, Pan-Fu Kao^{1,2}, Jui-Hung Weng¹

¹Department of Nuclear Medicine, Chung Shan Medical University Hospital, Taichung, Taiwan

²School of Medicine, Chung Shan Medical University, Taichung, Taiwan

Introduction: FUO is common in immunocompromised patients, e.g., those with liver cirrhosis. We presented a case of left adrenal abscess following injection sclerotherapy for gastric varices, which had not been identified until gallium scan with SPECT/CT.

Case report: A 49 y/o male had alcoholic liver cirrhosis and associated gastric and esophageal varices. He had several episodes of recurrent bleeding. He just received endoscopic injection sclerotherapy (EIS) for hemostasis two 2 months ago. Septic shock with *Streptococcus anginosus* bacteremia developed 6 weeks later. The infection seemed resolved after antibiotic treatment for 10 days. However, fever relapsed just one day after discharge. No abdominal pain was complained then. Abdominal sonography failed to identify the infectious focus while gallium scan later revealed a 5 cm abscess in left adrenal fossa. The mass was new as compared to the abdominal CT scan 20 days ago during last hospitalization. Of note, the left adrenal fossa where it located was close to the retained hyperdense histoacryl at gastric wall from prior EIS. The cause-and-effect relationship between EIS and left adrenal abscess seemed reasonable. Blood culture later yielded *Streptococcus anginosus* and *Candida albicans* bacteremia. After successful drainage, the abscess resolved as expected.

Discussion: Nuclear gallium scan with SPECT/CT has been the mainstay of surveying FUO. In this case report, we illustrated the value of gallium SPECT/CT to identify the etiology, even being a rare complication—left adrenal abscess, following injection sclerotherapy for gastric varices in a cirrhotic patient. Besides helping diagnosis, gallium scan SPECT/CT also guided decision in management.

PC122

Rugger-jersey Spine: A Rare Manifestation of Hyperparathyroidism Incidentally Identified on DXA Bone Densitometry

Jui-Hung Weng¹, Pan-Fu Kao^{1,2}

¹*Department of Nuclear Medicine, Chung Shan Medical University Hospital, Taichung, Taiwan*

²*School of Medicine, Chung Shan Medical University, Taichung, Taiwan*

Introduction: DXA bone densitometry is the gold standard for the diagnosis, risk stratification and treatment response monitoring of osteoporosis. We incidentally identified a distinctive radiographic manifestation of spine resulted from hyperparathyroidism in a patient with ESRD and fragility femur fracture, and presented it here.

Case report: A 49 year-old gentleman with end stage renal disease and hemodialysis for 19 years was admitted due to fragility fractures of both femurs. He received operation for both hips thereafter. An abnormal radiographic pattern called “Rugger-jersey spine” on DXA spine image for documenting osteoporosis was incidentally identified. The prominent endplate densities at multiple contiguous vertebral levels produced an alternating sclerotic-lucent-sclerotic appearance, which mimics the horizontal stripes of a “rugby jersey”. Hyperparathyroidism was later confirmed by hypercalcemia and high serum intact PTH value.

Discussion: The prevalence of osteoporosis is increasing as the result of aging country. Although osteoporosis resulted from hyperparathyroidism is not a rare clinical entity, Rugger jersey spine had not been met before in our experience until this case. As distinctive for hyperparathyroidism, those who present this special radiographic feature on either KUB or DXA study warrant a survey for hyperparathyroidism and thus an adequate management.

PC123

A Gallium-67 Scan Mimicking Bone Scan – An Interesting Case

Jing-Uei Hou¹, Yi-Ching Lin¹, Yu-Yu Lu¹, Shih-Chuan Tsai^{1,2}

¹Department of Nuclear Medicine, Taichung Veterans General Hospital, Taichung, Taiwan

²Institute of Radiological Science, Central Taiwan University of Science and Technology, Taichung, Taiwan

Introduction: Gallium-67 citrate is the first radiopharmaceutical which used to help the diagnostic evaluation of fever of unknown origin. Although there are other new tracers such as Indium-111-labeled leukocyte scan and FDG positron emission tomography, it is still used today.

Case report: Our case is a 65-year-old female who suffered from fever for 3 days. Thus, she came to our emergency department for help and then admitted to hospital. A Gallium-67 Scan was arranged for survey of fever of unknown origin. We acquired the image at 24 hours after intravenous injection of 2 mCi of Ga-67 citrate. However, the result only revealed diffusely increased gallium uptake in the skeletons, and the bilateral pulmonary hili. There was decreased radioactivity at the normal physiological sites. According to her history, she has been diagnosed essential thrombocythemia, which is a rare chronic blood cancer (myeloproliferative neoplasm), and received treatment for about 10 years. Chronic anemia was noted during the period of follow-up, and she received blood transfusion several times. We checked her hemogram and showed very high Ferritin level (8076 ng/mL, normal range 5-200 ng/mL). Thus, hyperferritinemia was diagnosed, which may result the gallium-67 scan mimicking bone scan.

Discussion: Gallium has the biological behavior similar to iron. Thus, the radionuclide Ga-67 may bound to transferrin and lactoferrin after intravenous injection, and then transported to the inflammatory site. Normal distribution of Ga-67 includes liver, bone and bone marrow, spleen, lacrimal and salivary glands, breast, thymus in children, kidneys and colon (route of excretion). In our case, multiple blood transfusions causes excess ferric ions, so the Ga-67 cannot bind to transferrin. Therefore, normal distribution is altered and may result the gallium-67 scan mimicking bone scan. In conclusion, it important to know the history of patient before receive this examination. Some examination, such as gadolinium MRI or whole-body irradiation, may led the Ga-67 image unable to interpret.

PC124

正子藥物自動注射機 對注射工作人員的輻射劑量評估

樊玲 蔡書汎 莊麗華 何恭之

林口長庚紀念醫院核子醫學部

背景介紹：林口長庚醫院核子醫學部使用正子藥物自動注射機 (Medrad® Intego PET Infusion System) 為氟-18 葡萄糖正子攝影患者進行藥物注射，本文探討操作正子藥物自動注射機對藥物注射工作人員的輻射劑量評估。

方法：本研究分為兩部份 (一) 針對自動注射機的操作環境使用手持式輻射偵測儀 (Thermo Scientific RadEye B20) 評估藥物分裝罐的傳送、安裝以及藥物注射等每個步驟劑量率，並針對手持藥物注射方式量測藥物注射時的劑量率，(二) 針對工作人員每日輻射劑量評估配戴電子式個人劑量計 (Thermo Scientific EPD Mk2) 在骨盆腔水平高度，並設定深部、淺部輻射劑量率警報值 (50 $\mu\text{Sv/hr}$) 即時回饋藥物注射工作人員操作時的輻射劑量。

結果：(一) 以自動注射機為病患注射正子藥物前，需將具有輻射屏蔽的正子藥罐以推車傳送 (248 $\mu\text{Sv/hr}$, 55 公分) 至自動注射機旁，提取藥罐裝入自動注射機 (1.45 mSv/hr , 17 公分) 始可對病患進行藥物注射；每位病患使用獨立無菌注射管線 (patient administration set) 連接自動注射機，以生理食鹽水測試連接管路順暢後，工作人員站立至屏蔽後方才開始注射正子藥物 (2.47 $\mu\text{Sv/hr}$, 145 公分)，藥物注射完移除注射管線 (112 $\mu\text{Sv/hr}$, 55 公分)，全日使用自動注射機之工作人員每日輻射劑量深部為 28.0 μSv ；針對手動注射藥物方式，注射工作人員站立在屏蔽後方 (47 公分) 僅以手持正子藥物直接為病患注射，其輻射劑量率為 4.20 $\mu\text{Sv/hr}$ 。(自動注射：手持注射之輻射劑量率 = 2.47 $\mu\text{Sv/hr}$: 4.20 $\mu\text{Sv/hr}$, $p < 0.001$) (二) 會超過 50 $\mu\text{Sv/hr}$ 的步驟為傳送、提取自動注射機的藥罐時、移除病患與自動注射機連接管線，以及手動、自動注射藥物時病患無法配合注射姿勢以至於工作人員無屏蔽防護時。

結論：使用自動注射機有顯著降低工作人員的輻射劑量。為更有效降低注射工作人員的人員劑量，在現有的空間、物力下，我們修正了自動注射機、屏蔽擺放位置、增加推車傳送、減少對藥物注射後患者的衛教，希冀正子藥物自動注射機能夠有效的減低注射工作人員不必要的輻射曝露。

PC125

以電腦斷層做腎臟深度校正 來測量移植腎之腎絲球過濾率

郭建瑋¹ 彭南靖^{1,2}¹ 高雄榮民總醫院核子醫學科² 國立陽明大學醫學院

背景介紹：Gates method 因其快速、方便、病人接受度高以及分腎功能等優點，常當作臨床上測量病人腎絲球過濾率的方法之一。然而 Gates method 用來深度校正的 Tonnesson equation 乃是利用病人身高體重來估算從斜後側測量兩側腎臟之深度，不同於病人實際從後方收集腎臟放射性藥物影像所受到衰減之深度，可能造成腎絲球過濾率以及分腎功能比例之誤差。另外 Tonnesson equation 也無法應用於移植腎之深度校正。故本研究探討調整 Gates method 的參數，利用電腦斷層測量實際腎臟之深度來校正，並應用於移植腎之病人評估。

方法：本研究回溯性收集接受 Tc-99m DTPA 腎絲球過濾率測定檢查、腹部電腦斷層以及收集 24 小時尿液計算肌酐廓清率的病人。利用電腦斷層測量腎臟深度做校正，可得到新的腎攝取百分比。將電腦斷層校正之腎攝取百分比與肌酐廓清率做線性迴歸分析後，可得一公式 ($Y = aX + b$)，並利用此公式計算移植腎病人的腎絲球過濾率。

另外回溯性收集接受 Tc-99m DTPA 腎絲球過濾率測定檢查、腹部電腦斷層及 eGFR 的病人，分別利用 Tonnesson equation 及電腦斷層做腎臟深度校正後，各自將腎攝取百分比與 eGFR 做線性迴歸分析。

結果與結論：電腦斷層校正之腎攝取百分比如預期大於 Tonnesson equation 校正所得到的值，而新公式其迴歸係數如預期比 Gates method 還要小，但決定係數相當低。由於電腦斷層比 Tonnesson equation 校正的腎攝取百分比對 eGFR 之迴歸分析有更高的決定係數，不排除電腦斷層校正是更為準確的計算。由於有些病人造影、尿液收集與採血有時間上的落差，導致離群值產生，未來需要前瞻性的設計，收集更多病人、更準確的尿液與血液數據來做分析。

PC126

Sudden Enlargement of Locally Advanced Thyroid Tumor After Recombinant Human TSH Administration – Case Report and Review of the Literature

Pei-Wen Wang, Shu-Hua Huang, Yung-Cheng Huang,
Chien-Chin Hsu, Yen-Hsiang, Chang

*Department of Nuclear Medicine, Kaohsiung Chang Gung Memorial Hospital
and Chang Gung University College of Medicine, Kaohsiung 833, Taiwan*

Background: Levothyroxine withdrawal is being increasingly replaced by recombinant human TSH (rhTSH) for radioactive iodine (RAI) therapy or follow-up scan in patients with differentiated thyroid cancer. Patients who received rhTSH do not experienced hypothyroidism and maintain a good quality of life. However, adverse reactions including hemiplegia due to hemorrhage in brain metastasis, airway obstruction by cervical tumor enlargement, respiratory distress caused by multiple lung tumor swelling, and ovarian hyperstimulation have been reported.

Case Report: A 65 y/o man, with history of hypertension, stroke, diabetes and gout, received total thyroidectomy in May 2009 for a big nodule (8x5x4 cm) in right lobe of the thyroid. Pathology revealed follicular carcinoma with capsule invasion and extra-thyroid extension (T4NxMx). First (80 mCi in Aug 2009) and 2nd (150 mCi in June 2010) doses of RAI therapy found superior and posterior mediastinum uptake of radioactivity, while stimulated thyroglobulin increased from 99.8 to 200 ng/ml during follow up. The 3rd dose of 150 mCi in May 2011 revealed anterior mediastinum tumor and diffuse lung uptake. The 4th dose of 200 mCi in Oct 2012 revealed the same picture. All the four doses of RAI were treated under thyroxine withdrawal preparation. In Mar 2015, his basal thyroglobulin level reached > 490 ng/ml, and was advised to take the 5th dose of RAI by rhTSH injection due to progressive weakness. However, after the 1st dose injection of rhTSH, he developed hoarseness and CT revealed a huge soft tissue mass at right lower neck and para-tracheal region with tracheal compression. He was immediately treated with dexamethasone and admitted to the hospital. The 2nd dose injection of rhTH and the RAI were cancelled. He received EBRT for local disease control, but general condition deteriorated progressively with frequent infection and GI bleeding, and lost follow-up in Oct 2015.

Conclusion: Our case demonstrated that the risk of abrupt tumor swelling following the use of rhTSH is a real concern. In patients with locally advanced tumor, brain metastasis, widely disseminated disease, or basal serum thyroglobulin levels > 5 ng/ml, rhTSH should be used carefully. Prophylactic steroid use and lower rhTSH doses are suggested to decrease the clinical complications.

PC127

Clinical Usefulness of Bone SPECT/CT Scan in Patients with Spondyloarthritis

Yi-Ching Lin^{1,2}, Shih-Chung Tsai²

¹*Department of Public Health, China medical University, Taichung, Taiwan*

²*Department of Nuclear Medicine, Taichung Veteran General Hospital, Taichung, Taiwan*

Spondyloarthritis (SpA) is an umbrella term for inflammatory diseases that involve the joints, tendons, and the entheses. In the traditional SpA classification system, SpA recognizes six separate diseases including Ankylosing Spondylitis (AS), Enteropathic Arthritis (EnA), Psoriatic Arthritis (PsA), Reactive Arthritis (ReA), Undifferentiated Spondyloarthritis (USpA), and Juvenile Spondyloarthritis (JSpA). In the newer SpA classification system, SpA divides into two broader categories as Axial Spondyloarthritis (AxSpA) and Peripheral Spondyloarthritis (pSpA). Axial SpA causes inflammation in the spine and/or pelvis that typically brings on inflammatory back pain while peripheral SpA commonly causes inflammation in joints and/or tendons in the hands, wrists, elbows, shoulders, knees, ankles, and feet. By demonstrating increased radionuclide uptake in the areas of accelerated bone turnover, bone scintigraphy may be used as a screening method to detect bone metabolism due to inflammation. Bone scan has high sensitivity, cumulative evidence for detection, and easy accessibility for detecting abnormal bone metabolism. Local single photon emission tomography/computed tomography (SPECT/CT) scan provides both functional and anatomic information, which is a better interpretation for comparison and adjusting. This report provides an overview of the applications of bone SPECT/CT images in patients with SpA.

PC128

意外發現術後傷口造成三相骨骼掃描中血池相的放射性異常吸收

朱秀蘭¹ 劉芝庭¹ 游慧貞² 莊雅雯¹

¹ 高雄醫學大學附設中和紀念醫院核子醫學部

² 高雄醫學大學附設中和紀念醫院影像醫學部

背景介紹：核醫三相骨骼掃描對於鑑別蜂窩性組織炎及急性骨髓炎具有重要地位，因臨床及 X 光檢查常難以區別。三相骨骼掃描流程為由靜脈注射放射性示蹤劑後，立即收集局部病灶之動態血流相、血池相和 2-4 小時後的延遲相。蜂窩性組織炎之影像為在血流相及血池相中的病灶會呈現放射線活性聚集，但在延遲相中並沒有放射線活性聚集，急性骨髓炎影像則是三相中的病灶皆呈現放射線活性聚集現象，由此可根據延遲相之差異來鑑別診斷。

病例報告：一位 47 歲男性病患被狗咬傷左手大拇指，因其皮膚膿瘍持續紅腫疼痛，故臨床醫生安排至核醫部進行三相骨掃描檢查。在血池相的影像中，病患左手大拇指有明顯的放射線活性聚集，而在延遲相中的左手大拇指已無放射性聚集現象，表示此病患為罹患蜂窩性組織炎。另外在血池相中，意外發現此病患的頭部軟組織也呈現異常的放射性活性累積，而後在延遲相中並無放射性聚集現象，經查詢病患之病歷紀錄後，發現在執行三相骨掃描檢查的前 2 個禮拜，病患有進行頭部拉皮手術，適逢檢查期間剛好為術後傷口癒合時期，故而意外發現其組織血流增加而造成頭部軟組織在血池相中有明顯異常的放射性活性增高現象。

結論：根據上述影像顯示，其手術的傷口會造成異常的放射性活性累積，因此應盡量避免在檢查期間進行非必要之手術，且其病患之病歷紀錄也要仔細正確填寫，才能避免偽陽性之診斷。

大會組織

大會組織

主辦單位 中華民國核醫學學會

承辦單位 奇美醫學中心永康總院

協辦單位 行政院原子能委員會核能研究所

會長 李將瑄會長

指導委員 (依姓氏筆畫順序, 尊稱省略)

王安美、王昱豐、李將瑄、杜高瑩、林立凡、周大凱、邱南津、邱創新、吳東信、吳彥雯、陳宜伶、陳輝墉、翁瑞鴻、許幼青、曹勤和、黃文盛、黃英峰、黃奕瑋、黃淑華、黃雅瑤、彭南靖、程紹智、詹勝傑、張智勇、楊邦宏、廖炎智、廖建國、鄭媚方、蔡世傳、樊裕明、顏若芳、謝德鈞

法律顧問 蔡雅琴

論文評選組 (依姓氏筆畫順序, 尊稱省略)

召集人 王昱豐

執行秘書 陳保良

口頭論文基礎組 張志賢、黃詠暉、黃雅瑤、陳傳霖

口頭論文臨床組 邱宇莉、邱創新、許幼青、詹勝傑

壁報論文基礎組 田育彰、陳宜伶、黃奕瑋、楊邦宏、羅彩月

壁報論文臨床組 王安美、林明賢、黃淑華、彭南靖、楊士頤、曹勤和

秘書處 (依姓氏筆畫順序, 尊稱省略)

秘書長 路景竹

執行秘書 莊佩儒、蔡思盈

秘書 羅尉文、楊月桂



贊助廠商

台灣新吉美碩股份有限公司
西門子醫療設備股份有限公司
奇異亞洲醫療設備股份有限公司
貝克西弗股份有限公司
臺灣拜耳股份有限公司
富特茂股份有限公司
恩典科研股份有限公司
洋貿易股份有限公司
冷泉港生物科技股份有限公司
士宣生技(股)有限公司
泰歷藥品儀器股份有限公司
元新儀器有限公司
台灣飛利浦股份有限公司
衛采製藥股份有限公司
量子輻射科技有限公司
常捷生醫科技股份有限公司
臺灣新吉美碩股份有限公司

